Dynamic Post-Translational Control of HDAC Activity in Breast Cancer and Implications for Drug Discovery

BY

THOMAS HANIGAN

B.S. Iowa State University, 2012

THESIS

Submitted as partial fulfillment of the requirements for the degree of Doctor of Philosophy in Medicinal Chemistry in the Graduate College of the University of Illinois at Chicago, 2018

Chicago, Illinois

Defense Committee:

Pavel A. Petukhov, Chair and Advisor
Jonna M. Frasor, Co-Advisor
Gregory R. J. Thatcher
Terry W. Moore
Nadim Mahmud (Department of Medicine)
Dennis Grayson (Department of Psychiatry)

This thesis is dedicated to William G.G. Miller and Daniel G. Gardner.

ACKNOWLEDGMENTS

First and foremost, I would like to thank Dr. Pavel Petukhov and Dr. Jonna Frasor for critically analyzing my ideas and for providing a fostering environment for research spanning the fields of chemistry and biology. An immense amount of time from both parties has been spent on my behalf and I will be forever indebted to you both. In particular, I would like to thank Dr. Petukhov for his guidance in chemical synthesis and life perspective and I would like to thank Dr. Frasor for help with biological experimentation and professional direction.

I would like to thank Dr. Petukhov and the National Cancer Institute/NIH grants R01 CA131970, R21 CA183627 and the Alzheimer's Drug Discovery Foundation grant ADDF #20101103 for funding this research. I would like to thank Dr. Jonna Frasor and the NIH R21 CA193627 for helping fund this research.

Additionally, I would like to thank the rest of my thesis committee members (Drs. Greg Thatcher, Nadim Mahmud, Terry Moore, and Dennis Grayson) for their active participation and guidance with the direction of my research. I would like to thank Taha Y. Taha and Shaimaa M. Aboukhatwa for experimental help with chapters three and four of this thesis.

I would like to thank my family and friends for supporting me through completion of my PhD. Without your words of encouragement, I could have never finished. I apologize for all the missed calls and lack of time. I love and care for you all very much.

I want to thank my parents for providing for my undergraduate education, pointing me in the direction of a career in science, and for always pushing me to do my best.

ACKNOWLEDGMENTS (Continued)

Above all else, I would like to thank Rachael Farhat for literally taking care of me during times when I was not able to take care of myself. I owe a lot of my successes to you my love, and I will never forget it.

TWH

Contribution of Authors

Chapters two through four of this thesis are adapted from published manuscripts or manuscripts currently under review. While Thomas W. Hanigan is the first author on all manuscripts, additional co-authors contributed substantially to these works. Below is an accounting of the contributions for each chapter.

Chapter two: T.W.H. and P.A.P conceived of the project. T.W.H. designed and performed all experiments and data analysis apart from determination of IC_{50} and comparison of enzymatic activity, which was done by S.M.A.. The manuscript was written by T.W.H., P.A.P. and J.M.F.

Chapter three: T.W.H. and P.A.P conceived of the project. T.W.H. and S.M.A designed and performed all experiments and data analysis. N.D.B aided in synthesis of PRP 11. The manuscript was written by T.W.H., S.M.A, P.A.P. and J.M.F.

Chapter four: T.W.H. and J.M.F conceived of the project. T.W.H. and T.Y.T. designed and performed all experiments and data analysis. The manuscript was written by T.W.H., T.Y.T., P.A.P. and J.M.F.

TABLE OF CONTENTS

TABLE OF CONTENTS (CONTINUED)

TABLE OF CONTENTS (CONTINUED)

LIST OF FIGURES

LIST OF ABBREVIATIONS

HDAC	Histone Deacetylase
HDACI	Histone Deacetylase Inhibitor
JNK	c-Jun N-terminal kinase
PRP	Photoreactive Probe
MAPK	Mitogen Activated Protein Kinase
PTM	Post-Translational Modification
ER	Estrogen Receptor
TFPA	Tetrafluoro Phenyl Azide
ZBG	Zinc Binding Group
SBG	Surface Binding Group
TNBC	Triple Negative Breast Cancer Cells
BC	Breast Cancer
SAR	Structure Activity Relationship
SAHA	Suberoyl anilide hydroxamic acid
NCOR	Nuclear Receptor Corepressor
GPS2	G Protein Pathway Suppressor 2
TBL1	Transducin Beta-like 1
CK2	Casein Kinase 2
GSK3b	Glycogen Synthase Kinase 3 Beta
TNF-α	Tumor Necrosis Factor Alpha
EGF	Epidermal Growth Factor
IGF-1	Insulin-like Growth Factor 1
EGFR	Epidermal Growth Factor Receptor
NFκB	Nuclear Factor kappa-light-chain-enhancer of Activated B Cells

LIST OF ABBREVIATIONS (CONTINUED)

ChIP	Chromatin Immunoprecipitation
ChIP-SEQ	Chromatin Immunoprecipitation followed by massively parallel DNA sequencing
ATAC-SEQ	Assay for Transposase-Accesible Chromatin with high throughput sequencing
DNASE-SEQ	DNase I hypersensitive sites sequencing
PBMC	Peripheral Blood Mononuclear Cells
DNMT	DNA Methyl Transferase

Summary

Multicellular organisms are comprised of genetically equivalent individual cells that rely on differential gene expression to manifest diverse functionality. This process is orchestrated by controlling the accessibility of DNA to transcriptional machinery through relaxation or compaction of chromatin at particular genomic loci. It is now well understood that this process is disrupted in cancer and a large effort to develop inhibitors of the enzymes that control this process is currently underway. Histone deaecetylase (HDAC) is a family of enzymes that is involved with this process, and inhibitors of this enzyme class have had some success for treatment of several cancer types, including breast cancer. As these enzymes are the final component in multiple converging signaling pathways that affect gene expression, their enzymatic activity is itself regulated by diverse mechanisms including formation of multi-protein complexes, subcellular compartmentalization and post translational modification.

This thesis focuses on the development and application of cell-based assays to identify whether the mechanisms known to regulate HDAC activity are transformed in breast cancer, as well as how these mechanism affect HDAC inhibitor binding. Understanding if and how these mechanisms are transformed will provide insight into disease relevant HDAC isoforms, as well as rationale for novel therapeutic strategies to improve HDAC inhibitor efficacy in breast cancer. Chapter one reviews the current understanding of how HDAC activity is regulated in cancer, paradigms for use and development of HDAC inhibitors, and introduction to methods used in following chapters. Chapter two focuses on the development of an assay to compare HDAC activity across multiple breast cancer cell types using a photoreactive histone decaetylase probe

(PRP). Using this PRP we discover a novel mechansim increasing HDAC3 activity in triple negative breast cancer cells. Chapter three focuses on a strategy to synthesize PRPs based on diverse HDAC inhbitor scaffolds and the application of these PRPs in triple negative breast cancer cells. Chapter four ascertains that the post-translational regulation of HDAC activity dynamically changes in response to HDAC inhibitors. Finally, chapter five discusses biological insights and future strategies to improve HDAC inhibitors for treatment of breast cancer, based off of the experimental endeavours outlined in chapters two through four.

Taken together this thesis demonstrates that HDAC activity is a highly regulated, cell type dependent, dynamic equilibrium, which must be taken into consideration when using and developing HDAC inhibitors to treat disease. Commonly, HDAC inhibitor drug discovery projects rely on biochemical assays using purified recombinant HDACs to measure inhibitor potency and selectivity under thermodynamic equilibirum. These compounds are then used in a context where the activity of these enzymes is dynamically regulated with the expectation that the inhibitor potency and selectivity will remain similar to biochemical predictions. The chapters of this thesis repeatedly reflect that this is not the case with respect to HDAC inhibitors, which may be mirrored in other therapeutically relevant epigenetic targets. As an alternative strategy this thesis describes several assays that can report on HDAC activity and inhibitor selectivity *in situ*. Using these techniques we identify important types of HDAC regulation and pathways that affect inhibitor binding and selectivity in cells, which should be useful to better predict, design and manipulate HDAC ihibitor selectivity and efficacy *in vivo*.

CHAPTER 1: INTRODUCTION.

1.1 Epigenetic deregulation in cancer

Multi-cellular organisms are composed of genetically equivalent but functionally diverse cell types. In humans, this means that all ~220 distinct cell types have the same DNA sequence [(1)]. The cell's functional transformations arise from differential gene expression, rather than DNA sequence alone [(2)]. This is accomplished through the packaging of DNA into chromatin. To package DNA into the nucleus of a cell, ~147 base pair units of DNA are wrapped around an octamer of histone proteins consisting of two copies of the histone isoforms H2A, H2B, H3 and H4, which together comprise a nucleosome. Nucleosomal arrangements are then further folded into higher order structures to make up chromatin [(3-5)]. This packaging provides a layer to control access of the transcriptional machinery to different genomic loci [(6)]. Chromatin can either be densely packed (heterochromatin) facilitating decreased transcription, or dispersed (euchromatin), facilitating increased transcription. Chromatin structure is differentially packaged throughout the genome depending on cell type, giving rise to variance in gene expression and functional diversity across cell types [(7)]. Taken together, gene expression, controlled through chromatin architecture, is generally referred to as epigenetic regulation [(8)].

Numerous mechanisms control chromatin architecture [(9)]. These mechanisms include shuffling histone octamers along DNA or eviction of histones at specific genomic loci. This is generally catalyzed by ATP-dependent multi-subunit complexes [(10)]. Additionally, it has been appreciated for decades that covalent modification of both DNA and histone proteins are associated with transcriptional activity [(11, 12)]. It is now understood that these modifications alter transcription by directly affecting DNA-protein interactions, altering long range nucleosome interactions or

inducing recruitment of remodeling complexes or other chromatin binding proteins. To date over 12 modifications at more than 130 sites on histones have been identified. These modifications include methylation, acetylation, phosphorylation, various acylations, ubiquitination and sumoylation [13]. Histone modifications are added, read and removed by a host of enzymes, many of which present as part of multi-component complexes that often contain several histone or DNA altering functional subunits [14]. It has been proposed that these marks represent a code of covalent histone modifications that are taken together to direct transcriptional activity [14]. The advent of genome wide studies, such as chromatin immunoprecipitation followed by high-throughput DNA sequencing (ChIP-seq) allowed identification of locus specific changes to histone and DNA modifications. Several concerted efforts to look at DNA elements, such as the ENCODE or roadmap epigenomics project, clearly demonstrated site specific individual or combinations of histone and DNA modifications can predict gene expression at discrete loci, supporting a histone code hypothesis [15, 16]. While these studies have demonstrated a correlation between histone modifications and gene expression, recent evidence shows that locus specific manipulation of histone modifications directly increases or decreases transcription of this locus, supporting a causative role for select histone modifications [17, 18].

These projects have also made it abundantly clear that aberrant DNA and histone modifications occur during oncogenesis. While a general hypomethylation of the genomic DNA and hyperacetylation of the histones of malignant neoplasms has been noted for some time [19-23], researchers have now begun to map patterns of DNA hypermethylation or histone modification at genes associated with oncogenesis, in a number of types of malignancies [15, 24], and it is now accepted that these aberrations are a general characteristic of most cancer cells [25]. Indeed, direct

point mutations to both DNA methylating as well as histone modifying enzymes are one of the most frequently occurring mutations in cancer [26]. For example, the DNA methyltransferase (DNMT) 3a gene is mutated in AML, histone methyltransferase enhancer of zeste homologue 2 (EZH2), is often mutated in myeloid leukemias and lymphomas [27]. Additionally, the histone demethylase family members 1a (KDM1a) and 5a (KDM5a), are mutated in a high number of solid and hematological tumors [27]. For a comprehensive review of epigenetic mutations in cancer, see [26, 27]. While our current perception of oncogenesis has been defined by genetic mutations, several recent studies suggest that epigenetic state may play a predominant role in causing DNA mutation. Several genome wide studies have shown local chromatin state in a large range of cell types correlates well with mutational frequency [24, 28, 29]. Thus, well-known mutations to oncogenes like *ras* or *p53* may be a function of the chromatin landscape at a genomic locus, suggesting epigenetic state may drive oncogenesis rather than genetic anomalies.

Given the clear connection between epigenetic aberrations and cancer, as well as the fact that these aberrations are reversible, large scale drug discovery projects to develop inhibitors of epigenetic enzymes are currently underway. In this review, we highlight initial successes of inhibitors that alter histone acetylation on a global scale. We review the current knowledge of how the enzymes responsible for deacetylation (HDACs) are regulated in hematological tumors to connect this regulation with inhibitor efficacy *in vivo*. Finally, using breast cancer as a model, we propose that looking at alternative mechanisms that regulate HDAC activity may help to identify cancer type specific vulnerabilities in the context of cell type specific chromatin architecture. This information should be useful to improve efficacy as well as increase specificity of HDAC inhibitors in a broad range of solid tumors.

1.2 Histone deacetylase enzymes, their substrates and inhibitors

HDACs, also known as lysine deacetylases (KDAC), are enzymes that catalyze the removal of acetyl moieties from lysine ε-amino group residues found on the terminal ends of histones as well as non-histone substrates. Deacetylation of histone tails is typically associated with chromatin condensation and transcriptional repression, with most differentiated eukaryotic cells consisting of hypoacetylated inactive chromatin [30, 31]. However, it is now understood that deacetylation of specific histone isoforms (e.x. Histone 3 or H3), at individual positions along histone tails (e.x. lysine 9 or K9) and the context of neighboring post-translational modifications can be associated not only with decreased transcription, but with increased transcription as well [32-38]. HDAC activity is directly opposed by histone acetyl transferases (HATs) which carefully regulate the equilibrium of histone acetylation [39].

The HDAC family is comprised of 18 isoforms, subdivided into four classes based on homology to yeast enzymes (Figure 1) [40]. Classes I, II and IV are dependent upon zinc to catalyze the deacetylation reaction, whereas Class III are NAD^+ dependent and will not be discussed further [40]. Class I HDACs consist of HDAC1, 2, 3 and 8, which show a high degree of homology, up to 83% between HDAC1 and 2. These isoforms are predominantly responsible for deacetylating histones [41], with the exception of HDAC8, and are ubiquitously expressed in all cell types [31, 42, 43]. Class II can be subdivided into class IIa (HDAC4, 7 and 9) and IIb (HDAC6 and 10), both of which show tissue specific expression [44, 45]. Class IV, comprised solely of HDAC11, is homologous to both class I and II HDACs and displays tissue specific expression [46, 47].

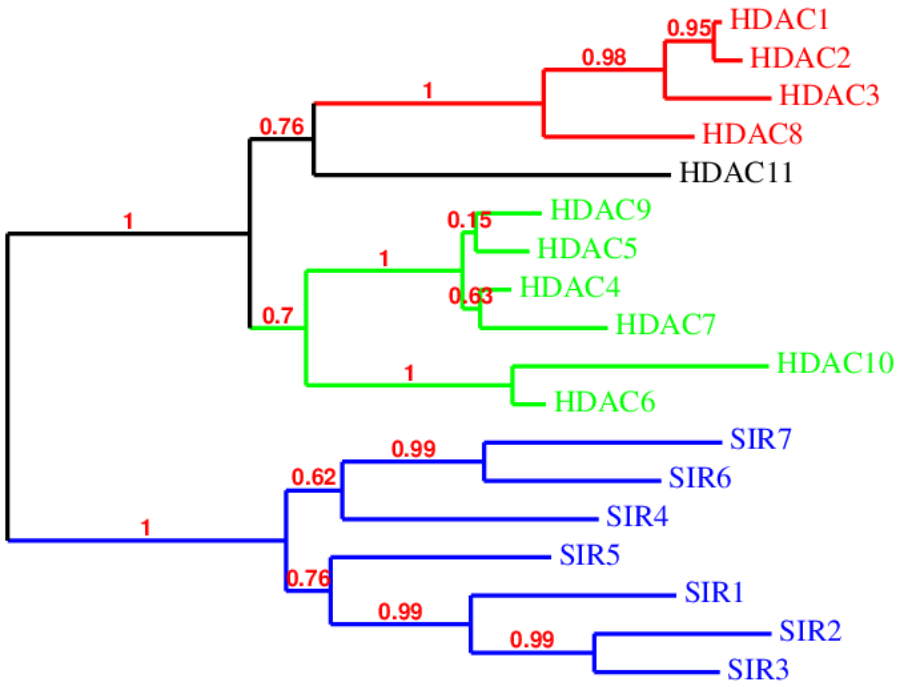

FIGURE 1: PHYLOGENETIC ANALYSIS OF CLASS I, II, III AND IV HDACS
Phylogeny was analyzed using the phylogeny.fr platform according to the methods outlined in [48-52]. Class I HDACs are in red, class II in green, class II in blue and class IV in black.

While many HDAC isoforms have the inherent ability to deacetylate histones, there is some evidence to suggest that individual isoforms non-redundantly deacetylate distinct substrates. For example, multiple studies have investigated which histone isoforms and/or discrete lysine residues are deacetylated by individual class I HDACs. Early cell-based experiments utilizing chromatin immunoprecipitation (ChIP) have indicated that while HDAC1, 2 and 3 could deacetylate all lysine positions and histone isoforms; they did so with variable efficiency [53]. More specifically, HDAC1 and 2 were found to prefer all lysine positions on H4 as well as H3K14, whereas HDAC3 preferred all lysine residues on H2A as well as H4K5, and H4K12 [53]. Studies using *in vitro* reconstituted acetylated histones suggests slightly different substrate

specificity, with HDAC1/2 preferring lysines on H3 and H4, and HDAC3 preferring only H3. Studies examining histone acetylation changes after knockout or knockdown of specific HDAC isoforms have been even more unclear. For example, multiple studies have observed knockdown of HDAC1 resulted in no overall change in histone acetylation levels, and only modest changes in acetylation of H3 and H4 [54-56]. Knockdown of HDAC3 did not change acetylation on H3K9 or H3K27 despite previous *in vitro* experiments showing efficient deacetylation of all lysines on H3 [57]. Another study examining HDAC3 knockout observed no change in total H3 or H4 acetylation [58]. What has become clear from transcriptional manipulation of individual HDAC isoforms is that various HDAC isoforms can compensate for each other resulting in no net change in substrate deacetylation [55, 59]. While histones are the most well characterized substrates of class I HDAC1, 2 and 3, it remains unclear if they are a substrate for HDAC8, class IIa, IIb and class IV members. And while there are well established substrates for some of these HDACs, for example the class IIb HDAC6 is predominantly responsible for deacetylating tubulin (HDAC6) [60], little is known regarding which isoforms deacetylate the 3,600 sites that have been discovered so far [61]. Clearly, additional work must be done to dissect the substrate specificity of individual HDAC isoforms.

HDACs were not isolated until several decades after demonstrating histone acetylation correlated with RNA production [11, 23, 30]. Interestingly, even inhibitors of this enzyme class were known long before the discovery of the first HDAC [22], and much of the biological insight regarding the function of HDACs has been driven and motivated by studies with small molecule inhibitors. Before the discovery of an enzyme with deacetylase activity, it was noted that the small molecule n-butyric acid (now known to inhibit HDACs) could both induce histone hyperacetylation [22], as

well as specifically induce the differentiation of erythroleukemic cells [62]. Several other small molecules that increased histone acetylation, as well specifically induced cancer cells were discovered shortly thereafter; including trapoxin A, trichostatin A, and SAHA [63-65]. Motivated by the functional consequences of changing histone acetylation in cancer cells, the first HDAC isoform was isolated using trapoxin A conjugated to solid support [30] and a revolution of HDAC inhibitor development ensued. Today there are four FDA approved HDAC inhibitors in clinical use for a limited subset of cancer types [66].

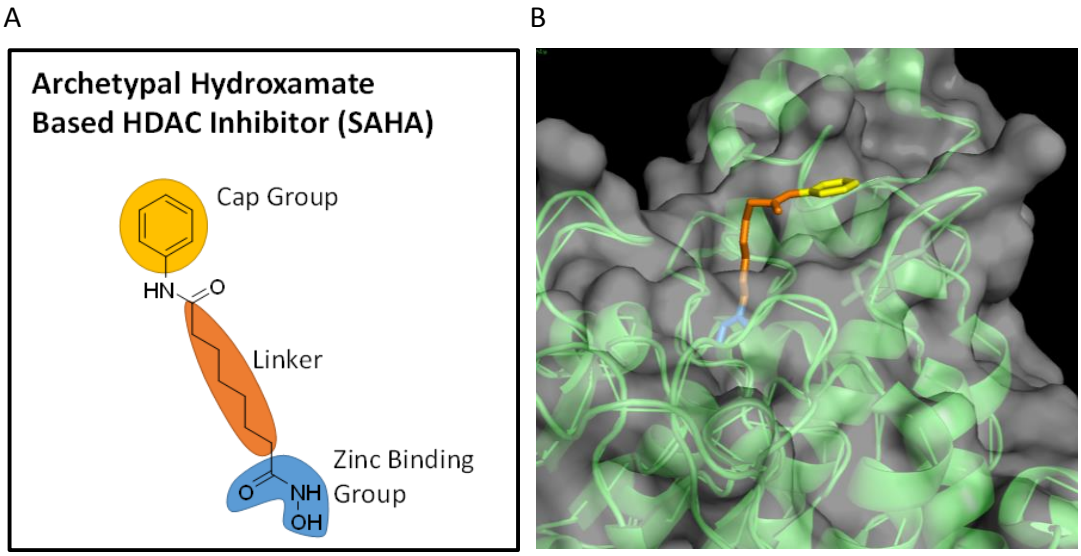

Figure 2: General structure of HDAC inhibitors.
A) Depiction of the components of first generation HDAC inhibitor SAHA. B) Crystal structure of SAHA in complex with HDAC2.

Extensive structural information on HDAC-inhibitor interactions have shown that these molecules bind in a catalytic active site pocket that is highly conserved across class I, II and IV

HDACs. HDAC inhibitors bind to this active site using three distinct structural components [67, 68]; a zinc binding group (ZBG), to chelate the catalytic zinc in the active site, a linker region to span the hydrophobic channel of the HDAC active site, and a surface binding group (SBG) to interact with hydrophilic active site rim (Figure 2) [40]. As HDAC inhibitors bind the HDAC active site, their effects are generally associated with inhibition of the deacetylase catalytic activity of multiple HDAC isoforms, given the similarity between the active site of class I, II and IV HDACs [69]. As first generation HDAC inhibitors target multiple HDAC isoforms, they induce genome wide changes to histone acetylation. In turn this change in acetylation has been shown to affect ~2-10% of the genome, depending on the cell type, treatment time and the small molecule examined, leading to a variety of effects [70-73].

Beyond inducing differentiation of transformed cells, HDAC inhibitors have been shown to arrest cells in G1 or G2, activate intrinsic or extrinsic apoptosis, increase production of reactive oxygen species, induce autophagy and mitotic defects, and impair DNA repair mechanisms (for review, see [69]). Remarkably, these effects seem to be specific for transformed cells, however, which effects and the extent to which they are induced in cancer cells is highly cell-type specific. Therefore, anti-cancer efficacy of HDAC inhibitors varies drastically between cancer cell types, making predictions of therapeutic potential *in vivo* difficult [74]. Thus, results from more than 350 clinical trials [75] have been diverse, with hematological malignancies showing the highest sensitivity [76, 77]. Currently, clinical use of HDAC inhibitors is limited to hematological malignancies, with FDA approval for non-Hodgkin's type lymphomas of T-cells, as well as multiple myeloma [40].

1.3 Aberrant HDAC recruitment in hematological tumors and HDAC inhibitor efficacy

Much work has been dedicated to understanding why HDAC inhibitors are more effective against hematological malignancies in comparison to solid tumors. One of the most important discoveries regarding HDAC inhibitor efficacy arose from examination of non-Hodgkin's lymphomas. Many of these lymphomas are driven by fusion transcription factors that result from chromosomal translocation and depend on aberrant recruitment of histone modifying enzymes to prevent differentiation and alter gene expression [(78, 79)]. This is epitomized in acute promyelocytic leukemias expressing the PML-RARα or PLZF-RARα fusions [(80)]. These fusion proteins recruit class I HDACs 1, 2 and/or 3, through protein-protein interaction to retinoic acid regulated genes. The deacetylase activity of this complex is directly responsible for the transforming capabilities of these fusion proteins and HDAC inhibitors are quite effective at inducing apoptosis of these cancer types *in vivo* [(78, 81, 82)]. This has also been observed in acute myeloid leukemia (AML), where the AML1-ETO fusion transcription factor recruits HDACs to repress key AML target genes [(81-83)]. These genes include *CDKN1A* (*P21*$^{Waf1/Cip1}$), which upon repression of its p21 cell cycle inhibitor product, allows cell cycle progression and uninhibited proliferation [(83)]. Aberrant HDAC recruitment has also been observed in non-Hodgkin's lymphoma, where the LAZ3 oncoprotein recruits HDAC1 to repress cell cycle related genes [(84)], as well as in certain types of multiple myeloma [(85)]. This type of regulation is not limited to histone deacetylation and a general reliance of hematological tumors on epigenetic enzymes for transformation is well characterized [(86)].

1.4 Histone deacetylase activity in Breast Cancer

Besides hematological malignancies, preclinical data support the notion that HDAC inhibitors should be efficacious in a number of solid tumor types including prostate, ovarian, colon, kidney, non-small cell lung, renal, and breast [74, 87]. However, clinical trials with HDAC inhibitors as monotherapy have repeatedly shown a lack of clinical response in many cases [76, 77]. Perhaps one of the most promising clinical responses to HDAC inhibitors has been observed in breast cancer [88-91]. What is starting to become clear is that some subtypes of breast cancer respond to HDAC inhibitors [90, 91]. As with hematological malignancies, preclinical research has been heavily focused on identification of aberrant HDAC activity in various subtypes of breast cancer cells.

Traditionally, molecular subtypes of breast cancer are classified based on the expression of the estrogen receptor (ER), progesterone receptor (PR) and amplification of HER-2/Neu [92-94]. Small molecules and antibodies targeting these pathways are some of the most effective primary therapeutic strategies in use today [95]. However, loss of expression of these receptors, either in response to endocrine therapy, or at initial presentation, limits treatment options, and is associated with a worse prognosis [95-97]. Multiple studies have shown HDAC activity plays a role in the loss of ER [95, 98-100]. Cell based data suggest that HDAC1 in conjunction with DNMT1a gets recruited to the ERα promoter to repress its transcription in ER negative cells [101, 102]. Indeed, treatment of ER negative cells with HDAC inhibitors has been shown to induce ERα expression [103-106], however, this is still a matter of open debate [107] and may require treatment with compounds targeting DNMT1a as well [108, 109]. Several researchers have hypothesized that treatment of ER negative cancers with an HDAC inhibitor as monotherapy or

in conjunction with endocrine therapy may be efficacious, however, limited data are available [(110, 111)]. Preclinical data does suggest that some HDAC inhibitors have increased efficacy in triple negative breast cancer cells as opposed to hormone receptor positive subtypes, but this seems to depend on the small molecule studied [(74, 99, 112)].

While, HDAC1 has been shown to be involved with repressing ER in triple negative disease and thus associated with worse prognosis, its expression has been correlated with better prognosis in some breast cancer subtypes [(113, 114)]. Many studies have looked at correlating HDAC expression with disease progression and prognosis. However, these correlational studies have been disparate and the results are often conflicting [(115-118)]. For example, high HDAC1 expression has been shown to correlate with longer disease-free and overall survival in estrogen receptor (ER) positive tumors and low expression of HDAC3 correlates with slower proliferation *in vivo* [(116, 119)]. Others have shown increased expression of HDAC2 and 3 is associated with more aggressive and less differentiated tumors [(117)]. Increased HDAC8 expression has been shown to be associated with poor prognosis in early-stage breast cancer [(118)]. These studies are not limited to class I HDACs either, with multiple groups citing class II HDACs as a contributing factor to disease initiation and progression [(115, 120, 121)]. Furthermore, it has been difficult to examine functional roles for individual isoforms based on these studies, and there is no experimental evidence to date suggesting overexpression of individual HDAC isoforms is transformative. In fact, some *in vivo* evidence supports the opposite, a tumor suppressive role for HDAC1, 2 and HDAC3 [(122-124)]. For example, liver specific knockout of HDAC3 induces hepatocellular carcinoma [(124)].

Given the pleiotropic nature of individual HDAC isoforms or subsets thereof in breast cancer, HDAC inhibitor drug discovery is now particularly focused on developing isoform selective inhibitors [(125)]. The overall strategy has been to modify the ZBG, linker, and SBG of these molecules [(126-128)]. Typically, libraries of potential isoform selective inhibitors are tested biochemically for their ability to inhibit an individual recombinant HDAC's ability to deacetylate a synthetic fluorogenic substrate under thermodynamic equilibrium. After testing against a panel of recombinant HDACs, potency for individual or subsets of isoforms can be compared to assess preference, hence referred to as biochemical selectivity. After development of biochemically potent and selective HDAC inhibitors, these compounds are tested in cells or *in vivo*, and findings with these inhibitors are often used to functionally dissect an HDAC isoform's contribution to disease [(129-131)]. However, HDAC activity is regulated *in vivo* by means other than expression, which is not represented during optimization of HDAC inhibitor potency and selectivity.

1.5 Mechanisms regulating HDAC activity *in vivo*

Almost all class I, II and IV HDACs function as part of multi-subunit protein complexes. As HDACs have no DNA binding affinity, it is generally accepted that they are recruited to specific genomic loci through interactions with transcription factors [(132, 133)] or other chromatin binding components [(134, 135)], to affect chromatin structure site-specifically. These complexes have been shown to directly affect HDAC catalytic activity [(136-138)]. The complexes of HDAC1, 2 and 3 are some of the most well studied. HDAC1 and 2 containing complexes include Sin3, Mi-2/NuRD, CoREST, and MiDAC, whereas HDAC3 acts as part of the NCoR/SMRT complex (Figure 3a) [(139-143)]. NCoR/SMRT can be looked at as a representative of these complexes, all of which

contain at least 5 stable components. One of these components is either NCoR or its isoform SMRT (NCOR2), both of which interact with HDAC3 through a deacetylase activating domain (DAD) [144, 145]. Unlike HDAC1 and 2, HDAC3 is inactive when purified away from it complex and depends on the DAD domain of NCoR or SMRT to become catalytically competent [146]. However, studies of deacetylase dead HDAC3 mutants have demonstrated the NCoR complex does not need deacetylase activity to alter gene expression, but does require the presence of HDAC3, suggesting HDAC3 plays an important non-catalytic scaffolding role in the NCoR/SMRT complexes ability to regulate gene expression [147]. Other members of the NCoR/SMRT complex include GPS2, a G-protein pathway suppressor, TBL1 and TBL1R, both of which are WD40 propeller containing proteins [148, 149]. Assembly of these components depends on the presence of multiple members, as documented by crystallographic and solution based NMR experiments with a c-terminal truncated HDAC3 [150]. Like the NCoR/SMRT complex, several class IIa HDACs possess no enzymatic activity when purified away from specific complex components, and it has been suggested these enzymes possess the ability to bind acetylated lysines rather than deacetylate them catalytically, and play important scaffolding roles to recruit other HDACs [136, 137].

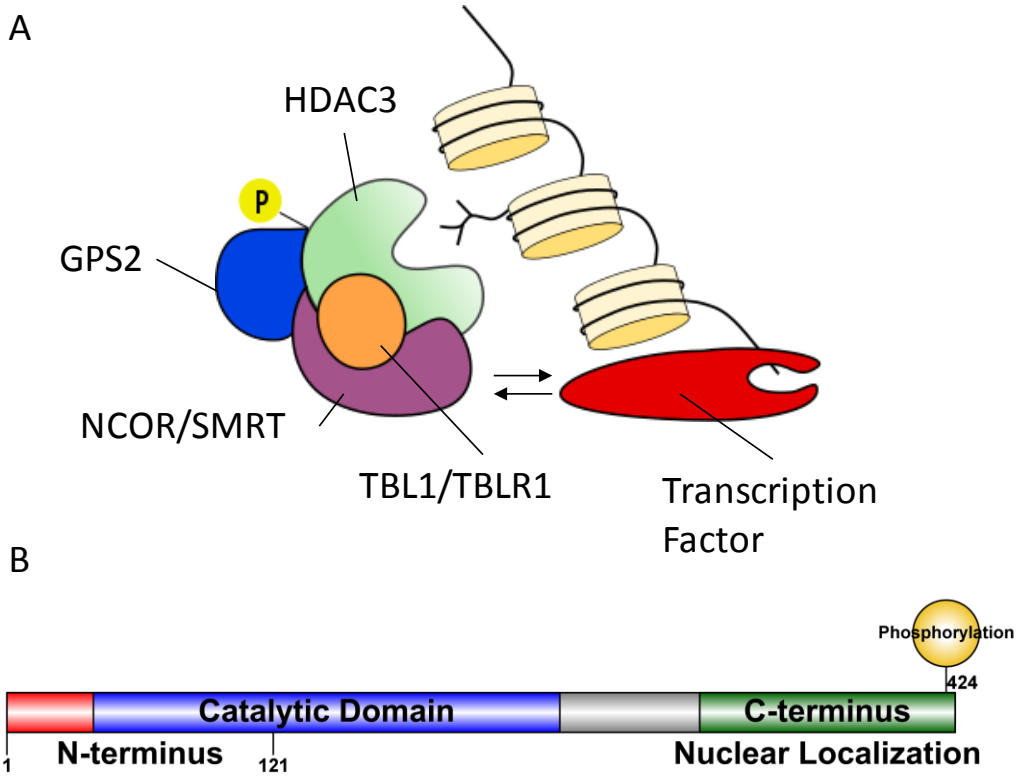

Figure 3: HDAC3 complex, post-translational modification and structural domains, post-translational modification and structural domains.
A) Depiction of the components of the NCOR/SMRT HDAC3 complex. B) Functional HDAC3 domains.

In addition to regulation by protein-protein interaction, HDAC activity is directly regulated by post-translation modifications (PTM) [(140, 151)]. While multiple covalent modifications have been identified, including acetylation, sumoylation, ubiquitination and nitrosylation [(152)], phosphorylation of class I and IIa HDACs has been the most extensively characterized [(140, 153, 154)]. Phosphorylation of both class I and II HDACs has been shown to directly increase deacetylase activity, for example phosphorylation of HDAC3 at serine 424 (Figure 3a), as well as indirectly affect activity through promoting complex formation (HDAC1/2) and subcellular

distribution (class II HDACs) [140, 153, 154]. While multiple phosphorylation sites have been identified on class I HDACs, modification of their loosely structured c-termini is a general trend (Figure 3b). Class II HDACs are modified at key protein-protein interaction sites mediating binding to proteins responsible for import and export from the nucleus [44, 155]. In addition to expression, complex formation and PTM, HDAC activity is regulated through nuclear/cytosolic shuttling. Whereas class I HDACs 1 and 2 have been shown to primarily reside in the nucleus, HDAC3 contains a nuclear export (Figure 3b) and import signal and has been shown to translocate from cytoplasm to nucleus to transduce NFκB mediated signals [156, 157]. The class I HDAC8, however, is primarily localized in the cytosol and has been shown to have multiple non-histone substrates [158, 159]. Class II HDACs are found both in the nucleus and cytosol and contain both nuclear import and export signals as part of their structures, likely to regulate substrate turnover through proximity [44, 160].

As made evident by studies looking at the regulation of HDAC activity, the mechanisms are complex. This is compulsory as these enzymes impinge on numerous signaling pathways to regulate transcription and thus many essential cellular processes. While much work has been done to identify the post-translational mechanisms that regulate HDAC activity, it is unclear whether these mechanisms are transformed in a particular disease state owing to a lack of methodology to easily quantify HDAC activity *in situ*. Furthermore, as HDAC inhibitors have been designed in a context that does not account for these mechanisms, it remains unclear if and which types of mechanisms may affect inhibitor binding and selectivity. This thesis outlines the development of chemical tools to simultaneously quantify the individual activity of all class I, II and IV HDACs and explore the mechanisms regulating HDAC activity in breast cancer cells.

This method is based on a set of novel photoreactive HDAC inhibitor probes (PRPs, Chapters 2 and 3), which also provides insight into how HDAC inhibitors in general are affected by these mechanisms.

1.6 Photoreactive probes

The use of photoreactive probes (PRPs) to study small molecule-protein interactions, termed photo-affinity labeling, was introduced in the 1960s [(161)]. The basic concept relies on introducing a photoreactive moiety as well as a reporter tag into a reversibly binding small molecule ligand (parent scaffold) with native affinity for macromolecular structures. The photoreactive group enables covalent attachment of the ligand to target biomolecules upon photolysis at a specific wavelength, whereas the reporter tag allows visualization or enrichment of labeled proteins. This method has been particularly useful to identify native protein-ligand interactions under physiologically relevant contexts [(162-164)].

To identify native protein interactions, the photoreactive and reporter groups must remain stable under physiological conditions, and minimally affect the native affinity of the parent scaffold. These constraints often require extensive optimization of position, size and electronic properties of the PRP constituents. Numerous photoreactive groups are synthetically accessible including, benzophenones, azides, and diazarines (for review, see [(165)]). Upon photolysis, these groups either form a diradical species, nitrene or carbene respectively, which can react relatively non-specifically with proximal carbon-hydrogen bonds on the surface of target biomolecules. Attractively, groups like azides and diazirines are very small in size, limiting steric interference when incorporated into parent ligands. However, azides must be positioned into an aromatic

residue to generate nitrenes upon photolysis and are prone to intramolecular aromatic ring expansion, which competes with protein intermolecular protein insertion, limiting their photolabeling efficiency [166]. To circumvent these limitations, fluorinated aryl azides were introduced, and afford much longer lived nitrene species and are excited at longer wavelengths, limiting degradation of biological samples [167]. While both diazirines and fluorinated aryl azides decompose irreversibly to reactive carbene/nitrene species, benzophenones reversibly form carbene diradical species upon photolysis, offering increased potential for reaction with protein targets [168, 169]. However this group is inherently bulky, often altering parent compound affinity, and preferentially acts with methionine amino acids, obscuring interpretation of target preference of the parent scaffold [169-171].

Historically, visualization of labeled proteins has been accomplished by incorporation of a radioactive isotope to visualize ligand-protein complexes after photolysis [172, 173]. While radioactive isotopes are minimally invasive to parent scaffolds, relatively easy to incorporate and provide low background signals, care must be taken during synthesis and use, and many commonly used isotopes have short half-lives, limiting the storage, experiment length, and physical location of where these compounds can be made [174]. Another commonly used reporting method is to directly incorporate affinity or fluorescent tags, such as biotin or fluorescein, into the parent scaffold. While this strategy eases synthesis and utility, and provides a means to isolate labeled targets in the case of an affinity tag, these groups often substantially change the steric and electronic properties of the parent scaffold as well as inhibit cellular uptake [175]. Development of the bioorgthogonal "click" reactions, including Huisgen 1,3-dipolar cyclization and Staudinger ligation [176] and adaptation of these reactions for use in photoaffinity

labeling [177] has substantially enabled widespread use of this technique, offering a minimally invasive handle to attach a wide variety of visualization and affinity tags after photoreaction with target biomolecules [175].

For example, copper catalyzed Huisgen 1,3-dipolar cyclization between alkyne and azide containing molecules has frequently been used to specifically connect affinity and fluorescent tags to labeled ligand-protein complexes in native proteomes [178, 179]. As the alkyne is sterically insignificant, rational incorporation of this group into parent scaffolds can be achieved without significantly altering parent scaffold affinity (for examples, see Chapter 3 and [162]). In fact, this strategy has been successfully adapted to identify targets of HDAC inhibitors in cells [162, 180-183].

1.7 Scope of the thesis.

Considering that photoreactive probes can be used to determine HDAC inhibitor targets in cells, this thesis focuses on synthesis (Chapter three) and the development of an assay (Chapter two and three) utilizing photoreactive probes to determine the effects that post-translational modification, protein complex formation and subcellular distribution have on both HDAC activity and inhibitor binding in breast cancer cells. Using this method, Chapter two and three, clearly demonstrate that HDAC3 phosphorylation alone, affects the potency and selectivity of diverse HDAC inhibitor scaffolds in cells.

As we found phosphorylation directly increases HDAC activity as well as affects HDAC inhibitor binding, we also demonstrate how theses probes can be used to quickly and simultaneously ascertain the overall enzymatic state of all class I, II and IV HDACs in any given

cell type of interest. This technique should open the door for functional characterization of the activity of individual HDAC isoforms, beyond expression, in any disease state of interest. In chapter two we also demonstrate that HDAC3 activity is increased in triple negative breast cancer cells (TNBC) in comparison to luminal subtypes, and identify a pathway involved in this regulation. This increase in activity may represent a cancer type dependent vulnerability, and provides rationale for the development and use of HDAC3 selective compounds in this disease, as well as strategies for combination therapy.

As shown in chapters two and three, the mechanisms regulating HDAC3 activity can affect inhibitor binding. In chapter four we investigate how inhibitor binding feeds back on these mechanisms. In particular, we examine subcellular distribution and phosphorylation of class I HDACs. We found that the subcellular localization of select class I HDACs is dose dependently altered in response to a subset of HDACi scaffolds without changing the total cellular abundance. This re-equilibration of subcellular localization was only observed for HDAC1. For HDAC3, on the other hand, we observed a change in the phosphorylation state in response to the treatment with HDAC inhibitors. In addition, we note that the re-equilibration of HDAC1 localization was subsequent to accumulation of histones and may be related to the cell cycle. This adds a spatial and post-translational component to the mechanism of action of HDACi in conjunction to inhibition of catalytic activity, and provides important insight into how individual class I HDACs are dynamically regulated in cells.

CHAPTER 2: DIVERGENT JNK PHOSPHORYLATION OF HDAC3 IN TRIPLE NEGATIVE BREAST CANCER CELLS DETERMINES HDAC INHIBITOR BINDING AND SELECTIVITY.

Thomas W. Hanigan[†], Shaimaa M. Aboukhatwa[†§], Taha Taha[†], Jonna Frasor[‡], Pavel A. Petukhov[†*]

[†] Department of Medicinal Chemistry and Pharmacognosy, College of Pharmacy, University of Illinois at Chicago, 833 South Wood Street, Chicago, IL 60612, USA.
[§] Department of Pharmaceutical Chemistry, Faculty of Pharmacy, Tanta University, Egypt 31527
[‡]Department of Physiology and Biophysics, University of Illinois at Chicago, Chicago, IL 60612.
*To whom correspondence should be addressed; Email: pap4@uic.edu

This chapter is adapted from the manuscript "Divergent JNK Phosphorylation of HDAC3 in Triple Negative Breast Cancer Cells Determines HDAC Inhibitor Binding and Selectivity" accepted for publication on July 18, 2017 in-press at *Cell Chemical Biology*. This manuscript is included in this thesis with permission from Cell Chemical Biology. Rights are shown in Appendix U.

2.4 Abstract

Histone deacetylase (HDAC) catalytic activity is regulated by formation of co-regulator complexes and post-translational modification. Whether these mechanisms are transformed in cancer and how this affects the binding and selectivity of HDAC inhibitors (HDACi) is unclear. In this study, we developed a method that identified a 3-16-fold increase in HDACi selectivity for HDAC3 in triple negative breast cancer cells (TNBC) in comparison to luminal subtypes that was not predicted by current practice measurements with recombinant proteins. We found this increase was caused by c-Jun N-terminal kinase (JNK) phosphorylation of HDAC3, was independent of HDAC3 complex composition or subcellular localization, and was associated with a 5-fold increase in HDAC3 enzymatic activity. This study points to HDAC3 and the JNK axes as targets in TNBC, highlights how HDAC phosphorylation affects HDACi binding and selectivity, and outlines a method to identify changes in individual HDAC isoforms catalytic activity, applicable to any disease state.

2.2 Introduction

Aberrant changes in the epigenetic landscape of chromatin is a hallmark of cancer [(15)]. These changes are a function of the enzymes that catalyze the reading, writing, and erasing of the post translational modifications (PTM) on DNA and associated histones. Histone deacetylase (HDAC) is a family of enzymes responsible for catalyzing the removal of acetyl marks from histone proteins and, as such, have been implicated in a number of different cancers, including breast cancer [(184)]. While HDAC inhibitors (HDACi) have shown promise as breast cancer therapeutics [(185, 186)], HDACs are intimately involved in normal cellular signaling and some of the 18 human isoforms or classes of these isoforms have been shown to be involved with tumor suppression [(187-191)]. Given the pleiotropic nature of HDACs in cancer, the current paradigm is to

selectively inhibit one or more of the 18 human isoforms associated with tumor initiation and progression [192-195]. However, it remains unclear which isoforms are important to target for efficacy in breast cancer. Correlational studies between individual isoform expression and disease state in breast cancer have been disparate [115-118]. In addition to expression, HDAC activity can be regulated through formation of multi-protein complexes and PTM [140, 141, 143, 151]. Whether these mechanisms are transformed in breast cancer, or any other disease state, remains unclear owing to a lack of methodology to easily identify changes in HDAC catalytic activity. If these changes are occurring, it will also be important to ascertain how this regulation affects HDACi binding in cells, subsequently termed target engagement.

Considering that photoreactive probes have already proven to be invaluable tools to probe HDACs in live cells [162, 180], we designed photomate, a novel photoreactive hydroxamic acid based HDAC inhibitor probe. We compared the inhibition and binding of photomate to recombinant HDACs with engagement of HDACs in a panel of diverse breast cancer cell lines. We found that a subset of HDAC isoforms was differentially engaged in a cell type dependent fashion, which was not predicted by assays with recombinant HDACs. Of particular interest, increased engagement of the class I HDAC3 was observed exclusively in TNBC cell lines. Following up on this observation, we systematically investigated the mechanisms contributing to photomate's divergent engagement of HDAC3 and found that its phosphorylation, through c-Jun N-terminal kinase, regulated HDACi target engagement. Ultimately, these differences reflected a change in the isoforms catalytic activity. Taken together we show a mechanism by which aggressive triple negative breast cancer (TNBC) cells regulate the catalytic activity of an individual HDAC isoform. Given the efficacy of HDACi in these cell types, this isoform may

serve as a pertinent drug target. In addition, we clearly show that regulation of this isoform affects inhibitor engagement and selectivity in cells, which should be useful to increase accuracy in predicting HDACi selectivity in vivo. Furthermore, the pathway responsible for this type of regulation could be used to attenuate the effect of HDACi given this pathway controls HDACi engagement.

2.3 Results

Design and synthesis of a photoreactive hydroxamate based probe (photomate)

In general, hydroxamic acid-based HDAC inhibitors, such as the archetypal inhibitor suberoyl anilide hydroxamic acid (SAHA) consist of three components: a) a zinc binding group, e.g. hydroxamic acid, to chelate the catalytic zinc in the active site of HDAC; b) a surface binding "cap" group to interact with the rim of the active site of HDAC; and c) a "linker" to connect the hydroxamic acid to the "cap" group (**Figure 4A**). Photomate incorporates a tetraflurophenyl azide (TFPA) photoactivatable moiety, and an alkyne arm as the "cap" group, joined at a tertiary amine and connected via a 5-carbon "linker" to a hydroxamic acid. This trifunctional design allows photomate to bind to the active site of HDACs and form covalent adducts with proximal proteins upon UV irradiation of the TFPA moiety. The alkyne arm facilitates the coupling of probe-protein adducts bioorthogonally via copper catalyzed 1,3-cycloaddition to an azide-conjugated fluorescent tag for visualization or biotin tag for enrichment and analysis.

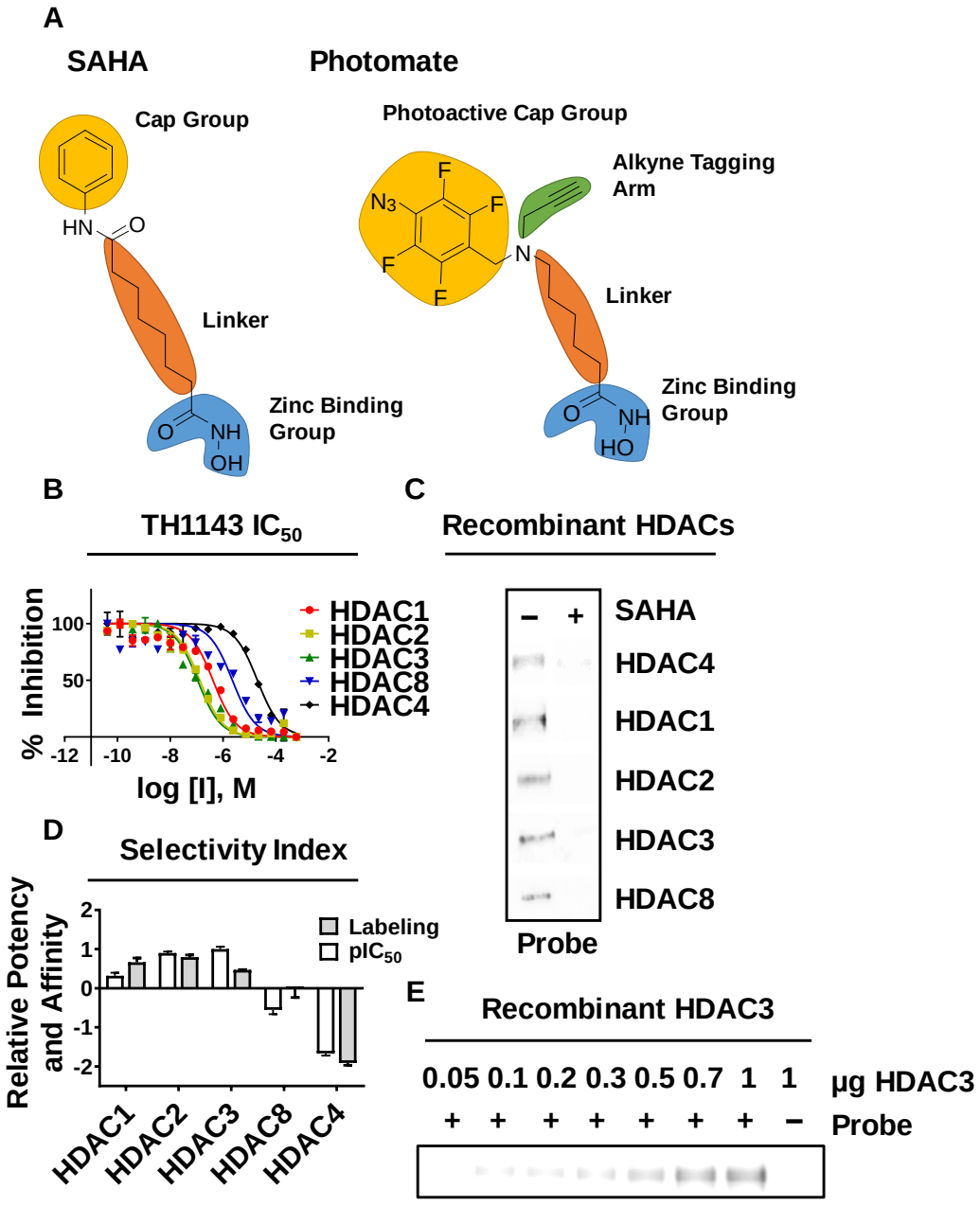

Figure 4: Photomate inhibits and labels class I and II recombinant HDACs.
A) Comparison of the archetypal pan HDAC inhibitor SAHA (Left) and photomate (right) B) IC50 measurements using recombinant class I or class II HDACs and fluorogenic substrates. C) Gel based visualization of recombinant proteins labeled with photomate (lane 1) or photomate and SAHA (lane 2) followed by click reaction with azide conjugated IRDye (gel is in greyscale). D) Relative potency or affinity as measured by pIC50 or labeling density. pIC50 or labeling density values were standardized to their mean and deviation and plotted. Data is shown as mean ± s.d. E) Gel based visualization as in B) with standard dilutions of recombinant HDAC3. All results are representative of at least 3 independent experiments.

Photomate inhibits and labels class I and II HDACs

Using a traditional assay of isoform selectivity, we first verified that photomate was an inhibitor of recombinant class I and II HDACs using a fluorogenic assay. We found photomate potently inhibits all class I HDACs with IC_{50} ranging from 0.109 μM (HDAC3) to 2.27 μM (HDAC8), and inhibited HDAC4, a representative class II HDAC with IC_{50} of 20.11 μM (**Figure 4B**). Next, we explored photomate binding to recombinant HDACs by photolabeling individual isoforms with photomate, or with photomate and excess SAHA (**Figure 4C**). Photomate-protein adducts were reacted with an azide conjugated 800CW IRDye for gel based visualization. We observed effective labeling of all the recombinant class I and representative class II HDACs (**Figure 4C**). Labeling of all HDAC isoforms was lost upon co-incubation with SAHA (**Figure 4C**), indicating the labeling was active site dependent. Additionally, we found photomate could detect at least 0.1 μg HDAC3 with this method (**Figure 4E**). Comparison of the relative potency or affinity based on inhibition or labeling respectively (**Figure 4D**) shows that photomate is non-selective for HDAC1, 2 and 3 but shows decreased potency and affinity with respect to HDAC8 and the class II HDAC4.

Photomate differentially targets HDACs depending on cell type

To characterize the HDAC isoforms targeted by photomate in a cellular context where the mechanisms that regulate HDAC activity are intact, we conducted *in situ* photolabeling experiments in a panel of seven breast cancer cell lines (**Figure 5**). Altogether these cell lines represent the spectrum of breast cancer molecular subtypes, including luminal A (MCF-7, T47D), luminal B (ZR75-1), basal A (BT-20, MDA-MB-468), basal B (MDA-MB-231) and an

additional cell line that does not fit into the classical breast cancer subtypes (MDA-MB-453). Cells growing in monoculture were incubated with photomate, photomate and excess SAHA or vehicle control, followed by irradiation with 365 nm light. We reacted photomate labeled samples with an azide conjugated biotin tag for enrichment with streptavidin coated beads and identification by western blot (**Figure 5**) and MS/MS analysis (MCF7 cells only, **Appendix D, Figure 6C**) or with an 800CW IRDye azide tag for gel based visualization (**Appendix B**). Proteins enriched in photomate labeled samples were compared to samples co-treated with excess SAHA, as well as samples treated with vehicle control and were considered specific if the fluorescence density or spectral count was decreased by greater than 50% in samples co-treated with photomate and excess SAHA and were not identified in vehicle controls. To account for variation in protein expression, we quantified the relative abundance of each class I and II HDAC in the cell lines (**Figure 5B**) and normalized the amount of each isoform that was specifically enriched to its relative abundance. These normalized values were then plotted with respect to the mean for each isoform across all cell types (**Figure 5D, E).**

In general, we found photomate ubiquitously targeted and enriched HDAC1, 2 and 9 from every cell line (**Figure 5A, D**). For these isoforms, the amounts enriched from each cell line correlated well with their relative expression in that cell line. This is reflected in the small range and standard deviation of the relative enriched amounts of these HDAC isoforms across all cell lines as shown in **Figure 5D**. However, all other class I and II HDACs were enriched only in a subset of cell types. For HDAC4 and 7, this was a result of only a subset of cell lines expressing this isoform (T47D, MDA-MB-468). On the other hand, the amounts of HDACs 3, 6, 8, 10 and 11 enriched by photomate did not correlate with their relative expression. For example, we found significantly ($P<.0001$) increased amounts of HDAC3 were enriched from TNBC cell lines

(black bars, **Figure 5E**) in comparison to luminal subtypes like MCF-7 (white bars, **Figure 5E**) despite increased

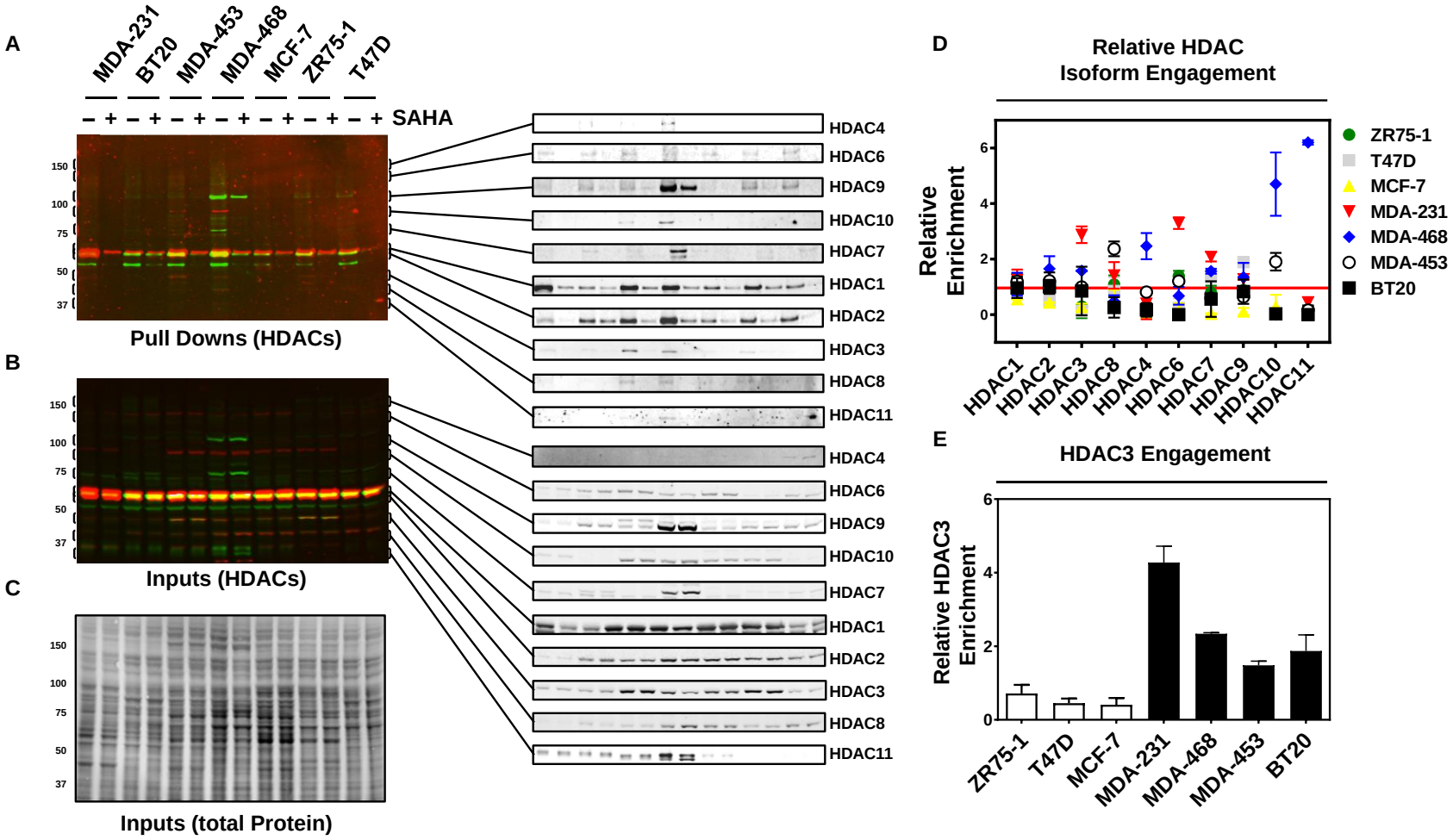

Figure 5: Photomate differentially targets HDACs depending on cell type.
A) Western blot analysis photomate enriched fractions from seven breast cancer cell lines labeled in situ with photomate or photomate and excess SAHA. Samples were reacted with biotin azide tag, and enriched with streptavidin coated magnetic beads. Antibodies for all class I and II HDACs were used for detection. Blot shows enriched fraction eluted off beads. Individual HDAC isoforms across all

cell lines are blown up to the right and shown in greyscale for clarity B) 10% input from each cell line used for enrichment experiments shown in A) HDAC Antibodies for all class I and II HDACs were used for detection. C) Total protein staining of gel featured in B). D) Quantification of enrichment experiments shown in A, B and C. Relative total abundance of each isoform across all cell types were normalized to total protein staining. Quantified enriched amounts of each isoform were then divided by the normalized total abundance of each isoform per cell line. These normalized values were then plotted with respect to the mean for each isoform across all cell types. All gels are representative of three individual experiments. Data is expressed as mean ± s.d. E) As in D) but only for HDAC3 and without normalizing to the mean. Significantly different ($P<0.0001$) values are separated by color (black and white). Data is expressed as mean ± s.d. For gel based visualization of photomate targets see Figure S2.

expression in many of the luminal subtypes (**Figure 5B**). To illustrate this point we quantified the absolute abundance of each class I HDAC in MCF-7 cells, a cell line where we found little to no HDAC3 enrichment by Western blot (**Figure 6B, Appendix A**). HDAC1, 2, and 3 expression was very similar, with $1.92x10^6$, $5.14x10^5$, and $8.37x10^5$ copies/cell, respectively. Notably, HDAC2 abundance is 1.6-fold lower than that of HDAC3, yet was enriched by photomate in this cell line while HDAC3 was not (**Figure 6A, Figure 6B**). This finding is of particular interest given the trend differentiating TNBC and luminal subtypes but also because it contradicts our *in vitro* experiments showing photomate should be equipotent for HDAC1, 2 and 3. In addition, we comprehensively analyzed photomate targets in MCF-7 cells by MS/MS (**Figure 6C, Appendix D**). This experiment matched Western blot analysis in that HDAC1 and 2 were the only HDAC targets in this cell line, and also helped characterize several other non-HDAC zinc containing enzymes or HDAC complex partners.

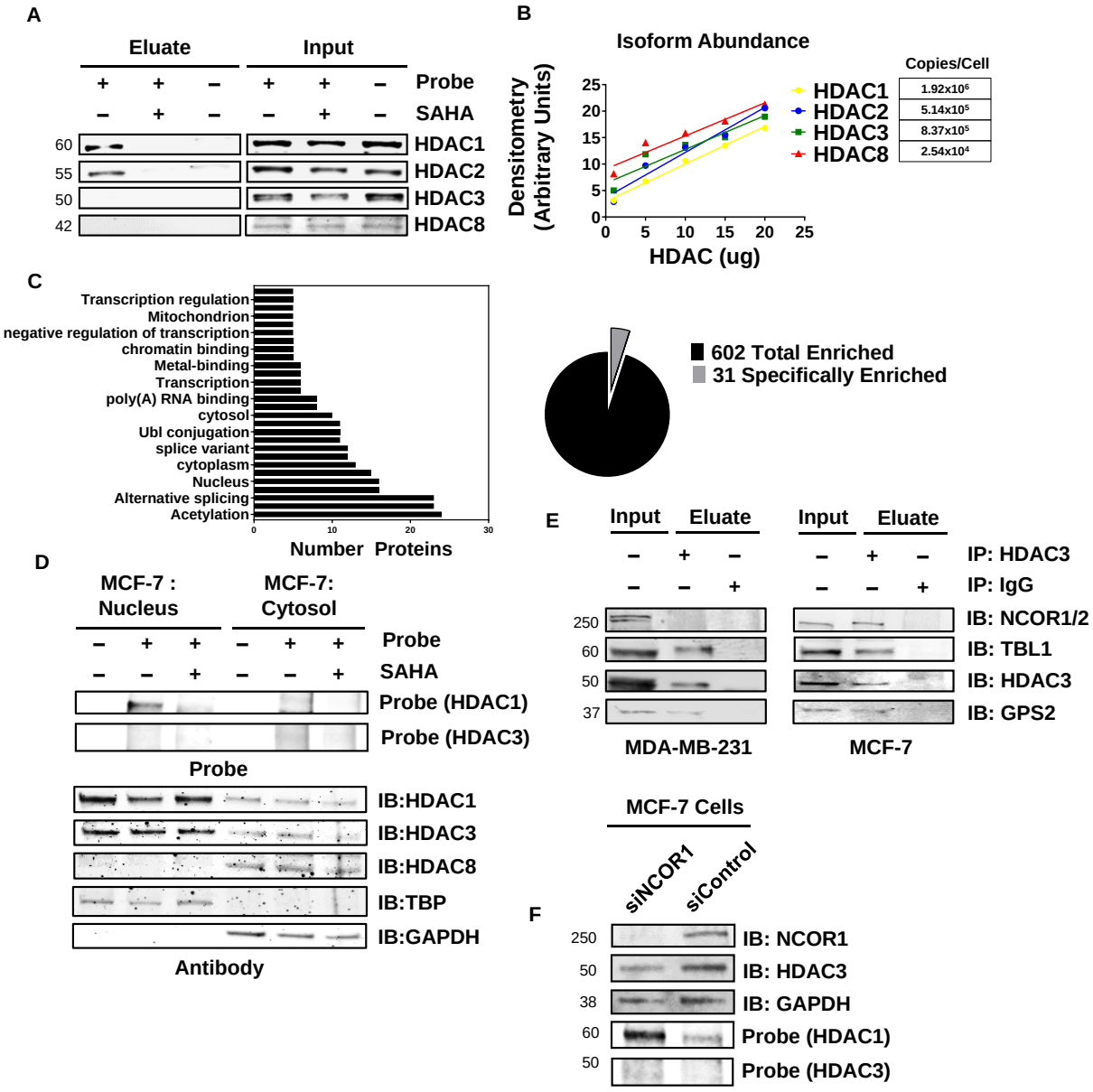

Figure 6: Divergent engagement of HDAC3 is independent of compartmentalization or protein complex composition.

A) Western blot analysis of MCF-7 cells labeled in situ with photomate (lane 1 and 4), photomate and SAHA (lane 3 and 5) or DMSO (lane 6), reacted with biotin azide tag, and enriched with streptavidin coated magnetic beads. Blot shows enriched fraction eluted off beads and 2.5% of input recognized by anti-HDAC1, 2 and 3 antibodies. B) Graph of the abundance of each class I HDAC in MCF-7 cells quantified by comparison of MCF-7 lysate to a standard curve of each recombinant class I HDACs; visualized by Western blot (Figure S1). C) MS/MS analysis of photomate enriched fractions, as in A). Pie chart on the right shows total number of proteins identified by MS/MS and the number that were specifically enriched when compared to a DMSO control and were decreased by at least 50% when co-treated with SAHA. On the left, bioinformatic annotation of enriched proteins. All specifically enriched proteins are shown in

Table S1. D) Gel based visualization of MCF-7 cells labeled with photomate in situ followed by fractionation into cytosol (right) and nucleus (left). Probe staining is shown above, and antibody recognition of the same gel is shown below. Gels are in grey scale for clarity. E) Western blot analysis of HDAC3 co-immunoprecipitates. MDA-MB-231 cells, or MCF-7 cells were lysed and enriched with polyclonal anti-HDAC3 (Abcam) or rabbit IgG protein A bead conjugates (Lanes 2 and 3 respectively). Eluates were analyzed by western blot along with 10% of Input (Lane 1) and blotted with antibodies for complex components. F) Small interfering RNA knockdown of NCOR1 in MCF-7 cells. MCF-7 cells were transfected with siNCOR1 or siControl, followed by labeling with photomate and electrophoretic separation. Antibody recognition of transfected cells is shown above, followed by gel based visualization of photomate engagement of HDAC1and HDAC3 below. Cells were either incubated with photomate (Lane 1) or photomate and excess SAHA (Lane 2) after transfection. All results are representative of at least 3 independent experiments.

Divergent engagement of HDAC3 is independent of compartmentalization or protein complex composition

Given the variation in HDAC3 and other class I and II HDAC engagement, we sought to gain insight into the mechanisms contributing to this variation. We investigated HDAC3 because its inhibition is generally thought to contribute to the efficacy of all FDA approved HDACi [(196)] and the mechanisms regulating its activity have been extensively explored. As HDAC3 translocates between nucleus and cytosol, we verified if photomate and HDAC3 have overlapping subcellular distribution. To do this we labeled MCF-7 cells, a cell line where photomate did not enrich HDAC3, followed by biochemical fractionation into cytosolic and nuclear portions (**Figure 6D**). Prominent labeling of HDAC1 and 2 was observed in the nucleus, showing photomate can permeate the nuclear membrane. Antibody staining of the nuclear fraction showed that the majority of HDAC3 was in the nucleus as well, however, no labeling event was observed (**Figure 6D**).

In addition to subcellular localization, HDAC3 activity is regulated by formation of multi protein complexes. Given this has been shown to affect HDACi selectivity, we analyzed the stable components of the HDAC3 complex from cell lines that do (MDA-MB-231) or do not (MCF-7) show distinct photomate engagement of HDAC3 by co-immunoprecipitation. **Figure 6E** shows Western blots of the immunoprecipitates enriched by a polyclonal HDAC3 antibody (Abcam). Known stable protein partners, TBL1, GPS2 and NCOR1, were co-immunoprecipitated with HDAC3 from MCF-7 cells, however, we noticed NCOR1 was not enriched from MDA-MB-231 cells, the cell line with robust labeling of HDAC3. As NCOR1 and 2 are capable of directly activating HDAC3 enzymatic activity, we envisioned that this might also be capable of influencing photomate engagement of HDAC3. However, siRNA knock down of NCOR1 in MCF-7 cells did not result in an increase in HDAC3 labeling (**Figure 6F**). Together these findings suggest NCOR1 and potentially the protein complex composition are in general, not the underlying cause of the lack of HDAC3 labeling.

Photomate engagement of HDAC3 is correlated with the phosphorylation status of HDAC3

In addition to transcriptional control of expression, subcellular localization, and co-repressor complex formation, HDAC3 is regulated by PTM. Phosphorylation of serine 424 occurs on the *c*-terminus of HDAC3 and increases its activity [(140)]. To investigate differences in HDAC3 phosphorylation, we utilized a phospho (ser-424) HDAC3 specific antibody. We first validated the phospho HDAC3 (pHDAC3) antibodies specificity by phosphorylating recombinant HDAC3 using casein kinase II (CK2) [(140)]. **Appendix E** shows HDAC3, incubated with CK2 in the presence of ATP, is recognized more by the pHDAC3 antibody, over HDAC3 incubated with CK2 only. Additionally, we found that the polyclonal HDAC3 antibody from Abcam, used previously in this paper, equally recognized both the phosphorylated and non-phosphorylated

forms of HDAC3 and that an antibody from Millipore recognized only the non-phosphorylated HDAC3 (**Appendix E**).

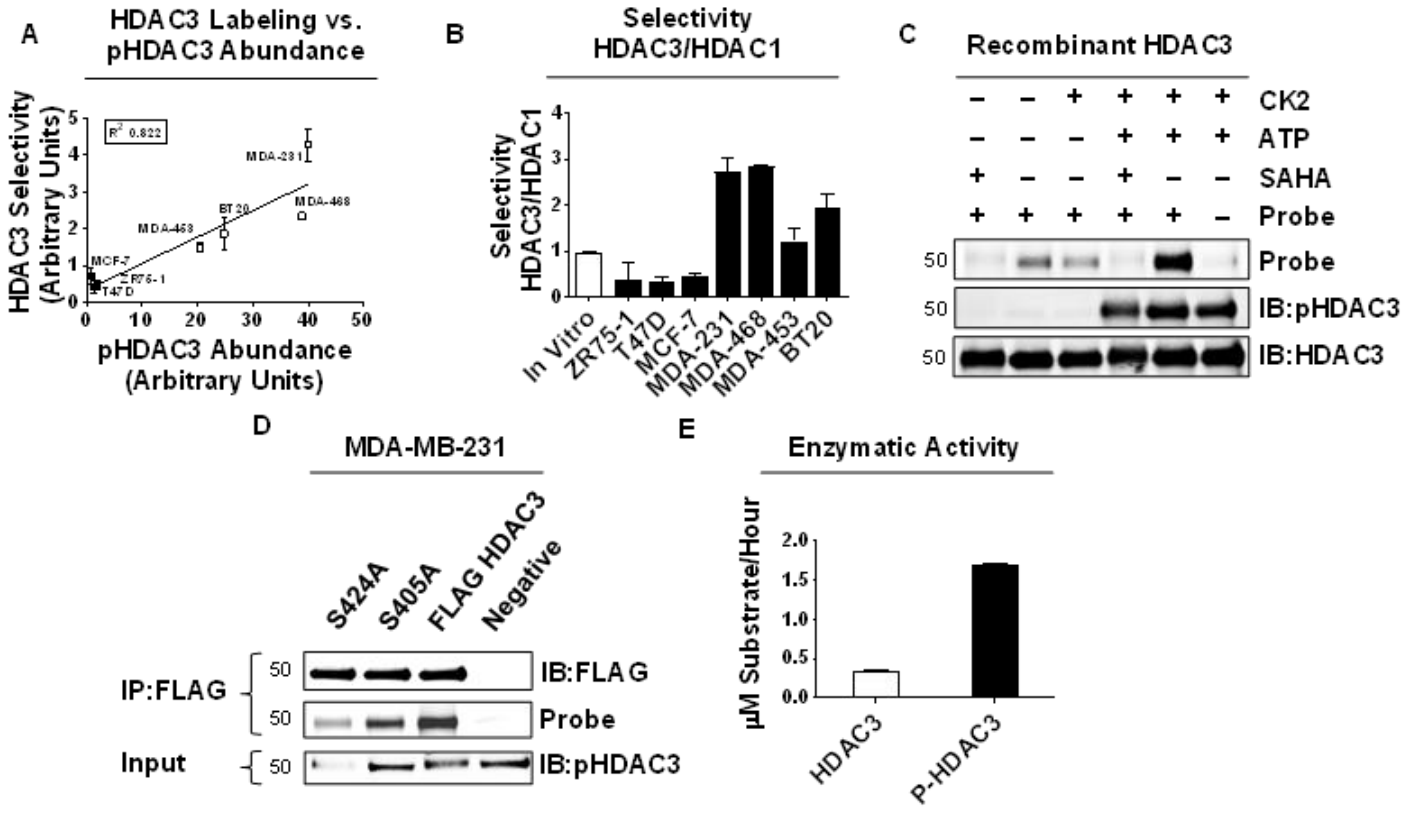

Figure 7: HDAC3 phosphorylation directly increases inhibitor binding.
A) Comparison of HDAC3 engagement versus relative abundance of phosphorylated HDAC3 (pHDAC3) protein; as quantified by Western blot (Figure S3). Linear regression and R square are shown. B) Statistically significant differences in photomate selectivity for HDAC3 compared to HDAC1 across cell lines and in comparison to selectivity based on in vitro potency. One way Anova shows P<.0001. Data is shown as mean ± s.d. C) Gel based visualization of recombinant HDAC3 incubated with CK2 and ATP or with CK2 and vehicle followed by labeling with photomate. Probe labeling is shown at the top followed by staining with antibody staining below. D) Differential labeling of FLAG tagged HDAC3 mutants. MDA-MB-231 cells were transfected with mutant or control HDAC3 plasmids, labeled with photomate (all lanes) and enriched with FLAG antibodies. Visualization of probe or antibody signals of the immunoprecipitates are shown above, and input staining of the phosphorylated HDAC3 below.

E) Enzymatic activity of HDAC3 and pHDAC3 was analyzed using a synthetic class I HDAC substrate. Activity is expressed in μM Substrate/Hour. Students t-test shows P<.0001. Data is expressed as mean ± s.d. All results are representative of at least 3 independent experiments.

Using these antibodies, we surveyed the phosphorylation state of HDAC3 in the panel of cell lines and found significant (P<0.0001) differences in the amounts of phosphorylated HDAC3 existed across cell types (**Appendix C**). Comparison of photomate's HDAC3 engagement and total pHDAC3 abundance shows a very high correlation ($R^2 = 0.822$) suggesting a linear relationship between photomate engagement of HDAC3 and its phosphorylation state (**Figure 7A**). Comparison of photomate's engagement of HDAC3 in comparison to HDAC1, normalized to their respective abundance (**Figure 7B**), shows that selectivity for HDAC3 is significantly increased in those cell lines with highly phosphorylated HDAC3 (P<.0001) and in comparison to *in vitro* experiments with recombinant HDACs.

Photomate binding of HDAC3 is directly affected by the phosphorylation of HDAC3

To test whether HDAC3 phosphorylation was capable of directly affecting photomate binding, we evaluated photomate's ability to label recombinant phosphorylated HDAC3 in comparison to recombinant HDAC3. What we observed was over 4-fold increase in photomate labeling of phosphorylated HDAC3 (**Figure 7C**). This experiment shows that HDAC3 phosphorylation alone is capable of causing an increase in photomate binding to HDAC3. We verified this was also the case in cells by transfecting plasmids for either a S424A, S405A, or control FLAG tagged HDAC3 into MDA-MB-231 cells followed by photomate labeling and enrichment with FLAG antibodies. In agreement with the binding experiments using recombinant phosphorylated HDAC3, we found the S424A mutant had decreased photomate labeling in comparison to the

S405A and control FLAG HDAC3, both of which became phosphorylated after expression (**Figure 7D**). This conclusion seems rationale as others have proposed that HDAC3 activity increases in cells upon phosphorylation [(140)]. A change in HDAC3 enzymatic activity is likely due to changes in its tertiary structure which would also interfere with photomate binding. To verify that the enzymatic activity of HDAC3 is indeed increased when phosphorylated, we compared phosphorylated HDAC3's ability to deacetylate a synthetic fluorogenic substrate to that of recombinant HDAC3. As seen in **Figure 7E**, the activity of phosphorylated HDAC3 is on average five times greater than that of the non-phosphorylated HDAC3. Taken together, these experiments suggest that phosphorylation of HDAC3 at serine 424 directly affects both photomate binding and HDAC3 activity *in vitro* and in cells.

MAPK signaling through c-Jun N-terminal kinase controls HDAC3 phosphorylation and photomate engagement of HDAC3

After establishing that phosphorylation of HDAC3 governs inhibitor binding, we sought to understand the cause of the differential HDAC3 phosphorylation between cell lines. Because CK2 readily phosphorylates recombinant HDAC3, we hypothesized that differential CK2 activity leads to the variation in HDAC3 phosphorylation. To test this hypothesis, we treated MDA-MB-231 cells with two structurally diverse kinase inhibitors that have been shown to potently inhibit CK2 activity (TBB, and LY294002) [(197, 198)], followed by labeling with photomate. Neither of the compounds induced any change in HDAC3 engagement or phosphorylation state, despite significantly changing phosphorylation of CK2 substrates AKT or c-Jun (**Appendix E, Figure 9H, I**). In addition to CK2, it has been shown that GSK3b, can phosphorylate HDAC3 in neurons [(199)]. However, addition of the GSK3b inhibitor AR-A014418 did not affect HDAC3 phosphorylation or photomate engagement (**Appendix F**). This is in line

with the experiment using LY294002, as it has been shown to increase GSK3b activity through AKT in MDA-MB-231 cells [(200)]. Taken together these experiments suggest that the activity of CK2 or GSK3b does not affect HDAC3 phosphorylation in MDA-MB-231 cells.

Given the TNBC cell lines show HDAC3 labeling, but estrogen receptor (ER) positive luminal cell lines do not, we initially thought ER may play a role in decreasing HDAC3 phosphorylation and photomate engagement. We tested this hypothesis by incubating MCF-7 cells with tamoxifen, at a concentration shown to antagonize ER activity in MCF-7 cells [(201)], or with siRNA specific for ERα, followed by labeling with photomate (**Appendix E**). We found no increase in HDAC3 labeling or HDAC3 phosphorylation as a result of either of these experiments indicating ER expression or activity does not affect photomate engagement of HDAC3.

While TNBC cell lines do not rely on ER signaling to proliferate, many have constitutive activation of MAPK signaling, through increased expression of epidermal growth factor receptor (EGFR), or Ras mutation [(202)]. As the NCOR-HDAC3 complex has been shown to be regulated by MAPK signaling [(203)] , we hypothesized that this signaling pathway may increase photomate engagement of HDAC3. To test this hypothesis, we tried either removal or addition of known MAPK stimulating agents followed by labeling with photomate in MCF-7 cells. In opposition to our hypothesis, we found that serum starvation as well as treatment with the proinflammatory cytokine TNF-α induces specific labeling of HDAC3 in MCF-7 cells (**Figure 8A-D**, **Figure S5A, I**), whereas the addition of MAPK stimulating growth factors, EGF, and IGF-1 had no effect despite inducing changes in phosphorylation of AKT (**Figure 8E**, **Appendix F**). In line with our experiments from **Figure 7**, showing photomate engagement of HDAC3 is associated with HDAC3 phosphorylation, the increase in HDAC3 labeling induced by serum starvation

corresponded with a concomitant increase in HDAC3 phosphorylation, which was labile to λ phosphatase (**Figure 8A, C)**. Additionally, we observed that most MCF-7 cells were aligned in G_0/G_1 upon serum starvation prior to labeling with photomate (**Appendix F**). Taken together, these experiments show mitogen removal and inflammatory cytokine stimulation induce HDAC3 phosphorylation and photomate engagement of HDAC3, whereas addition of growth factors has no effect.

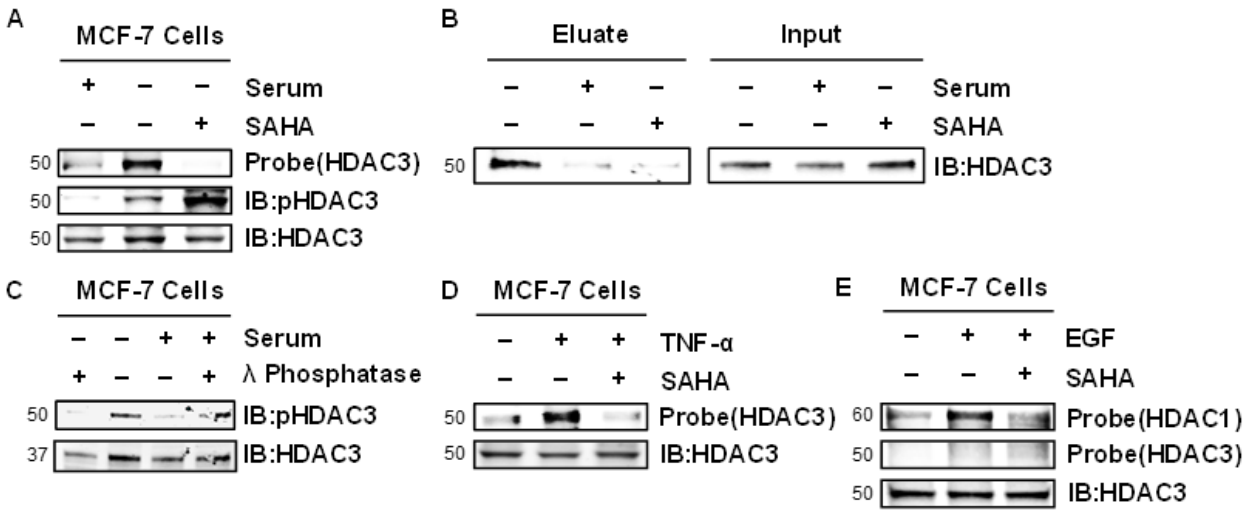

Figure 8: HDAC3 phosphorylation and photomate engagement is affected by cellular stress.
A) Gel based visualization of MCF-7 cells either serum starved or grown in medium supplemented with 10% FBS and labeled in situ with photomate or photomate and SAHA. Recognition of photomate labeled HDAC3 with antibodies is shown below. B) Western blot analysis of MCF-7 cells, serum starved, labeled with photomate or photomate and SAHA in situ, reacted with biotin azide tag, and enriched with streptavidin coated magnetic beads. Blot shows enriched fraction eluted off the beads and 2.5% of input stained with HDAC3 antibodies. C) Western blot analysis of pHDAC3 in MCF-7 cells either serum starved or grown in medium supplemented with 10% FBS. Each group was incubated with lambda phosphatase to remove any phosphate groups from HDAC3. D) Gel based visualization of MCF-7 cells either treated with TNF-α or vehicle and labeled in situ with photomate or phtoomate and SAHA. Recognition of the photomate labeled HDAC3 with antibodies is shown below. E) as in D) with EGF

treatment in place of TNF-α. All results are representative of at least 3 independent experiments. (For additional experiments and controls see Appendix E and F)

Because removal of serum or inflammatory cytokine signaling increased HDAC3 phosphorylation and photomate engagement, we hypothesized that a stress activated protein kinase pathway, either NF-κB, p38, or JNK was responsible. To test this hypothesis, we used inhibitors of IKK (IKK-16), p38 (SB202190) or JNK (SP600125) at concentrations that altered phosphorylation of known substrates of their respective enzymes (**Figure 9H, I**), followed by labeling with photomate. We found that the JNK inhibitor abolished the labeling of HDAC3 (**Figure 9A, B, Appendix F**), whereas the IKK inhibitor had no change and the p38 inhibitor increased labeling (**Appendix F**). Because the JNK inhibitor decreased labeling, we again measured the phosphorylation state of HDAC3 in comparison to control and observed a complete loss of HDAC3 phosphorylation (**Figure 9A, B**). In addition to SP600125, we used another structurally distinct specific JNK inhibitor (TCS 6o) in conjunction with photomate labeling and found both HDAC3 labeling and phosphorylation were decreased (**Figure 9C**). In agreement with JNK phosphorylating HDAC3, we identified activated JNK (phosphorylated), in MDA-MB-231 cell lysates immunoprecipitated with HDAC3 antibodies (**Figure 9G**). Furthermore, there were higher levels of phosphorylated JNK detected in the group of cell lines that were previously shown to have increased HDAC3 phosphorylation and photomate engagement (**Figure 9F**). Finally, we found recombinant JNK1 in the presence of ATP phosphorylates recombinant HDAC3 (**Figure 9E**). These experiments demonstrate that increased JNK activity, leads to an increase in HDAC3 phosphorylation and HDAC inhibitor engagement of HDAC3 in the basal type cell lines. To test whether JNK activity also controls HDAC3

phosphorylation in luminal subtypes, we pretreated MCF-7 cells with JNK inhibitor (TCS 6o) and stimulated with TNF-α. We observed a decrease in HDAC3 labeling and phosphorylation in comparison to cells treated with TNF-α alone, and similar levels to cells treated with neither TNF-α or JNK inhibitor (**Figure 9D**).

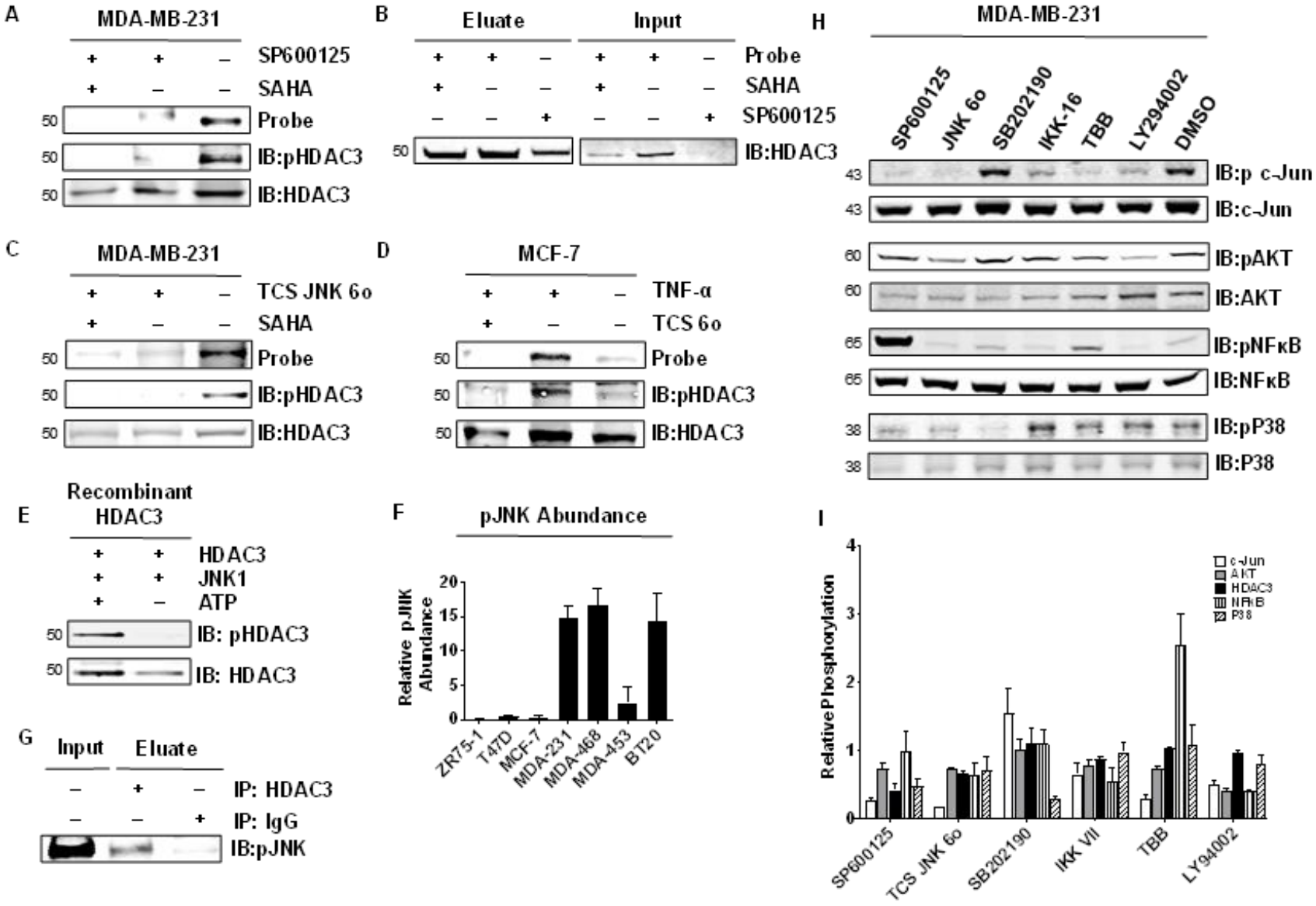
A
MDA-MB-231
SP600125
SAHA
Probe
IB:pHDAC3
IB:HDAC3
B
Eluate
Input
Probe
SAHA
SP600125
IB:HDAC3
C
MDA-MB-231
TCS JNK 6o
SAHA
Probe
IB:pHDAC3
IB:HDAC3
D
MCF-7
TNF-α
TCS 6o
Probe
IB:pHDAC3
IB:HDAC3
E
Recombinant HDAC3
HDAC3
JNK1
ATP
IB: pHDAC3
IB: HDAC3
F
pJNK Abundance
Relative pJNK Abundance
ZR75-1
T47D
MCF-7
MDA-231
MDA-468
MDA-453
BT20
G
Input
Eluate
IP: HDAC3
IP: IgG
IB:pJNK
H
MDA-MB-231
SP600125
JNK 6o
SB202190
IKK-16
TBB
LY294002
DMSO
IB:p c-Jun
IB:c-Jun
IB:pAKT
IB:AKT
IB:pNFκB
IB:NFκB
IB:pP38
IB:P38
I
Relative Phosphorylation
c-Jun
AKT
HDAC3
NFκB
P38
SP600125
TCS JNK 6o
SB202190
IKK VII
TBB
LY94002

Figure 9: JNK signaling controls HDAC3 phosphorylation.
A) Gel based visualization of MDA-MB-231 cells either treated with SP600125 or vehicle and labeled in situ with photomate or photomate and excess SAHA. Recognition of photomate labeled HDAC3 with antibodies is shown below. B) Western blot analysis of MCF-7 cells treated with SP600125, labeled with photomate or photomate and excess SAHA in situ, reacted with biotin azide tag, and enriched with streptavidin coated magnetic beads. Blot shows enriched fraction eluted off the beads and 2.5% of input stained with HDAC3 antibodies. C) As in A) substituting JNK 6o for SP600125. D) Gel based visualization of TNF-α treated cells either pretreated with TCS 6o or vehicle and labeled in situ with photomate (all lanes). Recognition of photomate labeled HDAC3 with antibodies is shown below. E) Western blot analysis of recombinant HDAC3 incubated with JNK in the presence or absence of ATP. F) Graph showing pJNK abundance in each cell line as quantified from Western blot in Figure S3. Data is shown as mean ± s.d. G) pJNK is detected in HDAC3 co-immunoprecipitates or IgG control. 10% of input is shown in lane 1. H) Western blot analysis of changes in several kinase pathways induced by treatment of MDA-MB-231 cells with all inhibitors used in this study and I) Quantification of H) normalized to treatment with vehicle. All results are representative of at least 3 independent experiments. Data is expressed as mean ± s.d.

2.4 Discussion

It has been shown that HDAC activity is aberrantly regulated in cancer by specific recruitment to genomic loci, and change in expression. In addition to these mechanisms, HDAC activity depends on formation of co-repressor complexes and PTM, however, it is unclear whether these mechanisms are transformed in cancer due to a lack of methodology. In this study, we provide the first evidence that HDAC phosphorylation is transformed in TNBC cell lines by analyzing the engagement of a novel photoreactive HDAC inhibitor probe. This method not only helps to understand a mechanism by which a subset of breast cancer cell lines regulate HDAC activity, but has implications for the future design and current understanding of the way HDAC inhibitors exert their effect.

Comparison of photomate's selectivity, based on inhibition of, or binding to recombinant HDACs, versus its engagement of HDACs in cells revealed significant differences with respect to HDAC3 that did not correlate with HDAC3 abundance. While photomate could bind to and inhibit HDAC3 under the conditions used for determination of IC_{50}, engagement in MCF-7 cells and other luminal cell types could not be detected. In contrast to this, we found TNBC cells had increased engagement of and selectivity for HDAC3 in comparison to recombinant HDACs. Differential engagement across cell types was also observed for most other class I and II HDACs, suggesting target engagement in cells can differ from *in vitro* predictions for these isoforms as well. As the development of selective HDACi is often guided by studies with recombinant HDACs, this variation clearly demonstrates that the actual target in a context of interest may be misrepresented by recombinant based assays.

Investigation into the mechanisms regulating HDAC3 binding revealed that HDAC3 phosphorylation, but not subcellular distribution or protein complex composition, directly controls photomate engagement. We found increased HDAC3 phosphorylation strongly correlated with engagement of HDAC3 in the cell lines under investigation. We validated that phosphorylation could directly control inhibitor binding, irrespective of other HDAC3 complex components, by comparing photomate binding to phosphorylated and non-phosphorylated recombinant HDAC3, which showed 4-fold higher photomate binding to phosphorylated HDAC3. We found this was true in cells as well because photomate engagement of a S424A HDAC3 mutant was decreased in comparison to control phosphorylated HDAC3. Furthermore, changing HDAC3 phosphorylation through inhibition of an HDAC3 kinase also significantly affects HDAC3 engagement in cells. In addition to differences in phosphorylation, we found that all known stable HDAC3 complex components were equally accounted for apart from NCOR1. Elimination of this discontinuity, however, did not influence photomate binding in cells, but tertiary structure of the remaining components, or binding of a transient or unknown component could potentially affect photomate binding concurrently with HDAC3 phosphorylation. Based on this data, accounting for phosphorylation when conducting *in vitro* assays may lead to a more accurate assessment of selectivity in cells.

In addition to its effect on inhibitor binding, we found phosphorylation of recombinant HDAC3 exhibits 5-fold higher catalytic activity compared to the non-phosphorylated protein. Because TNBC cells have increased HDAC3 phosphorylation in comparison to luminal subtypes and thus increased HDAC3 catalytic activity, they may be more reliant on its catalytic activity. As we have observed photomate (**Appendix B**), as well as other HDACi [(99, 204)], have increased efficacy in TNBC cells, HDAC3 may be a pertinent isoform to target for treatment of TNBC. However,

cell type based variation in other isoforms was observed, and likely contributes to the variation in efficacy as well. A follow up study with a larger set of cell lines or patient derived samples would be necessary to determine statistically significant correlations between targeted HDACs and efficacy.

Others have observed cell type dependent effects of HDACi in transformed cells as well, which may be explained by the differences in HDACi selectivity observed in this study. For example, many cell-based and *in vivo* studies have shown different mechanisms of cell death in response to HDACi, including activation of intrinsic [205, 206] versus extrinsic [207, 208] apoptotic pathways, or cell cycle arrest through induction of CDKN1A [71, 209] leading to cell type dependent efficacy. To account for these differences and determine where treatment with HDACi may be beneficial, diagnostic indicators of HDACi efficacy are needed. While several genomic approaches correlating HDACi response with mutational landscape or changes in basal gene expression serve as invaluable tools to identify prognostic markers associated with HDACi efficacy [74, 210], our study compliments this approach by identifying direct changes in HDAC binding, selectivity and enzymatic activity, which may also affect HDACi efficacy.

Although we explored a number of different key pathways shown to involve HDAC3, including ER [211], CK2 [140], NF-κB [212], p38 [213] and other MAPK mediated signaling, we found only the JNK pathway regulates HDAC3 phosphorylation. Others have observed a connection between JNK and HDAC3 as well [145, 214]; we add that increased JNK phosphorylation leads to HDAC3 phosphorylation, which affects both enzymatic activity and inhibitor binding in basal breast cancer cells in comparison to luminal subtypes. This is in line with other observations showing luminal breast cancer cells often have inactivating mutations to MAP3K1 and MAP2K7, the kinases directly upstream from JNK that are responsible for its phosphorylation and activation

[215]. We envision that measuring HDAC3 phosphorylation and/or JNK pathway mutations such as MAP3K1 and MAP2K7 could serve as diagnostic markers for predicting cellular response to treatment with HDACi. Finally, preclinical data suggests that inhibition of MAPK signaling, specifically the EGFR, in conjunction with HDACi is more effective in a broad range of cancer types [216, 217] and clinical trials are ongoing. Our study provides rationale for co-targeting the JNK pathway, a specific downstream component of an individual MAPK pathway, with HDAC3 to enhance the effects of HDACi in cancer therapy.

Beyond breast cancer, comparison of the differences in photomate binding to recombinant proteins against any disease state of interest should ultimately serve as a method to determine differences in catalytic activity of an individual HDAC isoform between these contexts; exposing novel drug targets and novel HDAC regulatory mechanisms.

2.5 Materials and Methods

Synthesis and characterization of photomate is outlined in Appendix N and key associated spectra is located in Appendix S.

Cell culture

Human cell lines MCF-7 and T47-D were obtained from Dr. Debra Tonetti (University of Illinois at Chicago) and were maintained in RPMI supplemented with 2 mM L-glutamine, 10% FBS, 1% non-essential amino acids, 1% antibiotics penicillin-streptomycin and 0.01 mg/ml human recombinant insulin at 37 ˚C in 5% CO2. The cell line ZR75-1 was obtained from ATCC and was maintained in RPMI supplemented with 2 mM L-glutamine, 1 mM sodium pyruvate, 10% FBS, 10 mM HEPES, 1% non-essential amino acids, and 1% antibiotics penicillin-streptomycin at 37 ˚C in 5% CO2. The breast cancer cell lines MDA-MB-231, MDA-MB-468, MDA-MB-453 and BT20, obtained from Dr. Clodia Osipo (Loyola University Chicago), Dr.

Elizaveta Benevolenskaya (University of Illinois at Chicago), Dr. Angela Tyner (University of Illinois at Chicago) and Dr. James Radosevich (University of Illinois at Chicago) respectively, were routinely maintained in IMEM media (Corning) supplemented with 2mM L-glutamine, 10 mM HEPES, 10% FBS, 1% non-essential amino acids and 1% antibiotics penicillin-streptomycin at 37 ˚C in 5% CO2.

Fluorogenic enzymatic assays for class I HDAC isoforms

Photomate IC50 for class I recombinant HDACs was measured using previously published procedures [(218, 219)]. All recombinant enzymes were purchased from BPS Bioscience. Photomate inhibits HDAC1, 2, 3 and 8 with LogIC50 of -6.38 ± .08, -6.88 ± 0.06, -6.96 ± 0.06, and -5.64 ± 0.06, respectively. The data is reported as the average ± s. e. (n=3).

General procedure for photolabeling in live cells

For whole cell analysis: cells were plated in 6 cm dishes and grown to 90% confluence in 2 mL culture medium. The medium was replaced with 1 mL culture medium and pretreated with competitor (SAHA, 200 µM or DMSO control where applicable and then treated with 10 µM photomate or DMSO control. After 40 min at 37 ˚C, the cells were cooled to 4 ˚C and irradiated with 366 nm light (35 J/cm2). The medium was removed and the cells gently washed twice with PBS and then covered with 1 mL PBS. Cells were scraped from plate into Eppendorf tubes, spun down at 1,000 g for 5 minutes at 4 ˚C, the supernatant removed and the cells resuspended in photolabeling lysis buffer (50 mM HEPES (pH 7.5), 150 mM NaCl, 0.7% Igepal, 5% glycerol, 1x protease inhibitor cocktail (Roche) and 1x phosphatase inhibitor cocktail (ThermoFisher)). Samples were homogenized by vortexing, incubated on a rotating stand at 4 ˚C for 1 hour, spun down at 20,000 g for 10 minutes at 4 ˚C and the protein concentrations were determined by bicinchoninic acid assay (BCA). For gel based visualization, 35.2 µg of total lysate was

incubated with 800CW azide conjugated IRDye at a concentration of 1.5x the probe, TCEP (0.25 mM), TBTA (0.1 mM), and CuSO4 (0.50 mM) for 90 minutes at rt. Samples were then diluted with sample loading buffer, heated to 70 ˚C for 10 minutes and separated by gel electrophoresis. Gels were transferred to nitrocellulose membranes with iBlot transfer system (P3 for 7 minutes) and visualized with Odyssey Sa imager. Membranes were then blocked with odyssey blocking buffer for 2 hours at 4 ˚C, incubated with desired antibodies overnight at 4 ˚C, washed 3x 5 minutes with PBST, incubated with relevant species of 680RD IRDye conjugated secondary antibody for 1 hour and simultaneously visualized at 700 and 800 nm with Odyssey Sa imager. Signals that 1) were competed by SAHA by at least 50% (quantified by densitometry) and 2) co-stained with a specific class I HDAC antibody were further analyzed.

For enrichment on streptavidin coated magnetic beads, 1 mg photomate labeled cell lysate was incubated with azide conjugated biotin according to 1.5x concentration of probe, TCEP (0.25 mM), TBTA (0.1 mM), and CuSO4 (0.50 mM) for 90 minutes at rt. Samples were then left at -20 ˚C overnight. Precipitated protein was spun down at 6,000 x g for 4 minutes at 4 ˚C, and resuspended with brief sonication in 1 mL cold methanol. This was repeated twice and the pellets were resuspended in 1 mL 0.22% SDS in PBS by brief sonication and 10 minutes of heating at 60 ˚C. Next, 20 uL of Dynabeads M-280 (ThermoFisher) were washed 2 x with 0.22% SDS in PBS, added into each reaction and incubated for 1.5 hours at rt. Beads were removed with a magnet and then washed 2 x with 0.22% SDS in PBS (500 µL), 2 x with modified PBS (500 mM NaCl) and 2 x with PBS.

For Western blot analysis, bound proteins were then suspended in LDS loading buffer and heated at 70 ˚C for 10 minutes. Beads were removed with magnet and samples separated by gel electrophoresis at 100 volts. Gels were transferred to nitrocellulose membranes with iBlot

transfer system (P3 for 7 minutes), blocked with odyssey blocking buffer for 2 hours at 4 ˚C, incubated with desired antibodies at 4 ˚C, washed 3x 5 minutes with PBST, incubated with relevant species of 680RD IRDye conjugated secondary antibody for 1 hour and visualized with Odyssey Sa imager.

For mass spectrometry based analysis, bound proteins were eluted in laemmli sample buffer, boiled for 10 minutes and eluant collected in a fresh Eppendorf tube. These samples were loaded onto a 15% gel and run into the gel approximately 1 inch at 20 volts (1 hour). One gel slab per lane was excised and gel pieces were destained in 50 mM NH4HCO3 in 50% ACN (v/v) until clear. Gel pieces were dehydrated with 100 µl of 100% ACN for 5 min, the liquid removed, and the gel pieces rehydrated in 10 mM DTT and incubated at 5 °C for 60 min. Gel pieces were again dehydrated in 100% ACN, liquid was removed and gel pieces were rehydrated with 55 mM IAA. Samples were incubated at room temperature, in the dark for 45 min. Gel pieces were washed with 50 mM NH4HCO3 and dehydrated with 100% ACN. Gel pieces were rehydrated with 10 ng/µl trypsin, resuspended in 50 mM NH4HCO3 on ice for 1 h. Excess liquid was removed and gel pieces were digested with trypsin at 37 °C overnight. Peptides were extracted with 50% ACN/5% FA, followed by 100% ACN. Peptides were dried to completion and resuspended in 2% ACN/0.1%FA. Peptides were cleaned with C18 ZipTips (Millipore) according to the manufacturer's instructions, followed by LC-MS/MS analysis.

Mass Spectrometry Analysis

The tryptic peptides were dissolved in 0.1% FA, directly loaded onto a reversed-phase pre-column (Acclaim PepMap 100, Thermo Scientific). Peptide separation was performed using a reversed-phase analytical column (Acclaim PepMap RSLC, Thermo Scientific). The gradient was comprised of an increase from 6% to 35% solvent B (0.1% FA in 98% ACN) over 12 min

and climbing to 80% in 4 min then holding at 80% for the last 4min, all at a constant flow rate of 400 nl/min on an EASY-nLC 1000 UPLC system, The resulting peptides were analyzed by Q ExactiveTM hybrid quadrupole-Orbitrap mass spectrometer (ThermoFisher Scientific). The peptides were subjected to NSI source followed by tandem mass spectrometry (MS/MS) in Q ExactiveTM (Thermo) coupled online to the UPLC. Intact peptides were detected in the Orbitrap at a resolution of 70,000. Peptides were selected for MS/MS using NCE setting as 28; ion fragments were detected in the Orbitrap at a resolution of 17,500. A data-dependent procedure that alternated between one MS scan followed by 20 MS/MS scans was applied for the top 20 precursor ions above a threshold ion count of 1E4 in the MS survey scan with 15.0 s dynamic exclusion. The electrospray voltage applied was 2.0 kV. Automatic gain control (AGC) was used to prevent overfilling of the Orbitrap; 5E4 ions were accumulated for generation of MS/MS spectra. For MS scans, the m/z scan range was 350 to 1800. The resulting MS/MS data were processed using Mascot search engine (v.2.3.0). Tandem mass spectra were searched against Swissprot Homo Sapeins database. Trypsin/P was specified as cleavage enzyme allowing up to 2 missing cleavages. Mass error was set to 10 ppm for precursor ions and 0.02 Da for fragment ions. Carbamidomethyl on Cys were specified as fixed modification and oxidation on Met, acetylation on Protein N-term were specified as variable modifications. Peptide ion score was set > 20. Datasets collected from probe collected samples were compared to DMSO treated samples to remove non-specific interactions. Proteins that were not enriched in DMSO treated samples were then compared to probe plus SAHA treated samples and any protein in probe treated samples that was decreased by at least 50% is shown in Table S1. This analysis was done using a custom Matlab script (**Appendix Y**).

Serum starvation followed by photolabeling

0.8x106 or 0.5x106 MCF-7 cells were plated in 6-well plates (corning) and grown in complete medium for 2 days. After 2 days the medium was replaced with either serum free medium (into the wells plated with 0.3x106 cells or complete medium (into the wells plated with 0.15x106 cells). The cells were incubated for an additional 48 hours followed by the "general procedure for photolabeling in live cells".

Treatment with inhibitors, cytokines and growth factors followed by photolabeling

0.3x106 MDA-MB-231 cells were plated in 6-well plates and grown in complete medium for 2 days. inhibitors of CK2 (TBB, 50 µM), JNK (SP600125, 10 µM or TCS 6o 20 µM), p38 (SB202190, 10 µM) and IKK/NF-kB (IKK-16, 10 µM), Pi3K (LY294002, 20µM), GSK3b (AR-A014418, 20 µM) or cytokines/growth factors EGF, TNF-α, IGF-1 (all at 10 ng/mL) were added to the growth medium at the indicated concentrations and incubated for 2-12 hours. After incubation, the "general procedure for photolabeling in live cells" was carried out or cells were lysed without further treatment for analysis by Western blot.

Trasnfection of mutant HDAC3 followed by photolabeling

2.1x106 MDA-MB-231 cells were plated in 10 cm plates (corning) and grown in complete medium for 2 days. After 2 days the medium was removed, the cells washed twice with PBS and medium containing 5% FBS without penicillin/streptomycin was added. 10 µg of S405A, S424A, or Flag-HDAC3 plasmids were diluted with 500 µL IMEM, and 500 µL of IMEM containing Lipofectamine 2000 was added and the samples incubated at room temperature for 30 minutes. Plasmid-lipofectamine complexes were added to the 10 cm plates and cells were transfected for 24 hours. The following day, the medium was removed and the cells washed

twice with PBS. Complete medium was added and the cells were incubated for 2 hours with complete medium followed by the "general procedure for photolabeling in live cells".

Western blotting

Protein samples were diluted with sample loading buffer containing DTT (Invitrogen), heated to 70 ˚C for 10 minutes and separated by gel electrophoresis at 100 volts. Gels were transferred to nitrocellulose membranes with iBlot transfer system (P3 for 7 minutes) and visualized with Odyssey Sa imager. Membranes were then blocked with Odyssey blocking buffer for 2 hours at 4 ˚C, incubated with desired antibodies overnight at 4 ˚C, washed 3x5 minutes with PBST, incubated with relevant species of IRDye conjugated secondary antibody for 1 hour and visualized with Odyssey Sa imager. If additional antibody probing was necessary, membranes were stripped with 0.2 N NaOH for 30 minutes and the Western blotting procedure was repeated starting from blocking with Odyssey buffer.

Quantitation of class I HDAC isoforms in breast cancer cell lines

A standard curve of individual recombinant proteins ranging from 1-20 ng as well as 30 µg cell lysate from MCF-7 cells were visualized by Western blotting procedure. Signal was quantified by densitometry, plotted and a linear regression fit using Graphpad Prism 6 software. Relative HDAC3 and phosphorylated HDAC3 abundance in the panel of breast cancer cell lines was quantified in a similar manner without use of a standard curve.

Photolabeling of recombinant proteins

Recombinant class I HDACs (500 ng/uL) in photolabeling lysis buffer were pretreated with competitor or DMSO control for 15 minutes when applicable and then treated with photomate or DMSO control. After a 40-minute incubation, samples were cooled to 0 ˚C and irradiated with 366 nm light (35 J/cm2). Samples were then incubated with azide conjugated 800CW IRDye at

a concentration 1.5x the probe, TCEP (0.25 mM), TBTA (50 uM), and CuSO4 (0.50 mM) for 90 minutes at rt. Samples were then diluted with loading buffer, heated to 70 ˚C for 10 minutes and separated by gel electrophoresis at 100 volts. Gels were transferred to nitrocellulose membranes with iBlot transfer system (P3 for 7 minutes) and visualized with Odyssey Sa imager. Membranes were then blocked with Odyssey blocking buffer for 2 hours at 4 ˚C, incubated with antibodies for class I HDACs overnight at 4 ˚C, washed 3x5 minutes with PBST, incubated with anti-rabbit 680RD IRDye conjugated secondary antibody for 1 hour and visualized with Odyssey Sa imager.

Phosphorylation of recombinant HDAC3

1 µg recombinant HDAC3 was diluted with 20 µL CK2 reaction buffer (New England Biolabs). 100 mM ATP was added, or vehicle for control reactions, followed by 200 U CK2 or 100 U JNK1. The reactions were incubated for 2 hours at 30 ˚C. Samples were then dialyzed into photolabeling lysis buffer for use in "photolabeling of recombinant proteins"

Enzymatic activity of HDAC3

Serial dilutions of deacetylated Fluor de Lys substrate (0-40 µM, Enzo Life Sciences) were prepared in KI-143 (25 mM Tris–HCl, pH 8.0, 137 mM NaCl, 2.7 mM KCl, and 1 mM MgCl2). The amount of acetylated fluor de lys substrate that phosphorylated HDAC3 and HDAC3 could deacetylate in 30 minutes was compared to this curve. Recombinant proteins were diluted with KI-311 (25 mM Tris–HCl, pH 8.0, 137 mM NaCl, 2.7 mM KCl, and 1 mM MgCl2, 1 mg/mL BSA) buffer to give 1 ng/µL stocks of each. 15 µL of enzyme stock and 25 µL of 5 mM substrate was added to a black half area 96 well plate (corning) alongside 50 µL of standard dilutions and incubated for 30 minutes rt. 50 µL of 1 mg/mL trypsin and 5 µM TSA in KI-143 buffer was added. The volume was made equal with KI-143 and the plate was read at excitation

wavelength 360 nm and emission wav elength 460nm using a Synergy 4 hybrid microplate reader from BioTek. Activity was determined using GraphPad Prism 6. Activity of 0.84 ± .006 and 0.17 ± .005 µM substrate/hour were found for phosphorylated HDAC3 and non-phsophorylated HDAC3 respectively. The data is reported as the average ± s. e. (n=3).

Immunoprecipitations

Six 10 cm plates were seeded with 0.8x106 MDA-MB-231 or MCF-7 cells and grown to 90% confluence according to general procedures. Cells were washed with PBS (2x 5 mL) followed by addition of 1 mL PBS. Cells were scraped from plate into Eppendorf tubes, spun down at 1000 rpm for 5 minutes at 4 °C, the supernatant removed, and the cells resuspended in hypotonic buffer (10 mM Hepes (pH 7.5), 10 mM KCl, 0.05% (for MDA-MB-231 cells) or 0.4% (for MCF-7 cells) Igepal CA-630, 1x Protease inhibitor cocktail and 1x phosphatase inhibitor cocktail) until cell walls were compromised (verified by microscopic inspection). The mixture was spun down at 1,000 g for 5 minutes to provide the cytosol (supernatant) and nuclei (pellet). The nuclei were than homogenized in 200 µL pull-down lysis buffer (20 mM Hepes (pH 7.5), 150 mM NaCl, 1.5 mM MgCl2, 0.5% Igepal CA-630, 1x protease inhibitor cocktail and 1x phosphatase inhibitor cocktail) and incubated for 1 hour at 4 °C on a rotating stand. Lysed nuclei were than centrifuged at 20,000 g for 10 minutes at 4 °C to provide nuclear fraction (supernatant). Protein concentration was determined using Bradford assay and then diluted to 2 mg/mL with pull-down lysis buffer. 0.8 mg of lysate was incubated with 35 µL protein A Dynabeads for 3 hours at rt and then stored for use at -20 °C. For antibody bead conjugation, 60 µL dynabeads (per reaction) were washed with PBS and separated into 2x 30 µL aliquots. 15 µg anti-HDAC3 (Abcam) antibodies or 15 µg rabbit IgG control, each diluted with 150 uL PBS, were added to either 30 µL washed dynabead aliquot and incubated at rt for 2 hours. Bead

antibody conjugates were then washed with 2x 1 mL PBS, 1 mL 0.2 N triethnolamine (pH 8.2) and incubated with 1 mL 25 mM dimethyl pimelidate in 0.2 N triethnolamine (pH 8.2) for 45 minutes at rt. After crosslinking bead-antibody conjugates were washed with 2x 1 mL 0.2 N triethanolamine (pH 8.2), resuspended in 0.1 N triethnolamine and incubated for 30 minutes at rt. Bead conjugates were then washed with 3x 1 mL PBS, 1 mL 0.2 N glycine (pH 2.6). Bead conjugates were then resuspended in 30 µL PBS, added into 0.8 mg of a pre-cleared, 2 mg/mL nuclear extract described above, and incubated overnight at 4 °C. The following day, beads were washed with 3x 1 mL pull-down lysis buffer and eluted with 3 x 50 mL 0.2 N glycine (pH 2.6). Eluates were pooled and 37.5 µL TCA (100 w/v) solution was added followed by 15 uL 1 M Tris (pH 8.5). Samples were incubated for 1.5 hours at 4 °C and spun down at 20,000 g for 10 minutes at 4 °C. The supernatant was removed and pellet was resuspended in 20 µL Laemmli buffer. Samples were boiled for 5 minutes and electrophoretically separated. Proteins were transferred to nitrocellulose membranes with iBlot transfer system (P3 for 7 minutes), blocked with odyssey blocking buffer for 2 hours at 4 °C, incubated with antibodies overnight at 4 °C, washed 3x 5 minutes with PBST, incubated with anti-rabbit IRDye conjugated secondary antibody for 1 hour and visualized with Odyssey Sa imager.

Statistical analyses

Statistical analyses were performed with GraphPad Prism 6 software. All data are shown as mean ± s.e. Student's t-test (two-tailed) was used to measure statistically significant differences between groups. P value < 0.0005 was considered statistically significant for this study. One way Anova was used to determine statistically significant variance. P<.0001 was considered statistically significant.

CHAPTER 3: SYNTHETIC STRATEGY TO ACCESS DIVERSE HISTONE DEACETYLASE PHOTOREACTIVE PROBES AND COMPARISON OF THEIR BIOCHEMICAL AND CELL-BASED SELECTIVITY.

Thomas W. Hanigan,[†,¶] Shaimaa M. Aboukhatwa,[†,§,¶] Jayaprakash Neerasa,[†] Taha Y. Taha,[†] Nathan D. Brown,[†] Eman E. El-Bastawissy,[§] Mohamed A. Elkersh,[§] Tarek F. El-Moselhy,[§] Jonna Frasor,[‡] Pavel A. Petukhov[†,*]

[†] Department of Medicinal Chemistry and Pharmacognosy, College of Pharmacy, University of Illinois at Chicago, IL 60612.
[§] Department of Pharmaceutical Chemistry, Faculty of Pharmacy, Tanta University, Egypt 31527.
[‡]Department of Physiology and Biophysics, University of Illinois at Chicago, IL 60612.

This chapter is adapted from the manuscript "Synthetic Strategy to Access Diverse Histone Deacetylase Photoreactive Probes and Comparison of Their Biochemical and Cell-Based Selectivity" under consideration at *ACS Chemical Biology*. This manuscript is included in this thesis with permission from *ACS Chemical Biology*. Rights are shown in Appendix .

3.1 Abstract

Histone deacetylase (HDAC) activity is modulated in vivo by post translational modifications and formation of multiprotein complexes. Given the interest in development of selective HDAC inhibitors (HDACi), it is important to evaluate how these factors affect their selectivity in live cells. In this study, we developed a general synthetic strategy to access chemically diverse photoreactive HDACi probes (PRPs) based on both pan and isoform-selective HDACi. Using this strategy, we demonstrated that rational incorporation of photoreactive groups only modestly affects potency without compromising selectivity for recombinant HDACs. Photolabeling studies in live MDA-MB-231 cells, a cell line where ca. 86% of HDAC3 is phosphorylated, revealed an increase in the binding and selectivity for HDAC3 for all chemical scaffolds evaluated, which was not predicted by biochemical assay. Given the stark contrast between the outcomes of these two assays, our synthetic strategy and PRP-based assay should be of broad interest to accurately assess the binding of ligands to their intended biological targets i.

3.2 Introduction, Results and Discussion

Histone deacetylases (HDACs) are a family of enzymes consisting of 18 human isoforms that are subdivided into four classes. HDACs catalyze the deacetylation of lysine residues in a variety of protein targets including histones, which regulates cell growth, cell cycle regulation, DNA repair, proliferation, differentiation, and apoptosis [(220)]. As many of these processes are altered in cancer, HDAC inhibitors (HDACi) have had success as anti-cancer therapeutics, and four HDACi have FDA approval for treatment of T-cell lymphoma or multiple myeloma.

Currently, all FDA approved HDACi are non-selective pan inhibitors of multiple class I and II HDACs. In general, these compounds consist of 1) a zinc binding group (ZBG), 2) a surface binding group (SBG) and 3) a linker to connect these components; for example, SAHA (**1**,

Figure 10) and panobinost (**6**, **Figure 10**). Much attention has been given to optimization of these components to increase affinity and selectivity for various HDAC isoforms, and multiple structural classes have emerged from these studies, such as pimelic diphenylamide 106 (**8**), a class I selective inhibitor, PCI-34051 (**10**), an HDAC8 selective inhibitor and TMP-269 (**12**) a class II selective inhibitor (**Figure 10**).

HDACi affinity and selectivity are typically evaluated in biochemical assays utilizing individual purified recombinant HDACs and a synthetic substrate where HDAC activity is measured under equilibrium conditions. This type of assay does not account for the regulation of HDAC activity that occurs in vivo through post-translational modifications [(151, 221)] and multi-protein complex formation [(138, 222)]. To determine if these factors can affect HDACi selectivity in live cells, we developed a general strategy to incorporate a photoreactive tetrafluorophenyl azide (TFPA) group and an alkyne reporter into the SBG of diverse HDACi scaffolds (**Figure 10**) and used the resulting photoreactive probes (PRPs) to measure HDAC selectivity in live cells. The TFPA moiety can be used to react covalently with cellular targets of the PRP upon UV irradiation, and labeled proteins visualized after biorthogonal reaction of the alkyne reporter with a near-infrared dye (IRDye).

To enable predictions regarding the selectivity of the parent compounds, the PRPs were rationally designed to incorporate the TFPA and alkyne moieties into the parent compound scaffold to retain structural and electronic properties similar to those of the parent compounds. This is opposed to previously described HDAC photoreactive probes, which have appended large photoreactive groups and biorthogonal handles onto parent scaffolds to optimize photocrosslinking and click reaction yields but do not retain structural and electronic properties of parent HDACi [(181, 182)]. Although many photoreactive groups are accessible synthetically, the

TFPA was chosen based on its similarity to aryl-based moieties present in the SBG of HDACi. In addition, the alkyne handle was chosen as it is small, electronically inert, and stable in biological systems, yet reactive under copper(I)-catalyzed "click reaction" conditions. Given the extensive structure activity relationships (SAR) available for most of the parent compounds, the alkyne handle was placed at positions deemed tolerant to same size substituents whenever possible [223-226] . The ZBG and linker region were unaltered as these components are often crucial for affinity and selectivity.

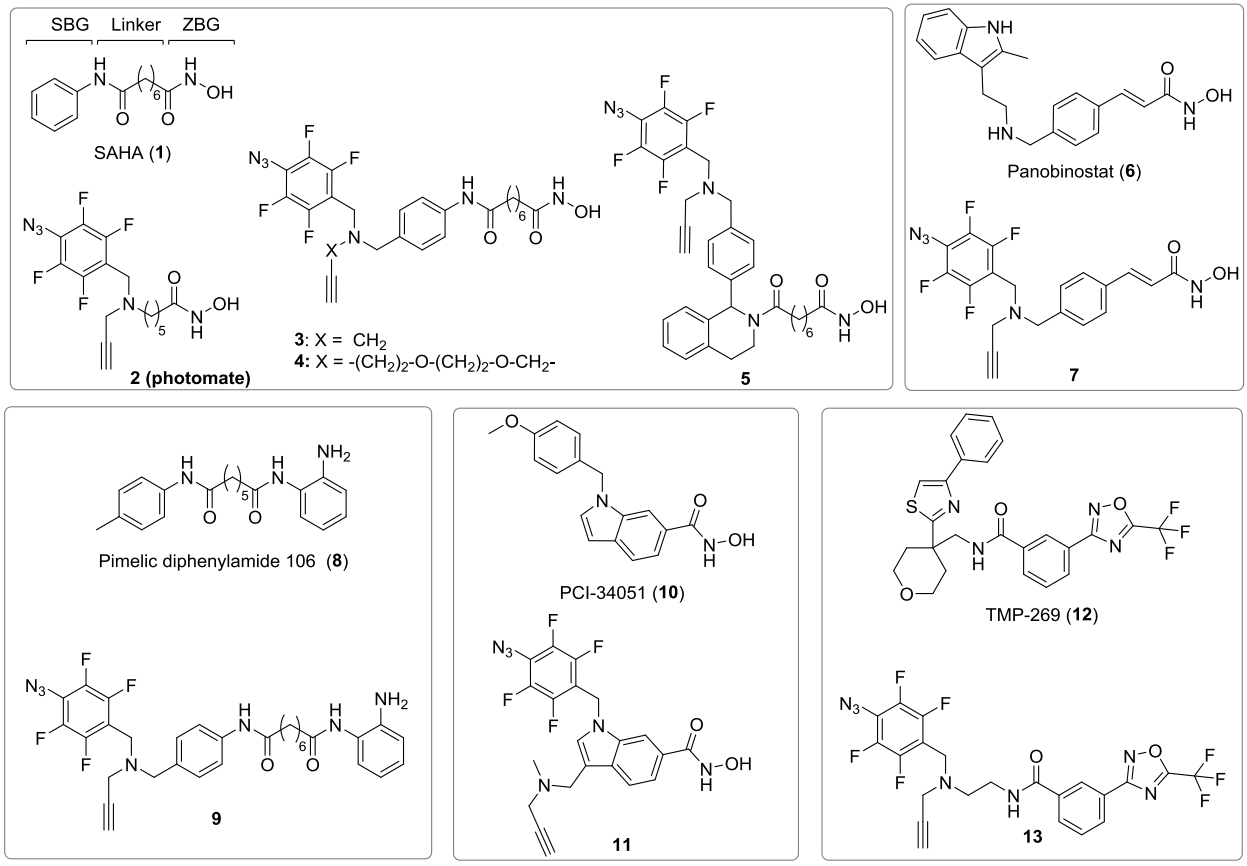

Figure 10: Parent HDACi scaffolds and corresponding PRPs based on these scaffolds
Associated PRPs and parents are grouped with boxes.

To incorporate the TFPA and alkyne into a diverse set of HDACi scaffolds, the PRP synthesis needed to be tolerant to the diverse reaction conditions used in the synthesis of the parent scaffolds. Our general strategy for synthesis of PRPs **2** (photomate)**-5**, **7**, **9**, **11**, and **13** is outlined in **Figure 11**. First, a protected ZBG and an amine bearing linker corresponding to the parent HDACi (**Figure 11**) were assembled separately. Next, a pentafluorophenyl precursor of TFPA, the alkyne moiety and the linker portion were connected via reductive amination followed by alkylation of the resulting secondary amine in few successive steps (**Figure 11**). The protected ZBG was then attached via coupling to the linker followed by azidation of the pentafluorophenyl group and deprotection of the ZBG. The azidation reaction was performed near the end of each synthesis as the resulting arylazido group is labile under reaction conditions typically used to prepare the parent HDACi. Specifically, we found that the TFPA group could not withstand conditions necessary for reductive amination, palladium-catalyzed cross-coupling, and reactions of hydroxylamine hydrochloride under basic conditions including amidoxime formation from nitriles and hydroxamic acid formation from esters.

PRPs **2** (photomate), **3**, **4** and **5** were built based on the scaffold of **1**. PRPs **3**, **4** and **5** include the TFPA and alkyne handle extended off the phenyl ring of **1** so that the amide linkage of the SBG and linker is retained, while PRP **2** (photomate) isosterically replaces SAHA's phenyl ring with the TFPA and alkyne so that only a single phenyl ring is present in the SBG. PRP **5** was designed to direct the TFPA group close to the surface of HDACs to increase the likelihood of reaction between them. PRP **4** includes an extended alkyne handle to direct this group away from the

surface of HDACs and into the solvent to increase the efficiency of click reaction with IRDye. The pan HDAC PRP **7** was designed based on compound **6**. PRP **7** isosterically replaces the indole SBG of **6** with TFPA and connects the alkyne handle at the terminal amine moiety, as compound 6 retains its activity as a tertiary amine in this position [(223)].

PRP **9** was based on the o-aminoanilide containing HDACi **8** reported to exhibit higher selectivity for HDAC1, 2, and 3 isoforms [(227)]. PRP **9** was designed by attaching TFPA and alkyne groups via a tertiary amine to the SBG of **8**. The scaffold of HDAC8 selective compound **10** was used to build PRP **11**. Isosteric replacement of the p-methoxy phenyl substituent at the indole nitrogen with the TFPA group and attachment of the alkyne handle at the indole C-3 were chosen as both positions could tolerate substituents of similar electronic and steric properties with only minor effect on potency and selectivity [(228)]. PRP **13** was designed by replacing the SBG of **12** with TFPA and alkyne moiety to develop a class-IIa selective PRP [(224)]. The synthetic schemes for each PRP and detailed experimental procedure are provided in the Supporting Information.

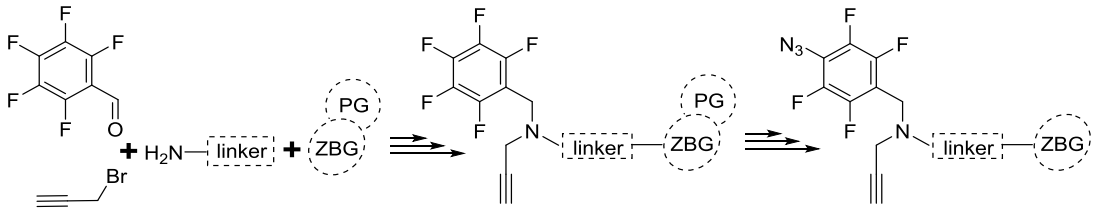

Figure 11: General synthetic strategy for PRPs.
Protecting group (PG), Zinc binding group (ZBG).

The PRPs and parent scaffolds were tested for HDAC inhibitory activity against a panel of recombinant class I HDACs as well as HDAC4 as a representative member of class II isoforms (**Appendices G and H**). The IC50 for each class I HDAC was normalized to that of HDAC1 and standardized around the mean to show relative selectivity for each isoform as a fold change. This data is summarized as a heat map in **Figure 12a**, and primary data can be found in **Appendices G-I**. Selectivity for HDAC4 was excluded from this analysis as only PRPs **2** (photomate) and **13** showed activity for HDAC4 below 50 μM.

Cell-based PRP selectivity was evaluated by photolabeling in live MDA-MB-231 cells (**Figure 12 and Appendix J**). Cells in culture were labeled with either PRP, PRP and excess SAHA, or DMSO control, reacted with an azide-conjugated 800CW IRDye and electrophoretically separated. Antibodies for individual HDAC isoforms were added followed by conjugation with 680RD labeled secondary antibodies. Visualization at both 800 and 700 nm revealed PRP labeled proteins as well as HDAC antibody labeled proteins. PRP bands (800 nm) were delineated as a particular isoform if they counter-stained with an individual HDAC antibody (700 nm); for example, see **Appendix K**. These bands were quantified by densitometry and were considered specific targets if probe signal was decreased by at least 50% upon co-treatment with SAHA and were absent from DMSO controls (**Figure 12d, e**).

Additionally, PRP **2** (photomate) selectivity was validated by reacting labeled proteins from MDA-MB-231 cells with an azide-conjugated biotin tag, enriching the covalently linked adducts using streptavidin coated magnetic beads, and identifying the enriched proteins by Western blot with specific antibodies for individual HDAC isoforms **Figure 5** (Chapter 1) [(229)]. The signal for

each class I HDAC was quantitated by densitometry and normalized to its relative abundance in MDA-MB-231 cells (**Appendix L**). The resulting normalized labeling for each class I HDAC was then taken as a fold change relative to HDAC1 labeling and standardized around the mean. This data is presented in **Figure 12a** as a heatmap where increased selectivity for individual isoforms is represented in red. Class II HDACs were excluded from this analysis as no PRP labeled bands at the molecular weight of the class II HDACs could be observed by gel-based visualization, except for PRP **2** (photomate) (**Figure 12d**, 150 kDa).

In general, the PRPs had equal or lower recombinant enzyme inhibitory activity in comparison to their parent scaffolds (**Appendices G and H**) and the selectivity profile for the PRPs often remained consistent with the parent compounds (**Appendix J**). Correlation coefficients between PRP and parent compound selectivity against recombinant HDAC proteins are ranked in **Figure 12c**. Probes **9**, **11** and **3** exhibited near perfect selectivity correlation with their parent scaffold (r = 1.00, 0.91 and 0.88, respectively), followed by PRP **5** and **4** (r = 0.63). Taken together, this data indicates the TFPA and alkyne groups can be rationally incorporated into the scaffolds of diverse HDACi without impacting potency and selectivity. Considering the similarity between the inhibitory profiles of the parent HDACi compounds and corresponding PRPs against recombinant HDAC enzymes, the cell-based selectivity of five of the eight total PRPs can be used to understand the selectivity of parent compounds in cells.

Comparison of the cell-based and biochemical PRP selectivity for class I HDACs given in **Figure 12a and 12c** (additional details are given in **Appendices I and J**) shows a general increase in selectivity for HDAC3 in MDA-MB-231 cells for all PRPs with the exception of PRP **9**, which was found to be selective for HDAC3 biochemically as well as in cells. For example,

PRP **7** was relatively selective for HDAC1 and 3 over HDAC2 and 8 in biochemical experiments, however it was 120-fold selective for HDAC3 over HDAC1 in cells. PRP **5** was predicted to be 3-5-fold selective for HDAC1 over other class I isoforms, but was found to be 6-31-fold selective for HDAC3 in cells. Even PRP **11**, based on the HDAC8 selective compound 10, which was 90-fold selective for HDAC8 over HDAC3 in biochemical experiments, was non-selective for HDAC8 over HDAC3 in cells.

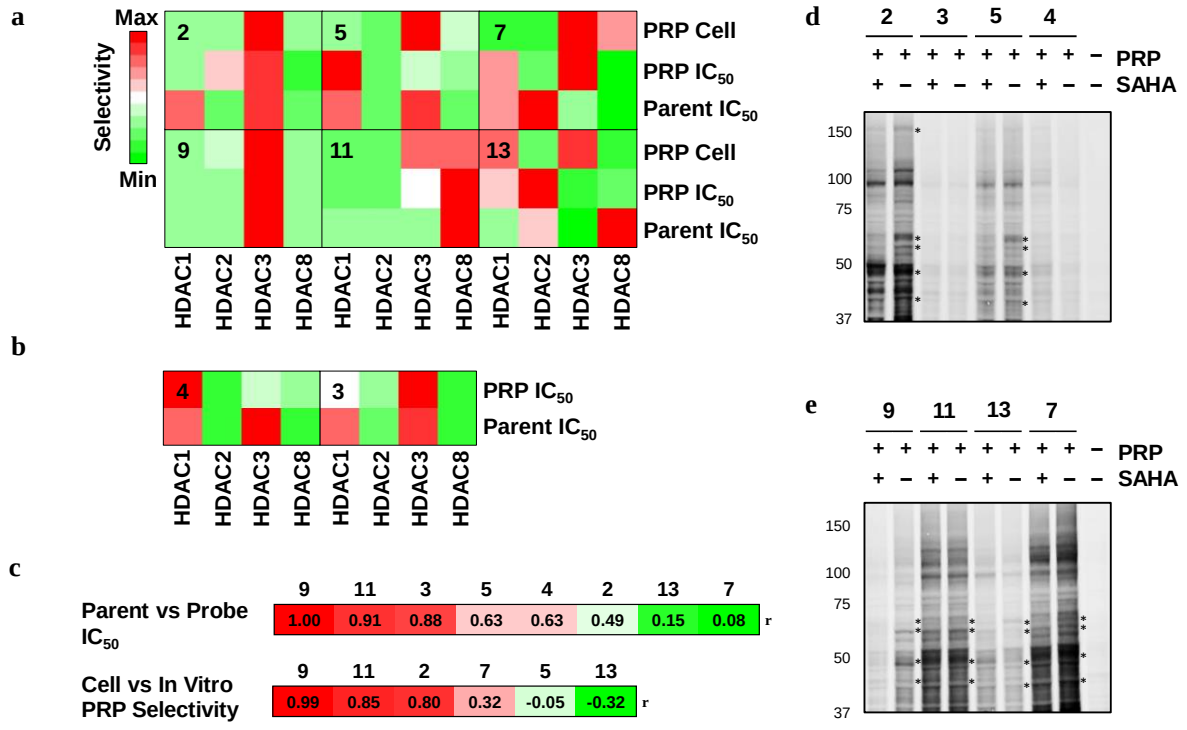

Figure 12: Biochemical vs cell-based selectivity comparison of PRPs and parent compounds.
(a) Heat map visualization of relative fold change in recombinant HDACs IC50 for PRPs and parent compounds or cell-based labeling for PRPs. Only PRPs with specific class I HDAC labeling in cells are shown. IC50 values or gel based photolabeling bands densitometry were taken as fold difference from HDAC1 and each row was standardized around a mean of zero

with standard deviation of 1. Each section of the heat map is presented with respect to an individual PRP corresponding parent scaffold, with PRPs numbered in the upper left hand corner of each section. Red indicates increased selectivity for a given isoform relative to the other class I isoforms. (b) as in (a) with respect to compounds that did not show labeling in cells. (c) Correlation coefficients comparing parent and PRP IC50-based selectivities, or IC50-based and cell-based PRP selectivity. (d) gel-based visualization of live MDA-MB231 cell photolabeling with PRPs 2-5, (e) as in (d) with respect to PRPs 7, 9, 11 and 13. In (e) and (d), stars indicate HDAC isoforms confirmed by immunoblotting with specific HDAC antibodies.

Interestingly, we found both PRP **13** and its parent inhibitor **12**, which was previously reported selective for class II HDACs [(224)], were not selective for the class II HDAC4 and were generally weak inhibitors of all class I and II isoforms tested (pIC50 ranging from 2.8-4.2). This finding highlights the well-known variability in the results of the biochemical assays used to measure HDACi selectivity. However, despite being a weak inhibitor of recombinant enzymes, we found PRP **12** could label HDAC1 and 3, but not 4 in cells. Only PRP **2** (photomate) was able to label HDAC4. This is in line with our IC50 experiments, as PRP **2** (photomate) was the only PRP able to inhibit HDAC4 at comparable potency to **1** and **12** (**Appendices G and H**).

On the other hand, PRPs **3** and **4**, despite being relatively potent inhibitors of all class I HDACs (pIC50 ranging from 3.65 to 6.35), did not show distinct labeling in cells. We hypothesize this may be due to positioning of the TFPA, rather than low yield of the click reaction, given PRP **4** has an extended polyethylene glycol alkyne reporter, which should be more accessible in comparison to the propargyl group found on other probes showing distinct labeling. Overall, however, six of the eight synthesized probes showed specific labeling of multiple HDAC isoforms, without extensive optimization of photoreactive and alkyne group positioning, highlighting the broad utility of our strategy.

Our previous studies have shown that phosphorylation status of HDAC3 directly increases the binding of one individual HDACi to HDAC3 in living cells [(229)]. Here we expand this observation and show that for all the HDACi scaffolds evaluated in this study, HDAC3 binding and selectivity was increased in MDA-MB-231, a cell type with a high percentage of phosphorylated HDAC3 (**Appendix M**), in comparison to selectivity based on recombinant HDAC3.

In summary, a novel synthetic strategy to access structurally diverse HDACi PRPs was developed. This method enabled the synthesis of eight structurally diverse PRPs, and should be widely applicable to other HDACi scaffolds. The strategy was successful in generating PRPs with HDAC selectivity profiles similar to those of their parent scaffolds in biochemical assay. While various PRP scaffolds showed distinct selectivity in MDA-MB-231 cells, this profile did not match biochemical predictions. We attribute these differences to the regulation of HDAC activity that occurs in live cells. Our synthetic strategy and PRP-based assay should be of broad interest to accurately assess the binding of ligands to their intended biological targets *in vivo*.

3.3 Materials and Methods

Synthesis and characterization of the PRPs is outlined in Appendices N-S.

Fluorogenic Enzymatic Assays for Class I HDAC Isoforms

Human recombinant HDAC1, HDAC2, HDAC3 (BPS Bioscience) and HDAC8 (In-house purified from E-coli) were diluted with assay buffer 1 (25 mM Tris–HCl, pH 8.0, 137 mM NaCl, 2.7 mM KCl, and 1 mM MgCl2, 1 mg/mL BSA) to give 4, 5, 1, and 8.5 ng/µL stocks of each isoform, respectively. Serial dilutions of the compounds/probes were made in assay buffer 2 (25

mM Tris–HCl, pH 8.0, 137 mM NaCl, 2.7 mM KCl, and 1 mM MgCl2) starting with the highest concentration at 1 mM. 10 µL of enzyme stock and 30 µL of each of the serial dilutions were mixed in a black half-area, low protein binding 96 well plate (Corning) and pre-incubated for 5 minutes (3 hours for the o-aminoanilide derivatives) at RT. Next, 10 µL of 125 µM BLA fluorescent substrate (Chem-Implex) for HDAC1-3 or 10µL of 25 µM Fluor de Lys® (BML-KI178) (Enzo Life Sciences) for HDAC8 was added to each welland incubated for 30 minutes at RT. The reaction was quenched by the addition of 50 µL of 1 mg/mL trypsin and 5 µM TSA in assay buffer 2 and incubated for an additional 30 minutes. The fluorescence signal was read at excitation wavelength 360nm and emission wavelength 460nm using a Synergy 4 hybrid microplate reader from BioTek. The statistical data analysis and IC50 values were determined using GraphPad Prism 7.02.

Fluorogenic Enzymatic Assay for HDAC4

HDAC4 inhibitory activity was determined using the fluorogenic HDAC4 assay kit (BPS Bioscience, catalogue # 50064) according to the manufacturer procedure. The statistical data analysis and IC50 values were determined using GraphPad Prism 7.02.

Cell Culture

The breast cancer cell lines MDA-MB-231, obtained from Dr. Clodia Osipo (Loyola University, Chicago), were routinely maintained in IMEM media (Corning) supplemented with 2mM L-glutamine, 10 mM HEPES, 10% FBS, 1% non-essential amino acids and 1% antibiotics penicillin-streptomycin at 37 °C in 5% CO2.

In-cell Photolabeling

For whole cell analysis: 0.15 × 106 cells were plated in 6 cm dishes and grown to 90% confluence in 2 mL culture medium. The medium was replaced with 1 mL culture medium and

pretreated with competitor or DMSO control for 15 minutes where applicable and then treated with the probe or DMSO control. After 30 min at 37 °C the cells were cooled to 4 °C and irradiated with 366 nm light (12 J/cm2). The medium was removed and the cells gently washed with 2 mL PBS and then covered with 1 mL PBS. Cells were scraped from the plate into Eppendorf tubes, spun down at 1000 rpm for 5 minutes at 4 °C, the supernatant removed, and the cells resuspended in whole cell lysis buffer (50 mM HEPES pH 7.5, 420 mM NaCl, 1% Igepal, 5% glycerol and 1x protease inhibitor cocktail (Roche)). Samples were homogenized by brief sonication and incubated on a rotating stand at 4 °C for 1 h, and spun down at 20,000 × g for 10 minutes at 4 °C. Lysates were then dialyzed into reaction buffer (10 mM HEPES pH 7.5, 150 mM NaCl, 1.5 mM MgCl2, 0.3% Igepal, 1x protease inhibitor cocktail (Roche)) and the protein concentrations were determined by BCA assay. Next, 50 µg total lysates were incubated with azide conjugated IRDye according to concentration of probe, TCEP (0.7 mM), TBTA (0.1 mM), and CuSO¬4 (0.50 mM) for 90 minutes at 29 °C.

Western Blot

Protein samples were diluted with sample loading buffer containing DTT (Invitrogen), heated to 70 °C for 10 minutes and separated by gel electrophoresis at 100 volts. Gels were transferred to nitrocellulose membranes with iBlot transfer system (P3 for 7 minutes) and visualized with Odyssey Sa imager. Membranes were then blocked with Odyssey blocking buffer for 2 hours at rt or overnight at 4 °C. The blots were incubated with desired antibodies (anti-HDAC1 (Abcam ab7028), anti-HDAC2 (Abcam, ab12169), anti-HDAC3 (Abcam, ab7030), anti-HDAC8 (Abcam, ab187139) and anti-HDAC4,5,9 (Abcam, ab131524)) at the recommended dilutions for each in Odyssey blocking buffer (Li-Cor) overnight at 4 °C. The blots were then washed 3 × 5 minutes with PBST, incubated with relevant species of IRDye conjugated secondary antibody for 1 hour

and visualized with Odyssey Sa imager. If additional antibody probing was necessary, membranes were stripped with 0.2 N NaOH for 30 minutes and the Western blotting procedure was repeated starting from blocking with Odyssey buffer.

Quantification of Class I HDAC isoforms availability in MDA-MB-231 cells

A standard dilutions of individual recombinant proteins ranging from 1 to 50 ng (for HDAC1), 1 to 20 ng (for HDACs2,3), 0.5 – 10 ng (for HDAC8) as well as 30 µg cell lysate from MCF-7 cells were analyzed by SDS-PAGE and western blotting procedure. The blot signals were quantified by densitometry and standard dilutions signals were plotted and a linear regression was fit using Graphpad Prism 7 software. HDACs 1,2,3 and 8 were quantified by comparing the density of their signal in cell lysate to their corresponding standard curve.

Calculation of biochemical and cell-based selectivity for PRP and parent compounds for generation of heat maps

Recombinant enzyme selectivity was calculated by taking the IC¬50 values (determined as per sections 1.1. and 1.2.) of PRPs and parent compounds for each class I HDAC divided by the IC50 value of HDAC1 to represent a fold change in selectivity. For cell-based selectivity, labeling signals corresponding to bands at the molecular weights of class I HDACs, that were decreased to at least 50% upon co-incubation with excess of the known HDAC inhibitor SAHA and cross reacted with specific antibodies for each individual class I HDAC were compared to PRP 2 signals. PRP 2 class I HDAC signals have been validated previously. If signals met all these criteria, and were at the same molecular weight as the bands of PRP 2, they were analyzed by densitometry. Densitometry signals were then normalized to the abundance of the corresponding HDAC isoform, which were derived in method 1.6. Normalized signals were taken as a fold change from HDAC1, to represent a fold change in selectivity. Both biochemical

and cell-based selectivity were analyzed in MATLAB 2015b using the heatmap function from this software suite. Each row was standardized around a mean of zero with standard deviation of 1 and plotted as a color, based on a custom colormap shown in figure 2a in the text.

CHAPTER 4: SCAFFOLD DEPENDENT HISTONE DEACETYLASE (HDAC) INHIBITOR INDUCED RE-EQUILIBRATION OF THE SUBCELLULAR LOCALIZATION AND POST-TRANSLATIONAL MODIFICATION STATE OF CLASS I HDACS.

Thomas W. Hanigan[1¶], Taha Y. Taha[1¶], Shaimaa M. Aboukhatwa[1], Jonna M. Frasor[2], Pavel A. Petukhov[1*]

[1] Department of Medicinal Chemistry and Pharmacognosy, University of Illinois at Chicago, Chicago, Illinois, United States of America

[2] Department of Physiology and Biophysics, University of Illinois at Chicago, Chicago, Illinois, United States of America

[*] Corresponding author E-mail: pap4@uic.edu (PAP)

[¶] These authors contributed equally to this work.

This chapter is adapted from the manuscript “Scaffold Dependent Histone Deacetylase Inhibitor Induced Re-Equilibration of the Subcellular Localization and Post-Translational Modification State of Class I HDACs” under consideration at PLOS one. This manuscript is licensed under Creative Commons Attribution, (https://creativecommons.org/licenses/by/4.0/). The text was altered to adapt the manuscript to the UIC thesis format.

4.1 Abstract

The mechanism of action of histone deacetylase inhibitors (HDACi) is mainly attributed to the inhibition of the deacetylase catalytic activity for their histone substrates. In this study, we analyzed the abundance of class I HDACs in the cytosolic, nuclear soluble and chromatin bound cellular fractions in breast cancer cells after HDACi treatment. We show that potent *N*-hydroxy propenamide-based HDACi induce a concentration dependent decrease in the HDAC1 associated with chromatin and a lasting concomitant increase in cytoplasmic HDAC1 while maintaining total protein expression. No such change occurred with HDAC2 or 8, however, an increase in cytoplasmic non-phosphorylated HDAC3 was also observed. We find the subcellular re-equilibration of HDAC1 is subsequent to the accumulation of acetylated histones and may be cell cycle dependent. This study suggests that the biological activity of a subset of HDACi may stem from both direct competition with histone substrates of HDACs as well as from spatial separation from their substrates in the nucleus or change in post-translational modification status.

4.2 Introduction

Gene expression is controlled through modification of histone tails, which relaxes or condenses chromatin at different loci and effectively promotes or prevents access of the transcriptional machinery to DNA. Histone deacetylase (HDAC) is a family of 18 human enzymes that catalyze the removal of acetyl marks form histones and other protein substrates. HDACs are classified based on sequence homology to yeast and the classical zinc-dependent HDACs are class I – HDAC1, 2, 3 and 8 – class II – HDAC4, 5, 6, 7, 9 and 10 – and class IV – HDAC11 [(230, 231)]. Although HDAC11 closely relates to class I HDACs, the sequence similarity is too low to be classified as a class I HDAC [(232)]. Deacetylation of histones is mainly attributed to the class I HDACs, which has been shown to regulate a variety of cellular processes including cell cycle,

proliferation, DNA repair, differentiation, and apoptosis [230, 233]. Given their role in gene regulation, sHDACs have emerged as promising targets for treating various cancers and a range of autoimmune and neurodegenerative diseases, with four HDAC inhibitors (HDACi) FDA-approved to treat cutaneous or peripheral T-cell lymphoma or multiple myeloma [230].

In general, HDACi consist of 1) a zinc binding group, 2) surface binding group and 3) a linker to connect these two components and span the hydrophobic active site channel. Several structural classes with variation of these components exist, including long chain hydroxamic acids like suberoylanilide hydroxamic acid (SAHA, **Figure 13**), a pan inhibitor of class I and II HDACs; *N*-hydroxy propenamides such as panobinostat and trichostatin A (**Figure 13**), also pan class I and II inhibitors; “linkerless” hydroxamic acids such as PCI-34051 (**Figure 13**), an HDAC8 selective inhibitor; and ortho-aminoanilides such as entinostat (**Figure 13**), a class I selective inhibitor.

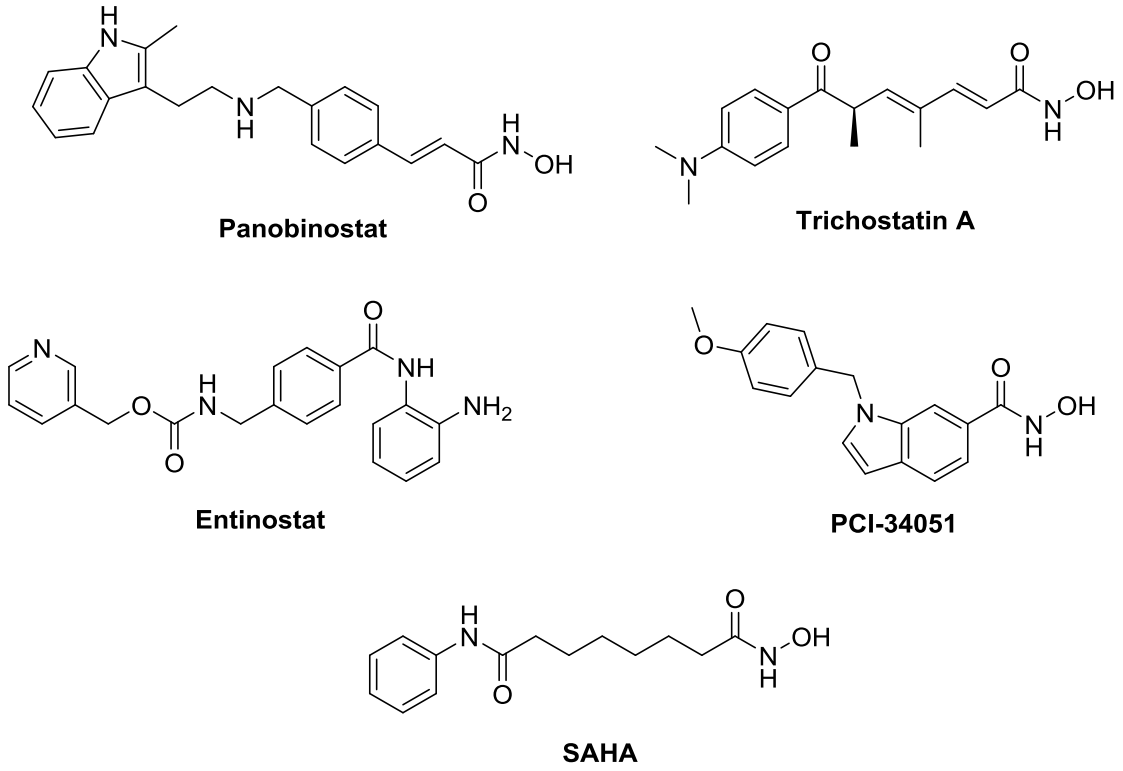

Figure 13: Structures of a diverse selection of HDACi.
Panobinostat, trichostatin A, and SAHA are pan-isoform inhibitors. Entinostat is a class I selective inhibitor. PCI-34051 is an HDAC8 selective inhibitor.

The effects of HDACi are mainly attributed to competitive inhibition of the deacetylase catalytic activity for their histone substrates. Under normal physiological conditions, HDAC catalytic activity is regulated through several mechanisms including subcellular localization and phosphorylation. In general, it has been shown that the class I HDACs reside in three separate pools: chromatin bound, soluble nuclear and cytosolic [234, 235]. HDAC1 and 2 are generally thought to be exclusively localized in the nucleus. Phosphorylation of HDAC1 and 2 promotes enzymatic activity and in the case of HDAC2 its association with chromatin [236]. HDAC3 has been shown to shuttle between the nucleus and cytosol, which is induced by cell cycle

progression [237], DNA repair [238] and differentiation [239]. Similar to HDAC1 and 2, HDAC3 phosphorylation also promotes enzymatic activity.

In this study, we investigated how HDACi affect the mechanisms that normally regulate the catalytic activity of class I HDACs in human breast cancer cell lines. MCF-7 and MDA-MB-231 cell lines were chosen as several HDACi have been shown to induce scaffold dependent effects on cell cycle and viability [195, 240-242]. We found that the subcellular localization of select class I HDACs is dose dependently altered in response to a subset of HDACi scaffolds without changing the total cellular abundance. This re-equilibration of subcellular localization was only observed for HDAC1. For HDAC3, on the other hand, we observed a change in the phosphorylation state in response to treatment with HDACi. In addition, we note that the re-equilibration of HDAC1 localization was subsequent to accumulation of histones and may be related to the cell cycle. This adds a spatial and post-translational component to the mechanism of action of HDACi in conjunction to inhibition of catalytic activity.

4.3 Results

HDACi affect the subcellular localization of HDAC1

As three separate pools of HDACs, cytosolic, nuclear soluble, and chromatin bound fractions have been previously reported [234, 235], we sought to analyze the effect that HDAC inhibition may have on the abundance of HDACs in these fractions. We treated serum starved MCF-7 cells with five structurally diverse pan and isoform selective HDACi (**Figure 13**) at 0.2, 10, and 50 µM for 12 hours followed by biochemical fractionation of cells into cytosolic, nuclear soluble, and chromatin bound portions. These concentrations of inhibitors were chosen as they span both above and below the reported cell-based EC_{50}'s [195, 240, 243, 244] and *in vivo* plasma concentrations

(245-249) for all the compounds evaluated in this study. We treated cells aligned at G_0/G_1 with HDACi so that only one cell cycle was analyzed, as the doubling time of MCF-7 cells is 24 hours *(250)*. Western blot analysis of these fractions shows that 12-hour treatment with panobinostat and trichostatin A, but not SAHA, entinostat or PCI-34051, induce a statistically significant concentration-dependent decrease of the chromatin bound HDAC1 fraction and a concomitant increase in the cytoplasmic fraction (**Figure 14a and 2b**, **Appendix U**). This was exclusive for HDAC1, in comparison to the other class I HDACs 2, 3 or 8 (**Appendix U**).

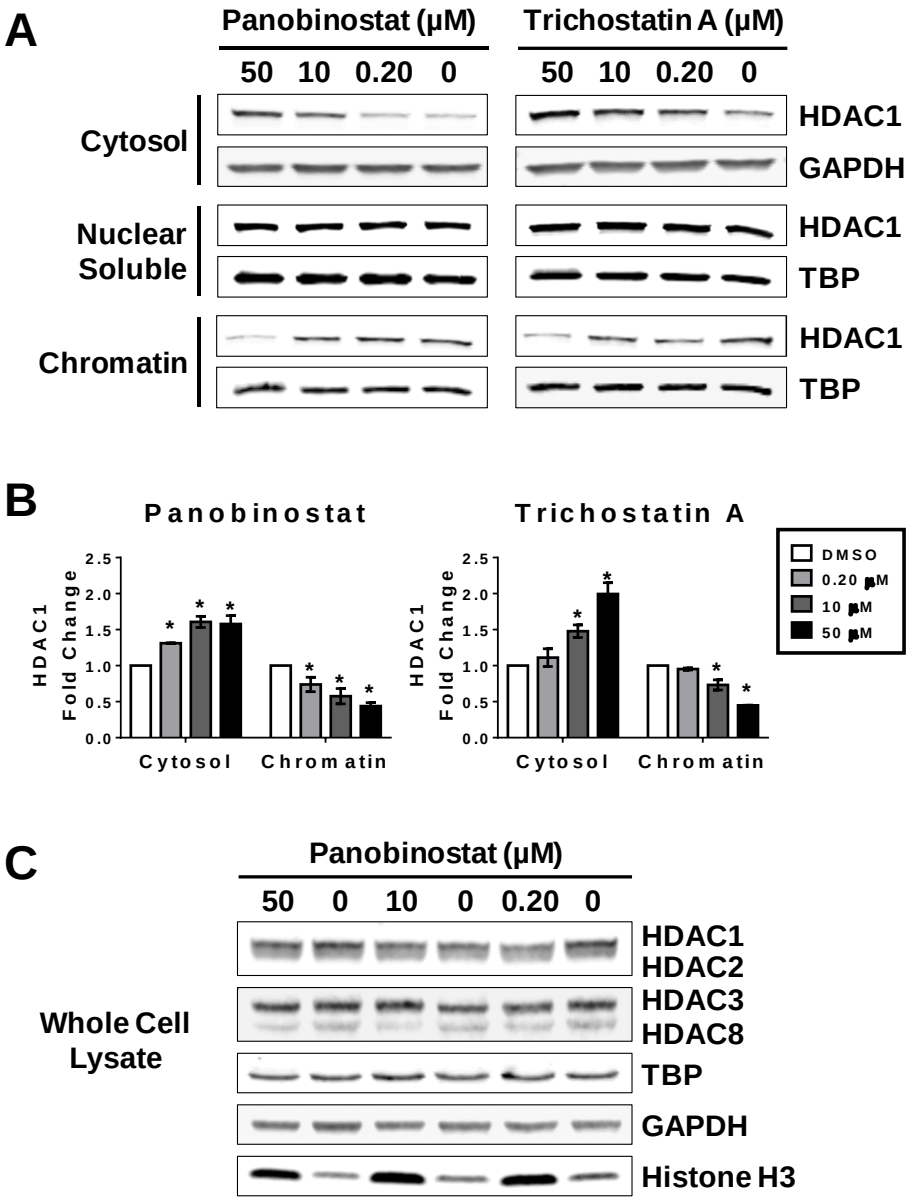

Figure 14: Potent HDACi alter the subcellular localization of HDAC1.
MCF-7 cells were treated with indicated concentrations of panobinostat or trichostatin A for 12 hours. A) Western blot analysis of the abundance of HDAC1 in the cytosolic, nuclear soluble, and chromatin bound fractions. B) Densitometry analysis of the abundance of HDAC1 normalized to GAPDH (cytosolic fraction) or to TATA-binding protein (TBP, nuclear soluble and chromatin bound fractions). C) Western blot analysis of the total abundance of class I HDACs and the loading controls TBP, GAPDH, and histone H3 after treatment with indicated concentrations of panobinostat for 12 hours. * Statistically significant difference compared with DMSO control (Student's t-test, $P<0.01$). Western blots shown are representative of at least two independent experiments. HDAC1 fold change is presented as the mean of at least two independent experiments ± standard deviation.

At 0.2, 10, and 50 µM, panobinostat reduced HDAC1 bound to chromatin to 74±10, 58±11 and 44±5.0 percent of the DMSO control, respectively. At the same concentrations, trichostatin A reduced the HDAC1 bound to chromatin to 95±1.5, 73±7.0 and 45±0.048 percent of the DMSO control, respectively. Both panobinostat and trichostatin A did not significantly affect cell viability compared with DMSO control (**Appendix V**). Neither of the HDACi affected the abundance of HDAC1 in the nuclear soluble cellular fraction (**Figure 14**). Similar to MCF-7 cells, we also observed trichostatin A, but not entinostat affected the subcellular distribution of HDAC1 in another cell line, MDA-MB-231 (**Appendix W**). To investigate whether the total abundance of HDAC1 was changing in response to the HDACi that were affecting its subcellular localization, we prepared whole cell lysates from cells treated with 0.2, 10, and 50 µM panobinostat. We observed no difference in the total abundance of HDAC1, HDAC2, 3 and 8 at any concentration of panobinostat in comparison to DMSO control (**Figure 14**). The validity of the biochemical fractionation was confirmed by the absence of GAPDH and HDAC8 *(251-253)* in the nuclear soluble and chromatin bound cellular fractions, and the absence of TATA-binding protein (TBP) in the cytosolic cellular fraction (data not shown). Moreover, HDACi treatment did not alter the total cellular abundance of these loading controls (**Figure 14**). We initially attempted to use histone H3 (H3) as the nuclear loading control, however, we observed that treatment with panobinostat increased its abundance in comparison to DMSO (**Figure 14**).

To confirm the HDACi-induced change in HDAC1 subcellular distribution in an orthogonal assay, we prepared MCF-7 cell microscope slides treated with HDACi under the same conditions as those for the biochemical fractionation. Optical sections were obtained for each HDACi by

laser scanning confocal microscopy (**Figure 15**, **Appendix X**) and correlated well with the results obtained by biochemical fractionation for HDAC1 (**Figure 14a and 14b**, **Appendix U**). HDAC1 colocalized with nuclear DAPI staining in the DMSO-treated cells for all experiments (**Figure 15**, optical sections A, E), whereas it localized in the cytosol when treated with panobinostat or trichostatin A (**Figure 15**, optical sections B-D and F-H, respectively). Both results were confirmed by quantitative colocalization analysis (**Figure 15**). The cells treated with SAHA or entinostat did not exhibit any significant change in subcellular localization of HDAC1 even at 50 µM, the highest concentration tested, (**Appendix X**, optical sections B-D and F-H, respectively) and were similar to the DMSO-treated cells **Appendix X**, optical sections A and E, respectively). Cells treated with PCI-34051 did not exhibit any change in subcellular localization of HDAC1 at 0.2 or 10 µM in comparison to DMSO control (**Appendix X**, optical sections I-K). At 50 µM PCI-34051, cells became elongated in morphology and did not adhere to the glass slide preventing reproducible staining (**Appendix X**, optical section L).

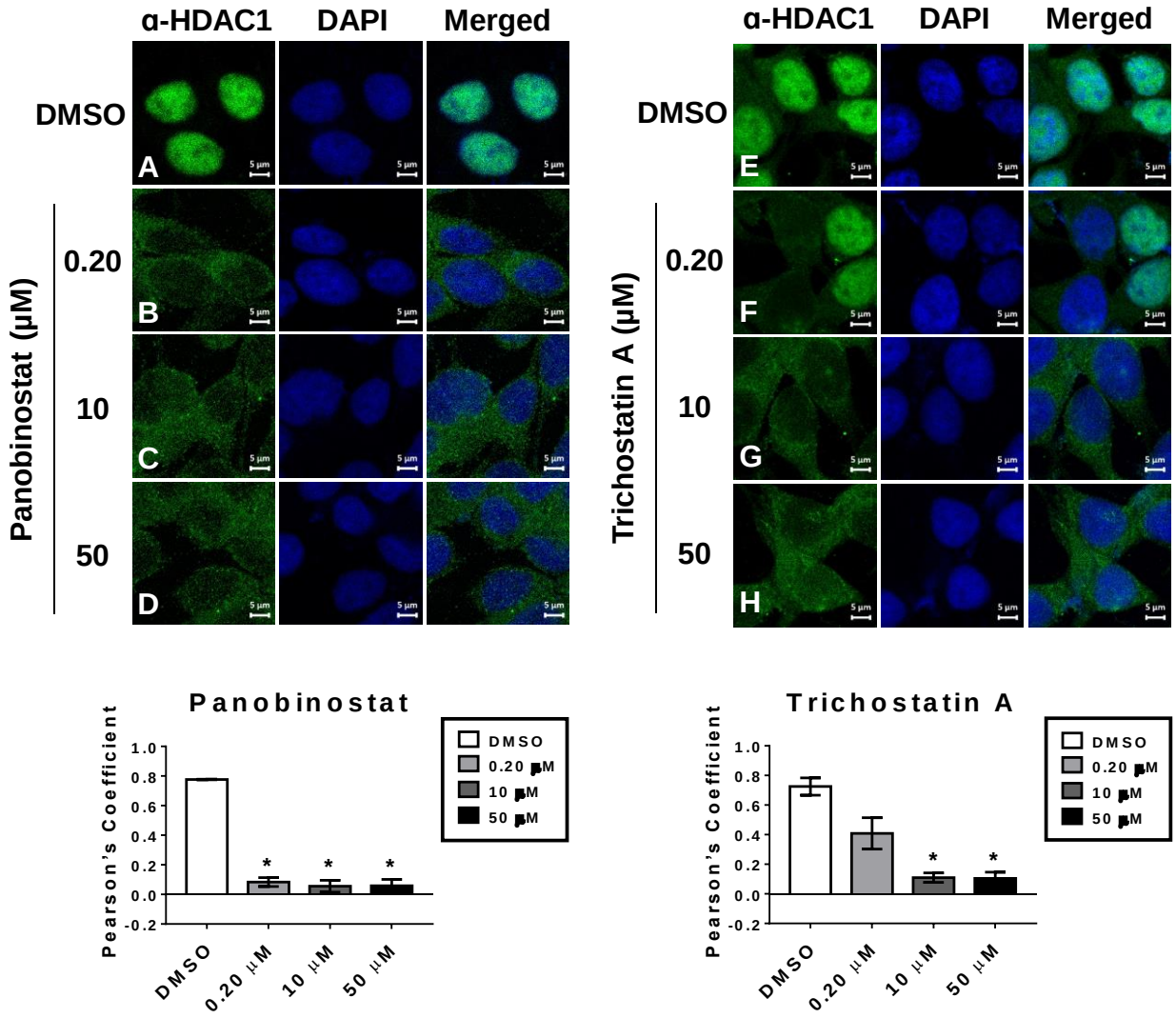

Figure 15: HDACi-induced re-equilibration of HDAC1 is confirmed by confocal microscopy.

MCF-7 cells were treated with indicated concentrations of panobinostat (optical sections A-D, respectively) or trichostatin A (optical sections E-H, respectively) for 12 hours, fixed, permeabilized and optical sections were obtained by laser scanning confocal microscopy. Fluorescence signal for HDAC1 is shown in green (left panels), DAPI staining is shown in blue (middle panels), and merged optical sections are shown in the right panels. Colocalization analysis of HDAC1 fluorescence signal and the DAPI stain signal was performed with JACoP (ImageJ) and shown below. * Statistically significant difference compared with DMSO control (Student's t-test, $P<0.01$). Pearson's Coefficient is presented as the mean of at least two independent experiments ± standard deviation. Optical sections shown are representatives of at least two independent experiments.

Re-equilibration of HDAC1 subcellular localization is subsequent to accumulation of acetylated histones and is affected by mitogens

The efficacy of HDACi is generally attributed to changing gene expression by leading to an accumulation of acetylated histones. As we have observed a change in the subcellular localization of HDAC1 induced by HDACi, we wondered whether this precedes or is subsequent to accumulation of histone acetylation. We tested this hypothesis by comparing histone acetylation after treatment with 10 μM trichostatin A for two and 12 hours, and compared to the abundance of HDAC1 in the cytosol (**Figure 16a and 16b**). We used 10 μM trichostatin A as this concentration robustly affected subcellular localization of HDAC1 (**Figure 14a and 14b**). At the two-hour time point, there was an accumulation of total acetylation of H3, a known HDAC1 substrate, whereas no increase in cytosolic HDAC1 was observed, suggesting acetylation precedes accumulation of HDAC1 in the cytosol (**Figure 16a and 16b**). We also analyzed the change in acetylation of H3 in response to 12-hour treatment with 0.2, 10, and 50 μM trichostatin A or the other four HDACi used in this study (**Figure 16c**). We found change in H3 acetylation correlated well with the previously reported in vitro IC_{50} values for each of the compounds [(241)]. However, the change in H3 acetylation did not correlate with the compounds' ability to change HDAC1 subcellular localization, given entinostat showed a large increase in H3 acetylation, but did not affect HDAC1 subcellular localization. Taken together, the in vitro HDAC inhibitor activity of the compounds reported previously ([(195, 241, 254, 255)]) and the increase in histone acetylation rule out cell permeability as the reason for the differences these compounds impose on HDAC1 subcellular localization.

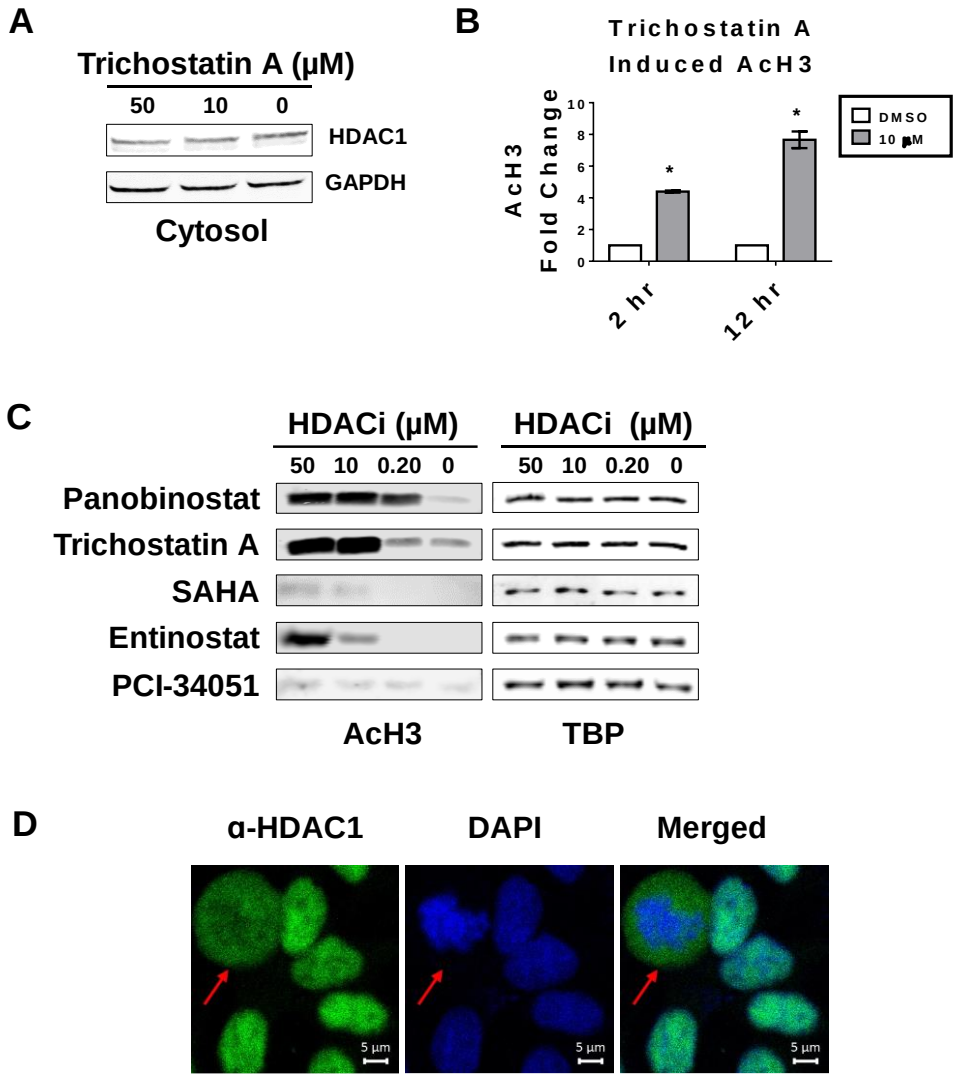

Figure 16: HDAC1 re-equilibration induced by HDACi is subsequent to histone acetylation and is affected by mitogenic stimuli.
A) Western blot analysis of cytosolic fractions of MCF-7 cells treated with indicated concentrations of trichostatin A for 2 hours. B) Densitometry analysis of western blots of chromatin fractions from MCF-7 cells treated with 10 μM trichostatin A for 2 and 12 hours; change in AcH3 was normalized to TBP. C) Western blot analysis of chromatin bound fractions from MCF-7 cells treated with indicated concentrations of HDACi for 12 hours. D) Laser

scanning confocal microscopy of MCF-7 cells, grown with 10% serum and treated with DMSO for 12 hours. Fluorescence signal for HDAC1 is shown in green (left panels), DAPI staining is shown in blue (middle panels), and merged optical sections are shown in the right panels. Representative optical section from two independent experiments is shown. Arrows indicate mitotic cells where HDAC1 is dispersed off chromatin, as indicated by DAPI staining. * Statistically significant difference compared with DMSO control (Student's t-test, $P<0.01$).

As others have noted a cell cycle dependent association of HDAC1 with chromatin [236, 256], our experimental investigation into its subcellular localization after treatment with HDACi was initially conducted after serum starvation (without mitogens). In addition, we obtained optical sections of cycling MCF-7 cells treated with 0.2, 10, and 50 μM panobinostat for 12 hours (data not shown). Unlike our experiments with quiescent cells, HDAC1 localization in DMSO controls depended on cell cycle (**Figure 16d**), with HDAC1 diffusing from chromatin during mitosis, confounding interpretation of samples treated with HDACi.

Re-equilibration of HDAC1 subcellular localization is sustained after removal of HDACi

As we saw a large percentage, up to 60%, decrease of the HDAC1 associated with chromatin upon treatment with panobinostat, we questioned whether this was a sustained change, or whether the cell could recover. To answer this question, we pulsed MCF-7 cells with 10 μM panobinostat treatment for 12 hours, and allowed the cells to recover for approximately one cell cycle (24 hours) in fresh media without the inhibitor. We observed that the cytosolic fraction of HDAC1 remained increased, and the chromatin bound fraction remained decreased in response to treatment with panobinostat (**Figure 17a and 17b**). In addition, the nuclear soluble fraction of HDAC1 decreased (**Figure 17a and 17b**), which did not occur with 12-hour treatment of

panobinostat (**Figure 14a**). Furthermore, H3 acetylation remained increased similar to 12-hour treatment with panobinostat (**Figure 16b**).

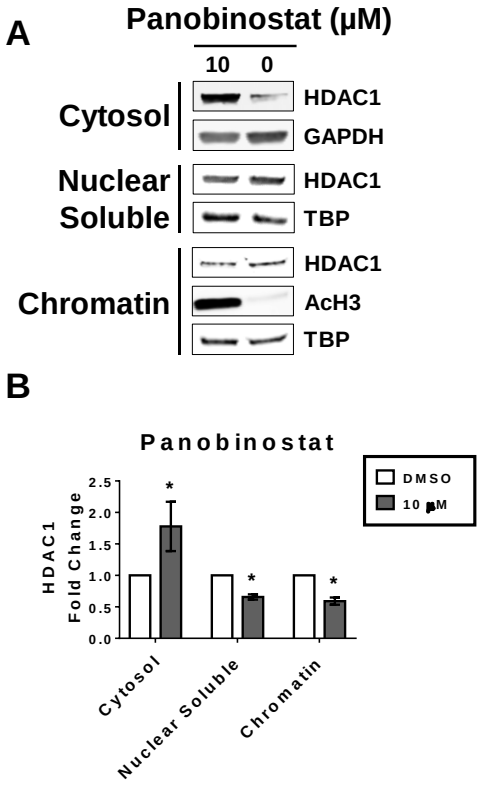

Figure 17: Increase in cytosolic HDAC1 is irreversible up to 24 hours
MCF-7 cells were treated with 10 μM panobinostat for 12 hours, the compound was then removed and cells allowed to recover for 24 hours. A) Western blot analysis of the abundance of HDAC1 in the cytosolic, nuclear soluble, and chromatin bound fractions. B) Densitometry analysis of the abundance of HDAC1 normalized to GAPDH (cytosolic fraction) or to TATA-binding protein (TBP, nuclear soluble and chromatin bound fractions). * Statistically significant difference compared with DMSO control (Student's t-test, $P<0.01$). Western blots shown are representative of at least two independent experiments. HDAC1 fold change is presented as the mean of at least two independent experiments ± standard deviation.

HDAC3 phosphorylation state is affected by HDACi treatment

In addition to subcellular localization, we also investigated HDAC3 phosphorylation state in response to HDACi treatment, as this isoform's subcellular localization was not affected (S1 Fig). Using an antibody found to be specific for non-phosphorylated HDAC3 [(257)], we analyzed the amount of non-phosphorylated HDAC3 after treatment with 0.2, 10 and 50 μM panobinostat, trichostatin A, SAHA, entinostat or PCI-34051 (**Figure 18a**). We observed 1.8-3.8 and 1.8-2.3-fold increase in non-phosphorylated HDAC3 in response to panobinostat and trichostatin A, respectively (**Figure 18b**). We found SAHA, entinostat, and PCI-34051 did not induce a significant change in non-phosphorylated HDAC3 (**Figure 18a and 18b**). These results along with the HDACi-induced re-equilibration of the subcellular localization are summarized in **Figure 19**.

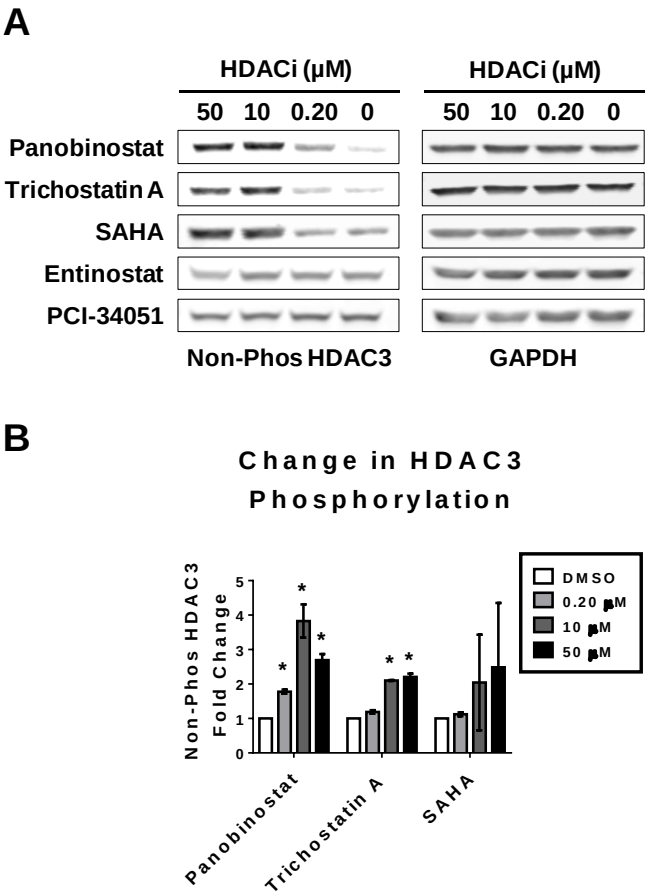

FIGURE 18: POTENT HDACI INCREASE THE ABUNDANCE OF NON-PHOSPHORYLATED HDAC3. MCF-7 cells were treated with indicated concentrations of panobinostat, trichostatin A, or SAHA for 12 hours and then biochemically fractionated. A) The abundance of non-phosphorylated HDAC3 was characterized by Western blot analysis in the cytosolic fraction. B) Densitometry analysis of the abundance of non-phosphorylated HDAC3 normalized to GAPDH. * Statistically significant difference compared with DMSO control (Student's t-test, $P<0.01$). Western blots shown are representative of at least two independent experiments. HDAC3 fold change is presented as the mean of at least two independent experiments ± standard deviation.

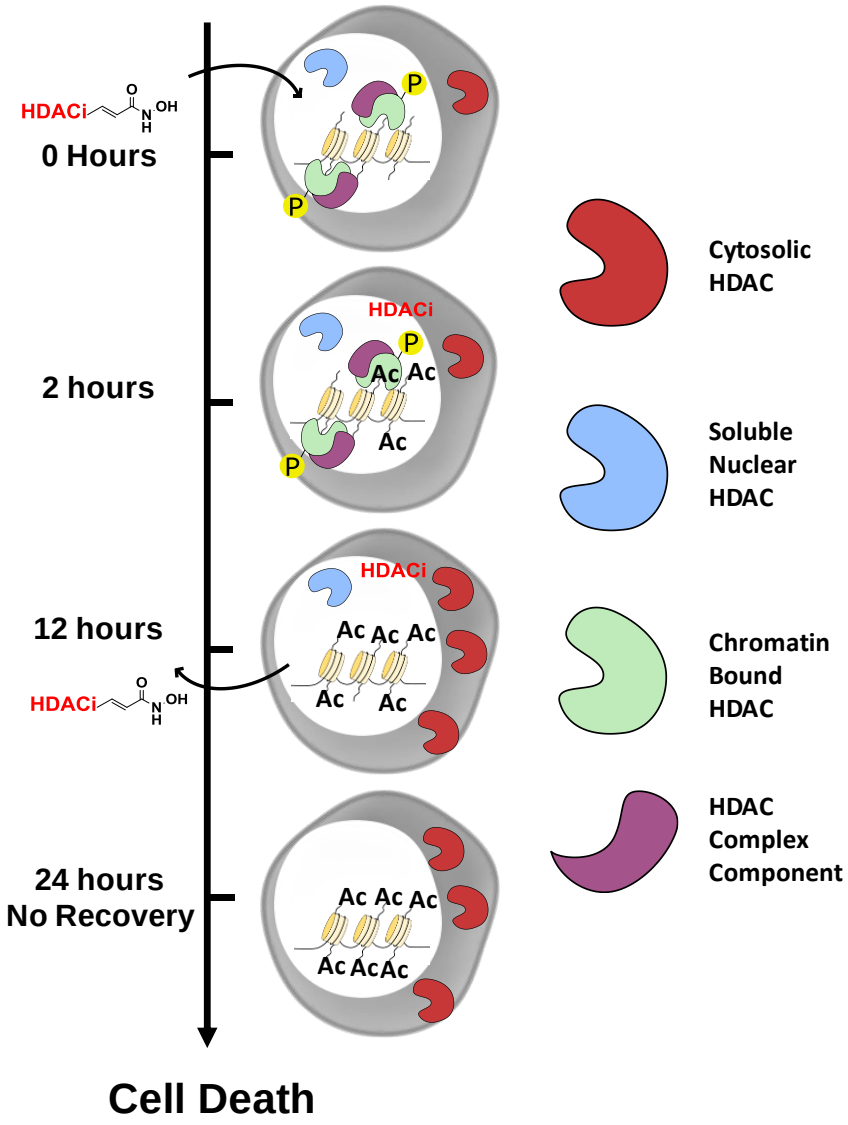

Figure 19: A model of the mechanism of action of propenamide-based HDACi including re-equilibration of the subcellular distribution and modulation of the post-translational modification of HDACs.
Treatment of with N-hydroxy propenamide-based HDACi increase histone acetylation at 2 hours without affecting the subcellular localization or the phosphorylation status of HDACs. At 12 hours, re-equilibration of subcellular localization as well as a decrease in phosphorylation of HDACs is observed, along with a greater increase in histone acetylation. The induced change in subcellular localization and phosphorylation of HDACs is sustained 24 hours after removal of HDACi. This is in line with the time necessary to induce commitment to cell death with HDACi.

4.4 Discussion

HDAC catalytic activity is normally regulated by controlling subcellular localization and phosphorylation status, among other mechanisms. In this study, we found that HDACi, whose effects are generally thought to be associated with competition with endogenous histone substrates, also affect subcellular localization and phosphorylation of class I HDACs in a chemotype dependent manner.

In particular, the pan HDACi panobinostat and trichostatin A induced a dose dependent increase in the cytosolic HDAC1 and a decrease in chromatin bound HDAC1 in MCF-7 and MDA-MB-231 cells. This response was not detected for the other class I HDACs. Instead, we observed a change in the phosphorylation state of HDAC3. Both panobinostat and trichostatin A dose dependently increased non-phosphorylated HDAC3 in the cytoplasm, with no change in total HDAC3 expression. Given that the total HDAC1 expression was not affected as well, the change in HDAC1 subcellular localization could either be caused by a translocation from chromatin to cytosol, or a degradation of chromatin bound HDAC1 coupled with a matching increase in translation of HDAC1 in the cytoplasm. HDACs are key regulators of gene expression, and the set of HDACi used in this study differentially affects gene expression in breast cancer cell lines used [243, 258-261]. Others have also observed that trichostatin A treatment increases HDAC1 mRNA levels [262]. As cells respond to trichostatin A by increasing HDAC1 mRNA production, a degradation/increased translation mechanism is likely responsible for our observation, which warrants future validation by blocking protein synthesis with cycloheximide or actinomycin D. The re-equilibration of HDAC1 subcellular localization likely play a role in the mechanism of action of HDACi given that it was significant starting at 200 nM and 10 μM for panobinostat and

trichostatin A, respectively, which are within concentrations reported *in vitro* and *in vivo* [243-247]. The observations appear to be independent of the estrogen receptor (ER) status considering that they were observed in ER+ MCF-7 and ER- MDA-MB-231 cells.

In addition, we observed that the re-equilibration of HDAC1 subcellular localization is sensitive to mitogenic stimuli. Re-equilibration of HDAC1 subcellular localization induced by panobinostat could be clearly observed by confocal microscopy only after cells were serum starved. When cells were cultured in the presence of serum, HDAC1 subcellular localization varied greatly in the DMSO control, depending on what part of the cell cycle an individual cell was in. Others have observed mitogens can induce HDAC1 dissociation from chromatin [263] and cell cycle dependent histone hyperacetylation has been noted going from G_1 to S phase [263] and hypoacetylation leading into mitosis [256]. In our study, we found that histone hyperacetylation precedes re-equilibration of HDAC1 subcellular localization. Taken together these data suggest that HDACi, initially induce histone hyperacetylation, which may be recognized by the cell as a G_1 to S phase transition, inducing a shift of HDAC1 from chromatin to cytosol, as would occur during normal cell cycle progression. As HDAC1 remains in the cytosol, the cell cannot progress from G_2 to M phase when deacetylation is necessary for chromatin condensation, leading to arrest, which is in line with the observed G_2/M arrest induced by HDACi (data not shown).

Curiously, we observed a sustained increase in cytosolic and decrease in chromatin bound HDAC1 after the pulse treatment with panobinostat followed by recovery for 24 hours, roughly one cell cycle. In addition, acetylation of H3 remained increased after 24-hour recovery. This model is depicted in **Figure 19**. Longer recovery times after pulse treatment of HDACi may

yield a return to basal HDAC1 levels in the cytosol; however, pulse treatment with panobinostat has been shown to induce cell death starting around 12 hours [(241)], which is the same time necessary to induce re-equilibration of HDAC1 subcellular localization. Therefore, re-equilibration of HDAC1 subcellular localization may be irreversible and may play role in HDACi induced cell death, given their similar kinetics. Others have observed inhibitor binding and histone acetylation kinetics do not correlate well with the time to induce cell death [(264)]. Our study identifies a plausible additional component of the mechanism of action of HDACi that may better correlate with induction of cell death. This mechanism may be useful in drug discovery efforts since this subset of HDACi is associated with increased efficacy in a number of cancer cell types [(241)].

The re-equilibration of HDAC1 subcellular distribution and change in HDAC3 phosphorylation was HDACi scaffold dependent. We only observed significant changes in either of these phenomena with panobinostat and trichostatin A, but not SAHA, entinostat or PCI-34051 treatment. Both trichostatin A and panobinostat feature alkenyl groups in the linker portion which have been shown to affect the tertiary structure of targeted HDACs differently than compounds with alkyl linkers like SAHA [(265)]. Changes in tertiary structure could potentially affect HDAC protein-protein interactions, which is known to control HDAC subcellular localization [(266)]. Indeed, others have shown that trichostatin A disrupts HDAC1 complex formation more potently than SAHA [(267)].

The changes in subcellular localization or phosphorylation were not dependent upon the relative induction of histone H3 acetylation. While panobinostat and trichostatin A, caused the largest

increase in H3 acetylation and the most significant change in HDAC1 subcellular localization or HDAC3 phosphorylation, SAHA and entinostat also induced H3 acetylation without significantly affecting HDAC1 subcellular localization. No change in histone acetylation was observed with PCI-34051 treatment, which is in line with reports showing it is an HDAC8 selective inhibitor; HDAC8 cannot deacetylate histones as we found it exclusively localized in the cytosol. Taken together our data show that only *N*-hydroxy propenamide-based HDACi scaffolds induce the change in HDAC subcellular localization or phosphorylation.

A large body of research has focused on the selective recruitment of HDACs to individual genes, to determine whether the gene is epigenetically silenced in a context of interest. These studies often employ chromatin immunoprecipitation (ChIP) and are typically validated with use of an HDACi to show that the HDAC activity is necessary for changing the expression of the gene. This study clearly demonstrates that some HDACi induce up to 60% dissociation of the total HDAC1 bound to chromatin, which should be taken into consideration when interpreting ChIP data.

This study suggests that the biological activity of a subset of *N*-hydroxy propenamide-based HDACi may stem from direct competition with histone substrates of HDACs as well as from spatial separation from their substrates in the nucleus and/or change in post-translational modification status of HDACs. Future studies are needed to investigate other HDACi chemotypes, elucidate the mechanism, expand beyond breast cancer cells, and determine if the same phenomenon is observed in vivo.

4.5 Materials and Methods

Cell culture and HDACi treatment

Human cell line MCF-7 was maintained in RPMI supplemented with 10% FBS, 1% non-essential amino acids, 2 mM L-glutamine, 1% Pen-Strep and 0.01 mg/mL human recombinant insulin at 37 °C in 5% CO2. MDA-MB-231 human cell line was maintained in IMEM media (Corning) supplemented with 10% FBS, 1% non-essential amino acids, 2 mM L-glutamine, 10 mM HEPES and 1% Pen-Strep at 37 °C in 5% CO2. Cells (2.1x106) were plated in 10-cm plates in culture media for biochemical fractionation and whole cell lysate analysis. For confocal microscopy, cells were plated in an 8-well chambered slide (Thermo Fischer) at a density of 35,000 cells per well. After 48 hours, culture media was replaced with serum free media. After 24 hours, cells (80-90% confluence) were treated with HDACi (Selleckchem) at a concentration of 0.2, 10, or 50 µM in serum free medium. These concentrations span above and below all previously reported cell-based IC50 [11, 12, 15, 16]. For cell cycle analysis, cells were seeded in a clear-bottom 96-well plate, serum starved for 24 hours followed by HDACi treatment for 12 hours. The cells were then fixed with ice-cold Methanol for 15 minutes, stained with propidium iodide for 40 minutes and imaged with Celigo image cytometer (Nexcelom Bioscience). Cell cycle analysis was conducted using FCS Express 6 Multicycle application (De Novo Software).

Biochemical cellular fractionation

Our method for biochemical fractionation was developed based on a previous work [17]. Briefly, cells were washed with phosphate buffered saline (PBS) and then scraped with a rubber policeman in PBS. Cells were then pelleted by centrifugation at 1,000g for 5 minutes at 4 °C in a 1.7 mL Eppendorf tube (Thermo Fischer). The pellet was then resuspended in 300 µL ice-cold cytosolic lysis buffer (10 mM HEPES, 10 mM KCl, Igepal CA-630 (Sigma-Aldrich, 0.2% for MCF-7 cells and 0.05% for MDA-MB-231 cells), 1X cOmplete Protease Inhibitor Cocktail (Roche), and 1:100 Phosphatase Inhibitor Cocktail Set II (EMD Millipore)) and vortexed for 10

seconds at room temperature (RT). The cells were allowed to swell for 10 minutes at RT and then vortexed again for 10 seconds at RT. Next, the nuclei were pelleted by centrifugation at 6,500g for 5 minutes at 4 °C, the supernatant (cytosolic fraction) was collected and the nuclear pellet was washed with ice-cold cytosolic lysis buffer without Igepal CA-630. The nuclei were again pelleted at 6,500g for 5 minutes at 4 °C and the supernatant discarded. The nuclear pellet was resuspended in 150 µL ice-cold no salt lysis buffer (3 mM EDTA, 1X cOmplete Protease Inhibitor Cocktail, and 1:100 Phosphatase Inhibitor Cocktail Set II) by sonication (5 seconds) on ice. The solution was then incubated with rotation for 30 minutes at 4 °C. Chromatin was pelleted by centrifugation at 6,500g for 5 minutes at 4 °C, the supernatant (nuclear soluble fraction) was collected and chromatin was resuspended in ice-cold high salt lysis buffer (50 mM HEPES, 0.5 M NaCl, 0.05% Igepal CA-630, 1X cOmplete Protease Inhibitor Cocktail, and 1:100 Phosphatase Inhibitor Cocktail Set II) by vortexing for 2 minutes in 30-second rounds at RT. The solution was then incubated with rotation for 30 minutes at 4 °C. The DNA and nuclear matrix were pelleted by centrifugation at 14,000g for 10 minutes at 4 °C. The supernatant (chromatin bound fraction) was collected and the pellet was discarded. The chromatin bound fraction was dialyzed into a lower salt concentration buffer (10 mM HEPES, 100 mM NaCl, 10 mM KCl, 5% glycerol, and 0.3% Igepal CA-630, 1X cOmplete Protease Inhibitor Cocktail, and 1:100 Phosphatase Inhibitor Cocktail Set II) to improve SDS-PAGE running conditions as described previously [18]. All fractions were kept on ice until further analysis and then stored at -20 °C.

Whole cell lysate preparation

Cells were washed with PBS, scraped with a rubber policeman in PBS and pelleted by centrifugation at 1,000g for 5 minutes at 4 °C in a 1.7 mL Eppendorf tube. Next, the pellet was resuspended in 300 µL ice-cold RIPA lysis buffer (150 mM NaCl, 0.5% sodium deoxycholate,

0.1% sodium dodecyl sulfate, 50 mM Tris pH 8.0, 1% Igepal CA-630, 1X cOmplete Protease Inhibitor Cocktail, and 1:100 Phosphatase Inhibitor Cocktail Set II) and incubated with rotation for 30 minutes at 4 °C. Insoluble cellular matrix was pelleted at 14,000g for 10 min at 4 °C and the supernatant was collected and kept on ice until further analysis and then stored at -20 °C.

Western blotting

Protein concentration of each cellular fraction was characterized with the Pierce BCA Assay Kit (Thermo Fischer). Proteins were diluted 3:1 with 4X Laemmli sample buffer containing 5% β-mercaptoethanol (Bio-Rad), boiled for 5 minutes, loaded onto a 12% polyacrylamide gel and electrophoretically separated (100 V, 1.5 hours). Equal portions of cytosolic, nuclear soluble and chromatin bound fractions were used for each experiment. After electrophoresis, proteins were transferred to a nitrocellulose membrane (iBlot 2 (Invitrogen) mode P3 for 7 minutes). Equal protein loading was confirmed with Ponceau S staining (Sigma-Aldrich). After staining, the membranes were blocked with Odyssey blocking buffer (Li-Cor) for 2 hours at RT, and then incubated with primary antibodies in blocking buffer for HDAC1 (Abcam, ab7028, lot GR188529-1, rabbit), HDAC2 (Abcam, ab124974, lot GR97402-7, rabbit), HDAC3 (Abcam, ab7030, lot GR121157, rabbit), non-phosphorylated HDAC3 (Ref [19]; Millipore, 05-813, lot 2726719, mouse), GAPDH (Abcam, ab128915, lot GR90965-22, rabbit), TATA-binding protein (Abcam, ab818, lot GR131329-14, mouse), H3 (Abcam, ab1791, lot GR242835-1, rabbit) and Acetyl-histone H3 (Millipore, 06-599, lot 2153150, rabbit) overnight at 4 °C. The membranes were then washed three times with PBS containing 0.1% Tween-20 (PBST) for 5 minutes at RT. The membranes were then incubated with an anti-rabbit or anti-mouse IRDye-conjugated secondary antibody (Li-Cor) for 1 hour at RT. The membranes were then washed 3 times with

PBST for 5 minutes and visualized using the Odyssey Sa scanner (Li-Cor). Densitometry analysis was performed with Image Studio version 5.2 (Li-Cor).

Confocal microscopy

Cells were washed two times with PBS and fixed by incubating with 4% formaldehyde (Sigma-Aldrich) in PBS for 10 minutes at RT. Cells were then washed two times with PBS for 5 minutes at RT. Next, the cells were permeabilized by incubating with 0.1% Triton X-100 (Thermo Fischer) in PBS for 1 min at RT. After permeabilization, the cells were washed two times with PBS and then blocked with 10% goat serum (Thermo Fischer) for 1 hour at RT. The blocking buffer was decanted and rabbit monoclonal HDAC1 antibody (Abcam) in blocking buffer was added. After incubation at 4 °C overnight, the cells were washed two times with PBS for 5 minutes at RT and then incubated for 1 hour at RT with Alexa Flour 488-conjugated goat anti-rabbit secondary antibody (Thermo Fischer) in 1% goat serum (Thermo Fischer). The cells were then washed two times with PBS for 5 minutes at RT, dried for 5 minutes, mounted with Prolong Gold Antifade Mountant containing DAPI (Thermo Fischer) and allowed to cure in the dark for 24 hours. The slide was visualized with a Zeiss LSM 710 (25 mW Multi-line Ar laser for Alexa Flour 488, 30 mW diode UV laser for DAPI) containing a 63x/1.46 Oil alpha Plan-Apochromat objective.

The correlation between the HDAC1 fluorescence signal and the DAPI stain signal was analyzed with JACoP (ImageJ) and the Pearson's coefficient calculated for each HDACi optical section. Pearson's coefficient range from 1 to −1, with 1 standing for complete positive correlation and −1 for a negative correlation, and zero standing for no correlation.

Statistical Analysis

Statistical analyses were performed with GraphPad Prism 7 software. All data are shown as mean ± standard deviation. Student's t-test (two-tailed) was used to measure statistically significant differences between groups. P value < 0.01 was considered statistically significant for this study.

CHAPTER 5: INSIGHTS FROM THE ANALYSIS OF HDAC REGULATION IN BREAST CANCER AND FUTURE DIRECTIONS FOR DRUG DISCOVERY

5.1 How do we find the relevant HDAC isoforms in breast cancer?

While preclinical and clinical data support the notion that HDAC inhibitors can be effective breast cancer therapeutics, no HDAC inhibitors have been approved for treatment of this disease. The current strategy to improve HDAC inhibitor efficacy has been to design selective HDAC inhibitors for the most disease relevant HDAC isoforms. However, which isoforms play a key role in breast cancer, as well as other disease states, remains unclear. To date, many studies have focused on correlating the expression of individual isoforms with disease. This information can be used to discern relevant HDAC inhibitor targets. However, in chapter two we saw HDAC3 expression had very poor correlation with HDAC3 phosphorylation and thus HDAC3 activity does not correlate well with HDAC3 expression (**Figure 20**).

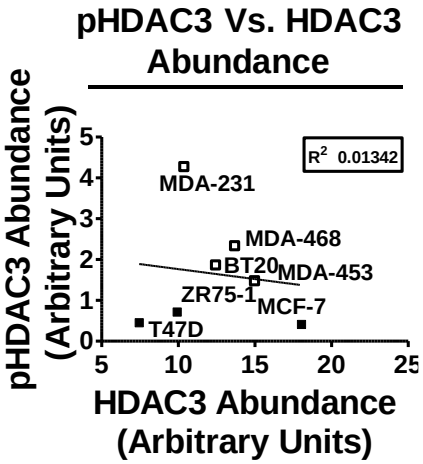

Figure 20: pHDAC3 versus HDAC3 expression.
Abundance of phosphorylated HDAC3 versus HDAC3 in panel of breast cancer cell lines.

Therefore, as current HDAC inhibitors inherently target the catalytic activity of HDACs, targeting HDAC isoforms based on expression in a disease of interest may not be an effective approach. Perhaps characterizing the activity state of known HDAC isoforms in a disease, and then developing inhibitors targeting the catalytic activity these isoforms would be more effective? We propose this approach as our data show that more aggressive triple negative cells have induced HDAC3 activity through phosphorylation in compared to less aggressive luminal breast cancer cells, which may indicate the HDAC3 activity, not expression, is important in disease progression.

Further rationale to support the importance of post-translational regulation of HDAC activity in disease, comes from the data in chapter four of this thesis. This chapter demonstrates that cells respond to HDAC inhibitors by altering the phosphorylation state, as well as the subcellular localization of select HDAC isoforms, not by changing the overall expression of these isoforms. We propose in chapter four, that breast cancer cells likely associate the histone hyperacetylation induced by HDAC inhibitors with a change in cell cycle and feedback on the HDAC activity through phosphorylation and subcellular localization, not by decreasing expression. We believe this highlights the importance of these post-translational mechanisms in regulating HDAC activity in breast cancer cells, and downplays the importance of transcriptional changes. This supports the proposed approach of tying activity, rather than expression, of individual isoforms to disease, and then designing inhibitors around this data. The assay presented in chapters two and three provides a tool to simultaneously quantify the activity state of all HDAC isoforms in any given cell type and should be useful to identify important isoforms contributing to disease.

Regardless of our suggestion to look at the activity state of HDAC isoforms, rather than overall abundance, previously collected data on HDAC isoform abundance may be useful elsewhere. While current HDAC inhibitors target the catalytic site and thus the enzymatic activity of HDACs, others have suggested that targeting the protein-protein interactions in native HDAC complexes may lead to more selective and diverse effects [(268-270)]. Others have shown that HDACs play an important scaffolding role in these complexes, and mutants that disrupt HDAC-protein interactions alter gene expression differently than inhibiting deacetylase activity [(147)]. Therefore, targeting these interactions may lead to different effects in comparison to inhibiting the deacetylase activity. As formation of protein-protein interactions is driven by the abundance of individual components, knowledge of the expression of these components may help to identify important disease relevant HDAC-protein interactions. This strategy may be guided by previously collected data correlating the expression of HDAC isoforms or known protein complex components with disease [(147)].

5.2 <u>How do we target the relevant HDAC isoforms?</u>

As shown in chapters two and three, phosphorylation of HDAC3, conclusively affects inhibitor binding to this isoform. As phosphorylation is not typically accounted for in the biochemical assays used during HDAC inhibitor development, it is not surprising that campaigns attempting to make selective inhibitors have not come up with solid, clinically effective compounds, as they may not bind their intended targets *in vivo*. The question that remains is how can we develop selective HDAC inhibitors that bind their intended targets? While accounting for phosphorylation of HDAC3 during biochemical analysis may help to improve selectivity and potency of HDAC inhibitors *in vivo*, other mechanisms likely affect HDAC inhibitor binding as

well [180, 271]. Furthermore, **Figure 5** shows that many, if not most other HDAC isoforms have altered drug binding between cell types and implies similar mechanisms may be at play with respect to these other isoforms. Therefore, it will be difficult to recreate the enzymatic state of multiple HDACs isoforms *ex vivo*, and thus accurately predict potency and selectivity *in vivo*.

Another strategy would be to directly measure target engagement and selectivity *in vivo*. As outlined in chapters two and three, small molecule HDAC inhibitors under development can be reformatted as photoreactive probes (PRPs) without drastically altering the biochemical potency using the synthetic strategy from chapter three. These PRPs can be used to report on target engagement and selectivity in a diverse set of cell lines, representative of a disease state of interest. However, this strategy requires synthesis of PRPs and validates parent compounds and PRPs have similar bioactivity based on biochemical experimentation (chapter three). One adaptation of the photolabeling strategy involves competition of pan-HDAC PRPs, like photomate, with potential isoform selective HDAC inhibitors under development (**Figure 21**). This strategy should be useful to simultaneously report on the selectivity of potential isoform selective HDAC inhibitors for photomate targets in cells. However, competition based experiments inherently depend on the native binding affinity and dissociation kinetics of the PRP to compare to potential isoform selective compounds, and use of multiple parent PRPs may be necessary. Furthermore, as observed in chapter four, pre-treatment of cells with HDAC inhibitors can alter the native enzymatic state of several HDAC isoforms, limiting kinetic studies using this method. Regardless, both photolabeling strategies have not been validated in animal models, which may be difficult as it is necessary to photoirradiate samples for covalent modification of PRPs.

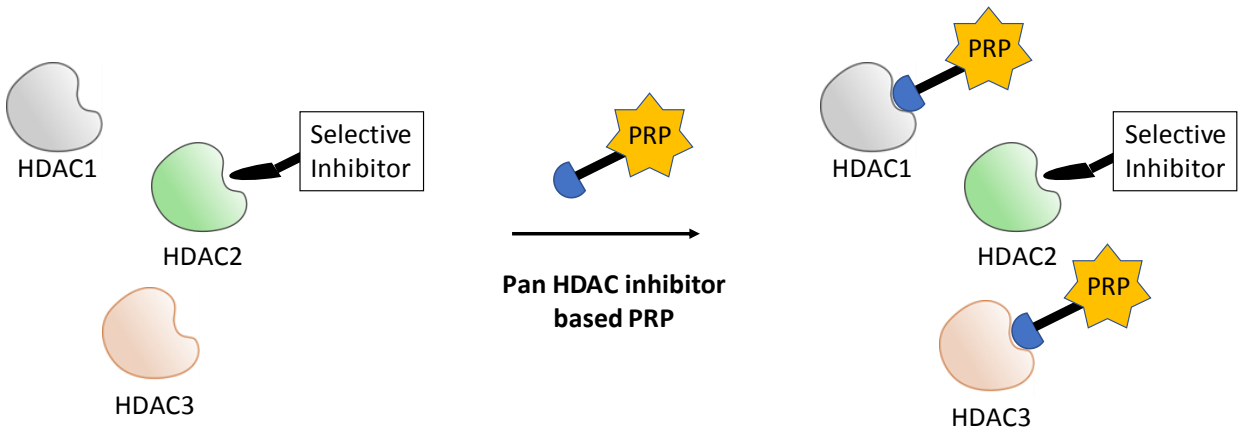

Figure 21:Competition based photolabeling experiment.
Graphical depiction of competition based photolabeling experiment with an isoform selective HDAC inhibitor.

One additional non-photolabeling type approach that successfully measured HDAC inhibitor target engagement and residence time in cells was recently reported [(272)]. This method depends on bioluminescence energy transfer (BRET) between a luciferase fused target HDAC and a fluorescently labeled HDAC inhibitor in competition with potential HDAC inhibitors of interest. While this method does not depend on photoirradiation of the samples, it does depend on the expression of a mutant fusion HDAC protein, which could potentially alter native enzymatic state of the HDAC isoform under investigation.

The easiest method with respect to enzymes, such as histone deacetylase, has historically been to monitor changes in substrate and product formation; i.e. the deacetylation of a specific substrate. This has been the preferred method of medicinal chemists working on HDACs after evaluating

their compounds biochemically. However, with respect to HDACs, this is not a straightforward task because of the compensatory mechanisms that regulate HDAC activity *in vivo*. As described in section 1.3, knockout or knockdown of one individual isoform results in the upregulation of other HDAC isoforms, which take over the responsibility for deacetylating substrates of the isoform that was transcriptionally manipulated. Therefore, it is a reasonable to assume inhibition of one individual isoform, likely results in increased activity of another, and thus no net change in substrate deacetylation can be measured because of this compensation. However, this compensation feedback mechanism may be useful if fully delineated. Take for example the feedback on HDAC3 activity that occurs through phosphorylation in response to HDAC inhibitors, shown in chapter four. Change in HDAC3 phosphorylation could serves as an indirect indication that an HDAC inhibitor is targeting HDAC3, which can easily be measured *ex vivo* after treating living systems with the HDAC inhibitor under question.

5.3 Combination therapy to improve HDAC inhibitors?

Another useful aspect of chapter two comes from the identification of pathways that converge on HDAC3, namely the JNK pathway. As HDAC inhibitors seem to lack efficacy in some disease states, multiple groups have begun combining HDAC inhibitors with other small molecule therapeutics in hopes of synergistically increasing efficacy. This approach has been evaluated in multiple clinical trials, for example treatment of triple negative breast cancer cells with an HDAC inhibitor in conjunction with endocrine therapy [90, 273], or treatment with multiple kinase inhibitors, such as those that target EGFR, in conjunction with an HDAC inhibitor [274, 275]. While these trials have had some success [273, 276], additional pathways that synergize with HDAC inhibitors are likely in existance. In chapter two we provide rationale that modulating the JNK pathway in conjunction with HDAC inhibition may enhance the effects of these compounds (**Figure 22**).

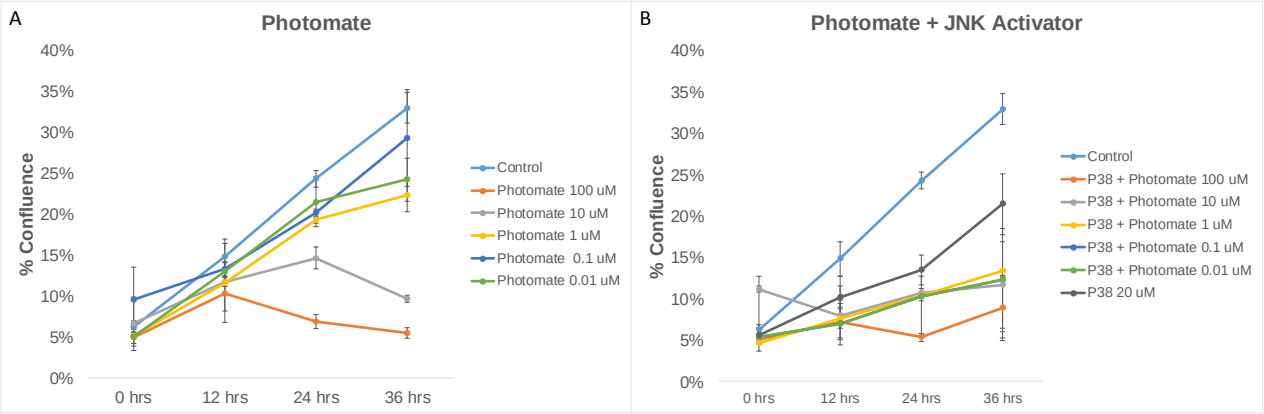

Figure 22: JNK activation sensitizes MCF-7 cells to HDAC inhibitor.

A) Treatment of cells with varying concentrations of HDAC inhibitor photomate (PRP 2), or B) photomate plus JNK pathway activating P38 inhibitor or control vehicle treatment.

5.4 Can we predict contexts where HDAC inhibitors will be effective?

Finally, clinical trials are expensive endeavors and require experimentation on human participants. As HDAC inhibitors seem to work in certain cases, but fail in others, better prognostic tools are desperately needed. Current studies have examined basal gene expression [(74)], changes in gene expression [(37)], genomic mutational state [(277)], changes in acetylated histones of circulating peripheral blood mononuclear cells (PBMCs) [(278-280)], and changes to chromatin accessibility [(281)], in order to develop an understanding of where HDAC inhibitors are going to be effective. Chapters two and three of this thesis suggest that variation in HDAC inhibitor target engagement between cell types may contribute to the disparity in response to HDAC inhibitors. Currently, measuring HDAC inhibitor engagement *in vivo* remains a challenge, as outlined in section 5.2, and no methods to examine these changes are available. Consequently, we propose that understanding the facets that contribute to HDAC inhibitor engagement in

cells may help predict their target engagement *in vivo*. For example, we can now say that measuring HDAC3 phosphorylation may be a good indication of HDAC inhibitor binding to HDAC3 *in vivo*. Therefore, development of a better understanding of other factors contributing to target engagement in cells represents an important endeavor to unlock the full potential of HDAC inhibitor efficacy for a variety of disease states.

APPENDICES

APPENDIX A: CLASS I HDAC QUANTIFICATION IN MCF-7 CELLS AS DETERMINED BY COMPARISON TO STANDARD DILUTIONS OF RECOMBINANT HDAC

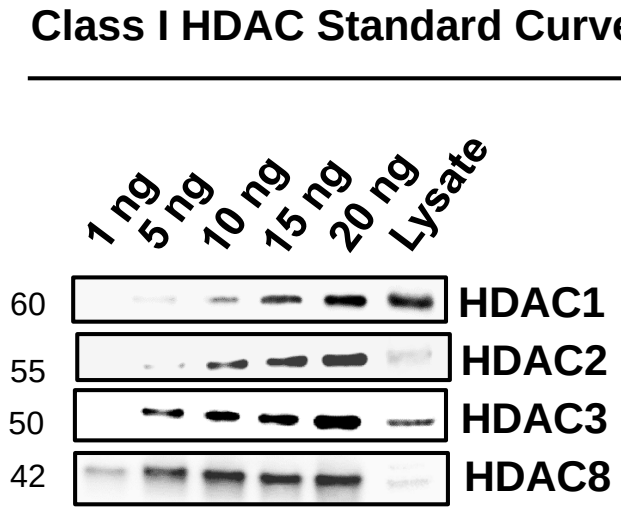

APPENDIX A: CLASS I HDAC QUANTIFICATION IN MCF-7 CELLS AS DETERMINED BY COMPARISON TO STANDARD DILUTIONS OF RECOMBINANT HDAC. WESTERN BLOTS OF INCREASING AMOUNTS OF RECOMBINANT HDACS FOLLOWED BY MCF-7 CELL LYSATE. ANTIBODIES FOR EACH INDIVIDUAL CLASS I HDAC WERE USED FOR VISUALIZATION.

APPENDIX B: PHOTOMATE SELECTIVITY IS DEPENDENT UPON BREAST CANCER CELL TYPE

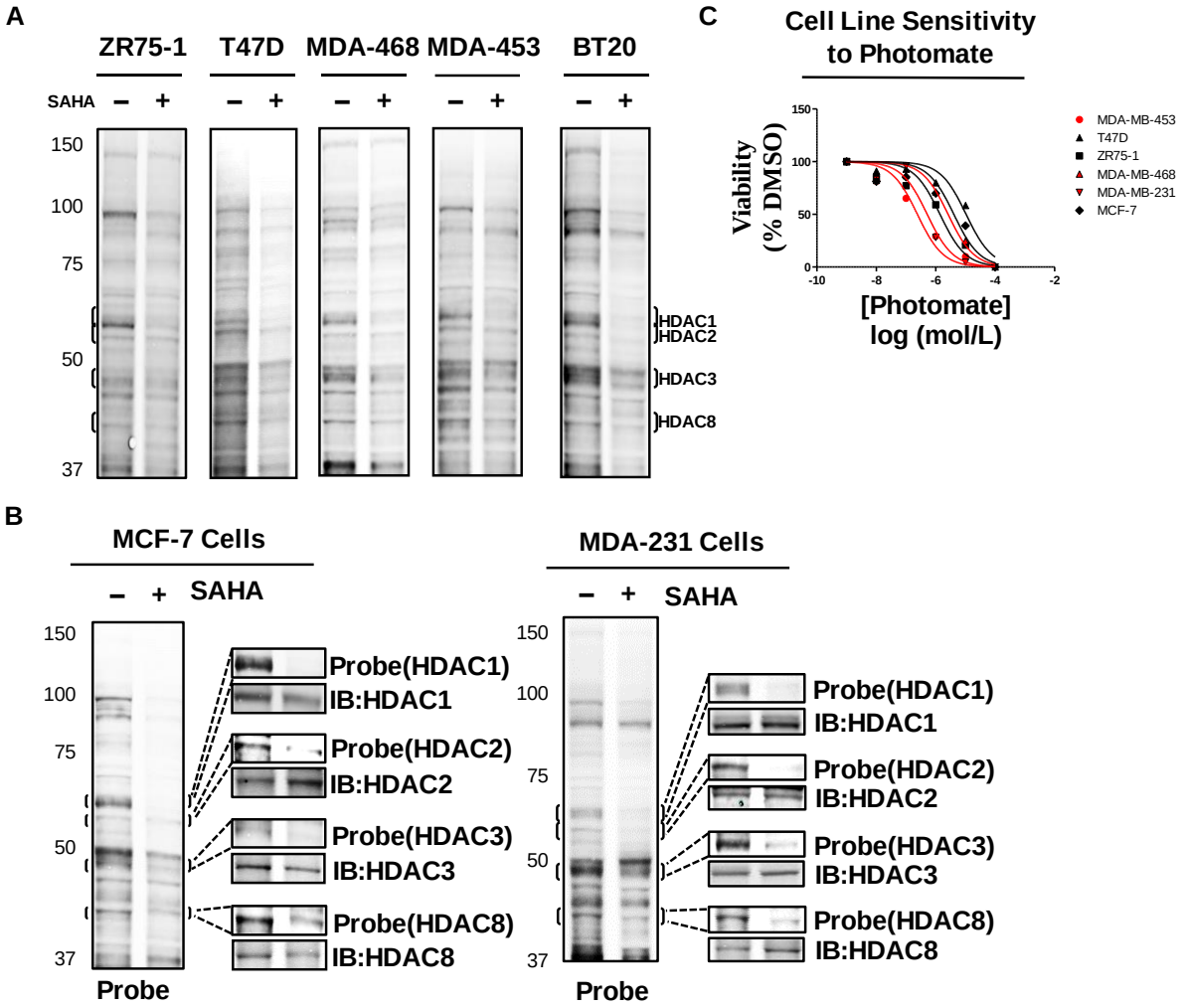

PHOTOMATE SELECTIVITY IS DEPENDENT UPON BREAST CANCER CELL TYPE. A) GEL BASED VISUALIZATION OF BREAST CANCER CELL LINES LABELED IN SITU WITH PHOTOMATE OR PHOTOMATE AND EXCESS SAHA. B) GEL BASED VISUALIZATION OF MCF-7 OR MDA-MB-231 CELLS LABELED WITH PHOTOMATE OR PHOTOMATE AND SAHA. TO THE RIGHT OF BLOT IS AN EXPANDED VIEW OF THE SAME GEL SHOWING PHOTOMATE SIGNAL (ABOVE) OR ANTIBODY RECOGNITION (BELOW) OF THE BANDS LABELED BY PHOTOMATE. INDIVIDUAL ANTIBODIES FOR CLASS I HDACS 1, 2, 3 AND 8 WERE USED. ALL RESULTS ARE REPRESENTATIVE OF AT LEAST 3 INDEPENDENT EXPERIMENTS. C) CRYSTAL VIOLET ANALYSIS OF CELL LINES TREATED WITH INCREASING CONCENTRATIONS OF PHOTOMATE FOR 48 HOURS. BASAL CELL LINES ARE SHOWN IN RED. DATA IS SHOWN AS MEAN ± S.D.

APPENDIX C: RELATIVE QUANTITATION OF HDAC3 PTM, HDAC1 AND PJNK

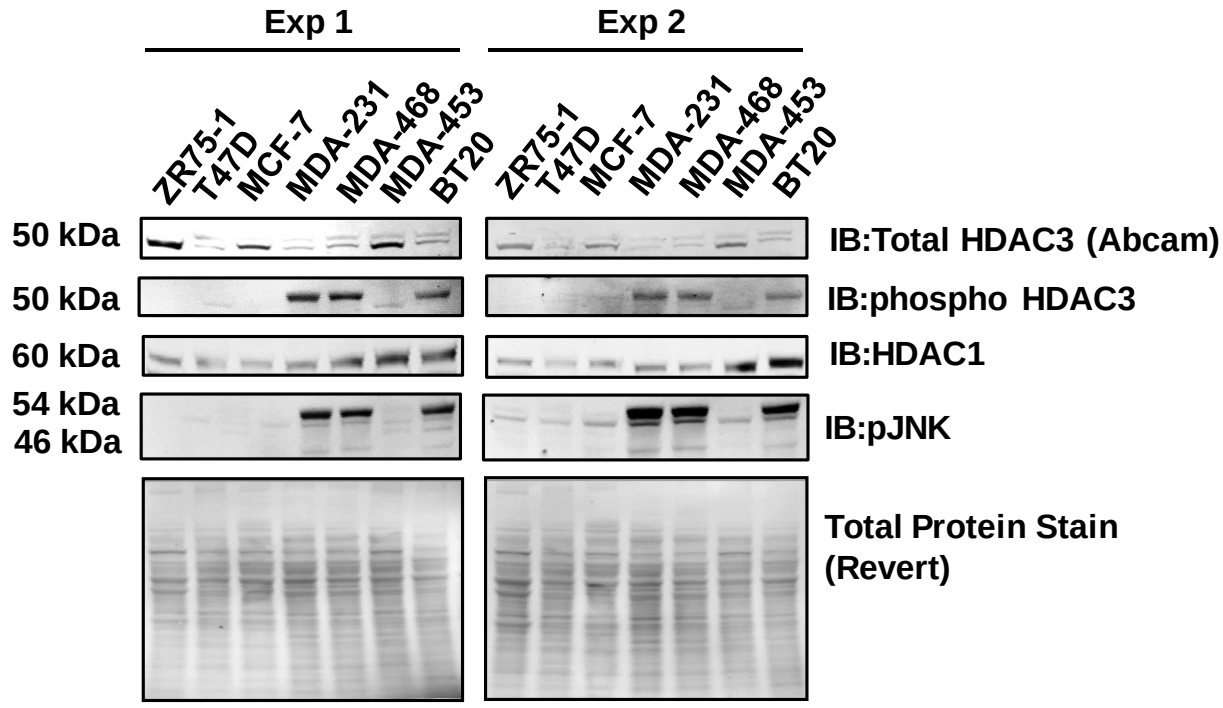

RELATIVE QUANTITATION OF HDAC3 PTM, HDAC1 AND PJNK. WESTERN BLOT ANALYSIS OF TOTAL HDAC3, PHOSPHORYLATED HDAC3, HDAC1 AND PHOSPHORYLATED JNK IDENTIFIED INDIVIDUALLY BY ANTIBODIES FOR EACH RESPECTIVE PHOSPHORYLATION STATE. TOTAL PROTEIN STAINING WAS USED FOR NORMALIZATION.

APPENDIX D: PHOTOMATE SPECIFICALLY ENRICHED PROTEINS IDENTIFIED BY MS/MS

Accession	Description	Score	Coverage	x_Proteins	x_UniquePeptides	x_Peptides	x_PSMs	x_AAs
Q96JB5	CDK5 regulatory subunit-associated protein 3 OS=Homo sapiens GN=CDK5RAP3 PE=1 SV=2 - [CK5P3_HUMAN]	76.78501	3.95	5	2	2	3	506
Q92769	Histone deacetylase 2 OS=Homo sapiens GN=HDAC2 PE=1 SV=1 - [HDAC2_HUMAN]	53.43072	3.11	3	3	3	3	482
Q13547	Histone deacetylase 1 OS=Homo sapiens GN=HDAC1 PE=1 SV=1 - [HDAC1_HUMAN]	53.43072	3.11	3	3	3	3	482
P29401	Transketolase OS=Homo sapiens GN=TKT PE=1 SV=3 - [TKT_HUMAN]	201.0585	9.95	2	6	6	7	623
P63010	AP-2 complex subunit beta OS=Homo sapiens GN=AP2B1 PE=1 SV=1 - [AP2B1_HUMAN]	72.61423	2.67	2	2	2	2	937
Q9Y6E2	Basic leucine zipper and W2 domain-containing protein 2 OS=Homo sapiens GN=BZW2 PE=1 SV=1 - [BZW2_HUMAN]	64.59809	3.58	2	2	2	2	419
P33991	DNA replication licensing factor MCM4 OS=Homo sapiens GN=MCM4 PE=1 SV=5 - [MCM4_HUMAN]	61.59709	2.09	2	2	2	2	863
Q8NF37	Lysophosphatidylcholine acyltransferase 1 OS=Homo	219.4714	14.04	1	7	7	7	534

APPENDIX D (CONTINUED)

	sapiens GN=LPCAT1 PE=1 SV=2 - [PCAT1_HUMAN]							
O60506	Heterogeneous nuclear ribonucleoprotein Q OS=Homo sapiens GN=SYNCRIP PE=1 SV=2 - [HNRPQ_HUMAN]	203.16	8.67	1	2	5	5	623
O94776	Metastasis-associated protein MTA2 OS=Homo sapiens GN=MTA2 PE=1 SV=1 - [MTA2_HUMAN]	58.74809	2.99	1	3	3	3	668
Q12874	Splicing factor 3A subunit 3 OS=Homo sapiens GN=SF3A3 PE=1 SV=1 - [SF3A3_HUMAN]	118.9505	7.58	1	4	4	4	501
Q02790	Peptidyl-prolyl cis-trans isomerase FKBP4 OS=Homo sapiens GN=FKBP4 PE=1 SV=3 - [FKBP4_HUMAN]	117.4873	10.68	1	4	4	4	459
Q9Y5Q8	General transcription factor 3C polypeptide 5 OS=Homo sapiens GN=GTF3C5 PE=1 SV=2 - [TF3C5_HUMAN]	102.7629	4.05	1	2	2	2	519
P10515	Dihydrolipoyllysine-residue acetyltransferase component of pyruvate dehydrogenase complex, mitochondrial OS=Homo sapiens GN=DLAT PE=1 SV=3 - [ODP2_HUMAN]	97.24697	4.95	1	3	3	3	647
O60341	Lysine-specific histone demethylase 1A OS=Homo sapiens GN=KDM1A PE=1 SV=2 - [KDM1A_HUMAN]	111.2377	3.64	1	3	3	3	852
P62495	Eukaryotic peptide chain release factor subunit 1 OS=Homo sapiens GN=ETF1	80.79855	7.78	1	3	3	3	437

APPENDIX D (CONTINUED)

	PE=1 SV=3 - [ERF1_HUMAN]							
O95433	Activator of 90 kDa heat shock protein ATPase homolog 1 OS=Homo sapiens GN=AHSA1 PE=1 SV=1 - [AHSA1_HUMAN]	75.60235	5.62	1	2	2	2	338
Q16401	26S proteasome non-ATPase regulatory subunit 5 OS=Homo sapiens GN=PSMD5 PE=1 SV=3 - [PSMD5_HUMAN]	72.8775	4.37	1	2	2	2	504
Q9NPQ8	Synembryn-A OS=Homo sapiens GN=RIC8A PE=1 SV=3 - [RIC8A_HUMAN]	72.14937	3.2	1	2	2	2	531
O95831	Apoptosis-inducing factor 1, mitochondrial OS=Homo sapiens GN=AIFM1 PE=1 SV=1 - [AIFM1_HUMAN]	69.91684	5.22	1	3	3	3	613
Q8WX92	Negative elongation factor B OS=Homo sapiens GN=NELFB PE=1 SV=1 - [NELFB_HUMAN]	66.60489	3.97	1	2	2	2	580
O00232	26S proteasome non-ATPase regulatory subunit 12 OS=Homo sapiens GN=PSMD12 PE=1 SV=3 - [PSD12_HUMAN]	64.39165	3.51	1	2	2	2	456
O14929	Histone acetyltransferase type B catalytic subunit OS=Homo sapiens GN=HAT1 PE=1 SV=1 - [HAT1_HUMAN]	58.54541	3.58	1	2	2	2	419
P49821	NADH dehydrogenase [ubiquinone] flavoprotein 1, mitochondrial OS=Homo sapiens GN=NDUFV1 PE=1 SV=4 - [NDUV1_HUMAN]	58.05232	4.96	1	3	3	3	464

APPENDIX D (CONTINUED)

P08559	Pyruvate dehydrogenase E1 component subunit alpha, somatic form, mitochondrial OS=Homo sapiens GN=PDHA1 PE=1 SV=3 - [ODPA_HUMAN]	57.27443	5.64	1	2	2	2	390
Q86VP6	Cullin-associated NEDD8-dissociated protein 1 OS=Homo sapiens GN=CAND1 PE=1 SV=2 - [CAND1_HUMAN]	57.22383	3.09	1	3	3	3	1230
Q9NSD9	Phenylalanine--tRNA ligase beta subunit OS=Homo sapiens GN=FARSB PE=1 SV=3 - [SYFB_HUMAN]	55.1099	3.4	1	2	2	2	589
P31948	Stress-induced-phosphoprotein 1 OS=Homo sapiens GN=STIP1 PE=1 SV=1 - [STIP1_HUMAN]	54.80635	4.6	1	2	2	2	543
Q13263	Transcription intermediary factor 1-beta OS=Homo sapiens GN=TRIM28 PE=1 SV=5 - [TIF1B_HUMAN]	50.0321	1.8	1	2	2	2	835
Q96A33	Coiled-coil domain-containing protein 47 OS=Homo sapiens GN=CCDC47 PE=1 SV=1 - [CCD47_HUMAN]	42.70394	3.52	1	2	2	2	483

PHOTOMATE SPECIFICALLY ENRICHED PROTEINS IDENTIFIED BY MS/MS

APPENDIX E: VALIDATION OF ANTIBODIES. HDAC3 PHOSPHORYLATION AND PHOTOMATE ENGAGEMENT IS NOT AFFECTED BY CASEIN KINASE 2 (CK2) INHIBITORS, ER EXPRESSION OR ER ACTIVITY

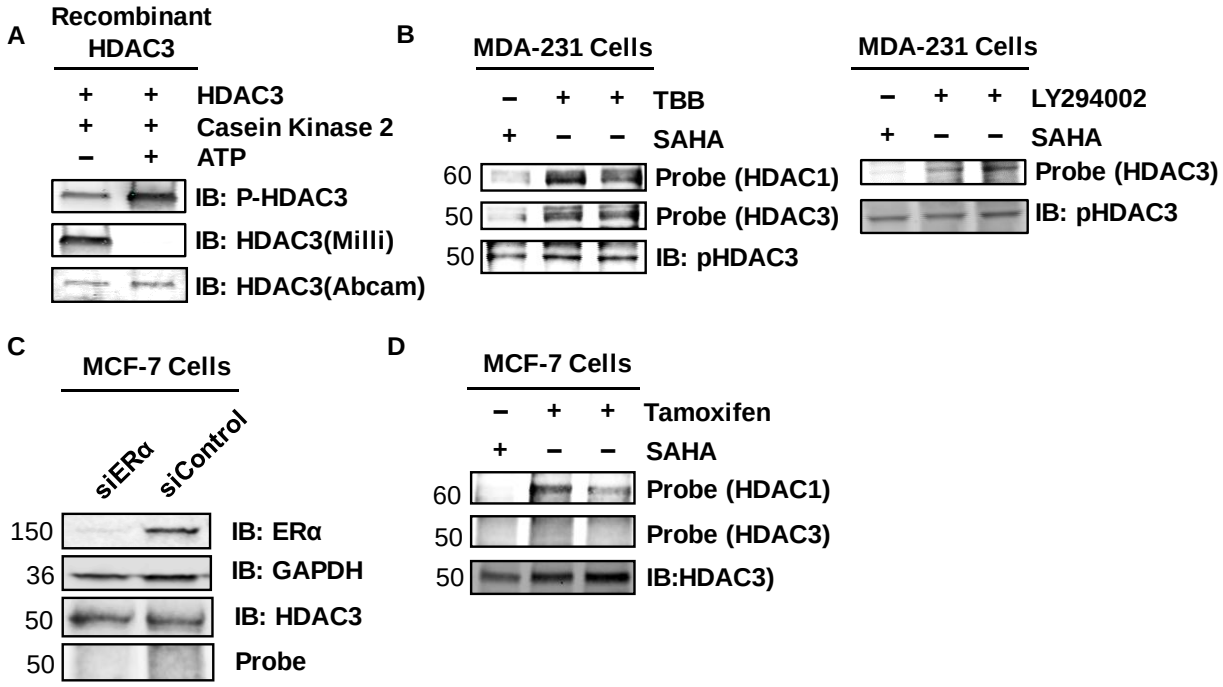

VALIDATION OF ANTIBODIES. HDAC3 PHOSPHORYLATION AND PHOTOMATE ENGAGEMENT IS NOT AFFECTED BY CASEIN KINASE 2 (CK2) INHIBITORS, ER EXPRESSION OR ER ACTIVITY. A) WESTERN BLOT ANALYSIS OF RECOMBINANT HDAC3 (LANE 1) AND RECOMBINANT HDAC3 PHOSPHORYLATED WITH CK2 (LANE 2). B) GEL BASED VISUALIZATION OF LIVE MCF-7 CELLS EITHER TREATED WITH TBB LY294002 OR VEHICLE FOLLOWED BY LABELING IN SITU WITH PHOTOMATE. C) GEL BASED VISUALIZATION OF LIVE MCF-7 CELLS EITHER TRANSFECTED WITH SIRNA FOR ERA OR VEHICLE FOLLOWED BY LABELING WITH PHOTOMATE. ANTIBODY RECOGNITION OF ERA, GAPDH OR HDAC3 IS SHOWN ABOVE FOLLOWED BY VISUALIZATION OF PHOTOMATE LABELING. D) GEL BASED VISUALIZATION OF LIVE MCF-7 CELLS EITHER TREATED WITH TAMOXIFEN OR VEHICLE (LANE 1) FOLLOWED BY LABELING WITH PHOTOMATE.

APPENDIX F: PHOTOMATE ENGAGEMENT OF HDAC3 IS AFFECTED BY SERUM, CYTOKINES AND SPECIFIC INHIBITORS OF JNK, BUT NOT P38 OR IKKB

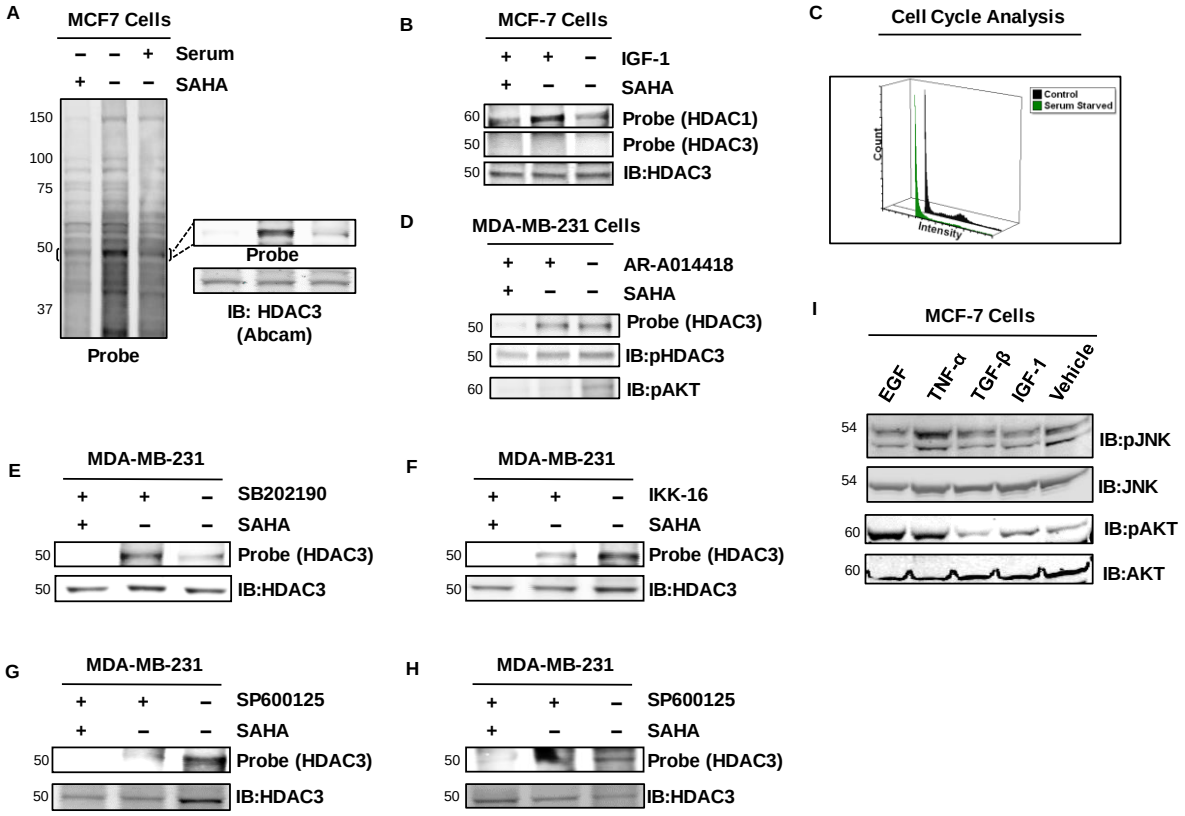

PHOTOMATE ENGAGEMENT OF HDAC3 IS AFFECTED BY SERUM, CYTOKINES AND SPECIFIC INHIBITORS OF JNK, BUT NOT P38 OR IKKB. A) REPLICATE GEL BASED VISUALIZATION OF LIVE MCF-7 CELLS EITHER SERUM STARVED FOR OR GROWN IN MEDIUM SUPPLEMENTED WITH 10% FBS, LABELED WITH PHOTOMATE OR PHOTOMATE AND SAHA AND SEPARATED ON A 12% BIS-TRIS GEL AS OPPOSED TO FIGURE 5 (FROM TEXT), WHERE A 4-12% BIS-TRIS GEL WAS USED. TO THE RIGHT IS AN EXPANDED VIEW OF THE HDAC3 LABELING AT THE 49 KDA RANGE FOR CLARITY B) GEL BASED VISUALIZATION OF LIVE MCF-7 CELLS TREATED WITH IGF-1 FOLLOWED BY LABELING WITH PHOTOMATE. PROBE LABELING OF HDAC1 IS SHOWN AS A POSITIVE LABELING CONTROL, FOLLOWED BY HDAC3 REGION. ANTIBODY BASED RECOGNITION OF HDAC3 IS SHOWN AT BOTTOM. C) HISTOGRAM OF PROPIDIUM IODIDE ANALYSIS SHOWING CELLS WERE ALIGNED IN A G0/G1 STATE AFTER SERUM STARVATION FOR 48 HOURS. D) GEL BASED VISUALIZATION OF LIVE MDA-MB-231 CELLS TREATED WITH SPECIFIC INHIBITOR OF GSK3B OR VEHICLE AND LABELED WITH PHOTOMATE OR PHOTOMATE AND EXCESS SAHA. E) AS IN D) BUT TREATMENT WITH P38 INHIBITOR OR VEHICLE F) AS IN D) BUT TREATMENT WITH IKKB INHIBITOR OR VEHICLE G) AND H) REPLICATE EXPERIMENTS FROM FIGURE 6A (FROM TEXT). I) WESTERN BLOT OF CHANGE IN PJNK OR PAKT IN RESPONSE TO CYTOKINE/GROWTH FACTOR TREATEMNT.

APPENDIX G: RECOMBINANT HDAC INHIBITOR DATA FOR PROBES AND THEIR PARENT SCAFFOLDS.

Compound	pIC_{50} ± SE				
	HDAC1	HDAC2	HDAC3	HDAC8	HDAC4
SAHA (1)	7.67 ± 0.01	6.92 ± 0.02	7.74 ± 0.02	6.61 ± 0.06	ND*
2 (PHOTOMATE)	6.26 ± 0.04	6.77 ± 0.04	6.96 ± 0.06	5.64 ± 0.11	4.42 ± 0.07
3	6.13 ± 0.07	5.95 ± 0.08	6.46 ± 0.10	5.30 ± 0.10	ND
4	6.35 ± 0.07	5.82 ± 0.04	3.65 ± 0.13	4.72 ± 0.06	ND
5	4.58 ± 0.05	3.92 ± 0.04	4.23 ± 0.05	4.12 ± 0.13	ND
Panobinostat (6)	9.52 ± 0.10	9.70 ± 0.46	9.20 ± 0.20	6.41 ± 0.20	ND
7	5.56 ± 0.07	5.32 ± 0.05	5.69 ± 0.06	5.12 ± 0.09	ND
PDA-106 (8)	6.33 ± 0.07	6.54 ± 0.05	7.66 ± 0.02	5.24 ± 0.09	ND
9	3.91 ± 0.05	3.37 ± 0.11	5.43 ± 0.08	< 3	ND
PCI-34051 (10)	5.50 ± 0.08	4.60 ± 0.03	4.94 ± 0.04	8.48 ± 0.06	ND
11	3.33 ± 0.14	4.19 ± 0.06	5.30 ± 0.03	5.67 ± 0.08	ND
TMP-269 (12)	4.33 ± 0.10	4.44 ± 0.11	4.24 ± 0.07	< 3	4.54 ± 0.11
13	3.95 ± 0.14	4.21 ± 0.04	< 3	2.81 ± 0.43	3.40 ± 0.78

*ND; not determined.

RECOMBINANT HDAC INHIBITOR DATA FOR PROBES AND THEIR PARENT SCAFFOLDS.

APPENDIX H: PERCENTAGE INHIBITION OF RECOMBINANT HDAC4

	HDAC4 % inhibition ± SD	
Compound	**10 µM**	**100 µM**
SAHA (1)	33 ± 3.8	77 ± 0.5
2	46 ± 0.9	92 ± 0.12
3	7 ± 2.5	18 ± 0.7
4	10 ± 4.6	17 ± 1.6
5	6 ± 1.8	11 ± 3.2
Panobinostat (6)	27 ± 6.6	83 ± 18.5
7	6 ± 1.5	19 ± 0.0
PDA-106 (8)	8 ± 0.9	9 ± 5.9
9	9 ± 3.5	12 ± 4.7
10	ND*	ND
11	5 ± 3.1	ND

*ND; not determined

PERCENTAGE INHIBITION OF RECOMBINANT HDAC4

APPENDIX I: RECOMBINANT ENZYME IC50-BASED SELECTIVITY RATIOS FOR PRPS AND PARENT COMPOUNDS.*

TMP-269 (12)	HDAC1	HDAC2	HDAC3	HDAC4
HDAC1		0.8	1.2	0.6
HDAC2	1.3		1.6	0.8
HDAC3	0.8	0.6		0.5
HDAC4	1.6	1.2	2.0	

PCI-34051 (10)	HDAC1	HDAC2	HDAC3	HDAC8
HDAC1		7.9	3.6	0.0
HDAC2	0.1		0.5	0.0
HDAC3	0.3	2.2		0.0
HDAC8	955.0	7516.2	3435.6	

PDA-106 (8)	HDAC1	HDAC2	HDAC3	HDAC8
HDAC1		0.6	0.0	12.4
HDAC2	1.6		0.1	20.2
HDAC3	21.2	13.1		263.6
HDAC8	0.1	0.0	0.0	

Panobinostat (6)	HDAC1	HDAC2	HDAC3	HDAC8
HDAC1		0.7	2.1	1312.2
HDAC2	1.5		3.1	1945.4
HDAC3	0.5	0.3		626.6
HDAC8	0.0	0.0	0.0	

SAHA (1)	HDAC1	HDAC2	HDAC3	HDAC8
HDAC1		5.6	0.9	11.5
HDAC2	0.2		0.2	2.1
HDAC3	1.2	6.6		13.6
HDAC8	0.1	0.5	0.1	

PRP 3	HDAC1	HDAC2	HDAC3	HDAC8
HDAC1		1.5	0.5	6.7
HDAC2	0.7		0.3	4.5
HDAC3	2.1	3.2		14.3
HDAC8	0.1	0.2	0.1	

PRP 13	HDAC1	HDAC2	HDAC8	HDAC4
HDAC1		0.6	13.8	3.6
HDAC2	1.8		25.1	6.5
HDAC8	0.1	0.0		0.3
HDAC4	0.3	0.2	3.9	

PRP 11	HDAC1	HDAC2	HDAC3	HDAC8
HDAC1		0.1	0.0	0.0
HDAC2	7.1		0.1	0.0
HDAC3	92.3	12.9		0.4
HDAC8	216.3	30.3	2.3	

PRP 9	HDAC1	HDAC2	HDAC3	HDAC8
HDAC1		3.5	0.0	8203.5
HDAC2	0.3		0.0	2365.9
HDAC3	32.6	113.0		267300.6
HDAC8	0.0	0.0	0.0	

PRP 7	HDAC1	HDAC2	HDAC3	HDAC8
HDAC1		1.8	0.7	2.8
HDAC2	0.6		0.4	1.6
HDAC3	1.3	2.4		3.7
HDAC8	0.4	0.6	0.3	

PRP 2	HDAC1	HDAC2	HDAC3	HDAC8
HDAC1		0.3	0.2	4.2
HDAC2	3.2		0.6	13.5
HDAC3	5.0	1.5		20.8
HDAC8	0.2	0.1	0.0	

PRP 4	HDAC1	HDAC2	HDAC3	HDAC8
HDAC1		3.4	498.9	43.1
HDAC2	0.3		146.2	12.6
HDAC3	0.0	0.0		0.1
HDAC8	0.0	0.1	11.6	

PRP 5	HDAC1	HDAC2	HDAC3	HDAC8
HDAC1		4.6	2.3	2.9
HDAC2	0.2		0.5	0.6
HDAC3	0.4	2.0		1.3
HDAC8	0.3	1.6	0.8	

***PARENT SCAFFOLD NAMES ARE IN RED AND PRPS NAMES ARE SHOWN IN GREEN. SELECTIVITY RATIO FOR EACH ISOFORM IS GIVEN IN THE CORRESPONDING ROW WITH RESPECT TO OTHER ISOFORMS IN INTERSECTING COLUMNS ACCORDING TO THE FORMULA: SELECTIVITY RATIO = 10^(ΔPIC50).**

APPENDIX J: CELL-BASED SELECTIVITY RATIOS FOR PRPS SHOWING LABELING OF HDACS IN MDA-MB-231 CELLS.

PRP 2	HDAC1	HDAC2	HDAC3	HDAC8
HDAC1	1.00	1.25	0.08	0.97
HDAC2	0.80	1.00	0.06	0.78
HDAC3	12.75	15.95	1.00	12.43
HDAC8	1.03	1.28	0.08	1.00

PRP 9	HDAC1	HDAC2	HDAC3	HDAC8
HDAC1	1.00	0.13	0.02	0.15
HDAC2	7.64	1.00	0.15	1.11
HDAC3	51.73	6.77	1.00	7.54
HDAC8	6.86	0.90	0.13	1.00

PRP 5	HDAC1	HDAC2	HDAC3	HDAC8
HDAC1	1.00	4.48	0.14	0.85
HDAC2	0.22	1.00	0.03	0.19
HDAC3	7.01	31.44	1.00	5.94
HDAC8	1.18	5.29	0.17	1.00

PRP 11	HDAC1	HDAC2	HDAC3	HDAC8
HDAC1	1.00	1.26	0.23	0.23
HDAC2	0.80	1.00	0.18	0.19
HDAC3	4.40	5.53	1.00	1.02
HDAC8	4.30	5.40	0.98	1.00

PRP 7	HDAC1	HDAC2	HDAC3	HDAC8
HDAC1	1.00	0.18	0.01	0.01
HDAC2	5.71	1.00	0.05	0.07
HDAC3	119.19	20.87	1.00	1.49
HDAC8	79.93	14.00	0.67	1.00

PRP 13	HDAC1	HDAC2	HDAC3	HDAC8
HDAC1	1.00	1.62	0.90	1.96
HDAC2	0.62	1.00	0.56	1.21
HDAC3	1.11	1.79	1.00	2.17
HDAC8	0.51	0.83	0.46	1.00

Cell-based selectivity ratios for PRPs showing labeling of HDACs in MDA-MB-231 cells.

APPENDIX K: PRP 2 LABELING AND HDAC1 ANTIBODY RECOGNITION OF LABELED HDAC1 IN MDA-MB-231.

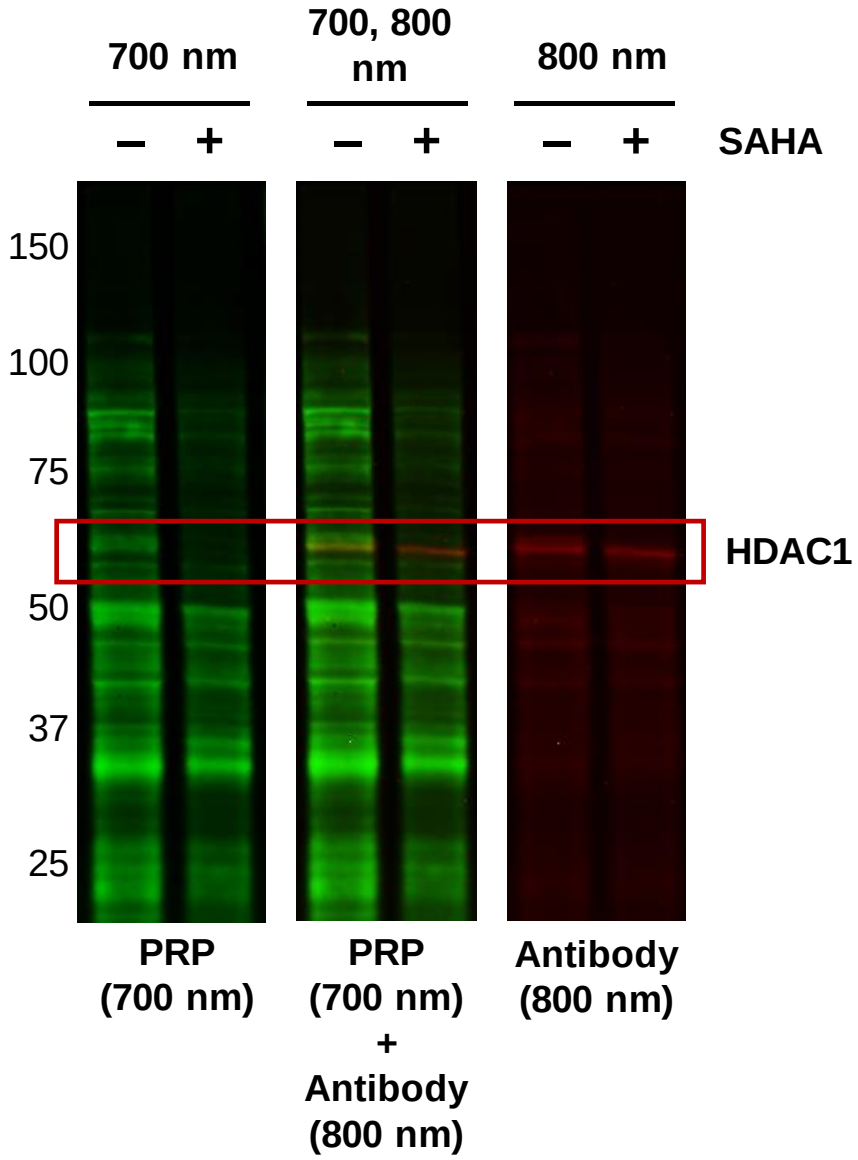

PRP 2 Labeling and HDAC1 antibody recognition of labeled HDAC1 in MDA-MB-231. Gel based visualization of live MDA-MB-231 cells labeled in situ with PRP2. Gel was visualized at 700 nm (left), showing PRP signal, 800 nm (right) to reveal HDAC1 signal, as well as 700 and 800 nm simultaneously (center), to show PRP and antibody signal overlap.

APPENDIX L: CLASS I HDAC QUANTIFICATION IN MDA-MB-231 CELLS AS DETERMINED BY COMPARISON TO STANDARD DILUTIONS OF RECOMBINANT HDAC ISOFORMS.

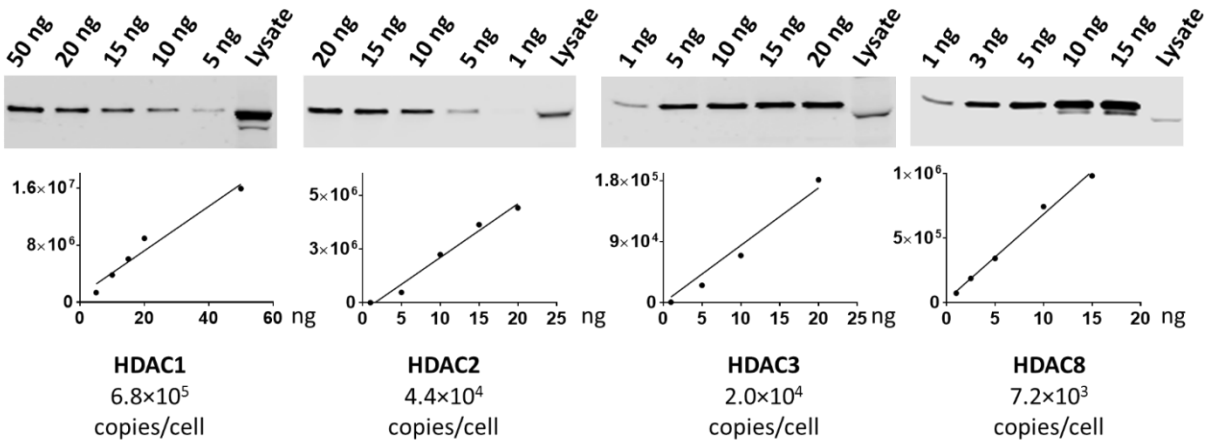

Class I HDAC quantification in MDA-MB-231 cells as determined by comparison to standard dilutions of recombinant HDAC isoforms. Standard curves were generated from densitometric analysis of western blots of serial dilutions of recombinant HDACs as shown for each isoform. Antibodies for each individual class I HDAC were used for visualization.

APPENDIX M: CALCULATION OF THE PERCENTAGE PHOSPHORYLATED HDAC3 IN MDA-MB-231 CELLS.

a

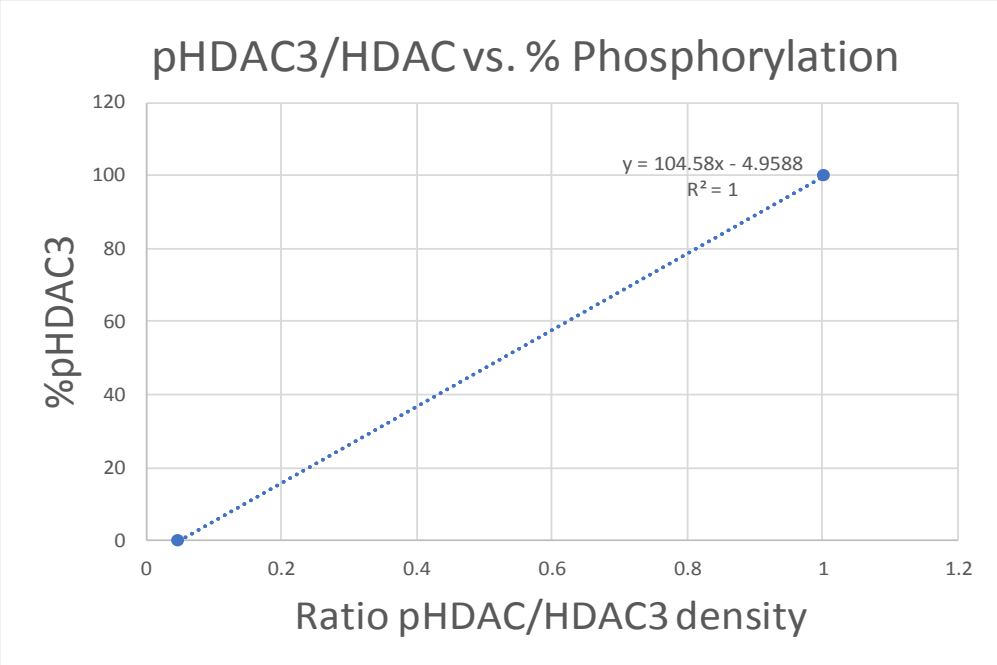

b

MDA-MB-231						
	exp1			exp 2		
	densisty	ratio to total HDAC3			ratio to total HDAC3	
Total Protein	19600000			17800000		
Total HDAC3	230000			280000		
PHDAC3	224000	0.973913043		215000	0.767857	
non pHDAC3	2220			9270		
Percent pHDAC3						
exp1	exp2	average	std deviation			
96.89302609	75.3437	86.11836304	10.77466			

Calculation of the percentage phosphorylated HDAC3 in MDA-MB-231 cells. a) Recombinant HDAC3 and recombinant phosphorylated HDAC3 (pHDAC3) were analyzed by western blot with specific antibodies for each and quantified by densitometry. The ratio pHDAC3/HDAC3 was plotted against percentage pHDAC3 and fit with a linear regression. b) Two biological replicates of lysates from MDA-MB-231 cells were then blotted with pHDAC3 and HDAC3 antibodies and the signal quantified by densitometry. The % pHDAC3 was then calculated with the linear regression from part a) using the ratio of pHDAC3/HDAC3 from MDA-MB-231 cells.

APPENDIX N: SYNTHESIS OF SAHA BASED PRP 2.

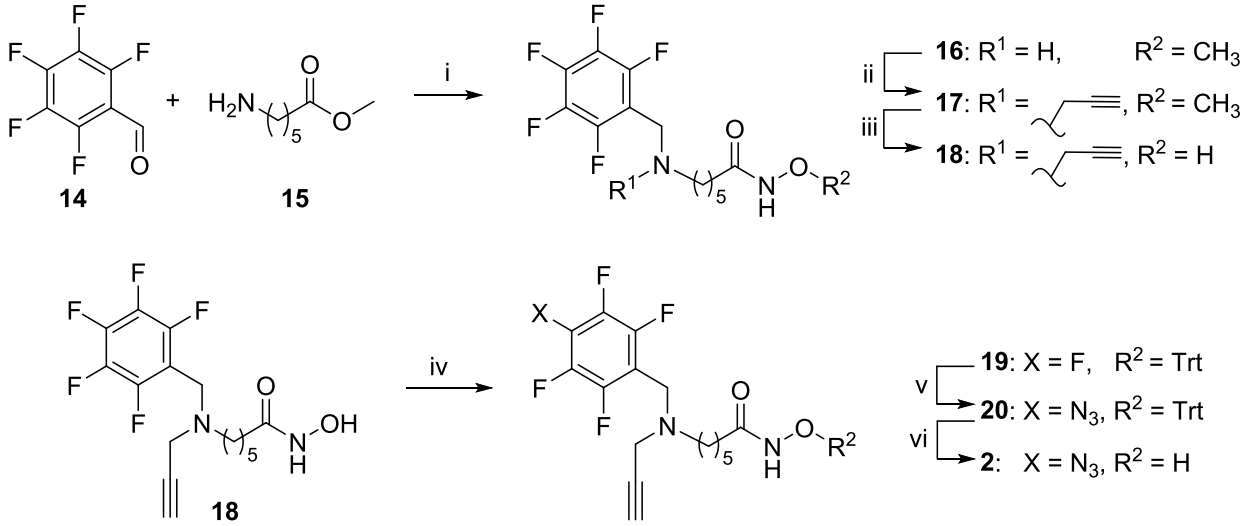

Reagents and conditions: (i) $NaBH_4$, CH_3OH, 0 °C–rt, 24 h (ii) propargyl bromide, CH_3CN, K_2CO_3, 12 h; (iii) NaOH, CH_3OH/H_2O (1:1), 3 h; (iv) *O*-tritylhydroxylamine, EDC·HCl, HOBt, DMAP, Et_3N, $CHCl_3$, 18 h; (v) NaN_3, Bu_4NN_3, DMF, 75 °C, 18 h; (vi) $MgBr_2$, DCM, 15 min.

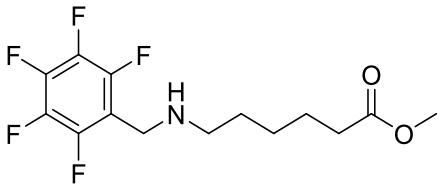

Methyl 6-(((perfluorophenyl)methyl)amino)hexanoate (16). Pentafluorbenzaldehyde, **14** (1.96 g, 10 mmol) and methyl 6-aminohexanoate hydrochloride, **15** (1.54 g, 10.6 mmol) were stirred in methanol (40 mL) with molecular sieves 4 Å under nitrogen for 3 h until imine formation was complete as monitored by TLC. After the imine had formed, the reaction was cooled to 0 °C and sodium tetrahydroborate (0.60 g, 16 mmol) was added portionwise over 20 minutes. The reaction was stirred for 24 h, filtered, concentrated in vacuo then diluted with water, made basic by addition of 10% sodium hydroxide and extracted with dichloromethane; DCM (3 × 30 mL). The combined DCM extracts were dried over anhydrous sodium sulfate, and concentrated in vacuo. The crude product was purified by silica gel chromatography eluting with gradient from 0-40% ethyl acetate; EtOAc in hexanes to give **16** as a colorless liquid (2.6 g, 80%). ^{1}H NMR (400 MHz, $CDCl_3$) δ 3.91 (s, 2H), 3.66 (s, 3H), 2.56 (t, J = 7.0 Hz, 2H), 2.30 (t, J = 7.4 Hz, 2H), 1.70 – 1.56 (m, 2H), 1.48 (m, 2H), 1.40 – 1.29 (m, 2H). ^{13}C NMR (101 MHz, $CDCl_3$) δ 174.05, 51.47, 48.57, 40.50, 33.92, 29.54, 26.71, 24.74. ^{19}F NMR (376 MHz, $CDCl_3$) δ -144.78 (dd, J = 22.8, 8.7 Hz, 2F), -156.24 (t, J = 20.7 Hz, 1F), -162.62 (td, J = 22.6, 8.8 Hz, 2F). HRMS (ESI-TOF) *m/z* calcd for $C_{14}H_{17}F_5NO_2$ $[M+H]^+$: 326.1174, found: 326.1193.

APPENDIX N (CONTINUED)

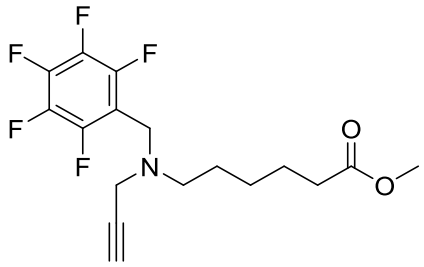

Methyl 6-(((perfluorophenyl)methyl)(prop-2-yn-1-yl)amino)hexanoate (17). The secondary amine **16** (0.88 g, 2.70 mmol) was dissolved in acetonitrile (30 mL), potassium carbonate (0.50 g, 3.60 mmol) and propargyl bromide (80% w/v in toluene, 0.34 mL, 3 mmol) were added and the mixture was stirred for 12 h. The reaction volume was reduced in vacuo, diluted with water, and extracted with DCM (3 × 30 mL). The organic phase was concentrated and the crude product was purified with silica gel chromatography eluting with gradient 5-35% EtOAc in hexanes to give **2** as a glassy solid (0.88 g, 90%). ^{1}H NMR (400 MHz, $CDCl_3$) δ 3.74 (s, 2H), 3.66 (s, 3H), 3.36 (s, 2H), 2.55 (t, *J* = 7.1 Hz, 2H), 2.29 (t, *J* = 7.5 Hz, 2H), 2.21 (t, *J* = 2.2 Hz, 1H), 1.66 – 1.54 (m, 2H), 1.49 (m, *J* = 14.5, 7.4 Hz, 2H), 1.32 (m, *J* = 15.0, 7.4 Hz, 2H). ^{13}C NMR (101 MHz, $CDCl_3$) δ 174.07, 73.22, 52.65, 51.45, 44.88, 41.90, 33.98, 26.96, 26.63, 24.70. ^{19}F NMR (376 MHz, $CDCl_3$) δ -142.06 (dd, *J* = 22.3, 8.1 Hz, 2F), -155.29 (t, *J* = 20.7 Hz, 2F), -162.41 (dt, *J* = 22.6, 8.0 Hz, 2F). HRMS (ESI-TOF) *m/z* calcd for $C_{17}H_{19}F_5NO_2$ $[M+H]^+$: 364.1331, found: 364.1354.

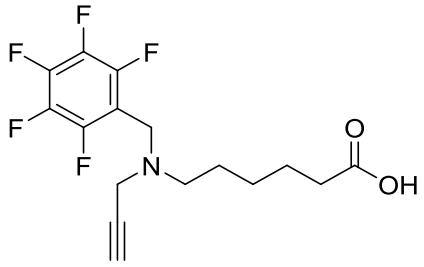

6-(((Perfluorophenyl)methyl)(prop-2-yn-1-yl)amino)hexanoic acid (18). The tertiary amine **17** (0.87 g, 2.4 mmol) was dissolved in methanol:water (1:1, 30 mL) and sodium hydroxide (0.24 g, 6 mmol) was added. The reaction was stirred at room temperature under nitrogen for 3 h. Upon completion, as monitored by TLC, the reaction was brought to pH ≈ 4.5 with 10% hydrochloric acid and extracted with DCM (3 × 30 mL). The crude product was obtained as white solid and used in the next reaction without further purification (0.76 g, 90%). ^{1}H NMR (400 MHz, $CDCl_3$) δ 3.76 (s, 2H), 3.37 (s, 2H), 2.57 (t, *J* = 6.9 Hz, 2H), 2.33 (t, *J* = 7.3 Hz, 2H), 2.21 (s, 1H), 1.62 (m, 2H), 1.55 – 1.44 (m, 2H), 1.36 (m, 2H). ^{13}C NMR (101 MHz, $CDCl_3$) δ 179.56, 73.53, 52.75, 44.97, 42.02, 34.06, 26.99, 26.71, 24.58. ^{19}F NMR (376 MHz, $CDCl_3$) δ -141.91 (dd, *J* = 15.7, 6.8 Hz, 2F), -155.12 (t, *J* = 20.3 Hz, 1F), -162.34 (td, *J* = 21.3, 7.6 Hz, 2F). HRMS (ESI-TOF) *m/z* calcd for $C_{16}H_{17}F_5NO_2$ $[M+H]^+$: 350.1174, found: 350.1196.

APPENDIX N (CONTINUED)

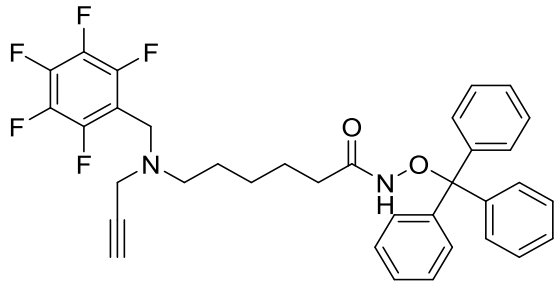

6-(((Perfluorophenyl)methyl)(prop-2-yn-1-yl)amino)-*N*-(trityloxy)hexanamide (19). To a mixture of intermediate **18** (0.70 g, 2 mmol), 3-(((ethylimino)methylene)amino)-*N*,*N*-dimethylpropan-1-amine; EDC.HCl (0.47 g, 3 mmol), 1-hydroxybenzotriazole hydrate; HOBt (0.34 g, 2.2 mmol) and 4-(dimethylamino)pyridine; DMAP (0.27 g, 2.2 mmol) in chloroform (30 mL) was added triethylamine (0.42 mL, 3 mmol) followed by immediate addition of *O*-tritylhydroxylamine (0.68 g, 2.5 mmol). The mixture was stirred at room temperature under nitrogen for 18 h. Upon completion, as monitored by TLC, the crude product was concentrated in vacuo, diluted with water, made acidic with 10% hydrochloric acid, washed with chloroform, neutralized with 10% sodium hydroxide (pH ≈ 7) and extracted with DCM (3 × 30 mL). The organic layers were collected and dried over anhydrous sodium sulfate. The crude product was then purified by silica gel chromatography eluting with a gradient of 5-35% EtOAc in hexanes to give **19** as a white solid (0.91 g, 75%). ^{1}H NMR (400 MHz, DMSO-d_6) δ 10.13 (s, 1H), 7.32 (m, 15H), 3.69 (s, 2H), 3.28 (s, 3H), 3.14 (s, 1H), 2.37 (t, J=6.9 Hz, 2H), 1.76 (t, J = 7.2 Hz 2H), 1.26 (m, 2H), 1.16 (m, 2H), 0.94 (m, 3H). ^{13}C NMR (101 MHz, DMSO-d_6) δ 170.65, 142.87, 129.35, 127.88, 127.77, 92.09, 78.60, 76.29, 52.56, 44.81, 41.57, 32.36, 26.75, 26.34, 24.98. ^{19}F NMR (376 MHz, DMSO-d_6) δ -142.41 (dd, *J* = 24.3, 6.5 Hz, 2F), -156.15 (t, *J* = 22.1 Hz, 1F), -163.01 – -163.26 (m, 2F).

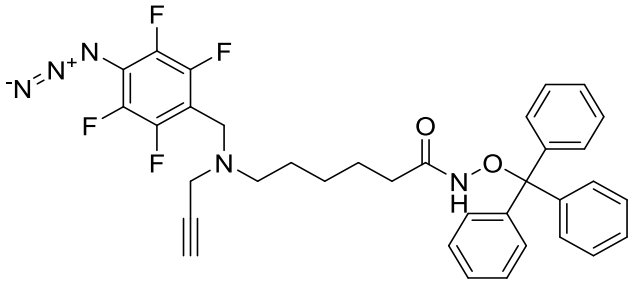

6-((4-Azido-2,3,5,6-tetrafluorobenzyl)(prop-2-yn-1-yl)amino)-*N*-(trityloxy)hexanamide (20). Sodium azide (0.91 g, 1.5 mmol), tetrabutylammonium azide (0.02 g, 0.077 mmol) and intermediate **19** (0.45 g, 0.75 mmol) were heated in dimethylformamide in a sealed pressure vessel under nitrogen atmosphere at 75 °C for 18 h. The crude product was concentrated in vacuo, and then diluted with water. The water layer was extracted with DCM (3 × 30 mL) and the organic phases combined and concentrated to afford a brown solid. The solid was then passed through a short silica gel column eluting with 37.5% EtOAc in hexanes to give **20** as a

APPENDIX N (CONTINUED)

colorless solid (0.19 g, 40%). ^{1}H NMR (400 MHz, DMSO-d_6) δ 10.14 (s, 1H), 7.32 (s, 15H), 3.67 (s, 2H), 3.28 (s, 2H), 3.15 (s, 1H), 2.37 (t, J = 6.9 Hz, 2H), 1.76 (t, J = 7.2 Hz, 2H), 1.25 (m, 2H), 1.16 (m, 2H), 0.94 (m, 2H). ^{13}C NMR (101 MHz, DMSO-d_6) δ 170.71, 142.93, 129.41, 127.94, 127.83, 112.72, 92.15, 78.69, 76.34, 52.52, 45.01, 41.71, 32.42, 26.81, 26.40, 25.03. ^{19}F NMR (376 MHz, DMSO-d_6) δ -143.32 (dd, J = 22.1, 9.5 Hz, 2F), -152.84 (dd, J = 22.4, 9.8 Hz, 2F).

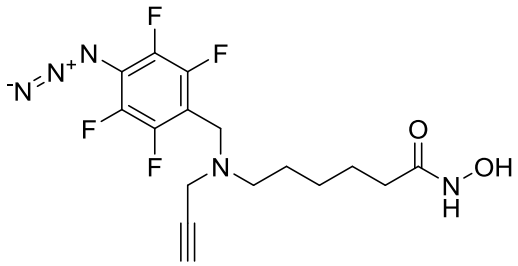

6-((4-Azido-2,3,5,6-tetrafluorobenzyl)(prop-2-yn-1-yl)amino)-*N*-hydroxyhexanamide (2). To a solution of **20** (0.19 g, 0.3 mmol) in DCM was added magnesium bromide (0.55 g, 3 mmol) and stirred at room temperature under nitrogen for 15 min. The solvent was evaporated, residue diluted with water and extracted with DCM (3 × 30 mL). The pooled extracts were concentrated, dried over anhydrous sodium sulfate and purified by silica gel chromatography eluting with a gradient of 0-10% methanol in DCM to give **2** as a colorless solid (0.09 g, 80%). ^{1}H NMR (400 MHz, DMSO-d_6) δ 10.30 (s, 1H), 8.63 (s, 1H), 3.69 (s, 2H), 3.35 – 3.27 (m, 2H), 3.13 (t, J = 2.1 Hz, 1H), 2.44 (t, J = 7.0 Hz, 2H), 1.91 (t, J = 7.3 Hz, 2H), 1.46 (m, 2H), 1.42 – 1.34 (m, 2H), 1.21 (m, 2H). ^{13}C NMR (101 MHz, DMSO-d_6) δ 169.06, 112.27, 78.32, 75.95, 52.16, 44.61, 41.32, 32.27, 26.41, 26.24, 24.98. ^{19}F NMR (376 MHz, DMSO-d_6) δ -143.32 (dd, J = 22.4, 9.8 Hz), -152.82 (dd, J = 22.7, 10.0 Hz). HRMS (ESI-TOF) *m/z* calcd for $C_{16}H_{18}F_4N_5O_2$ $[M+H]^+$: 388.1391, found: 388.1418.

APPENDIX O:. SYNTHESIS OF SAHA BASED PRPS 3 AND 4, AND O-AMINOANILIDE PRP 9

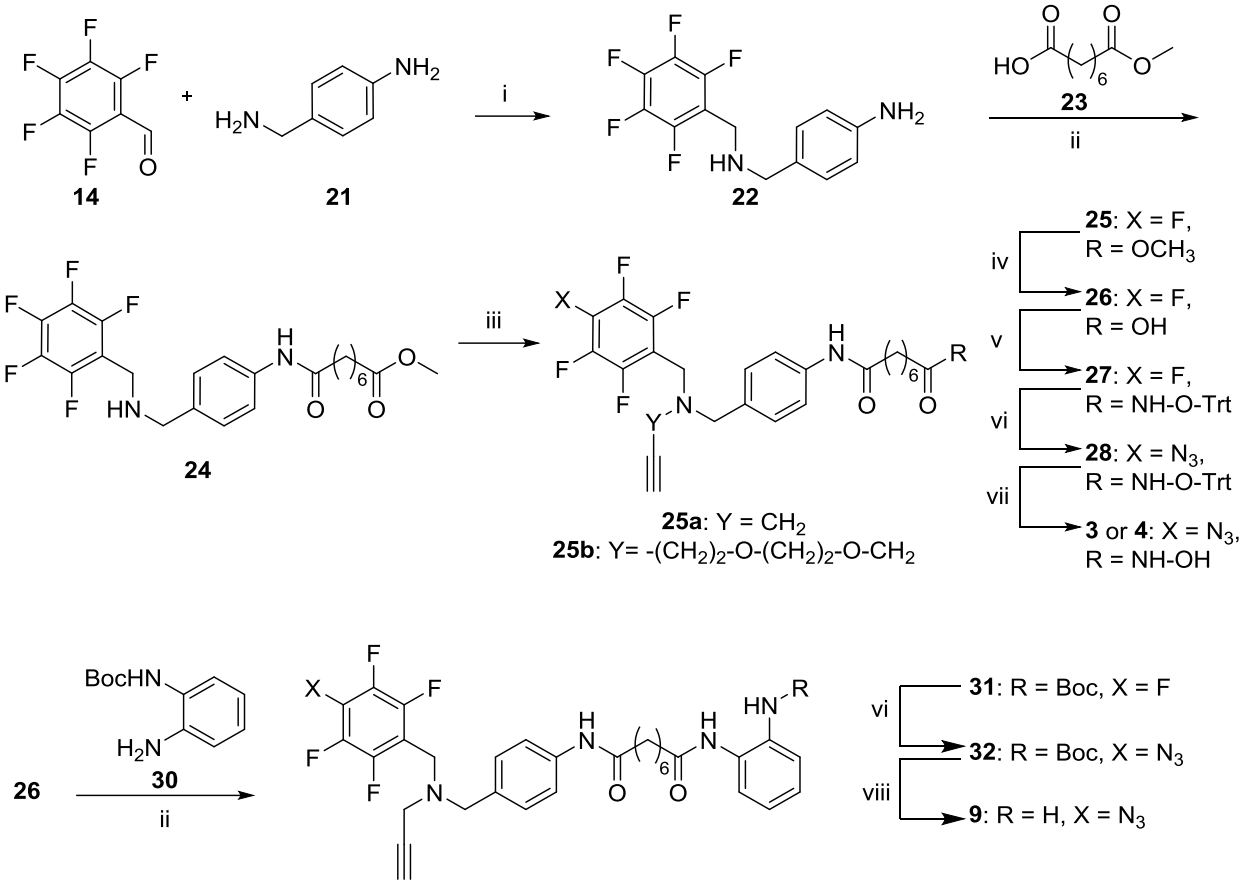

Reagents and conditions: (i) $NaBH_4$, CH_3OH, 4 h, 0 °C–rt; (ii) EDC·HCl, HOBt, Et_3N, DCM, 12h; (iii) propargyl bromide for **25a** (or 3-(2-(2-chloroethoxy)ethoxy)prop-1-yne) for **25b**, K_2CO_3, CH_3CN, 6h; (iv) LiOH, 2:1 THF/H_2O, 8h; (v) *O*-tritylhydroxylamine, EDC·HCl, HOBt, Et_3N, DCM, RT, 12h; (vi) NaN_3, Bu_4NN_3, DMF, 75-80 °C, 15 h for **28**, 20 h for **32**; (vii) $MgBr_2$, DCM, 10 min; (viii) 4M HCl in 1,4-dioxane, 1,4-dioxane, 3h.

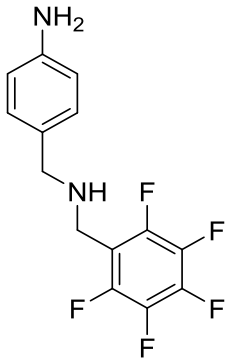

4-((((Perfluorophenyl)methyl)amino)methyl)aniline (22). A solution of perfluorobenzaldehyde **14** (1.0 g, 5.1 mmol) in methanol (20 mL) was added to a solution of 4-

APPENDIX O (CONTINUED)

(aminomethyl)aniline **21** (0.62 g, 5.1 mmol) in methanol over 4Å molecular sieves (0.5 g) and stirred for 1 h. After completion of reaction as monitored by TLC, sodium tetrahydroborate (0.77 g, 20.4 mmol) was added portionwise to the reaction mixture and stirred for additional 4 h at room temperature. Following filtration and solvent evaporation, water (20 mL) was added and extracted with ethyl acetate (2 × 20 mL). Resulted organic layers were dried over anhydrous sodium sulfate and concentrated in vacuo. The crude product was purified by silica gel chromatography eluting 30% EtOAc in hexane to give **22** in a 50 % yield. ^{1}H NMR (400 MHz, DMSO-d_6) δ 6.95 (d, J = 8.1 Hz, 2H), 6.49 (d, J = 8.2 Hz, 2H). 4.89 (bs, 2H), 3.74 (s, 2H), 3.50 (s, 2H). ^{13}C NMR (101 MHz, DMSO-d_6) δ 147.81, 129.06, 127.45, 114.04, 52.34.

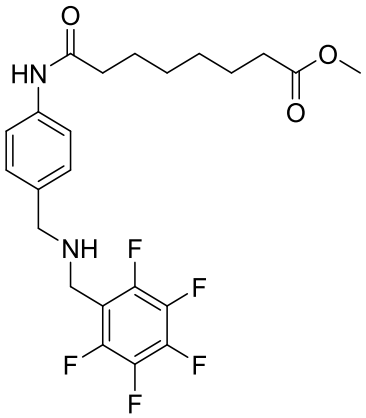

Methyl 8-oxo-8-((4-((((perfluorophenyl)methyl)amino)methyl)phenyl)amino)octanoate (24). To a solution of **22** (1.0 g, 3.31 mmol) and suberic acid monomethyl ester, **23** (0.62 g, 3.31 mmol) in dichloromethane (15 mL), HOBt (0.45 g, 3.31 mmol), EDC (0.63 g, 3.31 mmol), triethylamine (0.51 mL, 3.64 mmol) and DMAP (catalytic) were added. The reaction was stirred at room temperature for 16 h until completion then diluted with water (25mL). The DCM layer was washed with saturated sodium bicarbonate (10 mL) and brine sequentially, then dried over anhydrous sodium sulfate and solvent evaporated in vacuo. The crude product was purified by silica gel chromatography eluting 60% EtOAc in hexanes to give **24** in a 75% yield. ^{1}H NMR (400 MHz, DMSO-d_6) δ 9.79 (s, 1H), 7.50 (d, J = 8.1 Hz, 2H), 7.22 (d, J = 8.1 Hz, 2H), 3.76 (s, 2H), 3.62 (s, 2H), 3.58 (s, 3H), 2.31-2.26 (m, 4H), 1.57-1.55 (m, 4H), 1.32-1.29 (m, 4H). ^{13}C NMR (101 MHz, DMSO-d_6) δ 173.4, 128.1, 128.3, 118.8, 51.6, 51.2, 36.3, 33.3, 28.3, 25.0, 24.4.

APPENDIX O (CONTINUED)

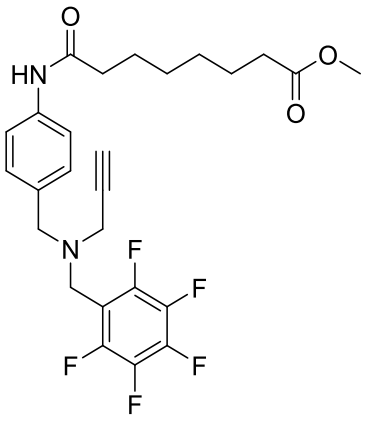

Methyl-8-oxo-8-((4-((((perfluorophenyl)methyl)(prop-2-yn-1-yl)amino)methyl)phenyl)amino)octanoate (25a). To a solution of **24** (800 mg, 1.69 mmol) and potassium carbonate (234 mg, 1.69 mmol) in acetonitrile (10 mL), propargyl bromide (241 mg, 2.03 mmol) was added dropwise. The reaction mixture was stirred for 2 h at room temperature then the solvent was evaporated. The residue was diluted with water (25 mL) and extracted with DCM (25 mL). The DCM layer was washed with saturated sodium bicarbonate solution (15 mL) and brine (5 mL) sequentially then dried over anhydrous sodium sulfate and solvent evaporated in vacuo. The crude was purified by silica gel chromatography eluting 30% EtOAc in hexanes to give **25a** in 90% yield. ^{1}H NMR (400 MHz, DMSO-d_6) δ 9.82 (s, 1H), 7.52 (d, J = 8.3 Hz, 2H), 7.18 (d, J = 8.3 Hz, 2H), 3.76 (s, 2H), 3.60 (s, 2H), 3.57 (s, 3H), 3.23 (s, 2H), 2.31-2.24 (m, 4H), 1.60-1.48 (m, 4H), 1.31-1.25 (m, 4H). ^{13}C NMR (101 MHz, DMSO-d_6) δ. 169.2, 138.6, 138.1, 132.3, 129.1, 118.8, 78.0, 76.4, 42.2, 36.4, 34.1, 28.5, 25.1, 24.6. HRMS (ESI-TOF) *m/z* calcd for $C_{26}H_{28}F_5N_2O_3$ $[M+H]^+$: 511.2015, found: 511.2012.

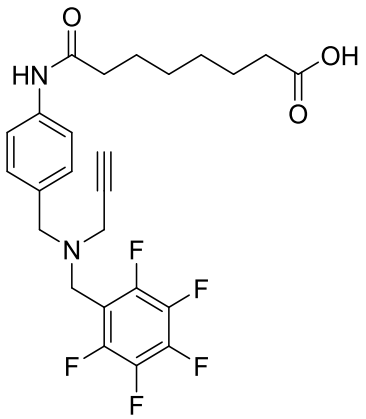

8-Oxo-8-((4-((((perfluorophenyl)methyl)(prop-2-yn-1-yl)amino)methyl)phenyl)amino)octanoic acid (26a). To a solution of **25a** (500 mg, 0.94 mmol) in 1:1 tetrahydrofuran/water (6 mL), lithium hydroxide (112 mg, 4.68 mmol) was added and stirred at room temperature for 4 h. After complete hydrolysis, the reaction mixture was concentrated in vacuo, acidified with 2N hydrochloric acid to pH ≈ 1, diluted with brine and

APPENDIX O (CONTINUED)

extracted with EtOAc (2 × 10 mL). The organic layers were dried over anhydrous sodium sulfate and concentrated to afford **26a** as a colorless oil (427 mg, 92%) that was used in next steps without further purification. ^{1}H NMR (400 MHz, DMSO-d_6) δ 9.85 (s, 1H), 7.52 (d, J = 8.3 Hz, 2H), 7.18 (d, J = 8.3 Hz, 2H), 3.75 (s, 2H), 3.59 (s, 2H), 3.22 (s, 2H), 2.27 (t, J = 7.4 Hz, 2H), 2.16 (t, J = 7.3 Hz, 2H), 1.87 (s, 1H), 1.61-1.44 (m, 4H), 1.31-1.25 (m, 4H). ^{13}C NMR (101 MHz, DMSO-d_6) δ 171.2, 138.6, 138.1, 132.3, 129.1, 118.8, 78.0, 76.4, 56.6, 42.2, 36.4, 34.1, 28.5, 25.1, 24.6. HRMS (ESI-TOF) *m/z* calcd for $C_{25}H_{26}F_5N_2O_3$ $[M+H]^+$: 497.1858, found: 497.1843.

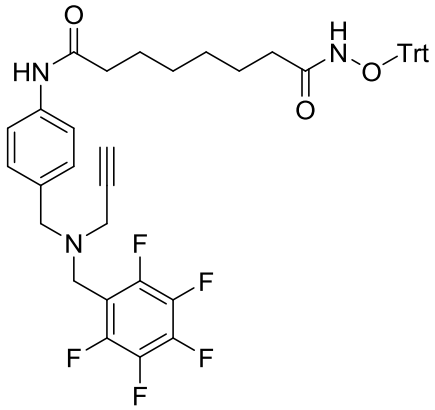

***N*^{1}-(4-((((Perfluorophenyl)methyl)(prop-2-yn-1-yl)amino)methyl)phenyl)-*N*^{8}-(trityloxy)octanediamide (27a).** To a stirred solution of **26a** (400 mg, 0.81 mmol) in DCM (10 mL) was added EDC (185 mg, 0.96 mmol), HOBt (131 mg, 0.96 mmol), triethylamine (96 mg, 0.81 mmol), and *O*-tritylhydroxylamine (222 mg, 0.81 mmol). The reaction mixture was stirred for 16 h and then diluted with DCM (10 mL), washed with water (10 mL) then brine (10 mL). The organic layer was dried over anhydrous sodium sulfate, filtered, and concentrated under reduced pressure. The crude product was purified by silica gel chromatography using 10-35% EtOAc in hexanes to afford **27a** as a white solid (485 mg, 80%). ^{1}H NMR (400 MHz, DMSO-d_6) δ 10.15 (s, 1H), 9.82 (s, 1H), 7.52 (d, J = 8.3 Hz, 2H), 7.37-7.26 (m, 15H), 7.19 (d, J = 8.3 Hz, 2H), 3.75 (s, 2H), 3.61 (s, 2H), 3.33 (s, 1H). 3.23 (s, 2H), 2.23 (t, J = 7.3 Hz, 2H), 1.80-1.74 (m, 2H), 1.52-1.44 (m, 2H), 1.22-1.10 (m, 4H), 1.03-0.96 (m, 2H). ^{13}C NMR (101 MHz, DMSO-d_6) δ 171.2, 142.5, 138.6, 132.3, 129.0, 127.5, 118.8, 91.8, 77.9, 76.4, 56.6, 44.2, 41.2, 36.4, 32.1, 28.4, 28.3, 25.0, 24.7. HRMS (ESI-TOF) *m/z* calcd for $C_{44}H_{39}F_5N_3O_3$ $[M-H]^-$: 752.2917, found: 752.2925.

APPENDIX O (CONTINUED)

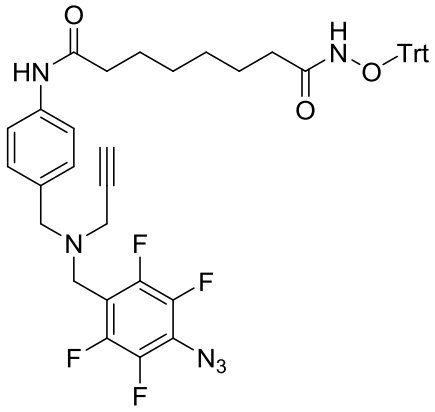

***N*[1]-(4-(((4-Azido-2,3,5,6-tetrafluorobenzyl)(prop-2-yn-1-yl)amino)methyl)phenyl)-*N*[8]-(trityloxy)octanediamide (28a).** To a solution of **27a** (300 mg, 0.39 mmol) in anhydrous dimethylformamide (5 mL), sodium azide (26 mg, 0.39 mmol) and tetrabutylammonium azide (catalytic) were added in a sealed pressure vessel. The reaction mixture was stirred at 80 °C for 20 h. After cooling, it was poured in an ice/water mixture and extracted with ethyl acetate (2 × 10 mL). The organic extract was dried over anhydrous magnesium sulfate, filtered and concentrated. The crude was purified by short silica gel column eluting EtOAc in hexanes to give **28a** in 60% yield. ^{1}H NMR (400 MHz, DMSO-d_6) δ 10.15 (s, 1H), 9.82 (s, 1H), 7.52 (d, J = 8.3 Hz, 2H), 7.37-7.26 (m, 15H), 7.19 (d, J = 8.3 Hz, 2H), 3.75 (s, 2H), 3.61 (s, 2H), 3.33 (s, 1H). 3.23 (s, 2H), 2.23 (t, J = 7.3 Hz, 2H), 1.80-1.74 (m, 2H), 1.52-1.44 (m, 2H), 1.22-1.10 (m, 4H), 1.03-0.96 (m, 2H). ^{13}C NMR (101 MHz, DMSO-d_6) δ 171.2, 142.5, 138.6, 132.3, 129.0, 127.5, 118.8, 91.8, 77.9, 76.4, 56.6, 44.2, 41.2, 36.4, 32.1, 28.4, 28.3, 25.0, 24.7.

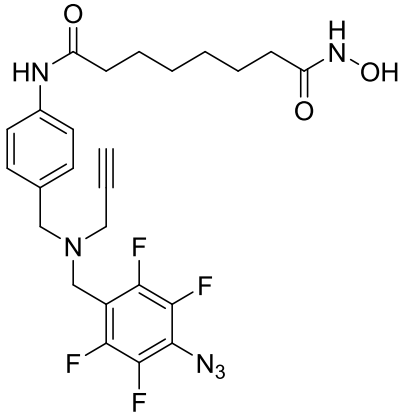

***N*[1]-(4-(((4-Azido-2,3,5,6-tetrafluorobenzyl)(prop-2-yn-1-yl)amino)methyl)phenyl)-*N*[8]-hydroxyoctanediamide (3)**. To a stirred solution of **28a** (200 mg, 0.26 mmol) in DCM (5 ml), magnesium bromide (220 mg, 2.06 mmol) was added and stirred at room temperature under nitrogen for 10 min. After completion the solvent was evaporated in vacuo, residue diluted with water and extracted with DCM. The DCM extract was dried over anhydrous magnesium sulfate, filtered and concentrated in vacuo. The crude product was purified by column chromatography

APPENDIX O (CONTINUED)

eluting 0-10% methanol in DCM to yield **3** in 65% yield. ^{1}H NMR (400 MHz, DMSO-d_6) δ 10.31 (s, 1H), 9.83 (s, 1H), 8.64 (s, 1H), 7.52 (d, *J* = 8.3 Hz, 2H), 7.33-7.28 (m, 2H), 3.74 (s, 2H), 3.59 (s, 2H), 3.22 (s, 2H). 2.91-2.87 (m, 1H), 2.74-2.72 (m, 1H), 2.30-2.23 (m, 2H), 1.95-1.88 (m, 2H), 1.60-1.44 (m, 2H), 1.31-1.20 (m, 4H). ^{13}C NMR (101 MHz, DMSO-d_6) δ 171.2, 169.1, 138.5, 132.3, 129.0, 126.7, 118.9, 80.6, 78.1, 76.5, 56.5, 44.3, 36.4, 32.3, 28.5, 25.1. HRMS (ESI-TOF) *m/z* calcd for $C_{25}H_{27}F_4N_6O_3$ $[M+H]^+$: 535.2076, found: 535.2077.

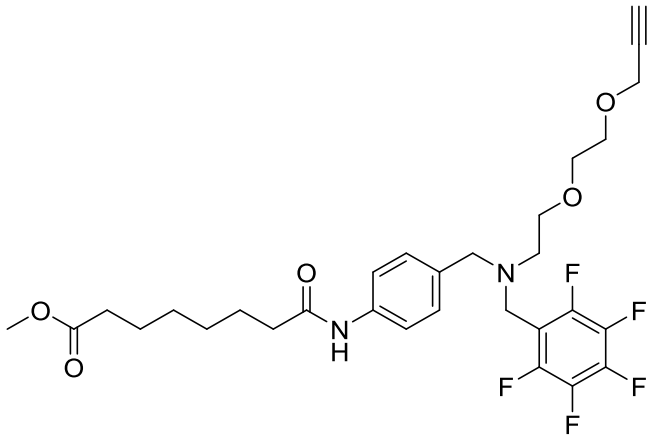

Methyl 8-oxo-8-((4-((((perfluorophenyl)methyl)(2-(2-(prop-2-yn-1-yloxy)ethoxy)ethyl)amino)methyl)phenyl)amino)octanoate (25b). Step 1: 2-(2-chloroethoxy)ethan-1-ol (1 g, 8 mmol) was dissolved in dimethylformamide (5 mL) and cooled in an ice-bath. Sodium hydride (480 mg, 12 mmol) was added and stirred for 15 min then propargyl bromide (80% w/v in toluene, 1.7 mL, 16 mmol) was added dropwise. The reaction was stirred for 3 h under nitrogen the reaction was quenched with 10% hydrochloric acid to pH ≈ 3, diluted with water and extracted with DCM (30 mL). The organic extract was washed with brine (2 × 30 mL), dried over anhydrous sodium sulfate, concentrated in vacuo. The crude was purified by column chromatography eluting 5-50% EtOAc in hexanes to give 3-(2-(2-chloroethoxy)ethoxy)prop-1-yne in 80% yield. ^{1}H NMR (400 MHz, $CDCl_3$) δ 4.21 (d, *J* = 2.3 Hz, 2H), 3.76 (t, *J* = 5.9 Hz, 2H), 3.71 (s, 4H), 3.64 (t, *J* = 5.9 Hz, 2H), 2.45 (t, *J* = 2.3 Hz, 1H). **Step 2:** To a solution of **24** (500 mg, 1.06 mmol) in acetonitrile (10 mL), 3-(2-(2-chloroethoxy)ethoxy)prop-1-yne (241 mg, 1.54 mmol), potassium carbonate (210 mg, 1.52 mmol) and potassium iodide (200 mg, 1.20 mmol) were added. The reaction mixture was stirred for 12 h at 70 °C then the solvent was evaporated. The residue was diluted with water (25 mL) and extracted with DCM (25 mL). The DCM layer was dried over anhydrous sodium sulfate and solvent evaporated in vacuo. The crude was purified by silica gel chromatography eluting 30% EtOAc in hexanes to give **25b** in 40% yield. ^{1}H NMR (400 MHz, $CDCl_3$) δ 7.43 (s, 2H), 7.25 (t, *J* = 9.5 Hz, 2H), 4.20 (d, *J* = 15.3 Hz, 2H), 3.81 (s, *J* = 41.2 Hz, 2H), 3.66 (d, *J* = 2.5 Hz, 6H), 3.59 (d, *J* = 7.1 Hz, 5H), 2.68 (s, 2H), 2.45 – 2.37 (m, 1H), 2.34 – 2.27 (m, 4H), 1.78 – 1.58 (m, 4H), 1.43 – 1.24 (m, 4H). ^{13}C NMR (101 MHz, $CDCl_3$) δ 173.83, 170.83, 145.81, 136.64, 134.28, 128.73, 127.09, 119.13, 114.93, 79.19, 74.11, 69.81, 69.32, 68.67, 57.97, 57.87, 52.18, 51.07, 45.44, 37.10, 33.53, 28.32, 24.92, 24.27.

APPENDIX O (CONTINUED)

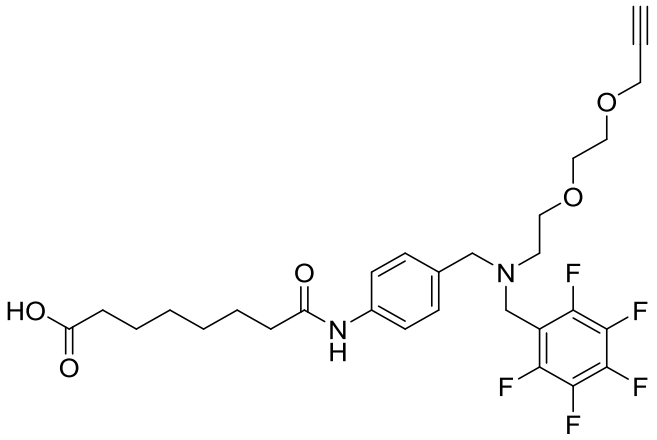

8-Oxo-8-((4-((((perfluorophenyl)methyl)(2-(2-(prop-2-yn-1-yloxy)ethoxy)ethyl)amino)methyl)phenyl)amino)octanoic acid (26b). To a solution of **JN-01-09** (300 mg, mmol) in 1:1 tetrahydrofuran/water (4 mL), lithium hydroxide (80 mg, mmol) was added and stirred at 35 °C for 4 h. After complete hydrolysis, the reaction mixture was concentrated in vacuo, acidified with 2N hydrochloric acid to pH ≈ 1, diluted with brine and extracted with EtOAc (2 × 10 mL). The organic layers were dried over anhydrous sodium sulfate and concentrated to afford **26b** in 92% yield that was used in next steps without further purification. ^{1}H NMR (400 MHz, $CDCl_3$) δ 8.09 (s, 9H), 7.46 (d, *J* = 8.0 Hz, 24H), 7.21 (d, *J* = 8.0 Hz, 24H), 7.16 – 6.78 (m, 20H), 6.61 (dt, *J* = 17.6, 8.3 Hz, 16H), 6.31 – 6.07 (m, 54H), 4.26 – 4.09 (m, 32H), 3.84 – 3.81 (m, 5H), 3.68 – 3.62 (m, 32H), 3.62 – 3.51 (m, 73H), 3.47 – 3.40 (m, 44H), 2.67 (t, *J* = 5.4 Hz, 23H), 2.29 (dt, *J* = 24.7, 7.1 Hz, 64H), 2.03 (d, *J* = 14.9 Hz, 29H), 1.62 (dd, *J* = 40.6, 6.2 Hz, 76H), 1.40 – 1.19 (m, 82H).

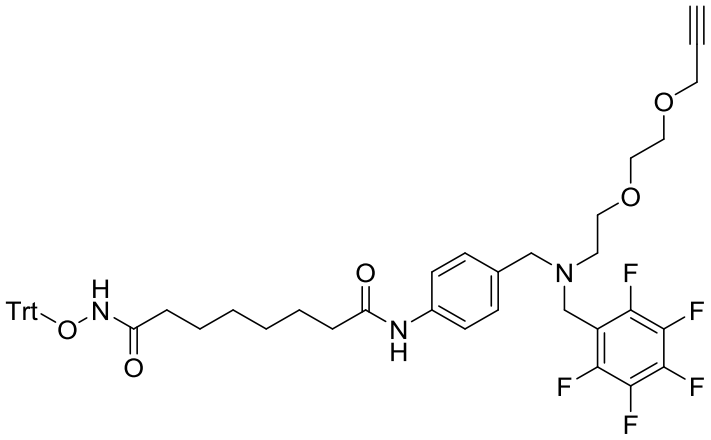

***N*^{1}-(4-((((perfluorophenyl)methyl)(2-(2-(prop-2-yn-1-yloxy)ethoxy)ethyl)amino)methyl)phenyl)-*N*^{8}-(trityloxy)octanediamide (27b).** To a stirred solution of **26b** (300 mg, 0.52 mmol) in DCM (7 mL) was added EDC (130 mg, 0.68 mmol), HOBt (100 mg, 0.74 mmol), triethylamine (0.1 mL, 0.72 mmol), and *O*-tritylhydroxylamine (168

APPENDIX O (CONTINUED)

mg, 0.61 mmol). The reaction mixture was stirred for 16 h and then diluted with DCM (10 mL), washed with water (10 mL) then brine (10 mL). The organic layer was dried over anhydrous sodium sulfate, filtered, and concentrated under reduced pressure. The crude product was purified by silica gel chromatography using 10-35% EtOAc in hexanes to afford **27b** in 70% yield. ^{1}H NMR (400 MHz, $CDCl_3$) δ 7.75 (t, *J* = 30.6 Hz, 2H), 7.57 – 7.27 (m, 20H), 7.24 (d, *J* = 7.4 Hz, 2H), 4.21 (d, *J* = 15.2 Hz, 2H), 3.83 (s, 2H), 3.67 (s, 2H), 3.61 (d, *J* = 5.5 Hz, 6H), 2.69 (s, 2H), 2.43 (s, 1H), 2.38 – 2.17 (m, 2H), 1.64 (d, *J* = 5.9 Hz, 4H), 1.26 (d, *J* = 13.0 Hz, 4H). ^{13}C NMR (101 MHz, $CDCl_3$) δ 177.21, 171.49, 144.39, 141.79, 141.07, 137.24, 136.08, 134.48, 129.09, 129.03, 128.12, 119.53, 115.37, 113.29, 112.35, 79.60, 74.55, 70.21, 69.74, 69.08, 58.38, 58.30, 52.57, 51.21, 45.86, 37.38, 33.07, 31.12, 28.66, 25.29, 23.20.

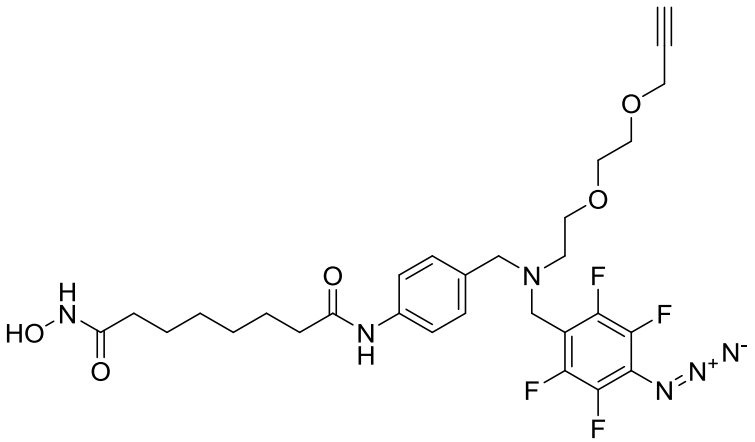

***N*^{1}-(4-(((4-azido-2,3,5,6-tetrafluorobenzyl)(2-(2-(prop-2-yn-1-yloxy)ethoxy)ethyl)amino)methyl)phenyl)-*N*^{8}-hydroxyoctanediamide (4).** Step 1: To a solution of **27b** (250 mg, 0.30 mmol) in anhydrous dimethylformamide (5 mL), sodium azide (20 mg, 0.31 mmol) and tetrabutylammonium azide (catalytic) were added in a sealed pressure vessel. The reaction mixture was stirred at 80 °C for 20 h. After cooling, it was poured in an ice/water mixture and extracted with ethyl acetate (2 × 10 mL). The organic extract was dried over anhydrous magnesium sulfate, filtered and concentrated. The crude was used for next step without purification. Step 2: To a stirred solution of **28b** (200 mg, 0.26 mmol) in DCM (5 ml), magnesium bromide (210 mg, 2.06 mmol) was added and stirred at room temperature for 10 min. After completion water was added reaction and extracted with DCM. The organic extract was dried over anhydrous magnesium sulfate, filtered and concentrated. The crude product was purified by silica gel chromatography eluting 0-10% methanol in DCM to give **4** in 60% yield. ^{1}H NMR (400 MHz, DMSO- d_6) δ 10.40 (s, 1H), 9.93 (s, 1H), 7.51 (d, *J* = 8.0 Hz, 2H), 7.12 (d, *J* = 8.0 Hz, 2H), 3.76 (s, 1H), 3.72 (d, *J* = 7.9 Hz, 2H), 3.61 – 3.51 (m, 9H), 3.47 – 3.41 (m, 5H), 3.37 (s, 2H), 3.30 (d, *J* = 4.1 Hz, 2H), 2.95 (d, *J* = 4.0 Hz, 1H), 2.52 (s, 1H), 2.27 (t, *J* = 7.3 Hz, 2H), 1.92 (d, *J* = 7.1 Hz, 1H), 1.85 (s, 1H), 1.52 (s, 2H), 1.44 (s, 2H), 1.24 (s, 5H). ^{13}C NMR (101 MHz, DMSO-d_6) δ 171.2, 169.1, 138.5, 132.3, 129.0, 126.7, 118.9, 98.2, 85.5, 80.6, 78.1, 76.5, 62.2, 58.7, 56.5, 44.3, 36.4, 32.3, 28.5, 25.1. HRMS (ESI-TOF) *m/z* calcd for $C_{29}H_{35}F_4N_6O_5$ $[M+H]^+$: 623.2600, found: 623.2604.

APPENDIX O (CONTINUED)

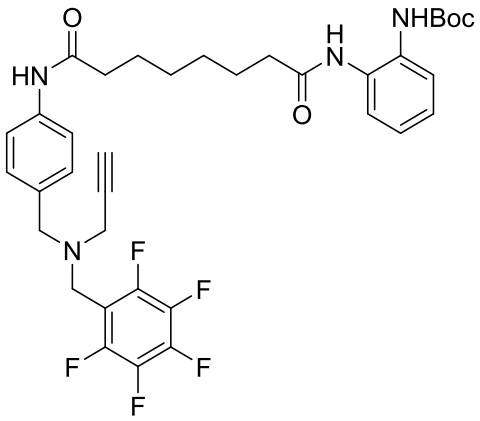

***tert*-Butyl(2-(8-oxo-8-((4-((((perfluorophenyl)methyl)(prop-2-yn-1-yl)amino)methyl)phenyl)amino)octanamido)phenyl)carbamate (31). Step 1:** di-tert-butyl dicarbonate (2.22 g, 10.19 mmol) solution in methanol (10 mL) was added dropwise to *O*-phenylenediamine (1 g, 9.26 mmol) solution in methanol (10 mL) over 45 min. The reaction was stirred at room temperature for 24 h. The solvent was evaporated in vacuo and crude product purified by silica gel chromatography eluting 10-50% EtOAc in hexanes to afford the desired product **30** as white shiny crystals (1.8 g, 90%). **Step 2:** to a stirred solution of **26a** (496 mg, 1.0 mmol) in DCM (10 mL) was added EDC (229 mg, 1.2 mmol), HOBt (183 mg, 1.2 mmol), triethylamine (0.17 mL, 1.2 mmol), and *tert*-butyl(2-aminophenyl)carbamate, **30** (210 mg, 1.64 mmol). The reaction mixture was stirred for 16 h and then diluted with DCM (10 mL), washed with water (10 mL) then brine (10 mL). The organic layer was dried over anhydrous sodium sulfate, filtered, and concentrated under reduced pressure. The resulting residue was purified by silica gel chromatography using 40% EtOAc in hexanes to afford a **30** as a white solid (609 mg, 88%). ^{1}H NMR (400 MHz, DMSO-d_6) δ 8.4 (bs, 1H), 7.8 (bs, 1H), 7.49-7.38 (m, 4H), 7.28-7.22 (m, 2H), 7.16-7.08 (m, 2H), 3.82 (s, 2H), 3.67 (s, 2H), 3.25 (s, 2H), 2.39-2.24 (m, 5H), 1.75-1.64 (m, 4H), 1.51 (s, 9H), 1.42-1.34 (m, 4H). ^{13}C NMR (101 MHz, DMSO-d_6) δ 172.2, 171.2, 153.8, 137.0, 133.0, 130.4, 129.1, 125.8, 124.9, 119.3, 80.5, 56.5, 44.4, 40.9, 36.8, 36.5, 24.8.

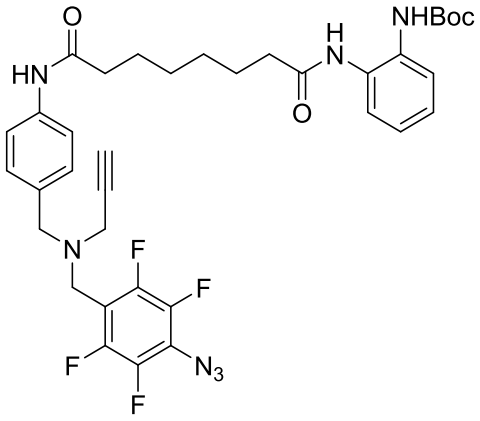

APPENDIX O (CONTINUED)

***tert*-Butyl (2-(8-((4-(((4-azido-2,3,5,6-tetrafluorobenzyl)(prop-2-yn-1-yl)amino)methyl)phenyl)amino)-8-oxooctanamido)phenyl)carbamate (32).** A solution of **30** (350 mg, 0.51 mmol), sodium azide (33 mg, 0.51 mmol) and tetrabutylammonium azide (catalytic) in anhydrous dimethylformamide (5 mL) in a sealed tube was heated at 80 °C under nitrogen for 20 h. After cooling, it was poured in an ice/water mixture and extracted with ethylacetate (2 × 5 ml). The organic extract was dried over anhydrous magnesium sulfate, filtered and concentrated. The crude was purified by silica gel chromatography eluting to afford **31** (235 mg, 65%). ^{1}H NMR (400 MHz, DMSO-d_6) δ 8.47 (bs, 1H), 7.95 (bs, 1H), 7.51-7.38 (m, 4H), 7.27-7.07 (m, 4H), 3.80 (s, 2H), 3.66(s, 2H), 3.24 (s, 2H), 2.40-2.24 (m, 4H), 1.75-1.62 (m, 4H), 1.51 (s, 9H), 1.42-1.32 (m, 4H). ^{13}C NMR (101 MHz, DMSO-d_6) δ 172.2, 171.3, 162.1, 153.8, 137.1, 130.5, 129.1, 125.8, 124.9, 119.3, 80.4, 73.3, 56.5, 41.0, 36.7, 36.1, 31.1, 27.9, 24.9. ^{19}F NMR (376 MHz, $CDCl_3$) δ -142.07 (dd, J = 20.7, 9.7 Hz), -152.33 (dd, J = 21.1, 10.0 Hz).

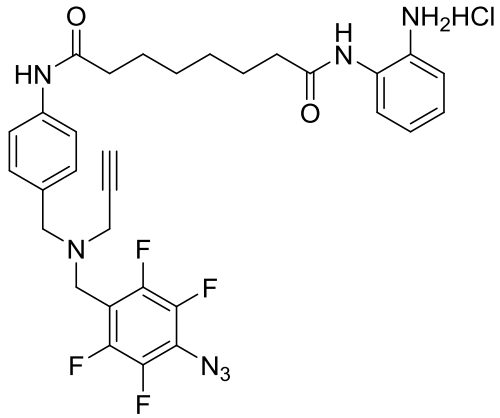

***N*^{1}-(2-Aminophenyl)-*N*^{8}-(4-(((4-azido-2,3,5,6-tetrafluorobenzyl)(prop-2-yn-1-yl)amino)methyl)phenyl)octanediamide hydrochloride (9).** To a solution of **31** (100 mg, 0.14 mmol) in 1,4-Dioxane, 4M hydrochloric acid in 1,4-Dioxane (1 mL) was added and stirred for 2 h at room temperature. The solvent was evaporated in vacuo and residue was triturated with ether and filtered. ^{1}H NMR (400 MHz, DMSO-d_6) δ 10.41 (bs, 1H), 10.12 (bs, 1H), 7.67-7.60 (m, 2H), 7.55-7.46 (m, 2H), 7.42-7.35 (m, 2H), 7.30-7.23 (m, 2H), 4.11-3.94 (m, 4H), 2.89-2.87 (m, 1H), 2.73-2.72 (m, 1H), 2.51-2.48 (m, 2H), 2.43-2.30 (m, 4H), 1.66-1.57 (m, 4H), 1.38-1.32 (m, 4H). ^{13}C NMR (101 MHz, DMSO-d_6) δ 172.2, 171.3, 162.1, 153.8, 137.1, 130.5, 129.1, 125.8, 124.9, 119.3, 80.4, 73.3, 56.5, 41.0, 36.7, 36.1, 31.1, 27.9, 24.9. HRMS (ESI-TOF) *m/z* calcd for $C_{31}H_{32}F_4N_7O_2$ $[M+H]^+$: 610.2548; found: 610.2545.

APPENDIX P: SYNTHESIS OF SAHA-BASED PRP 5.

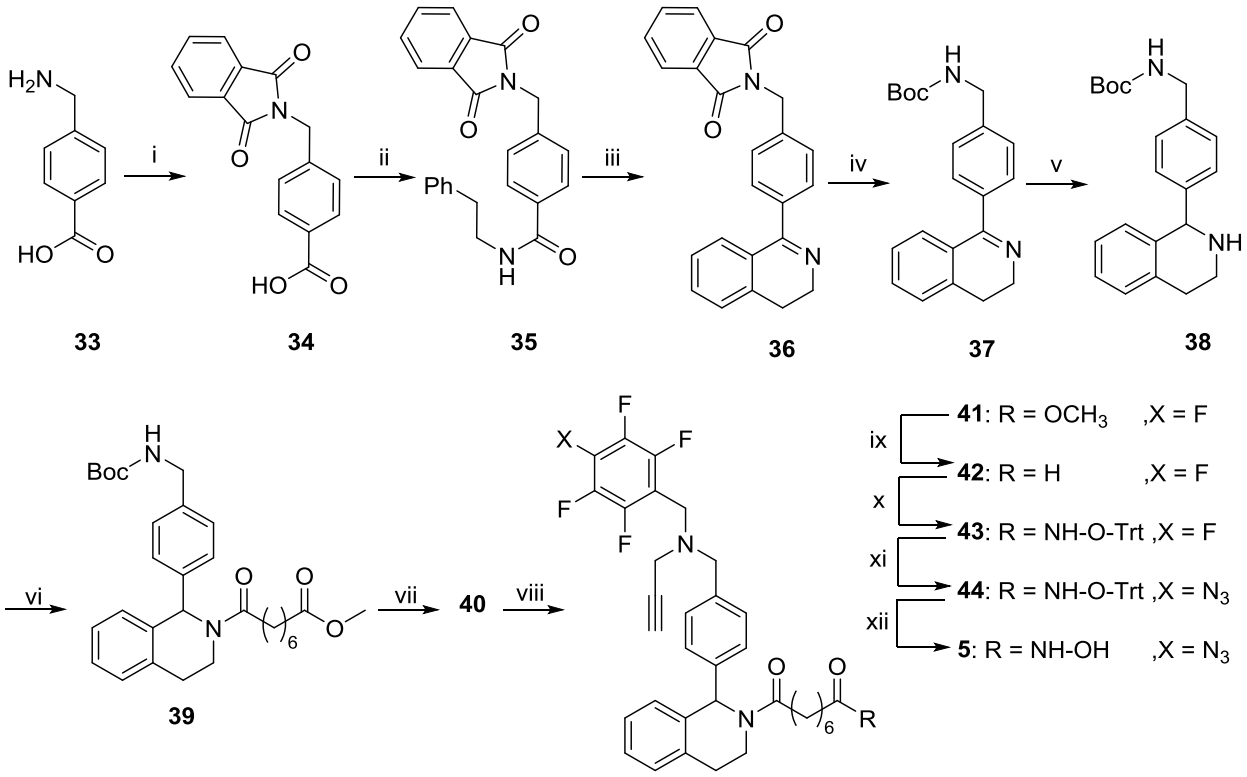

Reagents and conditions: (i) ethyl 1,3-dioxoisoindoline-2-carboxylate, Na_2CO_3, H_2O, 2 h; (ii) a. $(COCl)_2$, DCM, 0 °C, 3 h, b. phenytheleneamine, Et_3N, DCM, 4 h; (iii) $POCl_3$, PCl_5, xylene, 2 h, reflux; (iv) a. hydrazine hydrate, ethanol, 1 h, 65 °C; b. $(Boc)_2O$, THF, 12 h; (v) $NaBH_4$, CH_3OH, 1 h; (vi) suberic acid monomethyl ester, EDC·HCl, HOBt, Et_3N, DCM, 12 h; (vii) a. HCl, 1,4-dioxane, 4 h; b. **14**, Et_3N, DCM, 2 h; c. $NaBH_4$, CH_3OH, 1 h; (viii) propargyl bromide, K_2CO_3, CH_3CN, 4 h; (ix) LiOH, THF/H_2O, 8 h; (x) *O*-tritylhydroxylamine, EDC·HCl, HOBt, Et_3N, DCM, 12 h; (xi) NaN_3, Bu_3NN_3, DMF, 75 °C, 15 h; (xii) $MgBr_2$, DCM, 10 min.

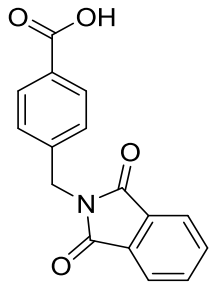

4-((1,3-Dioxoisoindolin-2-yl)methyl)benzoic acid (34)

A solution of 4-(aminomethyl)benzoic acid, **33** (2.0 g, 13 mmol), ethyl l,3-dioxo-2,3-dihydro-lH-isoindole-2-carboxylate (2.89 g, 13 mmol) and sodium carbonate (0.7 g, 6.5 mmol) in water (15 mL) was stirred for 3 h at room temperature. The pH of the solution was adjusted to ≈ 4 with 1 M hydrochloric acid. The product was filtered and filter cake was washed with 20 mL of water and dried to give **34** (3.34 g, 90%). ^{1}H NMR (400 MHz, DMSO-d_6) δ 7.92-7.80 (m, 6H), 7.44-

APPENDIX P (CONTINUED)

7.39 (m, 2H), 4.84 (s, 2H). ^{13}C NMR (101 MHz, DMSO-d_6) δ 167.7, 167.2, 141.4, 134.6, 131.6, 130.5, 129.7, 127.4, 123.3, 40.7. HRMS (ESI-TOF) *m/z* calcd for $C_{16}H_{10}NO_4$ [M-H]$^-$: 280.0615, found: 280.0617.

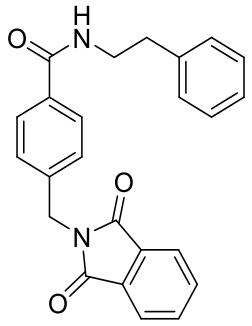

4-((1,3-Dioxoisoindolin-2-yl)methyl)-*N*-phenethylbenzamide (35). Step 1: To a suspension of **34** (2.0 g, 7.11 mmol) in DCM (50 ml) at 0 °C, Oxalyl chloride (1.36 g, 10.67 mmol) was added. dimethylformamide (10 µl) was added and stirring continued for 3 h at 0 °C.The solvents were evaporated to give a crude solid acid chloride (**35a**) which was used directly for next step.

Step 2: To a solution of acid chloride (**35a**) and phenethylamine (0.86 g, 7.11 mmol) in DCM (50 mL) was added triethylamine (1.5 mL, 10.67 mmol)) dropwise at 0 °C. The mixture was stirred at room temperature for 4 h then solvent evaporated in vacuo. The reaction residue was diluted with EtOAc and washed with 10% aq. HCl, saturated aqueous sodium bicarbonate, and brine. The EtOAc solution was dried over anhydrous sodium sulfate and solvent was removed under vacuum to afford the target amide **35** (2.5 g, 92%). ^{1}H NMR (400 MHz, DMSO-d_6) δ 7.93-7.82 (m, 8H), 7.32-7.20 (m, 5H), 4.79 (s, 2H), 3.04-2.98 (m, 2H), 2.92-2.86 (m, 2H). ^{13}C NMR (101 MHz, DMSO-d_6) δ 168.7, 167.7, 134.6, 131.6, 129.4, 128.6, 126.8, 123.3, 40.8, 33.9.

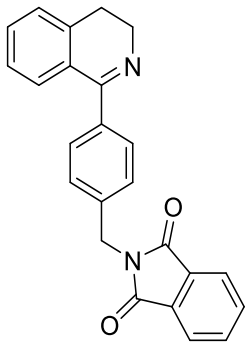

2-(4-(3,4-Dihydroisoquinolin-1-yl)benzyl)isoindoline-1,3-dione (36). Using Bischler-Napieralski reaction, to a solution of **35** (2.5 g, 6.5 mmol) in xylene (75 mL), phosphorous pentoxide (1.84 g, 13.1 mmol), and phosphorous oxychloride (1.82 mL, 19.5 mmol) were added. The reaction mixture was heated to 165 °C for 6 h, the hot solution was carefully poured into ice/water then 10 mL of a 20% potassium hydroxide solution was added to break up the oil. The mixture was stirred at room temperature for 5 min and an additional amount of potassium hydroxide solution was added until pH ≈ 7. EtOAc (50 mL) was added and the mixture was stirred at room temperature for 15 min. The organic layer was collected and the aqueous layer

APPENDIX P (CONTINUED)

was extracted with EtOAc (2 × 50 mL). The combined organic extracts were dried over anhydrous magnesium sulfate, concentrated in vacuo and purified by silica gel chromatography to give **36** (2.02 g, 85%). ^{1}H NMR (400 MHz, DMSO-d_6) δ 7.95-7.84 (m, 4H), 7.54-7.24 (m, 6H), 7.16-7.10 (m, 2H), 4.84 (s, 2H), 3.74-3.67 (m, 2H), 2.75-2.65 (m, 2H). ^{13}C NMR (101 MHz, DMSO-d_6) δ 167.8, 138.6, 137.8, 134.7, 131.7, 130.9, 128.9, 128.0, 127.1, 126.8, 123.4, 47.10, 42.6, 40.70, 25.6.

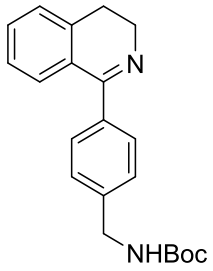

***tert*-Butyl (4-(3,4-dihydroisoquinolin-1-yl)benzyl)carbamate (37). Step 1:** To a solution of **36** (1.7 g, 4.64 mmol) in 25 mL ethanol was added hydrazine monohydrate (0.45 mL, 9.28 mmol) and stirred for 2 h at 70 °C. The reaction was allowed to cool to room temperature, quenched with 30 mL water then acidified to pH ≈ 3.5 using 2N hydrochloric acid. It was extracted with DCM (3 × 20 mL), organic layers combined, dried over anhydrous magnesium sulfate, filtered, concentrated to afford the hydrochloride amine salt (**37a**) which was used for the next step without further purification.

Step 2: To a solution of **37a** in 20 mL 1,4-dioxane/water (1:1), 1M sodium hydroxide was added to pH ~ 10-11. A solution of di-*tert*-butyl dicarbonate (1.1 g, 4.65 mmol) in 1,4-dioxane was added dropwise and the reaction was stirred at room temperature for 16 h. The mixture was concentrated in vacuo, acidified by 4M potassium hydrogen sulfate to pH ≈ 1-2, extracted by EtOAc (2 × 50 mL) and dried in vacuo. The crude was purified by silica gel chromatography to give **37** (1.24 g, 80% over two steps). ^{1}H NMR (400 MHz, DMSO-d_6) δ 7.58-7.51 (m, 4H), 7.40-7.21 (m, 4H), 5.05 (bs, 1H), 4.39-4.33 (m, 2H), 3.86-3.79 (m, 2H), 2.87-2.74 (m, 2H), 1.47 (s, 9H). ^{13}C NMR (101 MHz, DMSO-d_6) δ 167.7, 155.6, 139.8, 138.4, 137.5, 130.3, 128.7, 127.5, 127.0, 126.7, 126.2, 50.1, 47.1, 44.1, 28.0, 25.9.

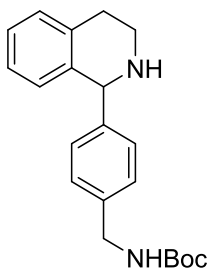

APPENDIX P (CONTINUED)

***tert*-Butyl (4-(1,2,3,4-tetrahydroisoquinolin-1-yl)benzyl)carbamate (38).** To a solution of **37** (1.5 g, 4.46 mmol) in anhydrous methanol (15 mL) was added sodium tetrahydroborate (255 mg, 6.69 mmol) and stirred at room temperature until completion ~2 h; as monitored by TLC. The reaction mixture was concentrated under vacuum, diluted with water and extracted with EtOAc (3 × 20 mL). The organic layer was washed with brine, dried over anhydrous sodium sulfate and solvent was removed under vacuum. The crude product was purified by silica gel chromatography eluting with EtOAc in hexanes to give **38** (1.29 g, 86%). ^{1}H NMR (400 MHz, DMSO-d_6) δ 7.29-7.20 (m, 4H), 7.19-7.12 (m, 2H), 7.08-7.02 (m, 2H), 6.71-6.67 (m, 1H), 5.11 (s, 1H), 4.88 (bs, 1H), 4.35-4.27 (m, 2H), 3.30-3.23 (m, 2H), 3.13-3.0 (m, 1H), 2.90-2.79 (m, 1H), 1.47 (s, 9H). ^{13}C NMR (101 MHz, DMSO-d_6) δ 155.5, 143.4, 137.7, 134.9, 128.8, 128.6, 127.6, 127.1, 125.9, 125.2, 79.1, 61.2, 44.0, 41.7, 29.2, 28.0.

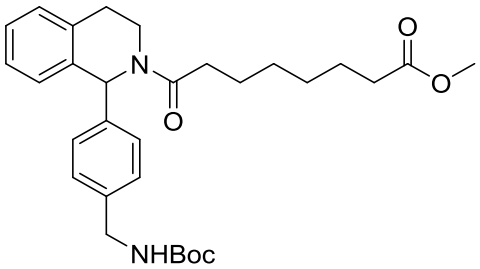

Methyl 8-(1-(4-(((*tert*-butoxycarbonyl)amino)methyl)phenyl)-3,4-dihydroisoquinolin-2(1*H*)-yl)-8-oxooctanoate (39). To a stirred solution of suberic acid monomethyl ester, **23** (0.86 g, 4.61 mmol) in DCM (20 mL) was added EDC (880 mg, 4.61 mmol), HOBt (700 mg, 4.61 mmol), triethylamine (0.9 mL, 4.6 mmol), and **38** (1.3 g, 3.84 mmol). The reaction mixture was stirred for 16 h then diluted with DCM (10 mL), washed with water (10 mL) and brine (10mL). The organic layer was dried over anhydrous sodium sulfate, filtered, and concentrated under vacuo. The crude residue was purified by silica gel chromatography eluting 75% EtOAc in hexanes to afford **39** as a white solid (1.65 g, 85%). ^{1}H NMR (400 MHz, DMSO-d_6) δ 7.21-7.07 (m, 6H), 7.03-7.69 (m, 1H), 6.90-6.84 (m, 1H), 5.10 (s, 1H), 4.25-4.16 (m, 2H), 3.77-3.68 (m, 1H), 3.44-3.55 (m, 1H), 2.97-2.74 (m, 2H), 2.38-2.19 (m, 4H), 1.65-1.53 (m, 4H), 1.39 (s, 9H), 1.34-1.26 (m, 4H). ^{13}C NMR (101 MHz, DMSO-d_6) δ 173.7, 171.0, 155.5, 141.3, 137.7, 134.9, 133.9, 128.4, 126.5, 125.8, 78.8, 54.3, 50.9, 43.7, 39.2, 33.5, 32.9, 28.4, 27.9, 24.3, 13.7.

APPENDIX P (CONTINUED)

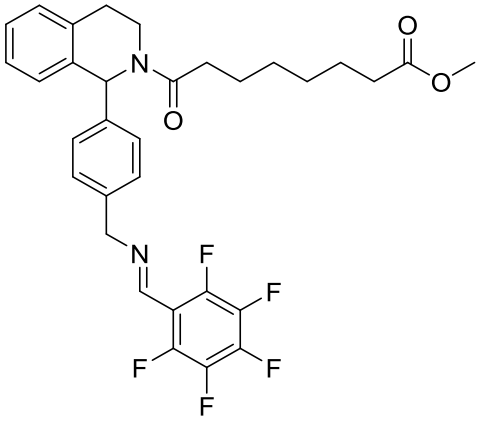

Methyl (*E*)-8-oxo-8-(1-(4-((((perfluorophenyl)methylene)amino)methyl)phenyl)-3,4-dihydroisoquinolin-2(1*H*)-yl)octanoate (40b). Step 1: To a solution of **39** (1.5 g, 4.46 mmol) in 1, 4-Dioxane, 4M hydrochloric acid in 1,4-Dioxane (5 mL) was added and stirred at room temperature for 2 h. Solvent was removed in vacuo and resultant solid was triturated with ether and filtered to give **40a**. **Step2:** To a solution of amine hydrochloride, **40a** in ethanol (20 mL), pentafluorobenzaldehyde (1.0 g, 3.54 mmol) was added. The solution was refluxed (90 °C) for 2 h then cooled to room temperature and solvent was removed under vacuum. The residue was purified by silica gel chromatography to give **40b** in 70% yield. ^{1}H NMR (400 MHz, DMSO-d_6) δ 8.59 (s, 1H), 7.38-7.11 (m, 7H), 6.72 (s, 1H), 4.82 (s, 1H), 3.88 (s, 2H), 3.77 (s, 3H), 3.39-3.34 (m, 2H), 2.90-2.79 (m, 2H), 2.51-2.37 (m, 2H), 2.36-2.25 (m, 4H), 1.50-1.27 (m, 4H), 1.20-1.16 (m, 4H). ^{13}C NMR (101 MHz, DMSO-d_6) δ 173.73, 171.45, 151.24, 141.96, 137.90, 135.93, 135.32, 129.04, 128.74, 128.32, 128.16, 127.52, 127.35, 126.49, 65.31, 54.81, 51.54, 33.64, 32.93, 24.96, 24.76.

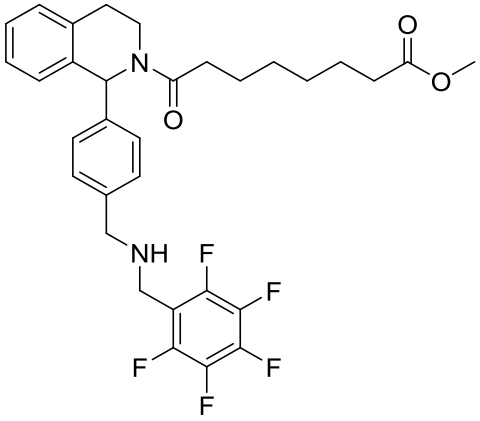

Methyl 8-oxo-8-(1-(4-((((perfluorophenyl)methyl)amino)methyl)phenyl)-3,4-dihydroisoquinolin-2(1*H*)-yl)octanoate (40). To a stirred solution of the **40b** (1.0 g, 1.7 mmol) in anhydrous methanol (20 mL) was added sodium tetrahydroborate (78 mg, 2.01 mmol) and stirred at room temperature for 2 h. The reaction mixture was concentrated in vacuo, residue dissolved in EtOAc (20 mL), washed with brine, dried over anhydrous sodium sulfate. The

APPENDIX P (CONTINUED)

solvent was removed under vacuum and crude product was purified by silica gel chromatography eluting with EtOAc in hexanes to give **41a** in 80% yield. ^{1}H NMR (400 MHz, $CDCl_3$) δ 7.29-7.07 (m, 8H), 6.95 (s, 1H), 3.95 (s, 2H), 3.75 (s, 2H), 3.68 (s, 3H), 3.47-3.41 (m, 1H), 3.35-2.96 (m, 2H), 2.87-2.83 (m, 2H), 2.45-2.30 (m, 4H), 1.70-1.64 (m, 4H), 1.37. ^{13}C NMR (101 MHz, $CDCl_3$) δ 174.19, 171.45, 141.74, 138.47, 135.41, 134.35, 128.90, 128.76, 128.65, 127.83, 126.95, 126.31, 54.74, 52.62, 51.44, 40.18, 39.63, 33.99, 33.47, 29.08, 28.93, 24.99, 24.78.

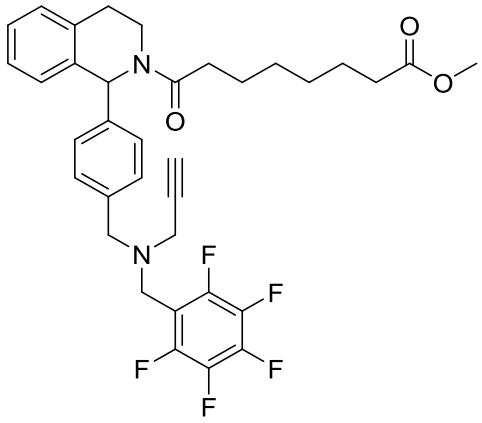

Methyl-8-oxo-8-(1-(4-((((perfluorophenyl)methyl)(prop-2-yn-1-yl)amino)methyl)phenyl)-3,4-dihydroisoquinolin-2(1*H*)-yl)octanoate (41). To a solution of **40** (500 mg, 0.85 mmol) in acetonitrile (15 mL), potassium carbonate (235 mg, 1.7 mmol) then dropwise propargyl bromide (80% w/v in toluene, 0.11 mL, 1 mmol) were added and reaction was stirred for 2 h at room temperature. After completion, solvent was evaporated, residue diluted with water (10 mL) and extracted with EtOAc (3 × 10mL). The organic extract was washed with saturated sodium bicarbonate and brine sequentially, dried over anhydrous sodium sulfate and solvent evaporated in vacuo. The crude product was purified by silica gel chromatography eluting 60% EtOAc in hexanes to give **41** (452 mg, 85%).^{1}H NMR (400 MHz, DMSO-d_6) δ 7.23 (t, J = 5.1 Hz, 3H), 7.19 (d, J = 8.1 Hz, 2H), 7.14 (t, J = 6.5 Hz, 1H), 7.04 (d, J = 7.9 Hz, 2H), 6.69 (s, 1H), 3.76 (s, 2H), 3.63 (s, 2H), 3.57 (s, 3H), 3.44 – 3.35 (m, 1H), 3.33 (s, 1H), 3.26 (s, 2H), 3.24 (d, J = 1.9 Hz, 1H), 2.93 (ddd, J = 15.4, 7.9, 5.9 Hz, 1H), 2.76 (dt, J = 9.4, 4.3 Hz, 1H), 2.47 – 2.31 (m, 2H), 2.27 (t, J = 7.4 Hz, 2H), 1.51 (dd, J = 13.3, 6.5 Hz, 4H), 1.29 (t, J = 8.8 Hz, 4H). ^{13}C NMR (101 MHz, DMSO-d_6) δ 173.39, 171.10, 141.66, 139.38, 136.92, 136.73, 135.58, 135.21, 134.96, 128.68, 128.35, 127.61, 127.04, 126.14, 78.05, 76.50, 59.80, 58.27, 56.70, 55.28, 54.96, 54.84, 54.37, 53.10, 51.18, 44.49, 43.45, 41.78, 41.44, 33.25, 32.48, 28.40, 28.33, 24.54, 24.36. HRMS (ESI-TOF) *m/z* calcd for $C_{35}H_{36}F_5N_2O_3$ $[M+H]^+$: 627.2641, found: 627.2651.

APPENDIX P (CONTINUED)

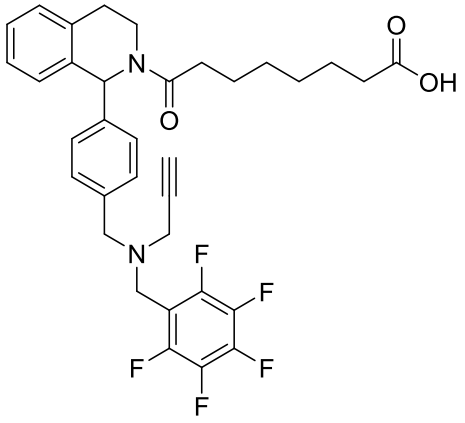

8-Oxo-8-(1-(4-((((perfluorophenyl)methyl)(prop-2-yn-1-yl)amino)methyl)phenyl)-3,4-dihydroisoquinolin-2(1*H*)-yl)octanoic acid (42). Lithium hydroxide (62 mg, 2.54 mmol) was added to a solution of **41** (400 mg, 0.64 mmol) in 4:1 tetrahydrofuran/water (10 mL) and stirred at room temperature for 4 h. The reaction mixture was concentrated in vacuo, acidified with 2N hydrochloric acid to pH ≈ 1, diluted with brine and extracted with EtOAc (2 × 10 mL). The organic phase was dried over anhydrous sodium sulfate and concentrated to afford **42** as a white solid (360 mg , 92%). ^{1}H NMR (400 MHz, DMSO-d_6) δ 11.95 (s, 1H), 7.23 (d, *J* = 6.0 Hz, 3H), 7.19 (d, *J* = 8.0 Hz, 2H), 7.13 (d, *J* = 7.0 Hz, 1H), 7.04 (d, *J* = 7.8 Hz, 2H), 6.69 (s, 1H), 3.76 (s, 2H), 3.63 (s, 2H), 3.44 – 3.35 (m, 1H), 3.33 (s, 1H), 3.26 (s, 2H), 3.24 (s, 1H), 2.99 – 2.86 (m, 1H), 2.78 (dd, *J* = 12.1, 8.4 Hz, 1H), 2.48 – 2.31 (m, 2H), 2.16 (dd, *J* = 24.8, 17.5 Hz, 2H), 1.49 (ddd, *J* = 14.1, 10.8, 7.2 Hz, 4H), 1.33 – 1.14 (m, 4H). ^{13}C NMR (101 MHz, $CDCl_3$) δ 178.89, 171.72, 141.80, 136.86, 135.37, 134.29, 128.89, 128.74, 128.63, 128.56, 127.13, 126.98, 126.33, 73.78, 57.00, 54.83, 45.04, 41.78, 39.73, 33.87, 33.43, 29.07, 29.00, 28.79, 24.98, 24.54. HRMS (ESI-TOF) *m/z* calcd for $C_{34}H_{34}F_5N_2O_3$ $[M+H]^+$: 613.2484, found: 613.2499.

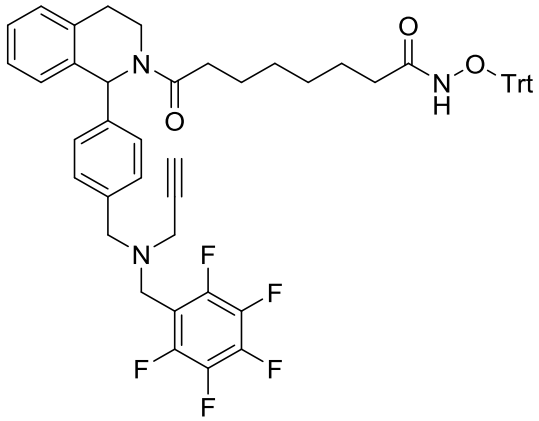

8-Oxo-8-(1-(4-((((perfluorophenyl)methyl)(prop-2-yn-1-yl)amino)methyl)phenyl)-3,4-dihydroisoquinolin-2(1*H*)-yl)-*N*-(trityloxy)octanamide (43). To a solution of **42** (300 mg, 0.49

APPENDIX P (CONTINUED)

mmol) in DCM (10 mL) was added EDC (112 mg, 0.58 mmol), HOBt (90 mg, 0.58 mmol), triethylamine (80 μL, 0.58 mmol), and *O*-tritylhydroxylamine (135 mg, 0.58 mmol).The reaction mixture was stirred for 16 h at room temperature under nitrogen and then diluted with DCM (10 mL), washed with water (10 mL) and brine (10mL). The organic layer was dried over anhydrous sodium sulfate, filtered, and concentrated under reduced pressure. The crude was purified by silica gel chromatography using 75% EtOAc in hexanes to afford **43** as a white solid (340 mg, 80%). ^{1}H NMR (400 MHz, DMSO-d_6) δ 10.14 (s, 1H), 7.31 (d, *J* = 13.0 Hz, 19H), 7.23 (s, 3H), 7.19 (d, *J* = 7.7 Hz, 2H), 7.13 (d, *J* = 7.2 Hz, 1H), 7.05 (d, *J* = 7.7 Hz, 2H), 6.69 (s, 1H), 3.76 (s, 2H), 3.63 (s, 2H), 3.39 (s, 1H), 3.33 (s, 1H), 3.25 (d, *J* = 5.2 Hz, 3H), 2.98 – 2.85 (m, 1H), 2.82 – 2.71 (m, 1H), 2.45 – 2.22 (m, 2H), 1.76 (d, *J* = 6.4 Hz, 2H), 1.43 (dq, *J* = 12.6, 6.4 Hz, 4H), 1.23 – 1.04 (m, 4H), 0.96 (dd, *J* = 19.9, 12.4 Hz, 2H). ^{13}C NMR (101 MHz, $CDCl_3$) δ 171.52, 141.86, 136.93, 135.48, 134.35, 129.03, 128.88, 128.68, 128.55, 128.09, 126.97, 126.30, 73.72, 57.04, 54.78, 45.06, 41.82, 39.69, 33.48, 29.08.

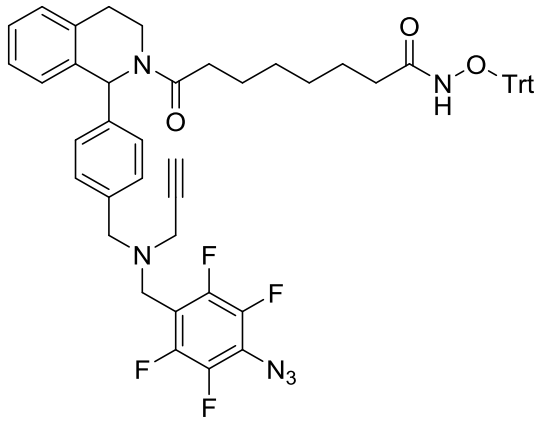

8-(1-(4-(((4-Azido-2,3,5,6-tetrafluorobenzyl)(prop-2-yn-1-yl)amino)methyl)phenyl)-3,4-dihydroisoquinolin-2(1*H*)-yl)-8-oxo-*N*-(trityloxy)octanamide (44). A solution of **43** (250 mg, 0.28 mmol) in anhydrous dimethylformamide (5 mL), sodium azide (19 mg, 0.28 mmol) and tetrabutylammonium azide (catalytic) were added in a sealed pressure vessel. The reaction mixture was stirred at 80 °C for 20h. After cooling, it was poured in an ice/water mixture and extracted with EtOAc (2 × 10 mL). The organic extract was dried over anhydrous magnesium sulfate, filtered and concentrated. The crude was purified by silica gel chromatography to give **44** (150 mg, 60%).^{1}H NMR (400 MHz, DMSO-d_6) ^{1}H NMR (400 MHz, DMSO) δ 10.15 (s, 1H), 7.37 – 7.25 (m, 15H), 7.23 (s, 3H), 7.19 (d, *J* = 8.1 Hz, 2H), 7.14 (s, 1H), 7.05 (d, *J* = 7.8 Hz, 2H), 6.69 (s, 1H), 3.96 (ddd, *J* = 67.9, 19.0, 9.1 Hz, 1H), 3.74 (s, 2H), 3.61 (s, 2H), 3.47 – 3.35 (m, 1H), 3.33 (s, 1H), 3.24 (d, *J* = 8.8 Hz, 2H), 2.98 – 2.64 (m, 2H), 2.45 – 2.21 (m, 2H), 2.04 (d, *J* = 39.0 Hz, 1H), 1.76 (d, *J* = 5.8 Hz, 2H), 1.43 (dt, *J* = 13.7, 7.0 Hz, 2H), 1.24 – 1.05 (m, 4H), 1.03 – 0.87 (m, 2H). ^{13}C NMR (101 MHz, DMSO-d_6) δ 171.11, 170.38, 142.54, 141.66, 136.90, 136.05, 135.61, 135.15, 134.96, 133.72, 129.02, 128.68, 128.36, 127.63, 127.53, 127.43, 127.05, 126.15, 91.77, 78.03, 76.49, 56.72, 56.54, 54.38, 44.50, 42.87, 41.58, 34.46, 32.57, 32.05, 28.46,

APPENDIX P (CONTINUED)

28.23, 24.70, 24.53. HRMS (ESI-TOF) *m/z* calcd for $C_{53}H_{47}F_4N_6O_3$ [M-H]$^-$: 891.3651, found: 891.3659.

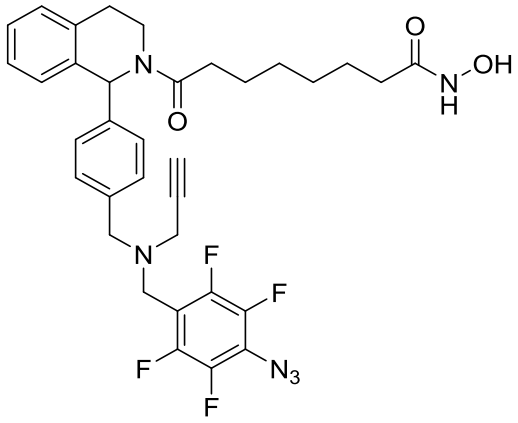

8-(1-(4-(((4-Azido-2,3,5,6-tetrafluorobenzyl)(prop-2-yn-1-yl)amino)methyl)phenyl)-3,4-dihydroisoquinolin-2(1*H*)-yl)-*N*-hydroxy-8-oxooctanamide (5). To a solution of **44** (100 mg, 0.11 mmol) in DCM (5 mL), magnesium bromide (103 mg, 0.56 mmol) was added and stirred at room temperature for 10 min. After completion, 10 mL water was added to the reaction and extracted with DCM (2 × 10 mL). The organic extract was dried over anhydrous magnesium sulfate, filtered and concentrated. The crude was purified by silica gel chromatography to give **5** (43 mg, 60%). ^{1}H NMR (400 MHz, DMSO-*d*$_6$) δ 10.14, 7.31, 7.30, 7.28, 7.22, 7.19, 7.17, 7.14, 7.13, 7.05, 7.03, 6.68, 3.82, 3.75, 3.74, 3.68, 3.62, 3.61, 3.39, 3.32, 3.29, 3.24, 3.22, 3.17, 2.91, 2.89, 2.77, 2.73, 2.38, 2.36, 2.34, 2.32, 2.30, 1.76, 1.50, 1.42, 1.41, 1.30, 1.29, 1.19, 1.17, 1.15, 1.14, 0.96. ^{13}C NMR (101 MHz, DMSO-*d*$_6$) δ 171.11, 170.38, 142.54, 141.66, 136.90, 136.05, 135.61, 135.15, 134.96, 133.72, 129.02, 128.68, 128.36, 127.63, 127.53, 127.43, 127.05, 126.15, 91.77, 78.03, 76.49, 56.72, 56.54, 54.38, 44.50, 42.87, 41.58, 34.46, 32.57, 32.05, 28.46, 28.23, 24.70, 24.53. HRMS (ESI-TOF) *m/z* calcd for $C_{34}H_{35}F_4N_6O_3$ [M+H]$^+$: 651.2702, found: 651.2706.

APPENDIX Q: SYNTHESIS OF PANOBINOSTAT BASED PRP

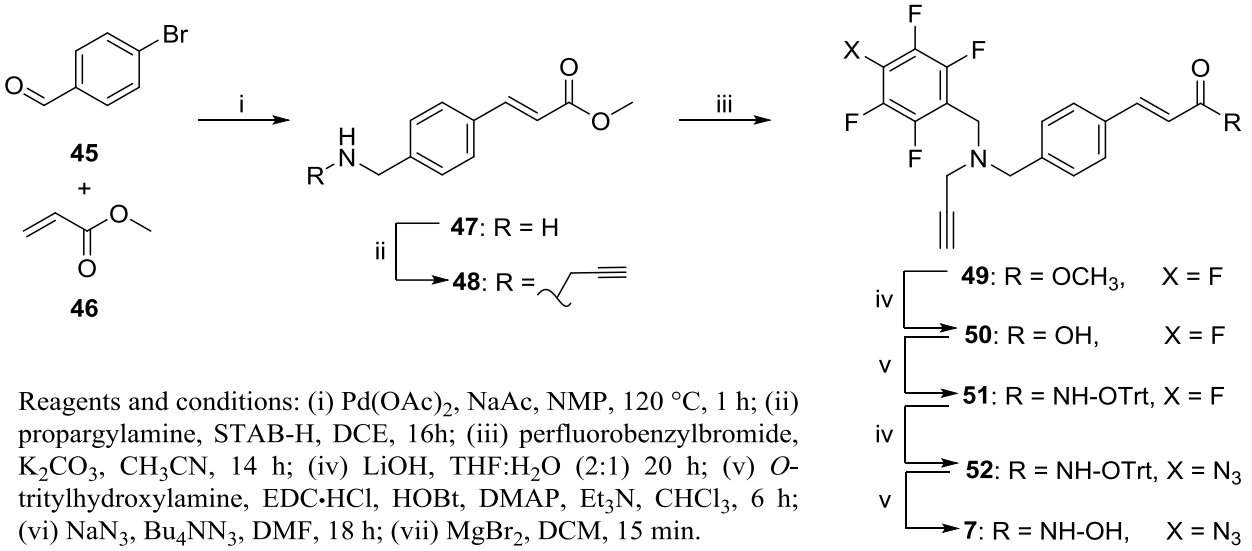

Reagents and conditions: (i) $Pd(OAc)_2$, NaAc, NMP, 120 °C, 1 h; (ii) propargylamine, STAB-H, DCE, 16h; (iii) perfluorobenzylbromide, K_2CO_3, CH_3CN, 14 h; (iv) LiOH, THF:H_2O (2:1) 20 h; (v) *O*-tritylhydroxylamine, EDC·HCl, HOBt, DMAP, Et_3N, $CHCl_3$, 6 h; (vi) NaN_3, Bu_4NN_3, DMF, 18 h; (vii) $MgBr_2$, DCM, 15 min.

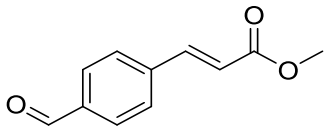

(*E*)-methyl 3-(4-formylphenyl)acrylate (47). To a solution of anhydrous sodium acetate (2.7 g, 33.0 mmol), *p*-bromobenzaldehyde, **45** (5.55 g, 30.0 mmol) and palladium acetate (2.6 mg, 0.04% mol) in anhydrous *N*-methyl-2-pyrrolidone (40 mL), methyl acrylate, **46** (3.9 mL, 43.3 mmol) was introduced via a syringe and the reaction mixture was heated at 120 °C for 60 min under nitrogen. The resulting red solution containing a white precipitate was diluted with water (100 mL) and extracted with ethyl acetate (2 × 70 mL). The combined organic layers were washed twice with water, once with brine, dried over anhydrous sodium sulfate, and filtered. The solvent was evaporated in vacuo to give **47** as a yellow solid (5.63 g, 99%) which was used in the next step without further purification. ^{1}H NMR (400 MHz, DMSO-d_6) δ 10.04 (s, 1H), 8.02 – 7.88 (m, 4H), 7.74 (d, J = 16.1 Hz, 1H), 6.83 (d, J = 16.1 Hz, 1H), 3.76 (s, 3H). ^{13}C NMR (101 MHz, DMSO-d_6) δ 193.11, 166.78, 143.52, 140.04, 137.46, 130.32, 129.42, 121.39, 52.15.

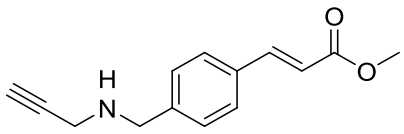

Methyl (*E*)-3-(4-(prop-2-yn-1-ylamino)phenyl)acrylate (48). To a solution of **47** (5.63 g, 29.63 mmol) in dichloroethane (70 mL), propargyl amine (2.6 mL, 32.59 mmol) was added. The reaction mixture was stirred under nitrogen gas at room temperature for 1 h. Sodium triacetoxyborohydride (12.56 g, 59.26 mmol) was added, reaction was stirred for 16 h. The reaction mixture was concentrated in vacuo, diluted with water (100 mL) and extracted with

APPENDIX Q (CONTINUED)

DCM (3 × 100 mL). The combined DCM extracts were washed with brine, dried over anhydrous sodium sulfate and concentrated under vacuo. The crude product was purified by silica gel chromatography eluting 10-70% EtOAc in hexanes to give **48** as a yellow solid (3.6 g, 70%). ^{1}H NMR (400 MHz, DMSO-d_6) δ 7.74 – 7.60 (m, 3H), 7.37 (d, J = 7.7 Hz, 2H), 6.61 (d, J = 16.0 Hz, 1H), 3.77 (s, 2H), 3.73 (s, 3H), 3.09 (s, 1H), 2.09 (d, J = 1.0 Hz, 2H), 1.94 – 1.88 (m, 1H). ^{13}C NMR (101 MHz, DMSO-d_6) δ 167.20, 144.91, 143.44, 132.92, 128.94, 128.71, 117.60, 83.16, 74.29, 51.89, 37.18, 31.15. HRMS (ESI-TOF) *m/z* calcd for $C_{14}H_{16}NO_2$ $[M+H]^+$: 230.1176, found: 230.1167.

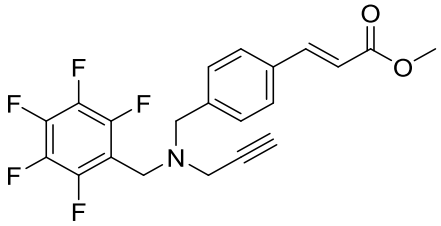

Methyl (*E*)-3-(4-((((perfluorophenyl)methyl)(prop-2-yn-1-yl)amino)methyl)phenyl)acrylate (49). To a solution of **48** (3.6 g, 16 mmol) in acetonitrile (40 mL), potassium carbonate (3.3 g, 24 mmol) was added and stirred for 5 min. Pentafluorobenzyl bromide (2.5 mL, 16 mmol) was added dropwise and the reaction was stirred under nitrogen for 14 h at room temperature. The mixure was concentrated under vacuum, diluted with water (50 mL) and extracted with DCM (3 × 50). The organic extracts were combined, washed with brine, dried over anhydrous sodium sulfate and concentrated under vacuum. The crude product was purified by silica gel chromatography eluting 5-25% EtOAc in hexanes to give **49** as yellowish white solid (6.41 g, 98%). ^{1}H NMR (400 MHz, DMSO-d_6) δ 7.65 (t, J = 12.1 Hz, 3H), 7.34 (d, J = 8.1 Hz, 2H), 6.61 (d, J = 16.0 Hz, 1H), 3.79 (s, 2H), 3.73 (s, 3H), 3.71 (s, 2H), 3.35 (s, 2H), 3.27 (s, J = 2.6 Hz, 3H). ^{13}C NMR (101 MHz, DMSO-d_6) δ 167.13, 144.69, 141.19, 133.52, 129.54, 128.72, 117.95, 78.38, 76.97, 57.09, 51.90, 44.76, 41.95. HRMS (ESI-TOF) *m/z* calcd for $C_{21}H_{17}F_5NO_2$ $[M+H]^+$: 410.1174, found: 410.1158.

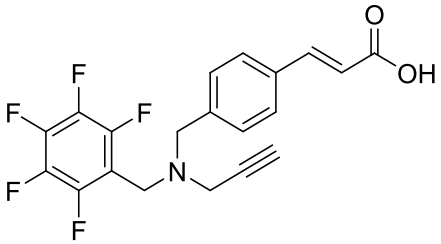

(*E*)-3-(4-((((perfluorophenyl)methyl)(prop-2-yn-1-yl)amino)methyl)phenyl)acrylic acid (50). To a solution of **49** (6.41 g, 15.68 mmol) in tetrahydrofuran (80 mL) and water (40 mL), lithium hydroxide (1.03 g, 43.98 mmol) was added and stirred at room temperature for 20 h. The reaction mixture was concentrated under vacuum and pH was made acidic (pH ≈ 5) by 10% hydrochloric acid and extracted with ethyl acetate (3 × 40 mL). The organic extracts were combined, washed with brine, dried over anhydrous sodium sulfate and solvent was removed under vacuum to yield **50** as a white solid (6.13 g, 99%) that was used in next step without

APPENDIX Q (CONTINUED)

further purification. ^{1}H NMR (400 MHz, DMSO-d_6) δ 12.37 (s, 1H), 7.63 (d, 2H), 7.56 (d, J = 16.0 Hz, 1H), 7.32 (d, J = 8.0 Hz, 2H), 6.49 (d, J = 16.0 Hz, 1H), 3.78 (s, 2H), 3.69 (s, 2H), 3.32 (s, 6H), 3.26 (s, 3H). ^{13}C NMR (101 MHz, DMSO-d_6) δ 168.04, 144.05, 140.87, 133.76, 129.54, 128.55, 119.39, 114.93, 87.19, 78.40, 76.97, 57.10, 1.95. HRMS (ESI-TOF) *m/z* calcd for $C_{20}H_{15}F_5NO_2$ $[M+H]^+$: 396.1018, found: 396.0994.

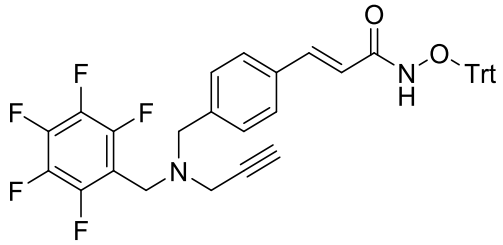

(*E*)-3-(4-((((perfluorophenyl)methyl)(prop-2-yn-1-yl)amino)methyl)phenyl)-*N*-(trityloxy)acrylamide (51). To a mixture of **50** (6.13 g, 15.52 mmol), EDC (4.45 g, 23.28 mmol), HOBt (2.61 g, 17.07 mmol) and DMAP (2.08 g, 17.07 mmol) in anhydrous chloroform (50 mL) was added triethylamine (3.3 mL, 23.28 mmol) followed by immediate addition of *O*-tritylhydroxylamine (5.34 g, 19.4 mmol). The mixture was stirred at room temperature under nitrogen for 6 hrs. Upon completion, reaction mixture was concentrated in vacuo, diluted with water and extracted with DCM (3 × 50 mL). The combined DCM extracts were dried over anhydrous sodium sulfate, solvent removed in vacuo. The crude product was then purified by silica gel chromatography eluting with a gradient of 0-35% EtOAc in hexanes to give **51** as a white solid (4.45 g, 75%). ^{1}H NMR (400 MHz, DMSO-d_6) δ 10.40 (s, 1H), 7.62 – 6.76 (m, 20H), 6.45 (d, J = 14.6 Hz, 1H), 3.76 (s, 2H), 3.66 (s, 2H), 3.31 (s, 1H), 3.25 (s, 3H).^{13}C NMR (101 MHz, DMSO-d_6) δ 170.86, 130.30 – 129.77, 128.51 – 127.49, 78.39, 76.95, 60.21, 57.09, 44.75, 41.90. HRMS (ESI-TOF) *m/z* calcd for $C_{39}H_{28}F_5N_2O_2$ $[M-H]^-$: 651.2076, found: 651.2078.

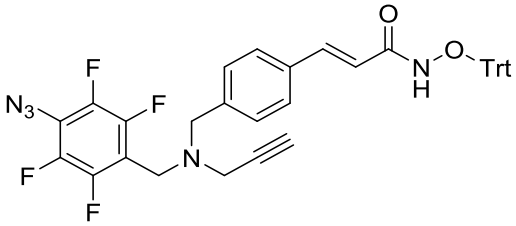

(*E*)-3-(4-(((4-azido-2,3,5,6-tetrafluorobenzyl)(prop-2-yn-1-yl)amino)methyl)phenyl)-*N*-(trityloxy)acrylamide (52). sodium azide (8.84 g, 13.6 mmmol), tetrabutylammonium azide (0.97 g, 3.41 mmol) and **51** (4.45 g, 6.8 mmol) were heated in anhydrous dimethylformamide (25 mL) at 80 °C in a pressure vessel under nitrogen gas for 15 h. The reaction mixture was concentrated in vacuo, diluted with water (100 mL) and extracted with DCM (30 mL). The DCM layer was washed with water (50 mL) then brine (50 mL) and solvent removed in vacuo. The brown crude product was purified by short silica gel column eluting with 20% EtOAc in hexane to give **52** as shiny yellow crystals (0.86 g, 25%). ^{1}H NMR (400 MHz, $CDCl_3$) δ 7.77 (d, J = 21.5 Hz, 1H), 7.61 – 7.03 (m, 24H), 6.10 (d, J = 15.8 Hz, 1H), 3.84 (s, 2H), 3.72 (s, 2H), 3.29 (s, 2H), 2.32 (s, 1H).^{13}C NMR (101 MHz, $CDCl_3$) δ 140.01, 129.06 (d, J = 19.5 Hz), 128.12 (d, J =

APPENDIX Q (CONTINUED)

15.2 Hz), 73.81, 57.01, 45.07, 41.71. HRMS (ESI-TOF) *m/z* calcd for $C_{39}H_{28}F_4N_5O_2$ $[M-H]^-$: 674.2184, found: 674.2206.

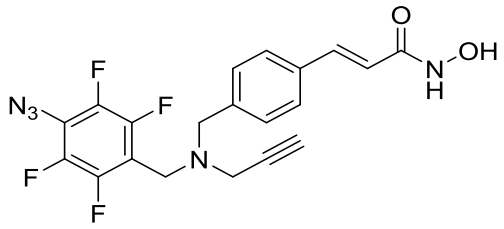

(*E*)-3-(4-(((4-azido-2,3,5,6-tetrafluorobenzyl)(prop-2-yn-1-yl)amino)methyl)phenyl)-*N*-hydroxyacrylamide (7). To a solution of **52** (0.70 g, 1.03 mmol) in DCM was added magnesium bromide (1.48 g, 10.06 mmol) and reaction was stirred at room temperature under nitrogen for 30 min. Upon completion, reaction mixture was concentrated under vacuum, diluted with water, pH adjusted to ≈ 8, the precipitate was filtered, washed with 20% EtOAc (10 × 10 mL). The pure product was dried under vacuum to yield a **7** as a light brown solid (0.2 g, 50%). ^{1}H NMR (400 MHz, DMSO-d_6) δ 7.67 – 7.00 (m, 6H), 6.48 (d, 1H), 5.75 (d, 1H), 3.76 (s, 2H), 3.24 (s, 2H), 3.17 (s, 2H), 1.23 (s, 1H). ^{13}C NMR (101 MHz, DMSO-d_6) δ 128.95 (d, J = 18.6 Hz), 127.61 (d, J = 25.0 Hz), 77.91, 76.18, 56.64, 48.61, 44.38, 41.33.^{19}F NMR (376 MHz, DMSO-d_6) δ -143.00 (dd, J = 22.3, 9.2 Hz), -152.91 (dd, J = 22.4, 9.5 Hz). HRMS (ESI-TOF) *m/z* calcd for $C_{20}H_{16}F_4N_5O_2$ $[M+H]^+$: 434.1235, found: 434.1236.

APPENDIX R: SYNTHESIS OF HDAC8 SELECTIVE PRP 11.

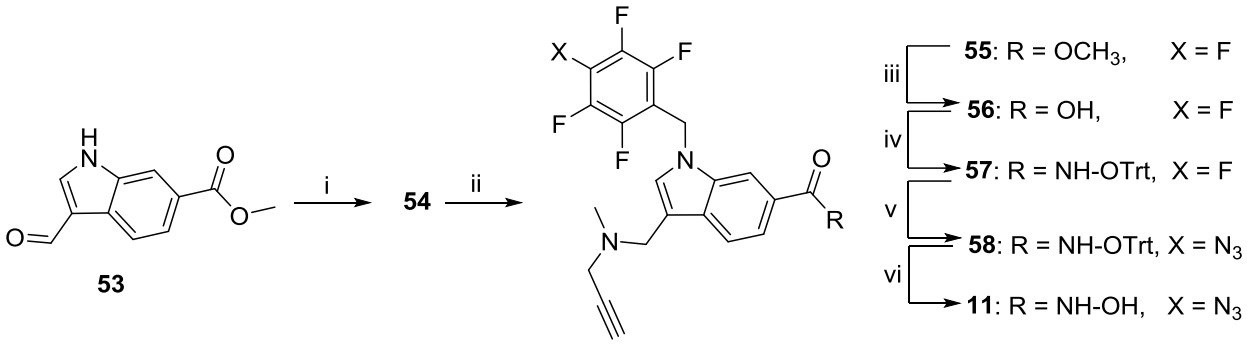

Reagents and conditions: (i) perfluotobenzylbromide, NaH, CH_3CN, 14 h; ii. N-methylpropargylamine, STAB-H, DCE, 5 h; (iii) LiOH, THF:H_2O:1,4-dioxane (6:3:1), 12 h; (iv) *O*-tritylhydroxylamine, EDC·HCl, HOBt, DMAP, Et_3N, $CHCl_3$, 6 h; (v) NaN_3, Bu_4NN_3, DMF, 50 °C, 22 h; (vi) $MgBr_2$, DCM, 3 h.

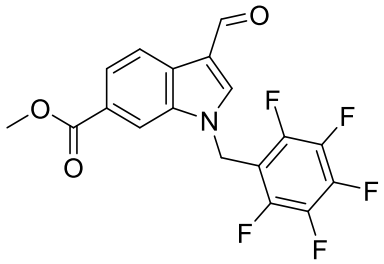

Methyl 3-formyl-1-((perfluorophenyl)methyl)-1*H*-indole-6-carboxylate (54). To a solution of methyl 3-formyl-1*H*-indole-6-carboxylate, **53** (230 mg, 1.13 mmol) and pentafluorobenzylbromide (0.17 mL, 1.13 mmol) in anhydrous dimethylformamide (3 mL) was added sodium hydride (60% mineral oil suspension, 67.9 mg, 1.69 mmol) and stirred at room temperature for 18 h. Upon completion, the reaction mixture was diluted with water (30 mL), extracted with ethyl acetate (3 × 30 mL). The combined organic extracts were washed with dilute sodium bicarbonate (30 mL) and brine (30 mL) then dried over anhydrous sodium sulfate, filtered and solvent removed in vacuo. The product **54** was obtained as orange-yellow solid (430 mg, 99%) and used in the next step without further purification. ^{1}H NMR (400 MHz, $CDCl_3$) δ 10.06 (s, 1H), 8.42 – 8.21 (m, 2H), 8.03 (d, *J* = 7.8 Hz, 1H), 7.94 (s, 1H), 5.52 (s, 2H), 3.99 (s, 3H). ^{13}C NMR (101 MHz, $CDCl_3$) δ 183.99, 166.75, 146.25, 143.74, 139.31, 138.61, 136.04, 128.33, 126.11, 123.93, 121.62, 118.82, 111.31, 99.59, 51.93, 37.63. HRMS (ESI-TOF) *m/z* calcd for $C_{18}H_{11}F_5NO_3$ $[M+H]^+$: 384.0654, found: 384.0655.

APPENDIX R (CONTINUED)

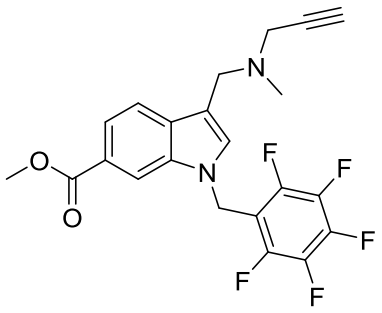

Methyl 3-((methyl(prop-2-yn-1-yl)amino)methyl)-1-((perfluorophenyl)methyl)-1*H*-indole-6-carboxylate (55). To a solution of **54** (360 mg, 0.94 mmol) in dichloroethane (3 mL) was added *N*-methylpropargylamine (0.237 mL, 2.8 mmol) and sodium triacetoxyborohydride (398.3 mg, 1.88 mmol). The reaction mixture was stirred at room temperature under nitrogen for 5 h then it was concentrated, diluted with water (3 mL), pH adjusted by 1N sodium hydroxide to ≈ 9 and extracted with DCM (3 × 3mL). The DCM extracts were combined, dried over anhydrous sodium sulfate and the solvent was evaporated in vacuo to yield **55** as an orange oil (400 mg, 97%) which was used in the next step without further purification. ^{1}H NMR (400 MHz, $CDCl_3$) δ 8.23 (s, 1H), 7.88 – 7.80 (m, 1H), 7.77 (dd, *J* = 7.7, 5.1 Hz, 1H), 7.28 (d, *J* = 3.3 Hz, 2H), 5.42 (s, 2H), 3.98 (d, *J* = 4.8 Hz, 3H), 3.75 (s, 2H), 3.33 (s, 2H), 2.38 (s, 3H), 2.31 (d, *J* = 2.2 Hz, 1H). ^{13}C NMR (101 MHz, $CDCl_3$) δ 167.53, 146.13, 143.72, 136.02, 135.27, 131.44, 129.77, 123.80, 120.54, 119.11, 113.54, 110.94, 109.91, 78.23, 73.01, 51.66, 49.79, 44.32, 41.39, 36.74.

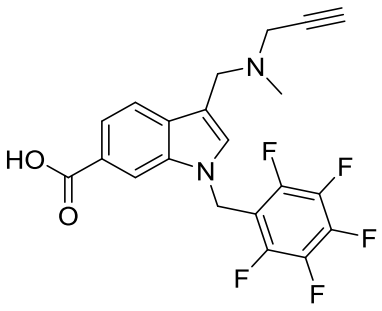

3-((Methyl(prop-2-yn-1-yl)amino)methyl)-1-((perfluorophenyl)methyl)-1*H*-indole-6-carboxylic acid (56). Intermediate **55** (400 mg, 0.92 mmol) was dissolved in 30 mL THF:water:dioxane (6:3:1) and lithium hydroxide (110.17 mg, 4.6 mmol) was added. The solution was stirred at RT under nitrogen till complete hydrolysis (120 h). The reaction mixture was concentrated in vacuo, the residue was taken in 10 mL iced-brine, pH adjusted to ≈ 5 by 1M hydrochloric acid and extracted with ethyl acetate (3 × 50 mL). The combined organic extracts were dried to give **56** as an orange brown solid (380 mg, 98%) that was employed for the next step without further purification. ^{1}H NMR (400 MHz, $CDCl_3$) δ 8.19 (s, 1H), 7.80 (d, *J* = 7.3 Hz, 1H), 7.69 (d, *J* = 6.5 Hz, 1H), 7.33 (s, 1H), 5.33 (s, 2H), 3.81 (s, 2H), 3.40 – 3.22 (m, 2H), 2.40 (s, 3H), 2.31 (s, 2H). ^{13}C NMR (101 MHz, $CDCl_3$) δ 171.21, 146.15, 143.70, 142.31, 139.77, 138.49, 135.96, 135.17, 131.38, 130.90, 124.94, 121.10, 118.59, 111.36, 111.07, 109.84, 76.79,

APPENDIX R (CONTINUED)

74.48, 48.68, 43.38, 40.39, 36.70. HRMS (ESI-TOF) *m/z* calcd for $C_{21}H_{16}F_5N_2O_2$ $[M-H]^-$: 421.0981, found: 421.0967.

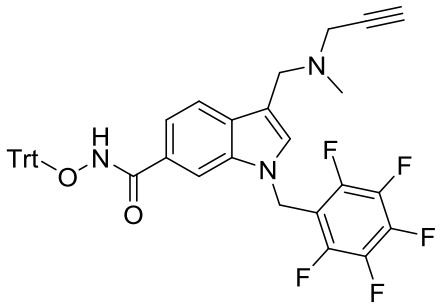

3-((Methyl(prop-2-yn-1-yl)amino)methyl)-1-((perfluorophenyl)methyl)-*N*-(trityloxy)-1*H*-indole-6-carboxamide (57). To a mixture of **56** (400 mg, 0.948mmol), EDC (271.738 mg, 1.421 mmol), HOBt (159.622 mg, 1.042 mmol) and DMAP (127.255 mg, 1.042 mmol) in anhydrous chloroform (10 mL) was added triethylamine (0.201 mL, 1.421 mmol) followed by *O*-tritylhydroxylamine (325.902 mg, 1.185 mmol). The mixture was stirred at room temperature under nitrogen for 6 hrs. The reaction mixture was concentrated in vacuo, diluted with water and extracted with DCM (3 × 10 mL). The combined organic layers were dried over anhydrous sodium sulfate and solvent was removed in vacuo. The crude product was purified by silica gel chromatography eluting a gradient of 10-80% EtOAc in hexanes to give **57** as white solid (300 mg, 50%). ^{1}H NMR (400 MHz, $CDCl_3$) δ 7.92 (s, 1H), 7.76 (s, 1H), 7.66 – 7.53 (m, 7H), 7.42 – 7.19 (m, 13H), 7.10 (d, *J* = 7.3 Hz, 1H), 5.33 (s, 2H), 3.70 (s, 2H), 3.28 (s, 2H), 2.33 (s, 3H), 2.28 (s, 1H). ^{13}C NMR (101 MHz, $CDCl_3$) δ 166.39, 147.25, 143.63, 141.60, 139.86, 135.27, 130.56, 129.30, 128.52, 127.63, 127.39, 125.89, 119.40, 117.44, 113.39, 108.75, 92.83, 78.16, 78.16, 73.03, 49.75, 44.24, 41.34, 36.75. HRMS (ESI-TOF) *m/z* calcd for $C_{40}H_{31}F_5N_3O_2$ $[M+H]^+$: 680.2331, found: 680.2312.

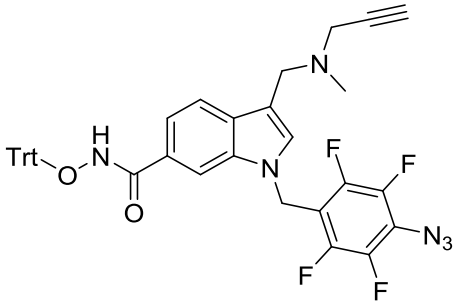

1-(4-Azido-2,3,5,6-tetrafluorobenzyl)-3-((methyl(prop-2-yn-1-yl)amino)methyl)-*N*-(trityloxy)-1*H*-indole-6-carboxamide (58). A solution of **57** (300 mg, 0.442 mmol) in anhydrous dimethylformamide (3 mL) was added sodium azide (57.427 mg, 0.883 mmol) and tetrabutylammonium azide (62.824 mg, 0.221 mmol) and the reaction was stirred under nitrogen at 50 °C for 22 h. LCMS and ^{19}F NMR were used to confirm complete azidation of the starting material. The mixture was allowed to cool to room temperature then diluted with water (30 mL),

APPENDIX R (CONTINUED)

extracted with ethyl acetate, the organic layer was washed twice with brine then dried over anhydrous sodium sulfate. The solvent was evaporated in vacuo to give **58** as a brown solid (305 mg, 98%) which was used for the next step without further purification. ^{1}H NMR (400 MHz, $CDCl_3$) δ 8.02 (s, 1H), 7.93 (s, 1H), 7.75 (s, 2H), 7.60 (s, 12H), 7.43 – 7.20 (m, 19H), 7.11 (s, 2H), 5.31 (s, 3H), 3.70 (s, 3H), 3.28 (s, 3H), 2.33 (s, 4H), 2.29 (d, *J* = 2.2 Hz, 3H). ^{13}C NMR (101 MHz, $CDCl_3$) δ 166.70, 141.61, 135.24, 130.57, 129.43, 128.54, 127.64, 127.39, 125.84, 119.35, 117.46, 113.15, 108.76, 92.83, 78.11, 73.10, 49.70, 44.19, 41.29, 36.85. ^{19}F NMR (376 MHz, $CDCl_3$) δ -139.96 – -140.95 (m), -149.04 (d, *J* = 21.2 Hz). HRMS (ESI-TOF) *m/z* calcd for $C_{40}H_{29}F_4N_6O_2$ $[M-H]^-$: 701.2293, found: 701.2295.

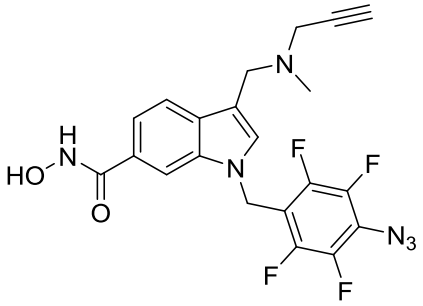

1-(4-Azido-2,3,5,6-tetrafluorobenzyl)-N-hydroxy-3-((methyl(prop-2-yn-1-yl)amino)methyl)-1H-indole-6-carboxamide (11). To a solution of 58 (210 mg, 0.299 mmol) in anhydrous DCM (10 mL), magnesium bromide (5.43 g, 29.91 mmol) was added and the mixture was stirred for 3 h at room temperature under nitrogen atmosphere. The mixture was concentered, diluted with water, pH adjusted to ≈ 8 by 1N sodium hydroxide and extracted with Ethyl acetate (3 × 20 mL). The product was purified using silica gel chromatography eluting 0-10% methanol in ethyl acetate. The pure product was obtained as a brown solid (50 mg, 36%). 1H NMR (400 MHz, CDCl3) δ 8.01 (s, 1H), 7.77 (s, 1H), 7.41 (s, 1H), 7.29 (s, 1H), 5.39 (s, 2H), 3.76 (s, 2H), 3.33 (s, 2H), 2.38 (s, 3H), 2.32 (s, 1H). 13C NMR (101 MHz, DMSO-d6) δ 165.78, 135.82, 130.65, 130.35, 126.88, 119.58, 118.13, 112.68, 111.24, 109.47, 79.62, 76.34, 50.40, 44.73, 41.45, 37.59. 19F NMR (376 MHz, DMSO-d6) δ -143.36 (dd, J = 22.3, 9.1 Hz), -151.78 (dd, J = 22.3, 9.2 Hz). HRMS (ESI-TOF) m/z calcd for C21H17F4N6O2 [M-H]-: 459.1198, found: 459.1196.

APPENDIX S: SYNTHESIS OF TRIFLUOROMETHYLOXADIAZOLE PRP 13.

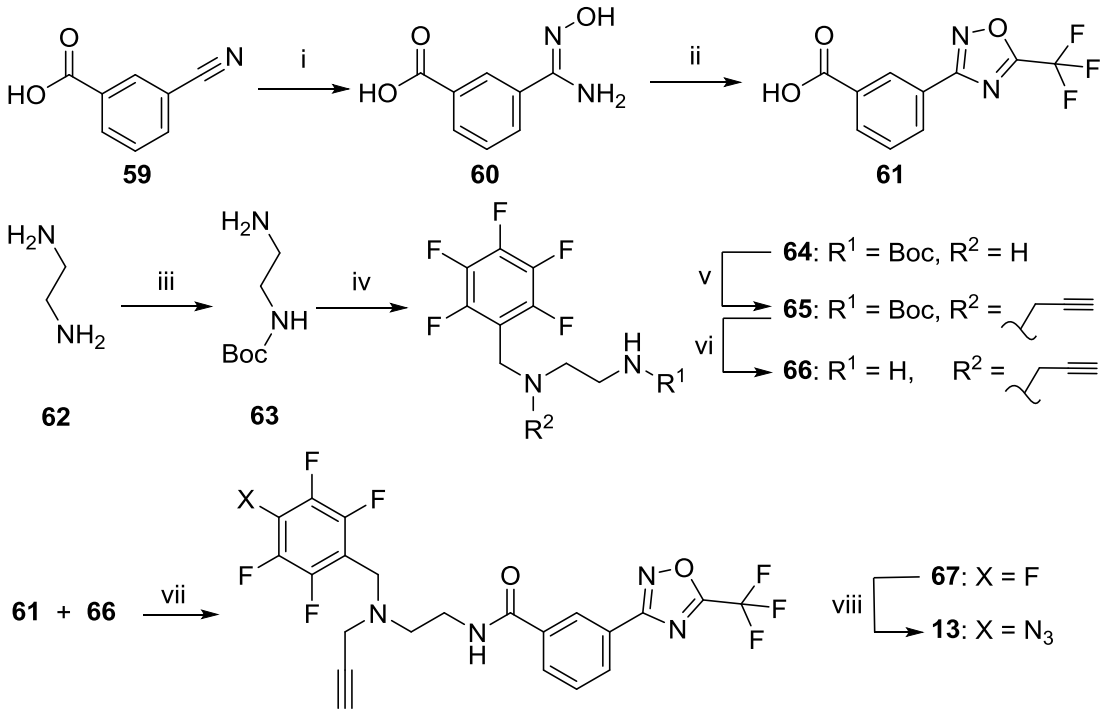

Reagents and conditions: (i) NH_2OH, Na_2CO_3, CH_3OH/H_2O, Reflux 4 h; (ii) TFAA, 0–50 °C, pyridine, 5 h; (iii) $(Boc)_2O$, $CHCl_3$, 0 °C–rt; (iv) **14**, $NaBH_4$, CH_3OH, 8 h; (v) propargyl bromide, K_2CO_3, CH_3CN, 48 h; (vi) 4M HCl, 1,4-dioxane, 1 h; (vii) EDC·HCl, HOBt, DMAP, Et_3N, $CHCl_3$, 12 h; (viii) NaN_3, Bu_4NN_3, DMF, 80 °C.

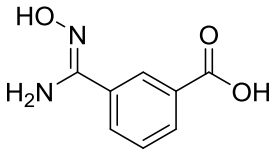

(*Z*)-3-(*N*'-hydroxycarbamimidoyl)benzoic acid (60). To a solution of 3-cyanobenzoic acid **59** (1g, 6.8 mmol) in ethanol (50 mL), 8-hydroxyquinoline (5 mg, 0.03 mmol) was added. A solution of hydroxylamine hydrochloride (950 mg, 13.6 mmol) in water (8 mL) and sodium carbonate (1.2 g, 10.9 mmol) in water (12 mL) were added successively. The reaction was refluxed for 4 h (85 °C). Upon completion, ethanol was removed under vacuum, the residue was diluted with water and set in an ice-bath. The cooled mixture was acidified to pH ≈ 3.5, the product **60** was precipitated as a greyish-white solid (500 mg, 41%), filtered, washed with iced water and dried in vacuo. ^{1}H NMR (400 MHz, DMSO-*d*$_6$) δ 9.73 (s, 1H), 8.27 (s, 1H), 7.93 (d, *J* = 6.9 Hz, 1H), 7.88 (d, *J* = 6.9 Hz, 1H), 7.49 (t, *J* = 7.0 Hz, 1H), 5.89 (s, 2H). ^{13}C NMR (101 MHz, DMSO-*d*$_6$) δ 159.26, 150.36, 133.70, 129.63, 129.44, 128.42, 128.39, 126.41. HRMS (ESI-TOF) *m/z* calcd for $C_8H_9N_2O_3$ $[M+H]^+$: 181.0608, found: 181.0603.

APPENDIX S (CONTINUED)

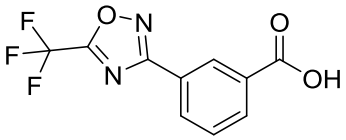

3-(5-(Trifluoromethyl)-1,2,4-oxadiazol-3-yl)benzoic acid (61). A suspension of the benzamidoxime **60** (500 mg, 2.8 mmol) in anhydrous pyridine (8 mL) was cooled in ice bath. Trifluoroacetic anhydride (1.62 mL, 8.34 mmol) was added dropwise over 20 min. The reaction was slowly warmed to room temperature and further heated to 50 °C for 3 h. The reaction mixture was poured into ice-water and pH adjusted to ≈ 4 by 10% hydrochloric acid. The product was extracted by ethyl acetate and the solvent was removed under reduced pressure. The crude was purified by silica gel chromatography running 3-20% ethyl acetate in hexanes where **61** was separated as white crystals (200 mg, 25%). ^{1}H NMR (400 MHz, DMSO-d_6) δ 13.42 (s, 1H), 8.57 (s, 1H), 8.30 (d, J = 7.8 Hz, 1H), 8.21 (d, J = 7.8 Hz, 1H), 7.77 (t, J = 7.8 Hz, 1H). ^{13}C NMR (101 MHz, DMSO-d_6) δ 168.49, 167.97, 166.35, 133.12, 132.11, 131.44, 130.27, 128.00, 124.99, 120.81. HRMS (ESI-TOF) *m/z* calcd for $C_{10}H_4F_3N_2O_3$ $[M-H]^-$: 257.0179, found: 257.0191.

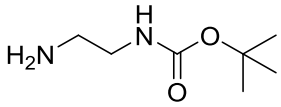

***tert*-Butyl (2-aminoethyl)carbamate (63).** Di-*tert*-butyl dicarbonate (2.5 g, 12 mmol) solution in 60 mL of chloroform was added dropwise to a solution of 1,2-diamimoethane **62** (8.3 mL, 125 mmol) in 125 mL of chloroform over 3 h with vigorous stirring and cooling in an ice bath. The reaction mixture was stirred for additional 16 h at room temperature. The reaction mixture was concentrated in vacuo then washed with (6 × 60 mL) of water. The chloroform layer was dried over anhydrous sodium sulfate, evaporated to give **63** as a colorless oil (1.5 g, 80%) which was used for the next step without further purification. ^{1}H NMR (400 MHz, $CDCl_3$) δ 4.87 (bs, 1H), 3.27 – 3.11 (m, 2H), 2.80 (dd, J = 7.8, 3.7 Hz, 2H), 1.46 (s, 9H), 1.35 (s, 2H). ^{13}C NMR (101 MHz, $CDCl_3$) δ 156.19, 79.22, 41.89, 28.40, 28.37. HRMS (ESI-TOF) *m/z* calcd for $C_7H_{17}N_2O_2$ $[M+H]^+$: 161.1285, found: 161.1284.

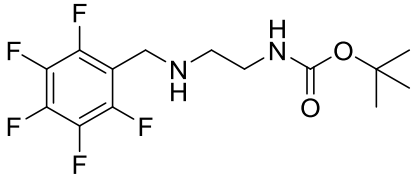

tert-Butyl (2-(((perfluorophenyl)methyl)amino)ethyl)carbamate (64).
Pentafluorobenzaldehyde (1.53 g, 7.81 mmol) was added to a solution of 63 (1.4 g, 8.72 mmol) in anhydrous methanol (40 mL) and stirred for 3 h over molecular sieves 4 Å. The reaction was placed in an ice-bath and sodium borohydride (1.2 g, 31.64 mmol) was added portionwise with 10 min interval during 30 min. The reaction was stirred at room temperature for 5 h under

APPENDIX S (CONTINUED)

nitrogen atmosphere. Upon completion, the solvent was removed in vacuo, the crude was washed by saturated sodium bicarbonate till pH ≈ 8 then extracted with EtOAc (3 × 40 mL). The product was purified by silica gel chromatography eluting with 15-50% EtOAc in hexanes to give 64 as an oily colorless viscous liquid (1.5 g, 56%). 1H NMR (400 MHz, CDCl3) δ 4.86 (bs, 1H), 3.93 (s, 2H), 3.23 (d, J = 3.7 Hz, 2H), 2.71 (s, 2H), 2.06 (d, J = 2.5 Hz, 1H), 1.45 (d, J = 2.3 Hz, 13H). 13C NMR (101 MHz, CDCl3) δ 155.65, 143.66, 143.02, 142.67, 104.76, 78.95, 47.66, 39.72, 39.72, 27.96. HRMS (ESI-TOF) m/z calcd for C14H18F5N2O2 [M+H]+: 341.1283, found: 341.1254.

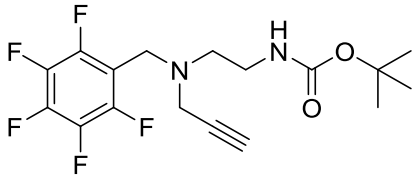

***tert*-Butyl (2-(((perfluorophenyl)methyl)(prop-2-yn-1-yl)amino)ethyl)carbamate (65).** To a solution of **64** (500 mg, 1.47 mmol) in acetonitrile (15 mL) was added potassium carbonate (504.29 mg, 3.7 mmol) and stirred for 15 min. Propargyl bromide (80% w/v in toluene, 0.48 mL, 4.41 mmol) was added dropwise. The reaction mixture was stirred for 24 h under nitrogen atmosphere then acetonitrile was removed under vacuo, the crude was washed with brine, extracted by ethyl acetate (3 × 20 mL), the combined organic extracts were combined and solvent evaporated in vacuo to give **65** an orange solid (550 mg, 98%) which was used in the next step without further purification. ^{1}H NMR (400 MHz, $CDCl_3$) δ 4.83 (s, 1H), 3.81 (s, 2H), 3.37 (d, 2H), 3.24 (s, 2H), 2.72 (t, *J* = 5.3 Hz, 2H), 2.25 (d, *J* = 1.8 Hz, 1H), 1.44 (s, 12H). ^{13}C NMR (101 MHz, $CDCl_3$) δ 155.91, 148.30, 148.03, 130.49, 108.67, 79.22, 77.45, 73.64, 52.24, 44.68, 41.88, 37.70, 28.34. HRMS (ESI-TOF) *m/z* calcd for $C_{17}H_{20}F_5N_2O_2$ $[M+H]^+$: 379.1439, found: 379.1426.

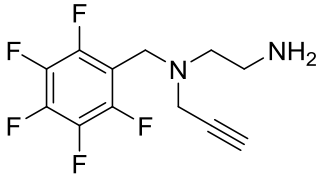

***N*^{1}-((perfluorophenyl)methyl)-*N*^{1}-(prop-2-yn-1-yl)ethane-1,2-diamine (66).** To a solution of **65** (550 mg, 1.45 mmol) in 1,4-dioxane (6 mL) was added 4M hydrochloric acid in 1,4-dioxane (10 mL) and stirred for 3 h at room temperature. The solvent was then evaporated under vacuo to yield a brown sticky solid (453 mg, 99%). The amine hydrochloride salt was converted into the free amine base by adding trimethylamine (0.2 mL) to a DCM suspension till complete dissolution then the solvent was evaporated yielding **66** as a light brown crystalline solid (400 mg). NMR data for HCl salt: ^{1}H NMR (400 MHz, DMSO-d_6) δ 7.96 (bs, 3H), 4.37 (bs, 11H), 3.84 (s, 2H), 3.48 (d, *J* = 1.3 Hz, 2H), 3.29 (s, 1H), 2.91 (dd, *J* = 11.3, 5.6 Hz, 2H), 2.79 (t, *J* = 6.1 Hz, 2H). ^{13}C NMR (101 MHz, DMSO-d_6) δ 146.23, 130.36, 118.34, 110.93, 77.63, 76.91, 49.18, 44.44, 41.55, 36.10. HRMS (ESI-TOF) *m/z* calcd for $C_{12}H_{12}F_5N_2$ $[M+H]^+$: 279.0915, found: 279.0907.

APPENDIX S (CONTINUED)

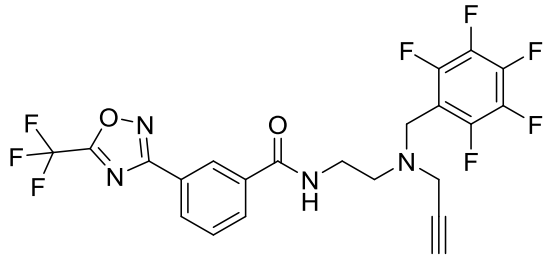

***N*-(2-(((Perfluorophenyl)methyl)(prop-2-yn-1-yl)amino)ethyl)-3-(5-(trifluoromethyl)-1,2,4-oxadiazol-3-yl)benzamide (67).** To a solution of **61** (200 mg, 0.77 mmol) in anhydrous DCM (10 mL), EDC.HCl (220.8 mg, 1.15 mmol), HOBt (114.379 mg, 0.87 mmol) and DMAP (106.21 mg, 0.87 mmol), triethylamine (0.16 mL, 1.16 mmol) were added and the solution was stirred for 15 min. **66** (214.23 mg, 0.97 mmol) was added, the reaction was stirred at room temperature under nitrogen for 20 h. The solvent was evaporated, residue diluted with water, made moderately basic (pH ≈ 9) extracted with DCM (3 × 10 mL). The combined organic extracts were dried over anhydrous sodium sulfate and solvent evaporated. The crude product was purified by silica gel chromatography eluting 5-35% EtOAc in hexanes to give **63** as a white solid (220 mg, 55%). ^{1}H NMR (400 MHz, $CDCl_3$) δ 8.46 (s, 1H), 8.27 (d, *J* = 7.6 Hz, 1H), 8.01 (d, *J* = 7.6 Hz, 1H), 7.64 (t, *J* = 7.7 Hz, 1H), 6.74 (bs, 1H), 3.89 (s, 2H), 3.62 (d, *J* = 4.6 Hz, 2H), 3.42 (s, 2H), 2.93 (s, 2H), 2.33 (s, 1H). ^{13}C NMR (101 MHz, $CDCl_3$) δ 173.10, 168.20, 165.60, 135.16, 130.48, 130.02, 129.23, 125.36, 125.01, 76.42, 73.63, 51.26, 44.49, 41.30, 36.60. HRMS (ESI-TOF) *m/z* calcd for $C_{22}H_{15}F_8N_4O_2$ $[M+H]^+$: 519.1062, found: 519.1048.

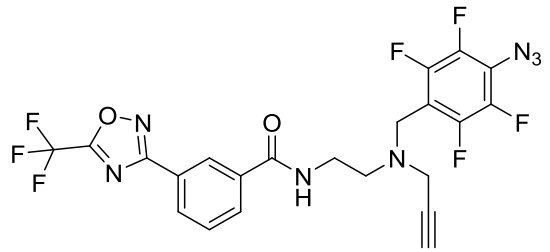

***N*-(2-((4-Azido-2,3,5,6-tetrafluorobenzyl)(prop-2-yn-1-yl)amino)ethyl)-3-(5-(trifluoromethyl)-1,2,4-oxadiazol-3-yl)benzamide (13).** To a solution of **67** (200 mg, 0.38 mmol) in anhydrous dimethylformamide (2 mL) were added sodium azide (50.16 mg, 0.76 mmol) and tetrabutylammonium azide (44.05 mg, 0.18 mmol). The reaction was heated at 80 °C for 18 h under nitrogen. After complete azidation as confirmed by LC-MS, the mixture was concentrated under vacuo, diluted with water and extracted with DCM (3 × 2 mL). The combined DCM extracts were dried over anhydrous sodium sulfate and the solvent was evaporated. The crude was purified by a short silica gel column eluting 25% EtOAc in hexanes to give **13** as white crystals (20 mg, 10%). ^{1}H NMR (400 MHz, $CDCl_3$) δ 8.47 (s, 1H), 8.28 (d, *J* = 6.7 Hz, 1H), 8.01 (d, *J* = 7.0 Hz, 1H), 7.65 (dd, *J* = 12.6, 4.9 Hz, 1H), 6.74 (bs, 1H), 3.87 (s, 2H), 3.68 – 3.53 (m, 2H), 3.43 (t, *J* = 6.1 Hz, 2H), 2.99 – 2.79 (m, 2H), 2.32 (t, *J* = 4.2 Hz, 1H). ^{13}C NMR (101 MHz, $CDCl_3$) δ 182.90, 168.23, 165.56, 144.07, 142.97, 140.57, 135.17, 130.45,

APPENDIX S (CONTINUED)

130.01, 129.21, 125.40, 125.05, 125.02, 111.53, 88.42, 73.58, 51.19, 44.61, 41.38, 36.61. ^{19}F NMR (376 MHz, $CDCl_3$) δ -65.36 (s), -142.81 (dd, *J* = 21.7, 10.6 Hz), -151.66 (dd, *J* = 21.2, 9.9 Hz). HRMS (ESI-TOF) *m/z* calcd for $C_{22}H_{15}F_7N_7O_2$ $[M+H]^+$: 542.1170, found: 542.1166.

APPENDIX T: NMR SPECTRA FOR KEY COMPOUNDS.

^{1}H NMR spectrum for PRP **2**

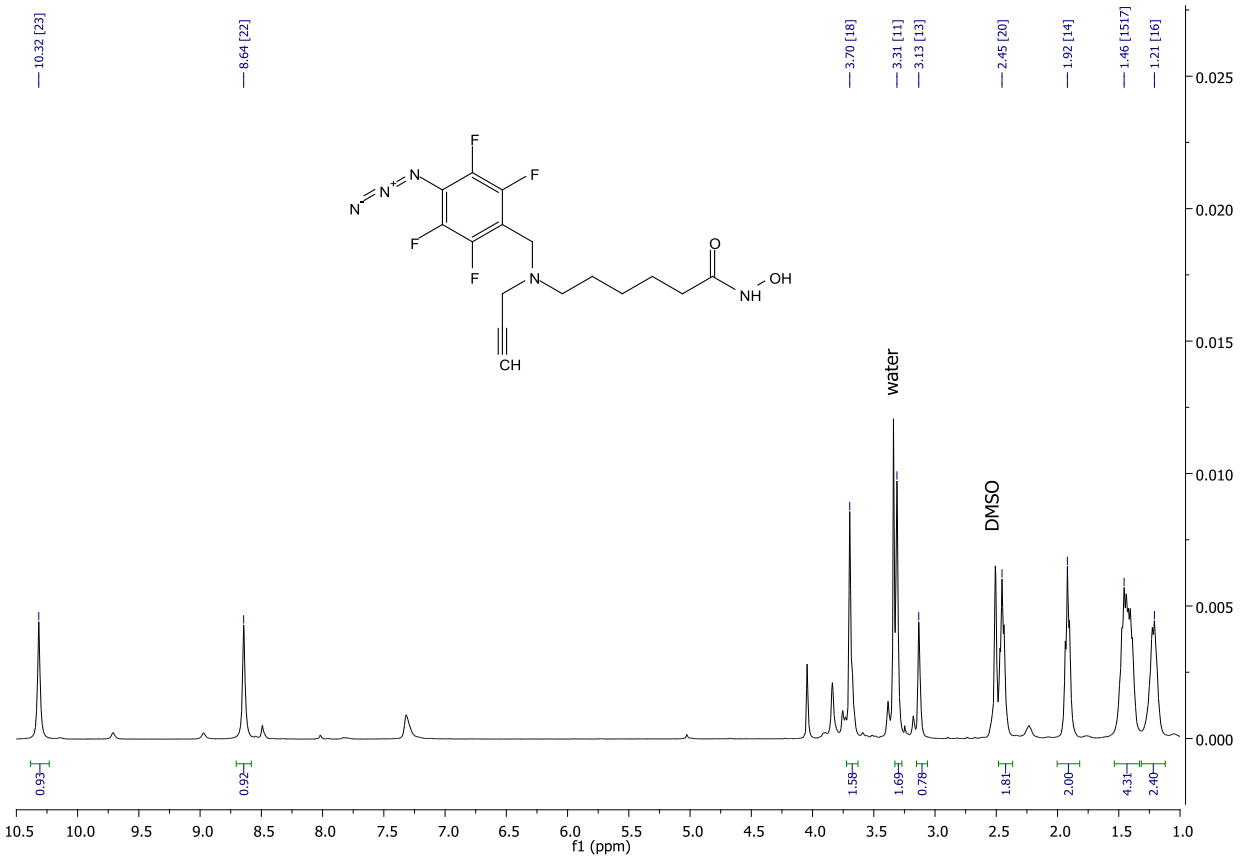

APPENDIX T (CONTINUED)

^{13}C NMR spectrum for PRP **2**

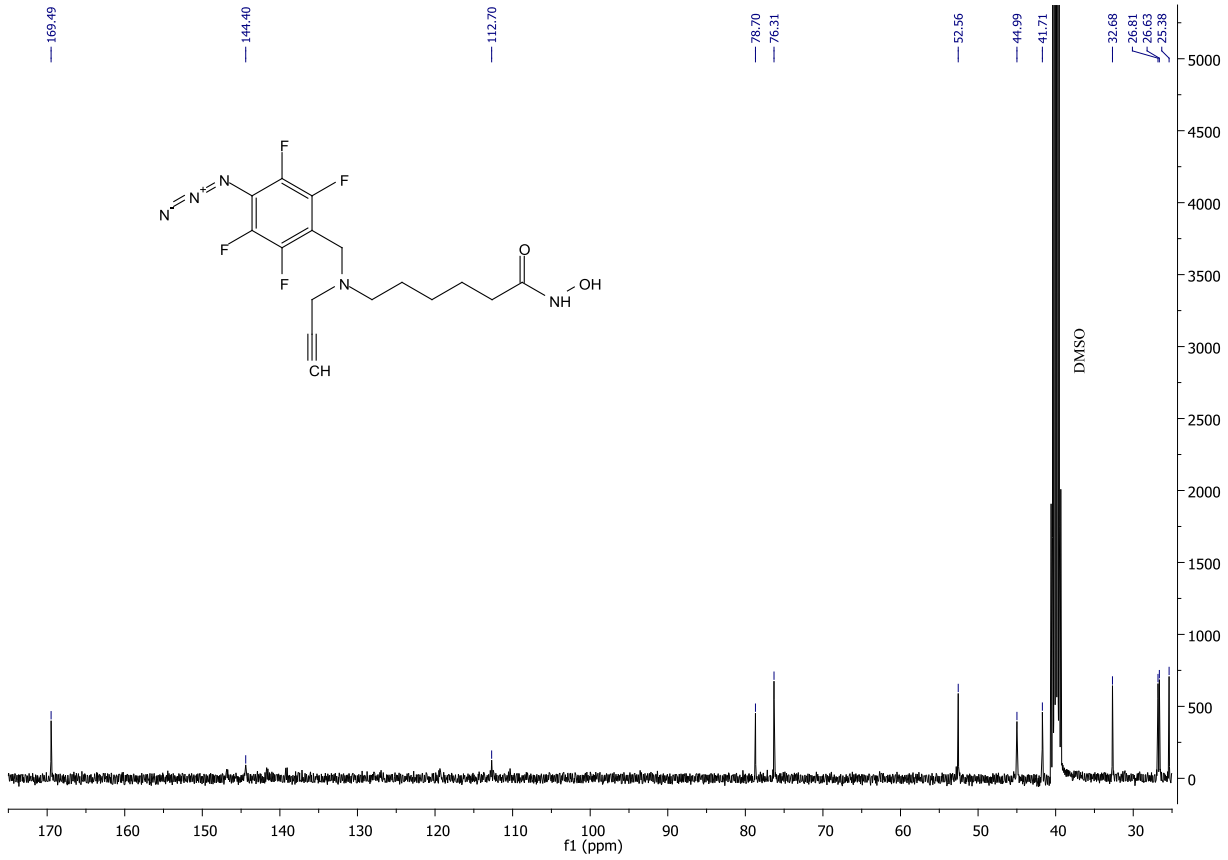

APPENDIX T (CONTINUED)

^{19}F NMR spectrum for PRP **2**

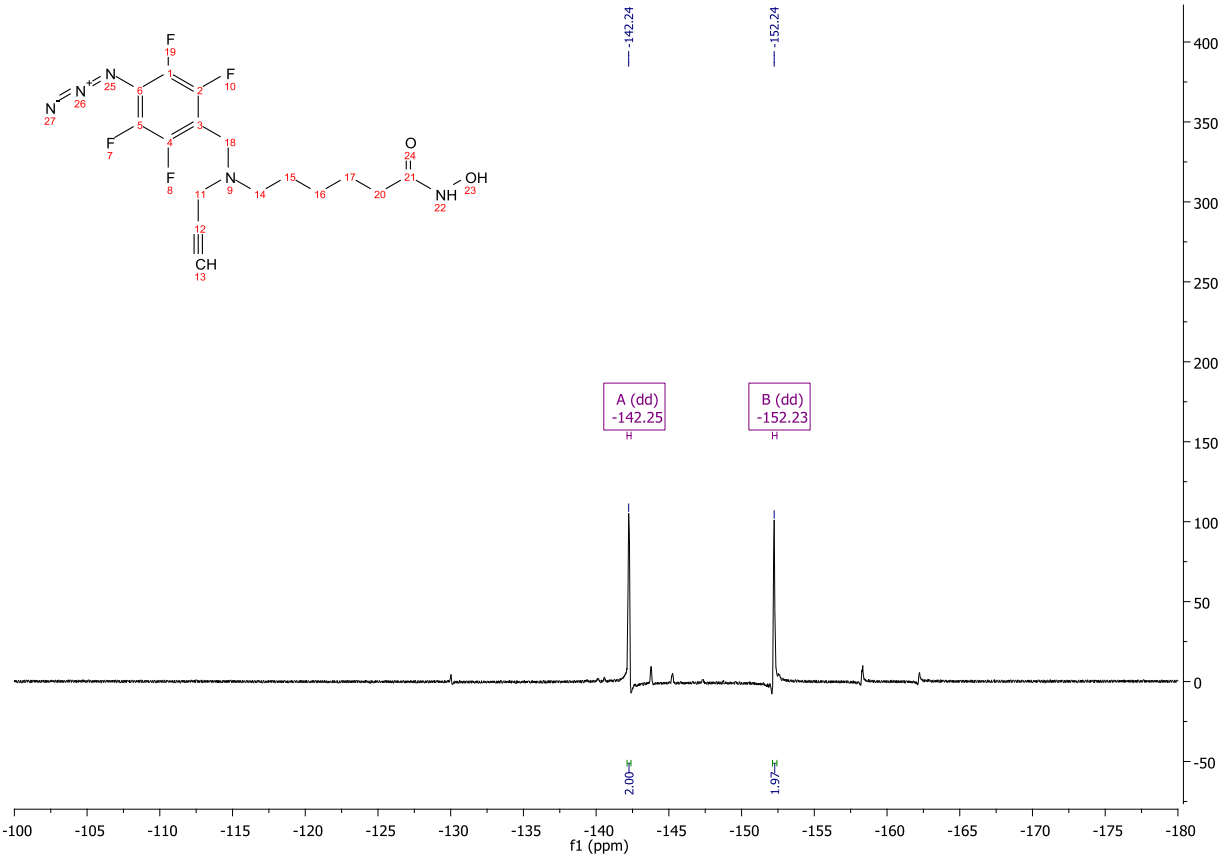

APPENDIX T (CONTINUED)

^{1}H NMR spectrum for PRP **3**

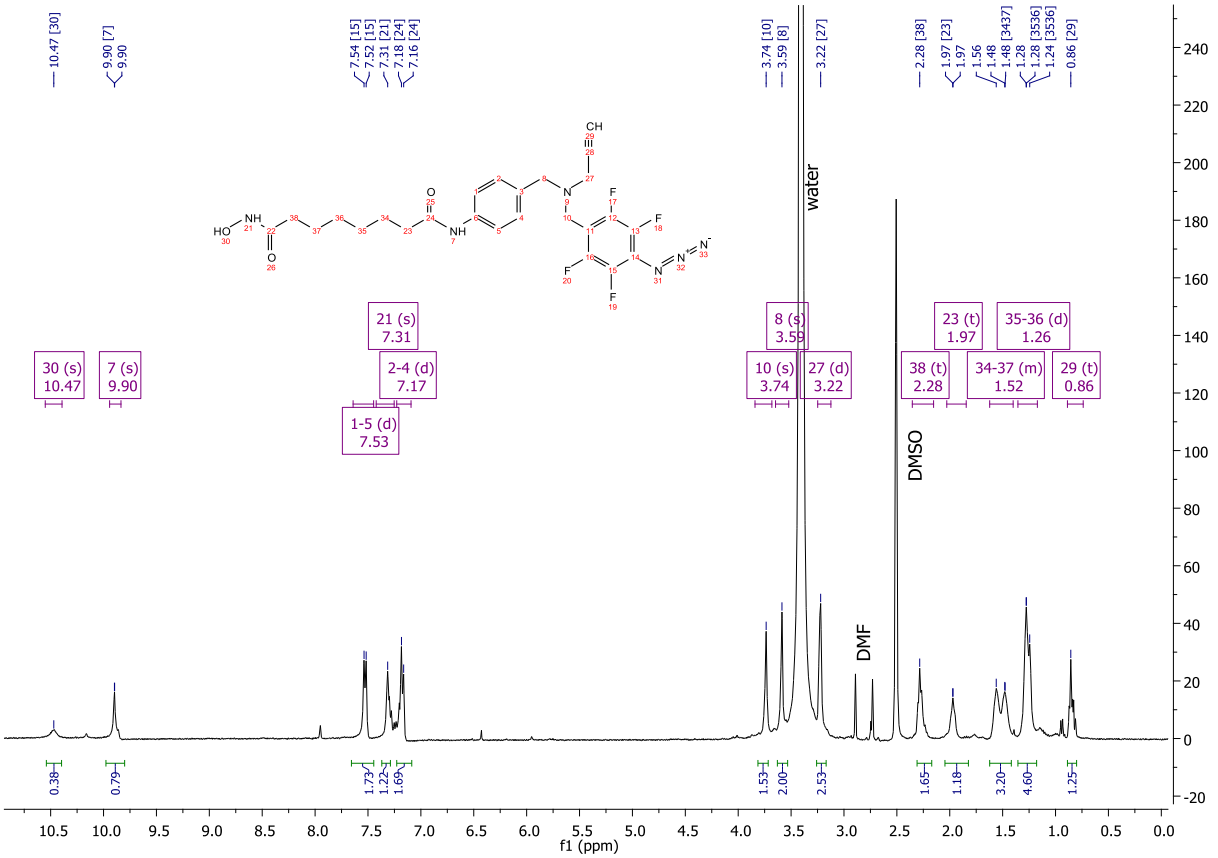

APPENDIX T (CONTINUED)

^{13}C NMR spectrum for PRP **3**

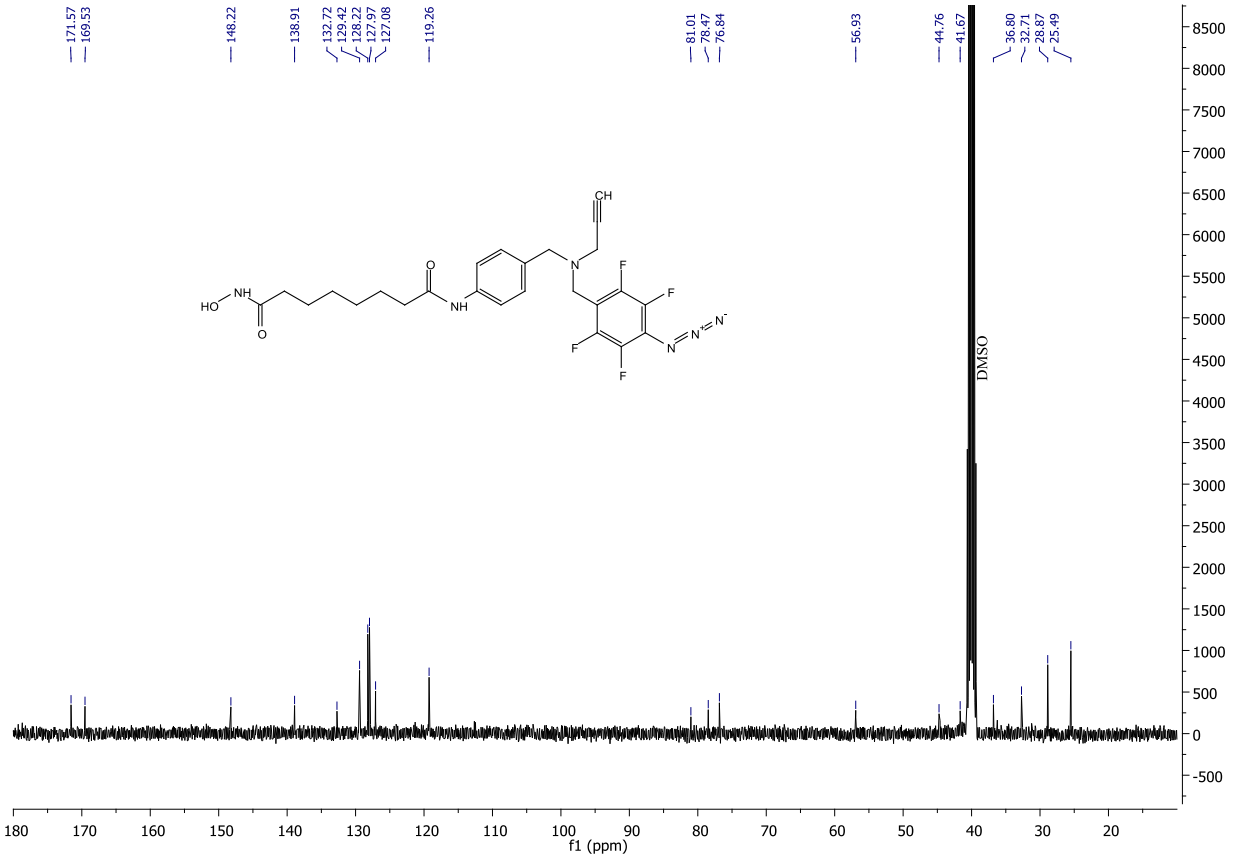

APPENDIX T (CONTINUED)

^{19}F NMR spectrum for PRP **3**

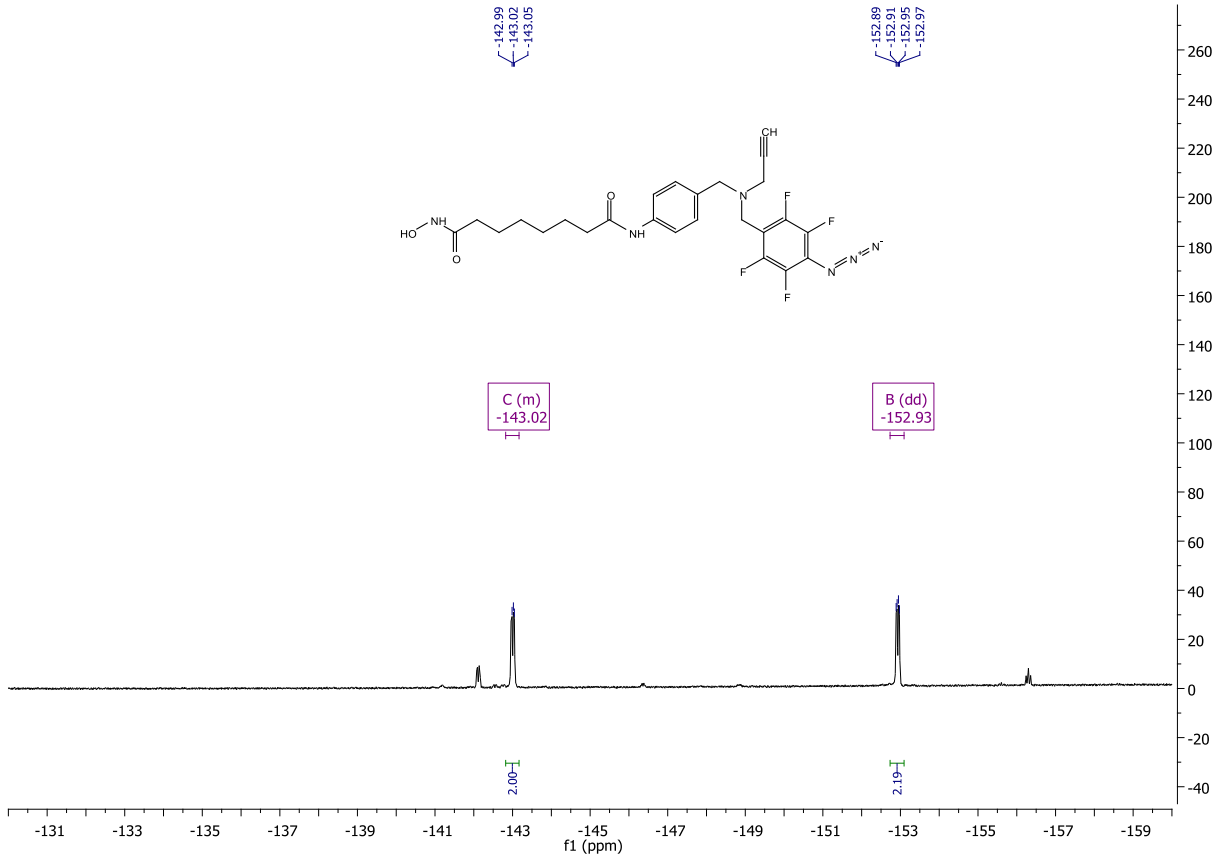

APPENDIX T (CONTINUED)

^{1}H NMR spectrum for PRP **4**

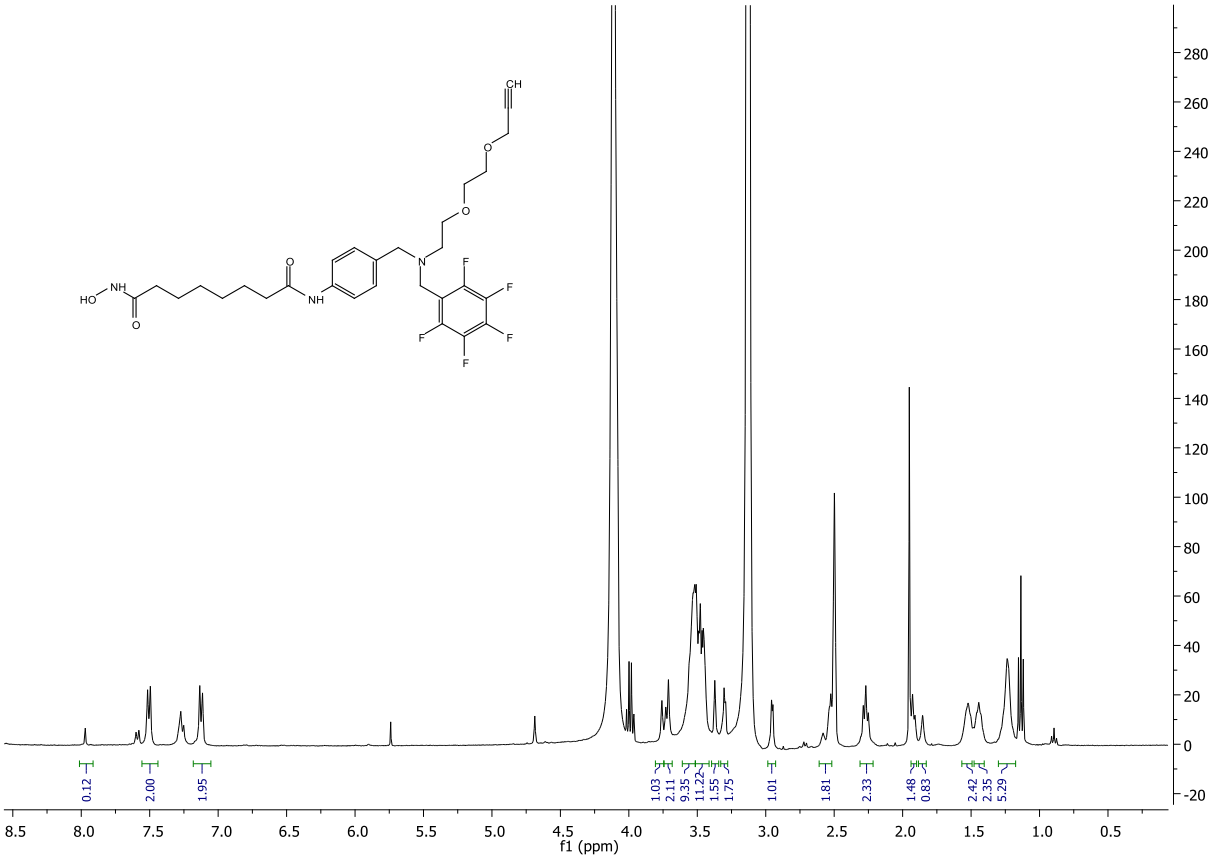

APPENDIX T (CONTINUED)

^{13}C NMR spectrum for PRP **4**

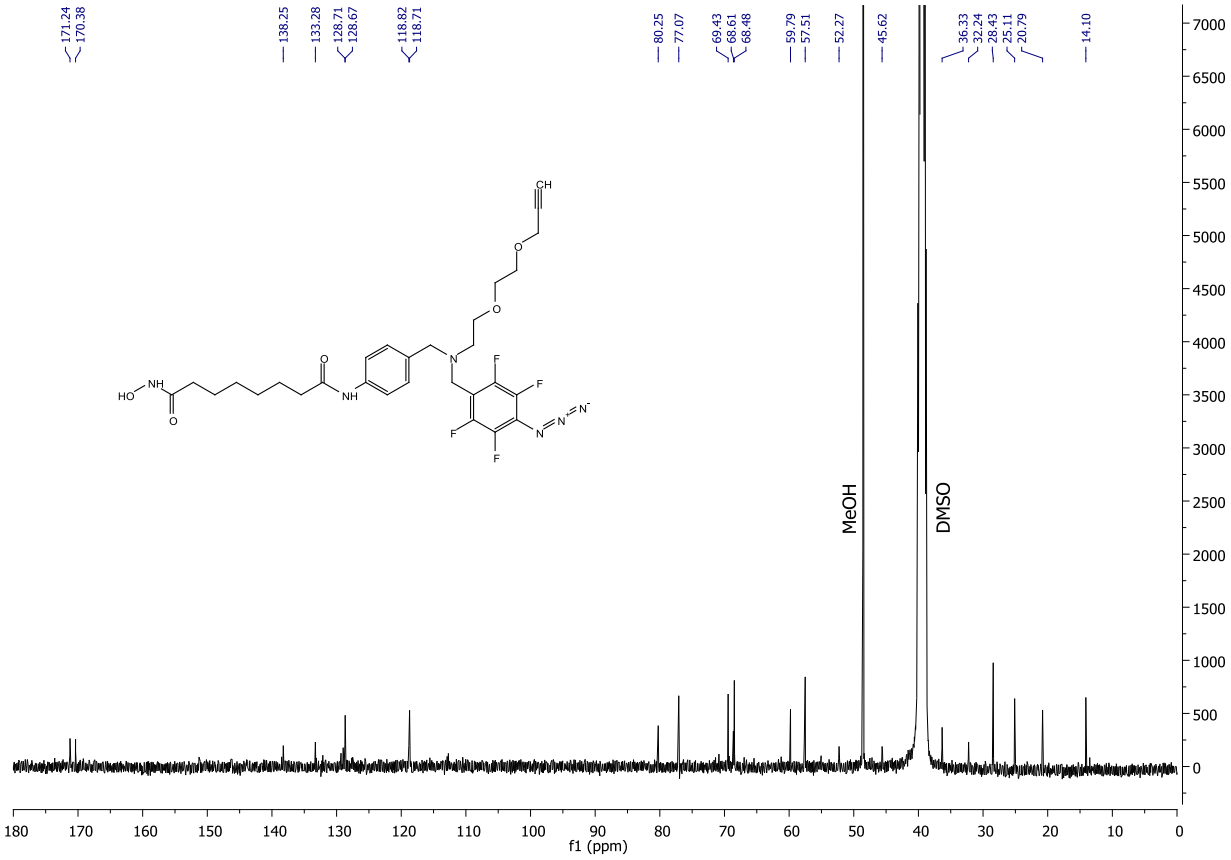

APPENDIX T (CONTINUED)

^{1}H NMR spectrum for PRP **9**

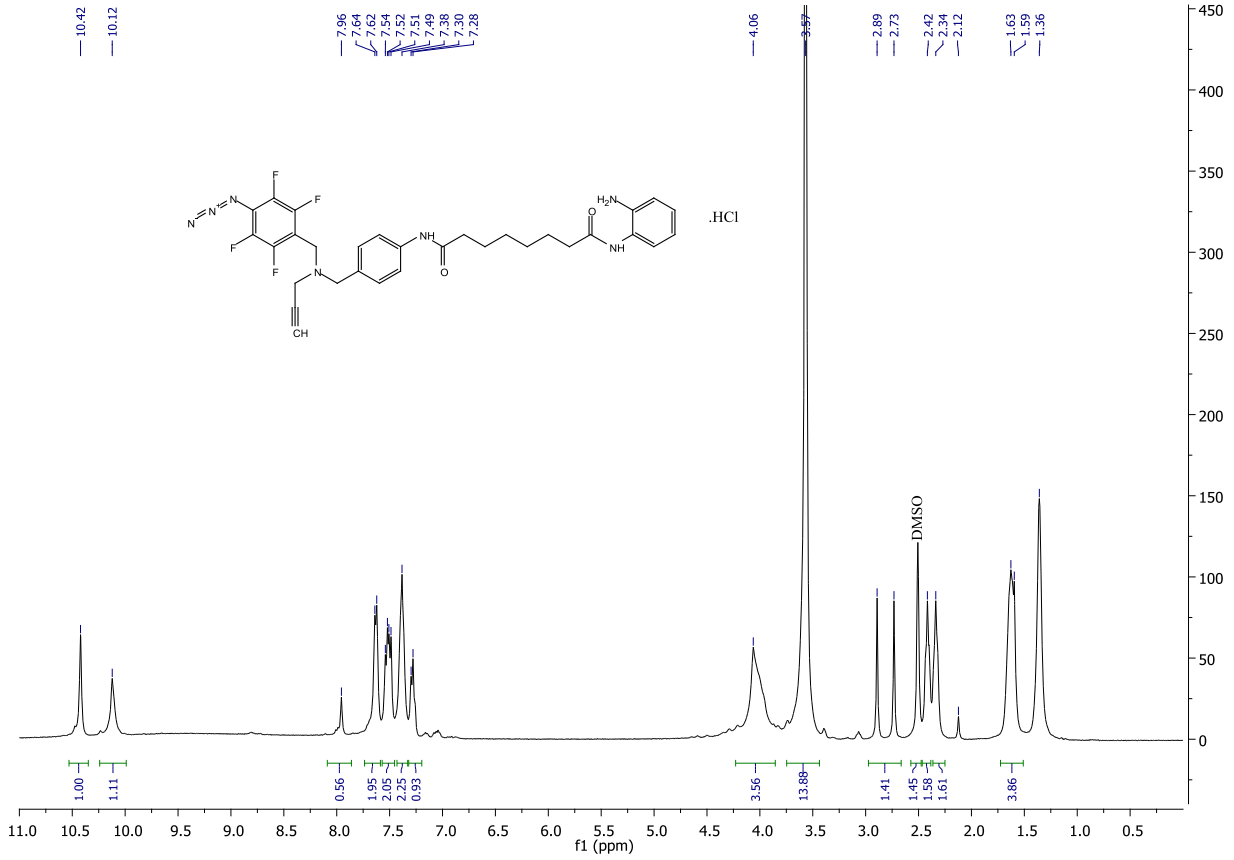

APPENDIX T (CONTINUED)

^{13}C NMR spectrum for PRP **9**

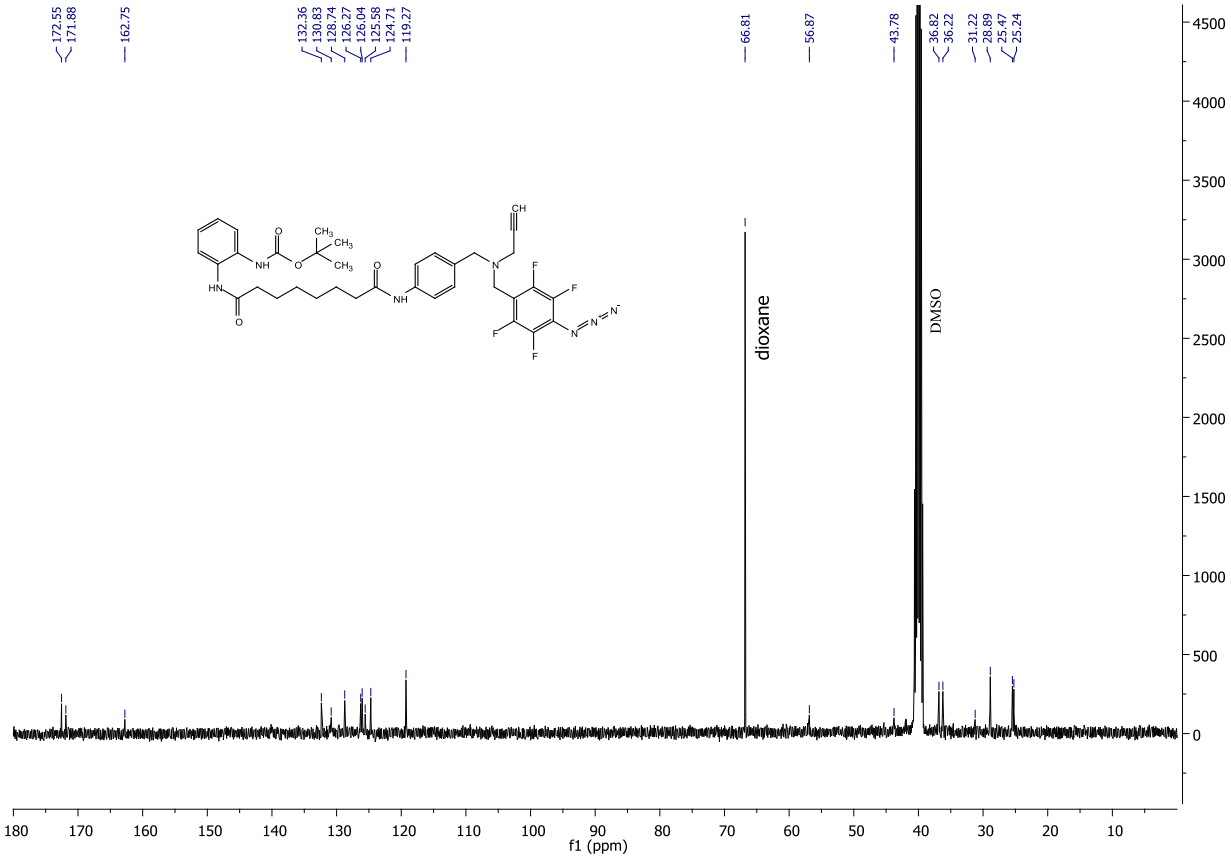

APPENDIX T (CONTINUED)

^{19}F NMR spectrum for intermediate **32**

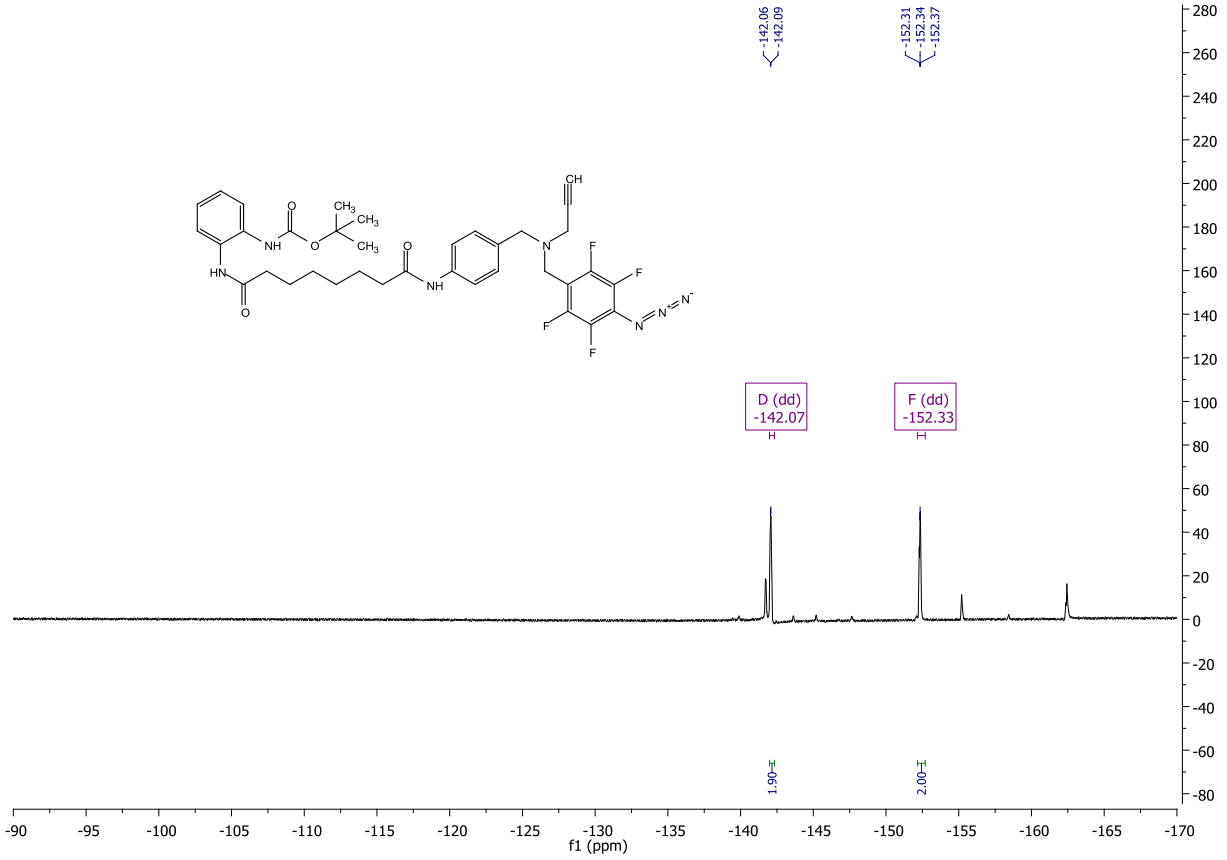

APPENDIX T (CONTINUED)

^{1}H NMR spectrum for PRP **5**

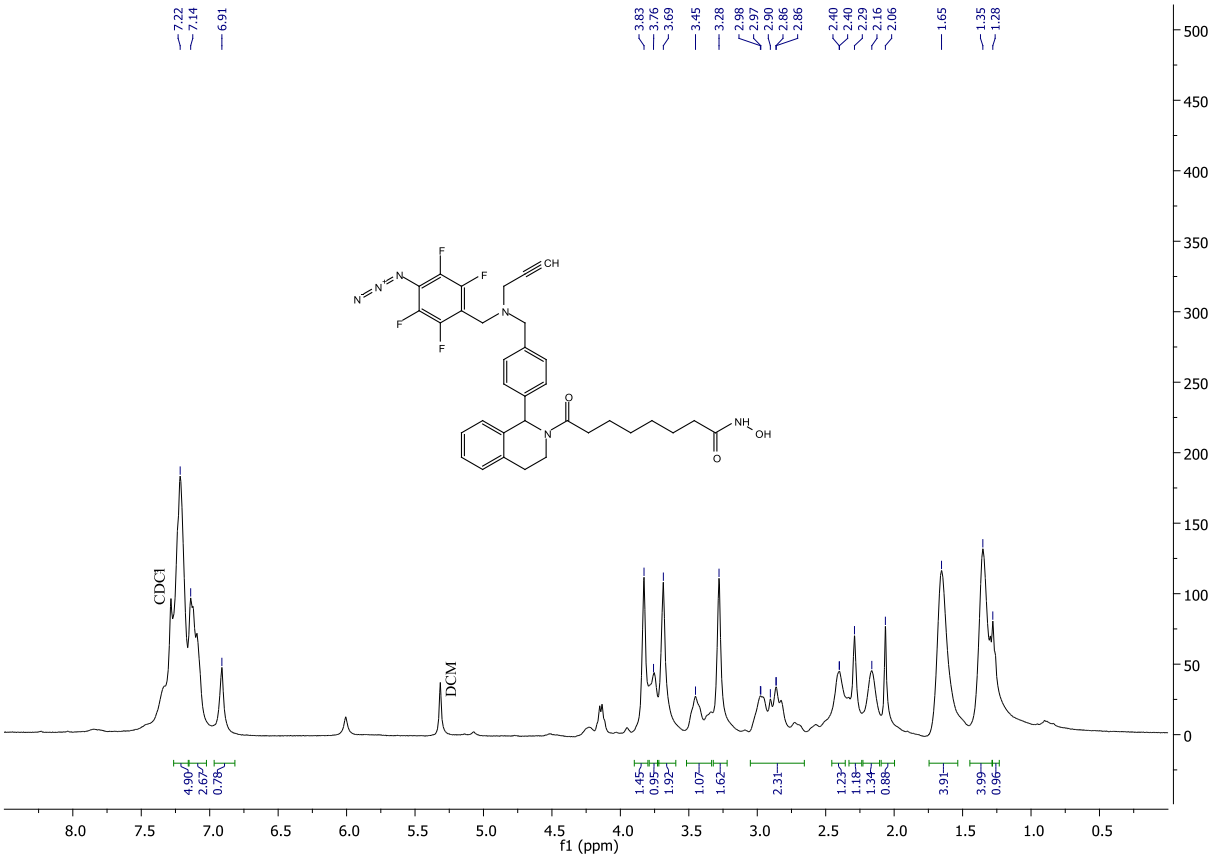

APPENDIX T (CONTINUED)

^{13}C NMR spectrum for PRP **5**

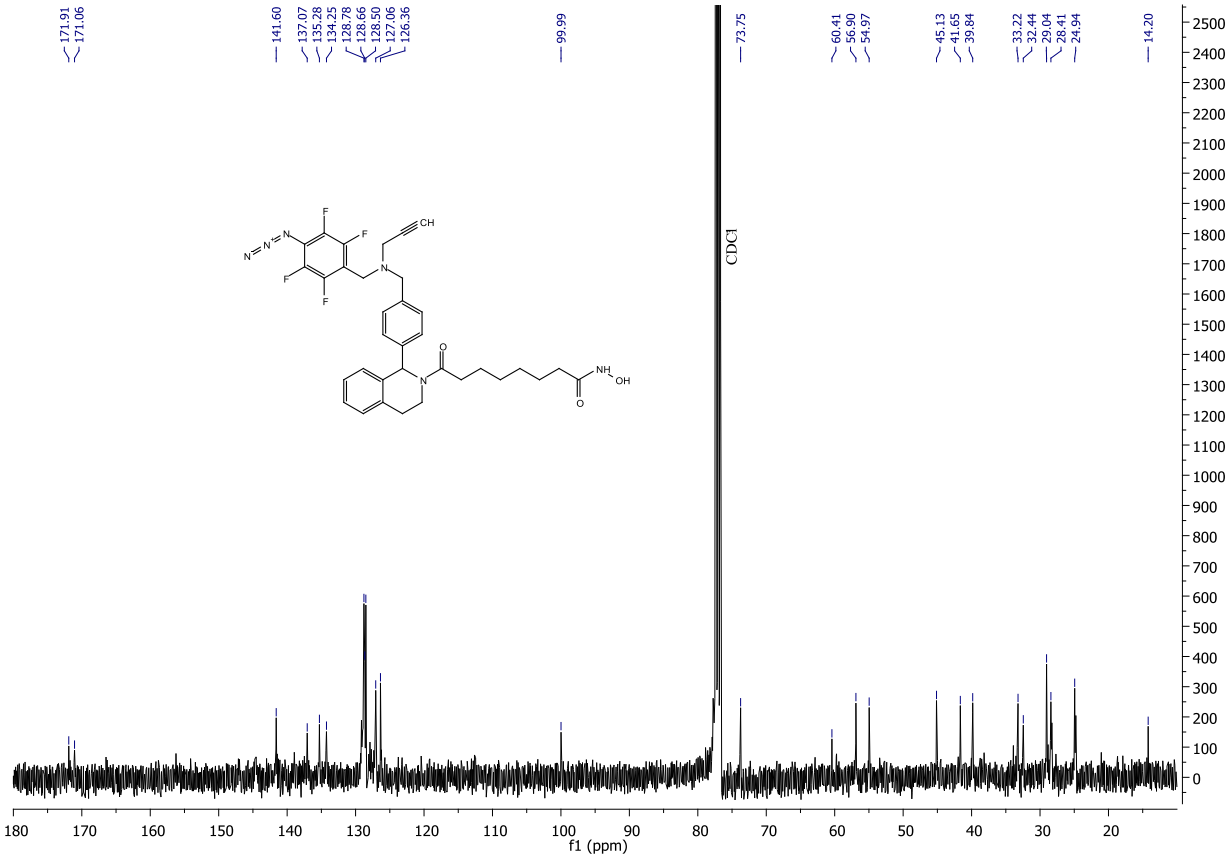

APPENDIX T (CONTINUED)

^{19}F NMR spectrum for PRP **5**

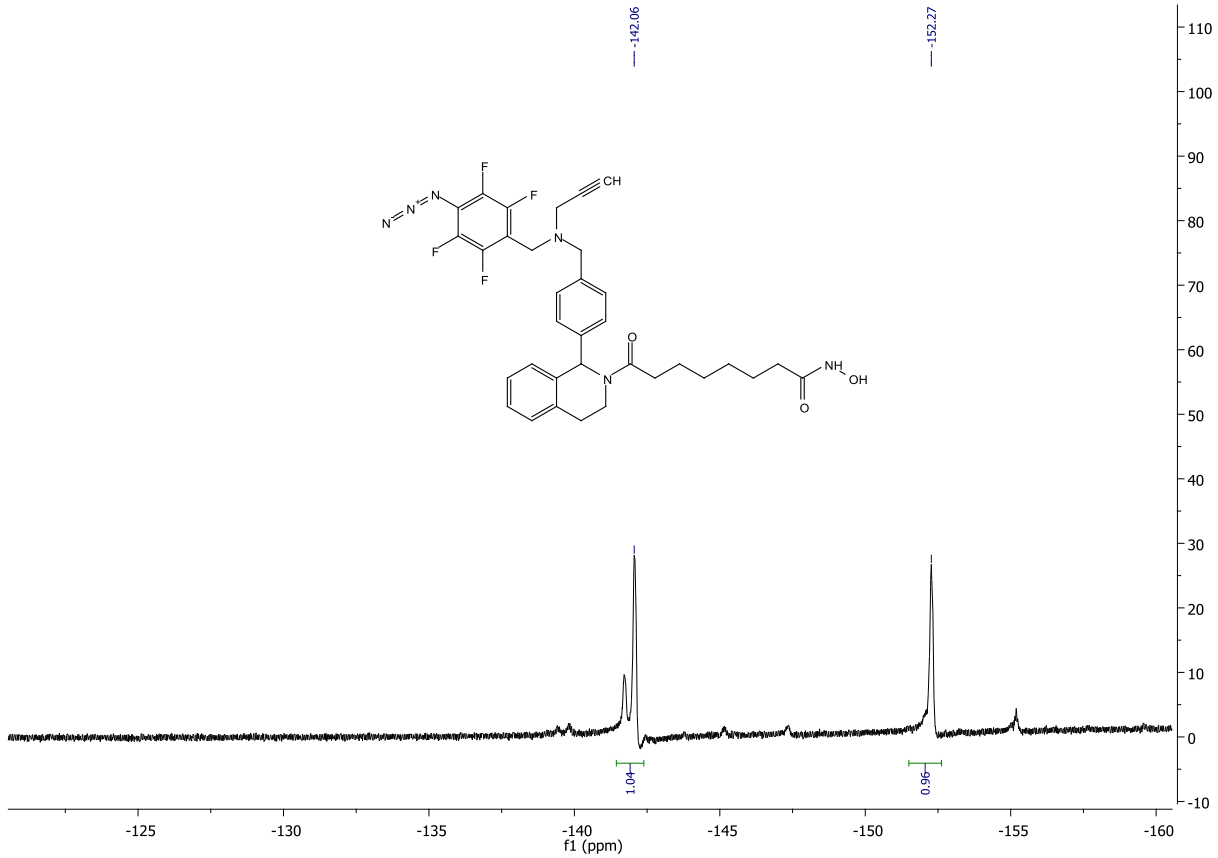

APPENDIX T (CONTINUED)

^{1}H NMR spectrum for PRP **7**

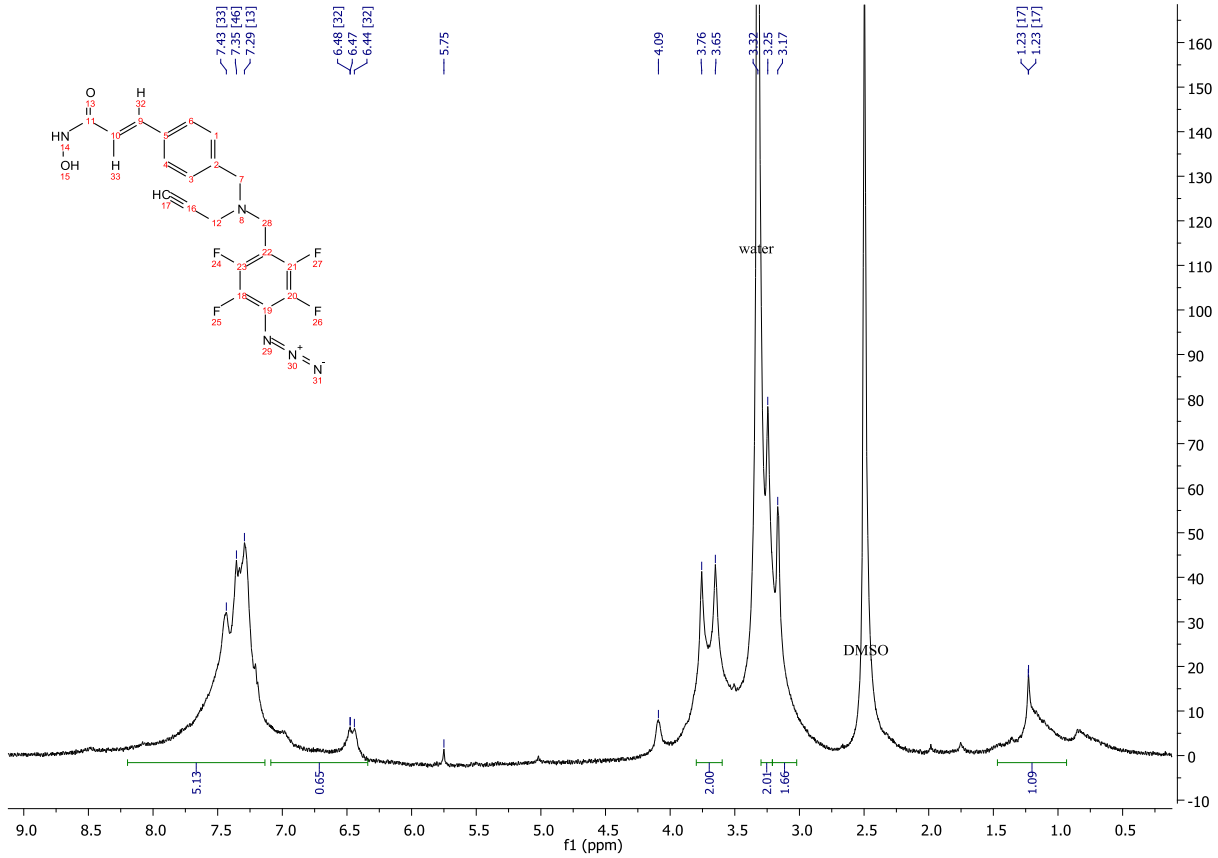

APPENDIX T (CONTINUED)

^{13}C NMR spectrum for PRP **7**

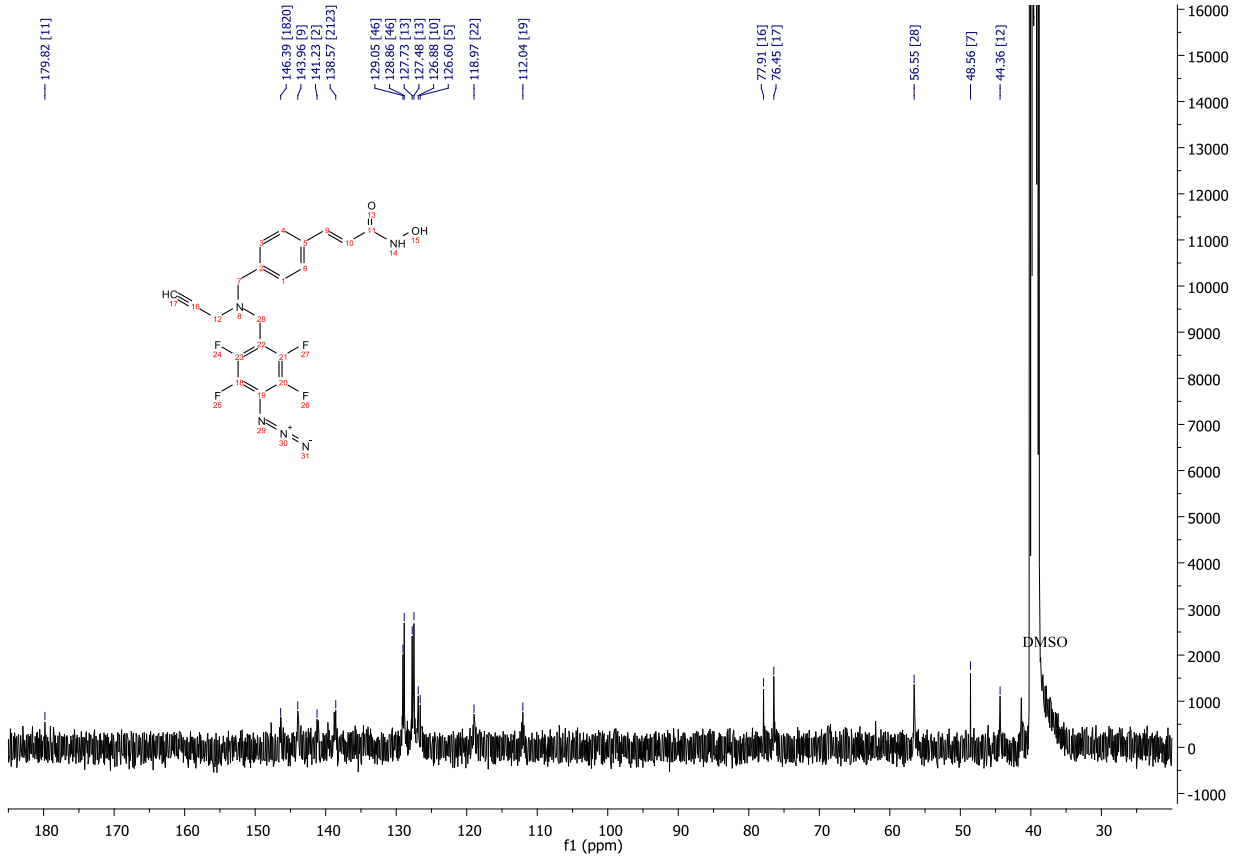

APPENDIX T (CONTINUED)

^{19}F NMR spectrum for PRP **7**

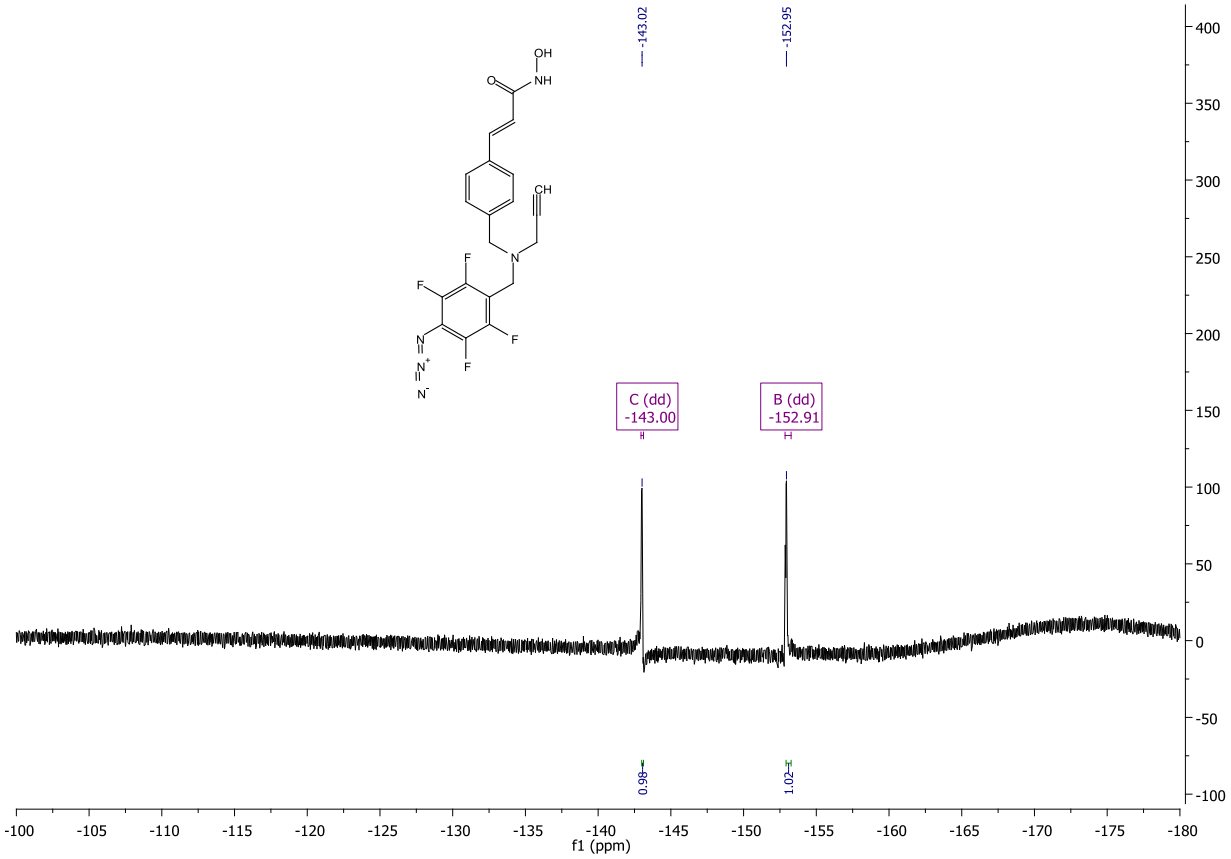

APPENDIX T (CONTINUED)

^{1}H NMR for intermediate **55**

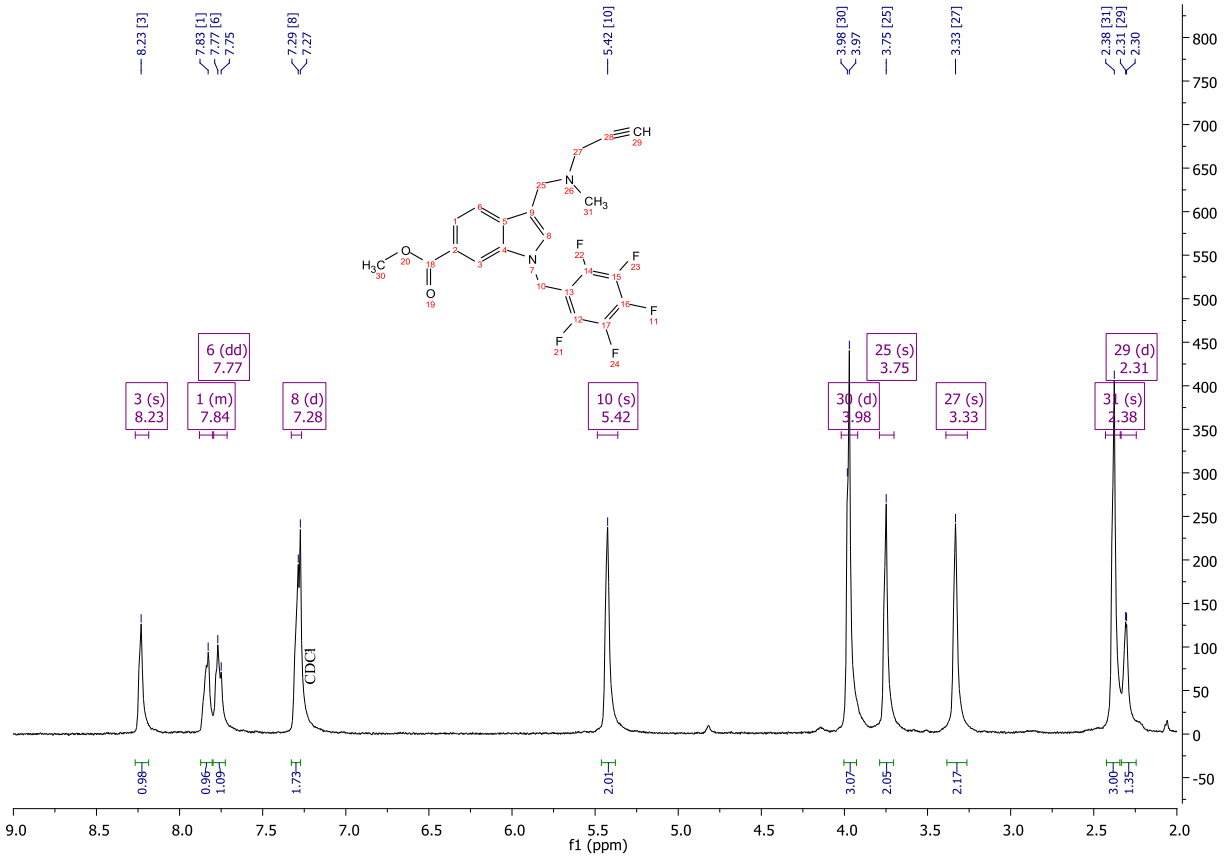

APPENDIX T (CONTINUED)

^{13}C NMR for intermediate **55**

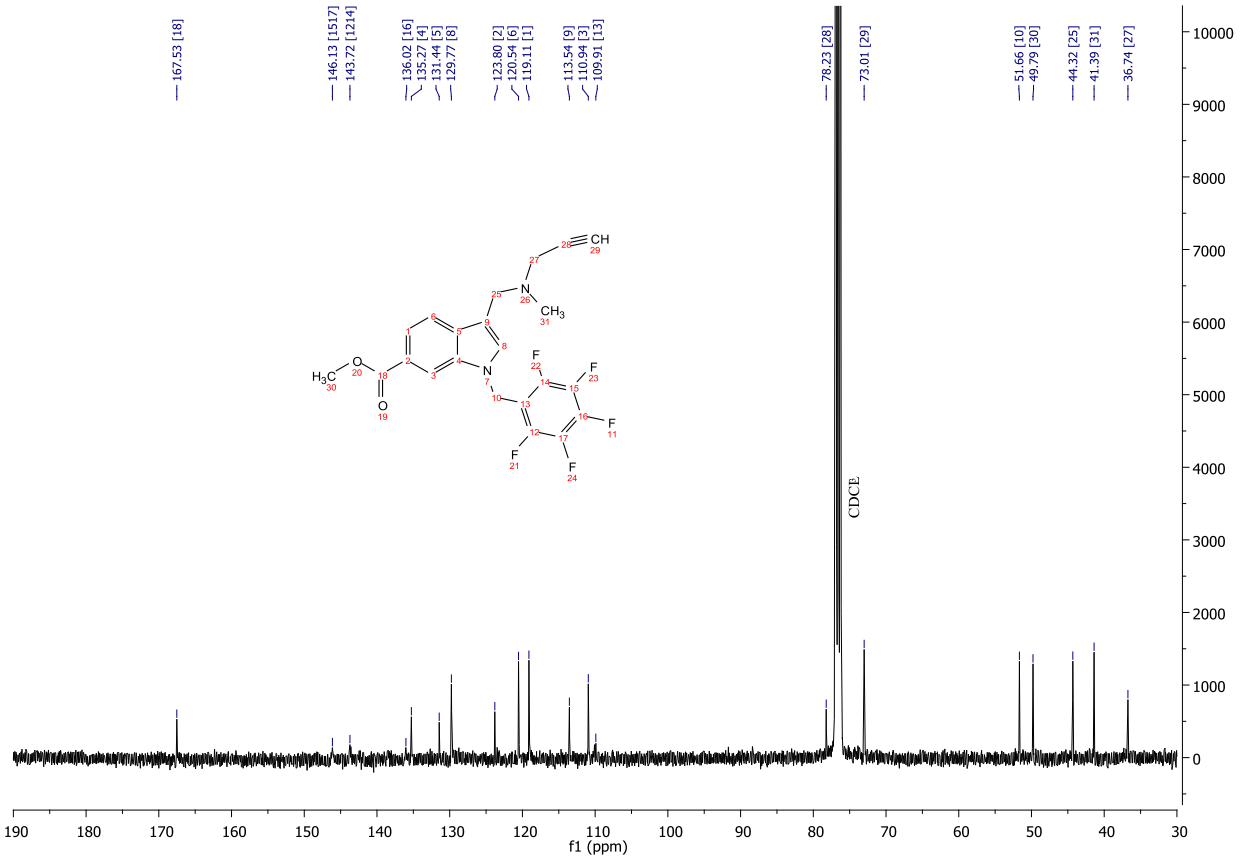

APPENDIX T (CONTINUED)

^{1}H NMR for intermediate **57**

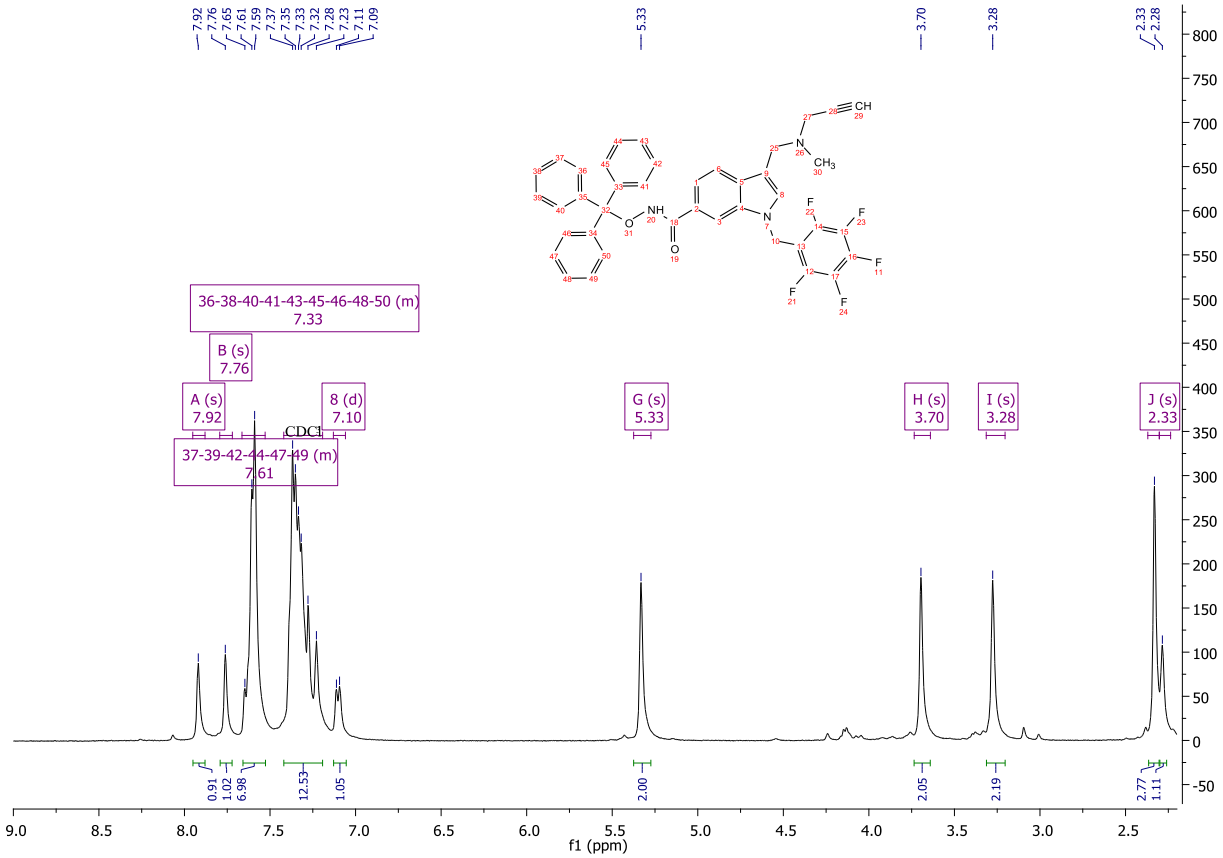

APPENDIX T (CONTINUED)

^{13}C NMR for intermediate **57**

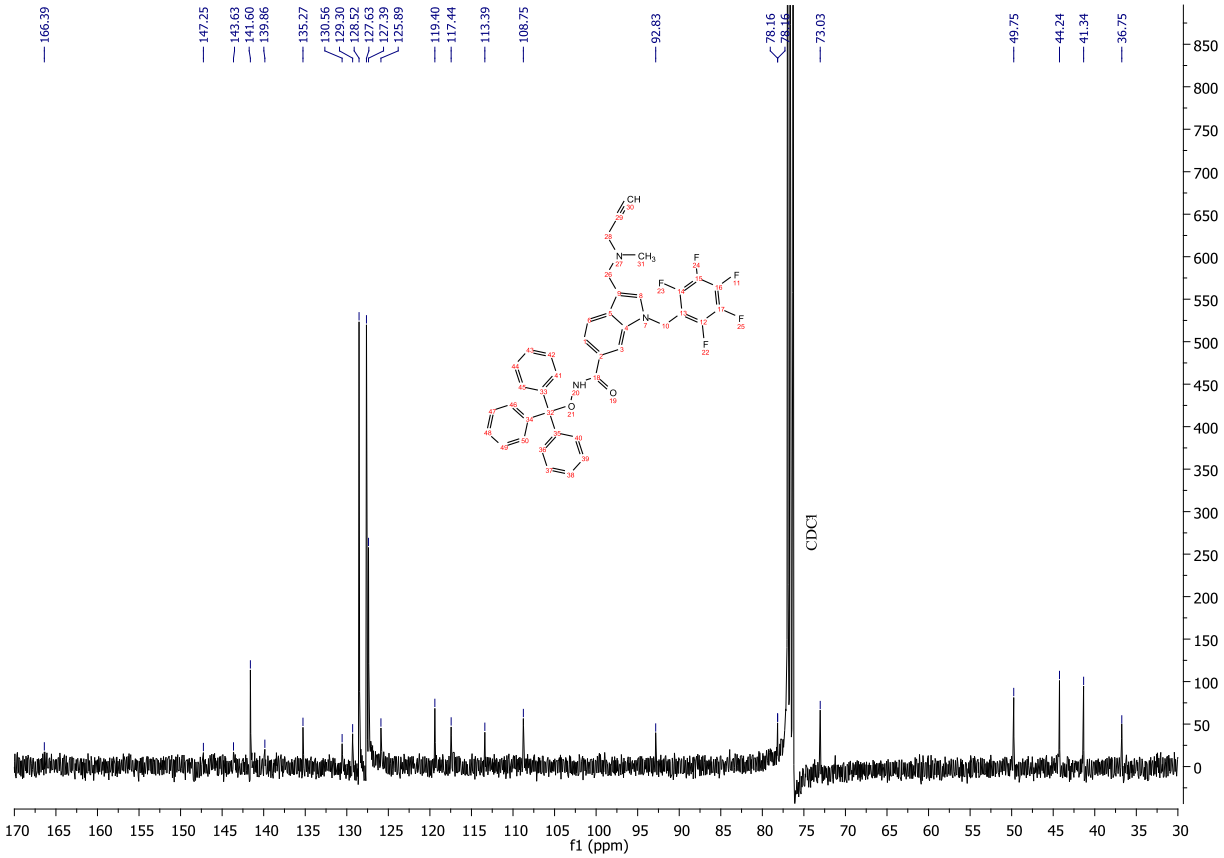

APPENDIX T (CONTINUED)

^{19}F NMR spectrum for intermediate **58**

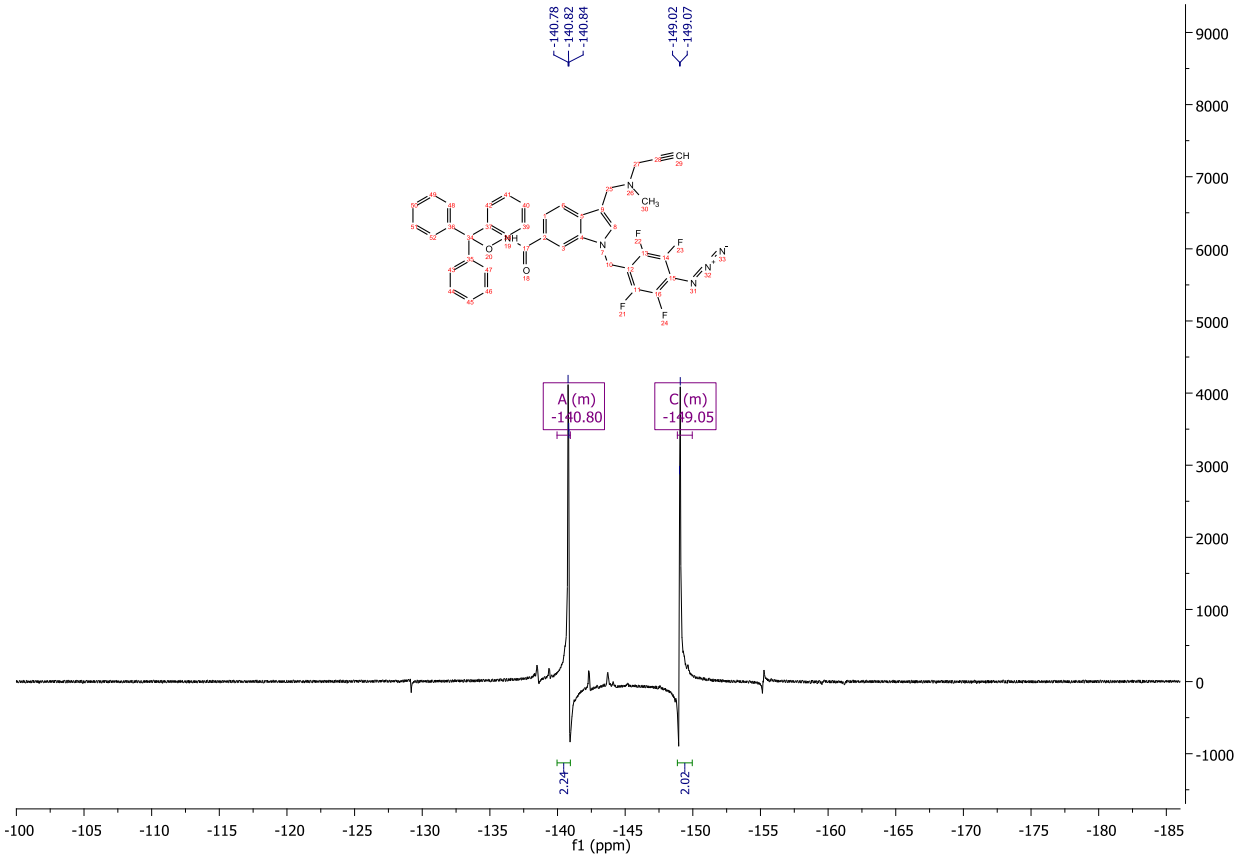

APPENDIX T (CONTINUED)

^{1}H NMR spectrum for PRP **11**

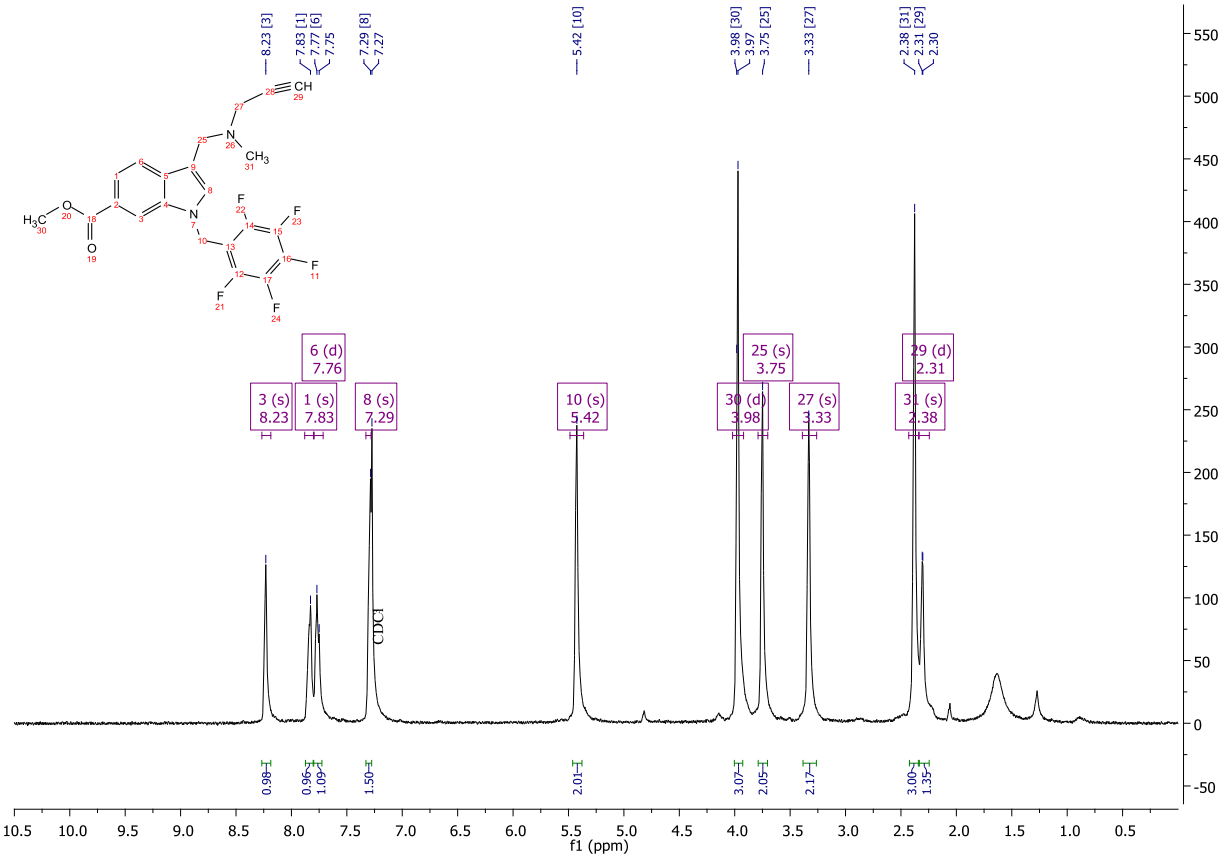

APPENDIX T (CONTINUED)

^{13}C NMR spectrum for PRP **11**

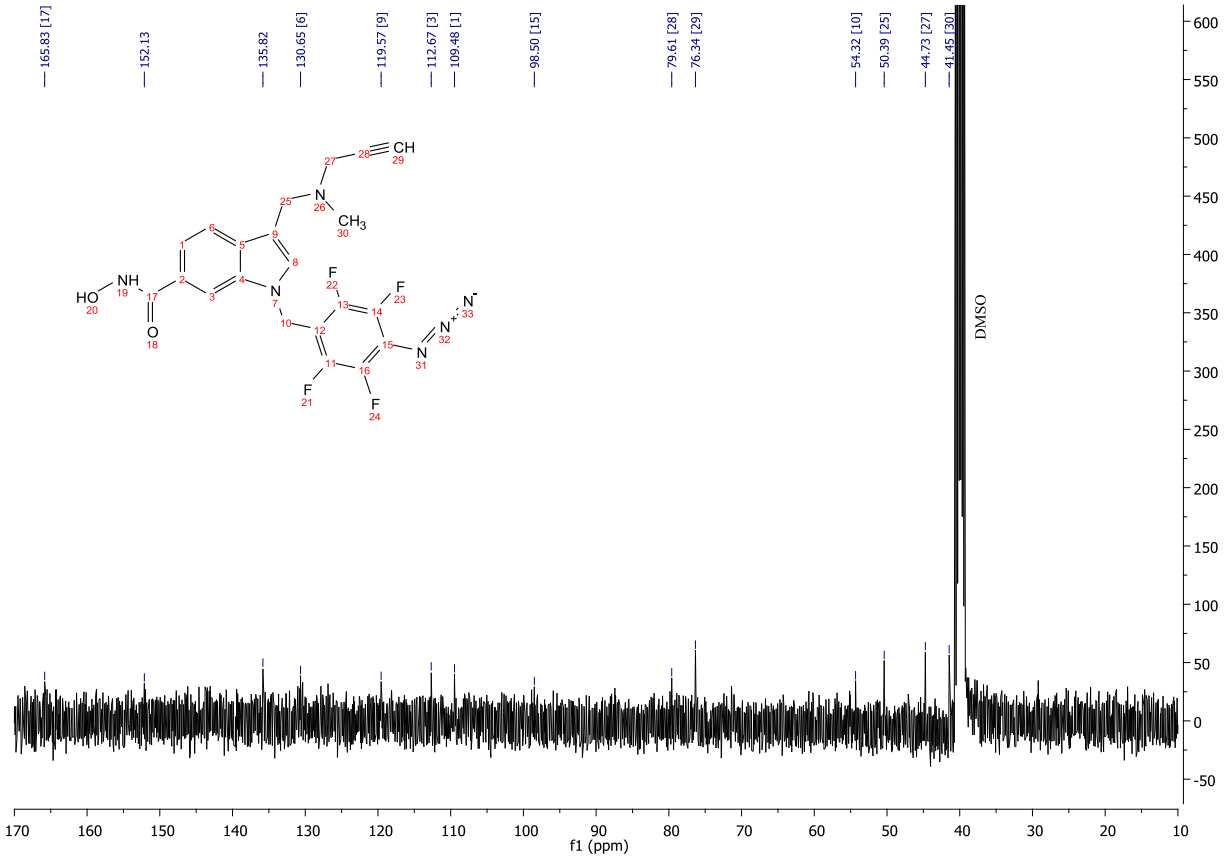

APPENDIX T (CONTINUED)

^{19}F NMR spectrum for PRP **11**

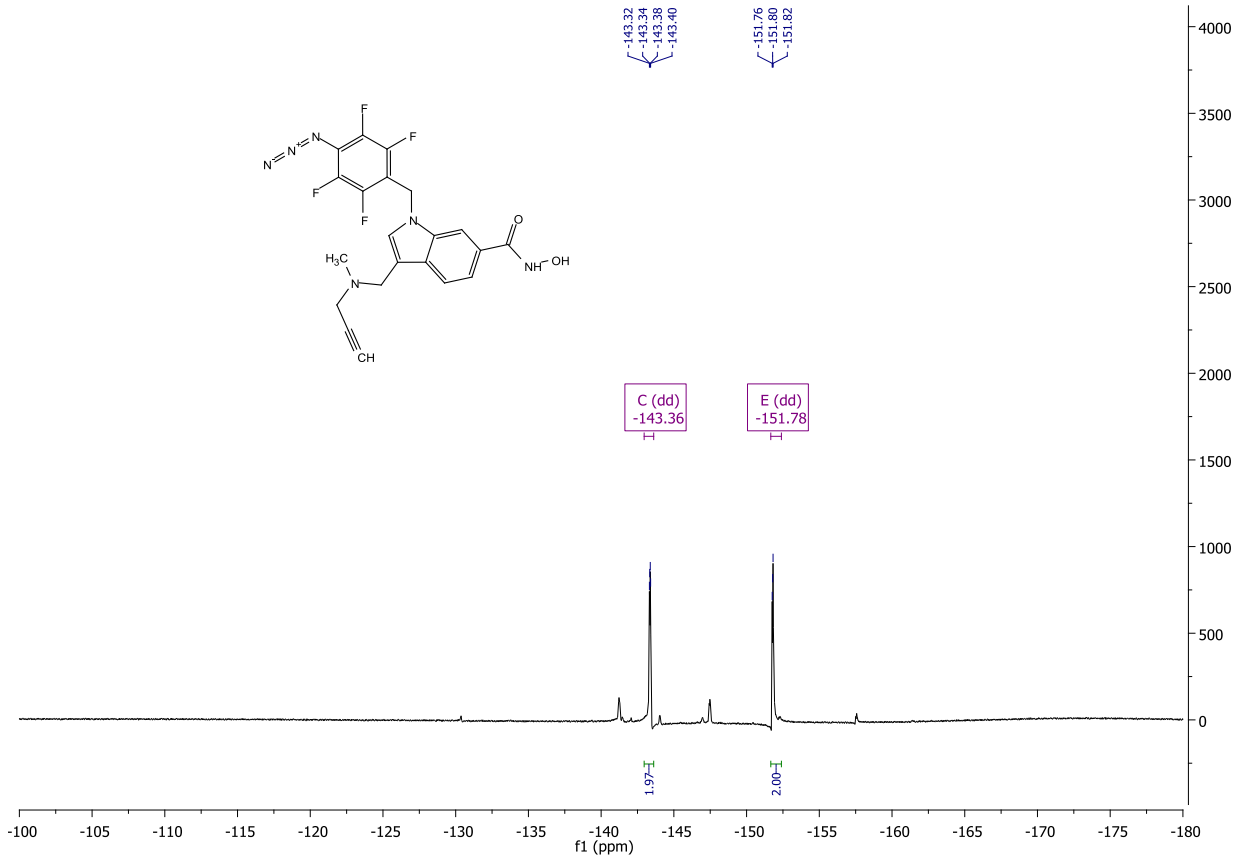

APPENDIX T (CONTINUED)

^{1}H NMR spectrum for PRP **13**

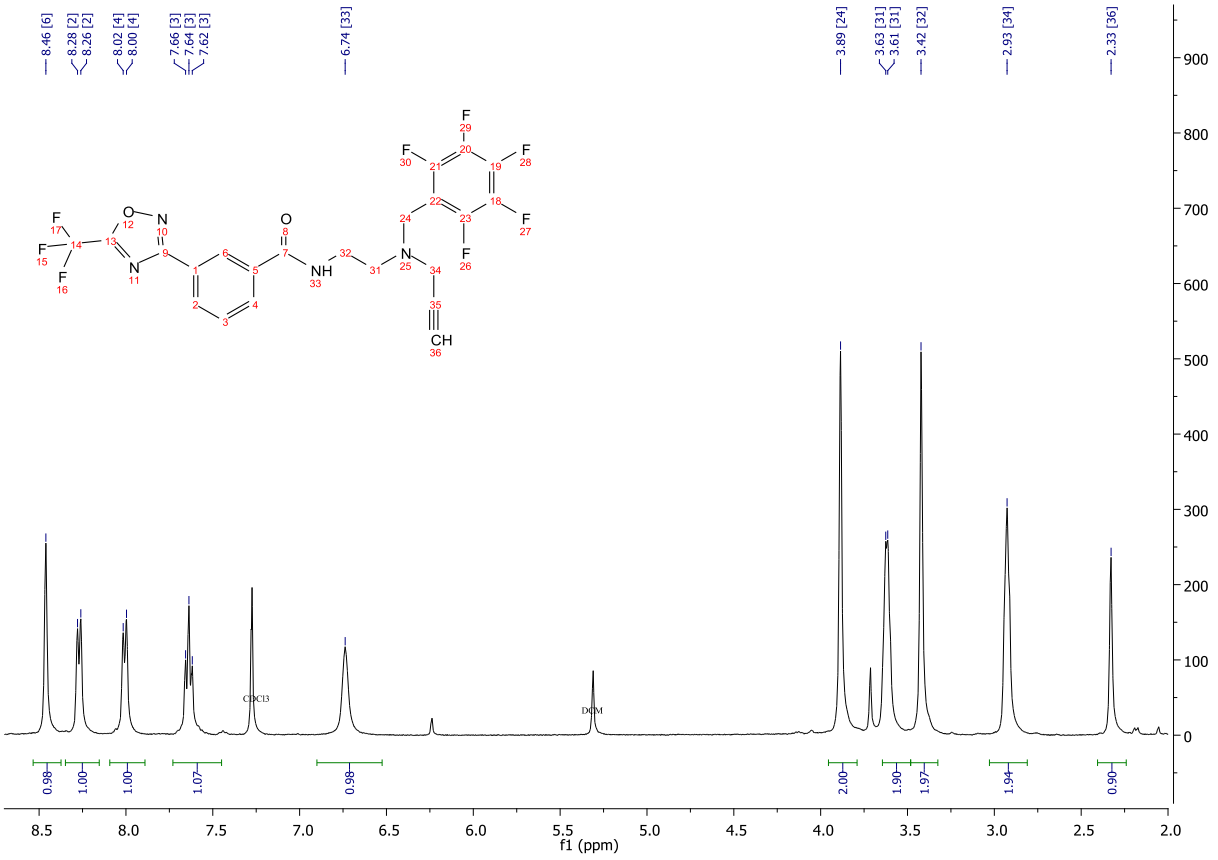

APPENDIX T (CONTINUED)

^{13}C NMR spectrum for PRP **13**

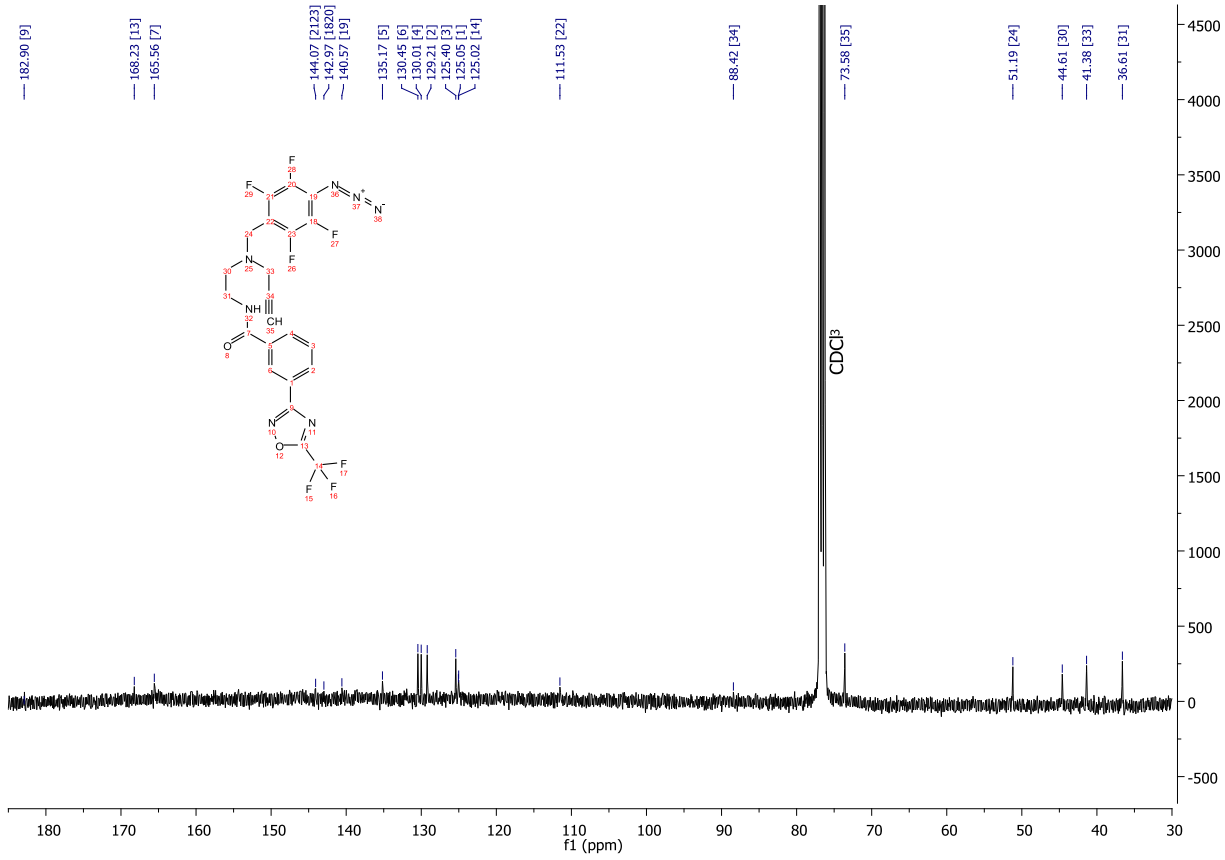

APPENDIX T (CONTINUED)

^{19}F NMR spectrum for PRP **13**

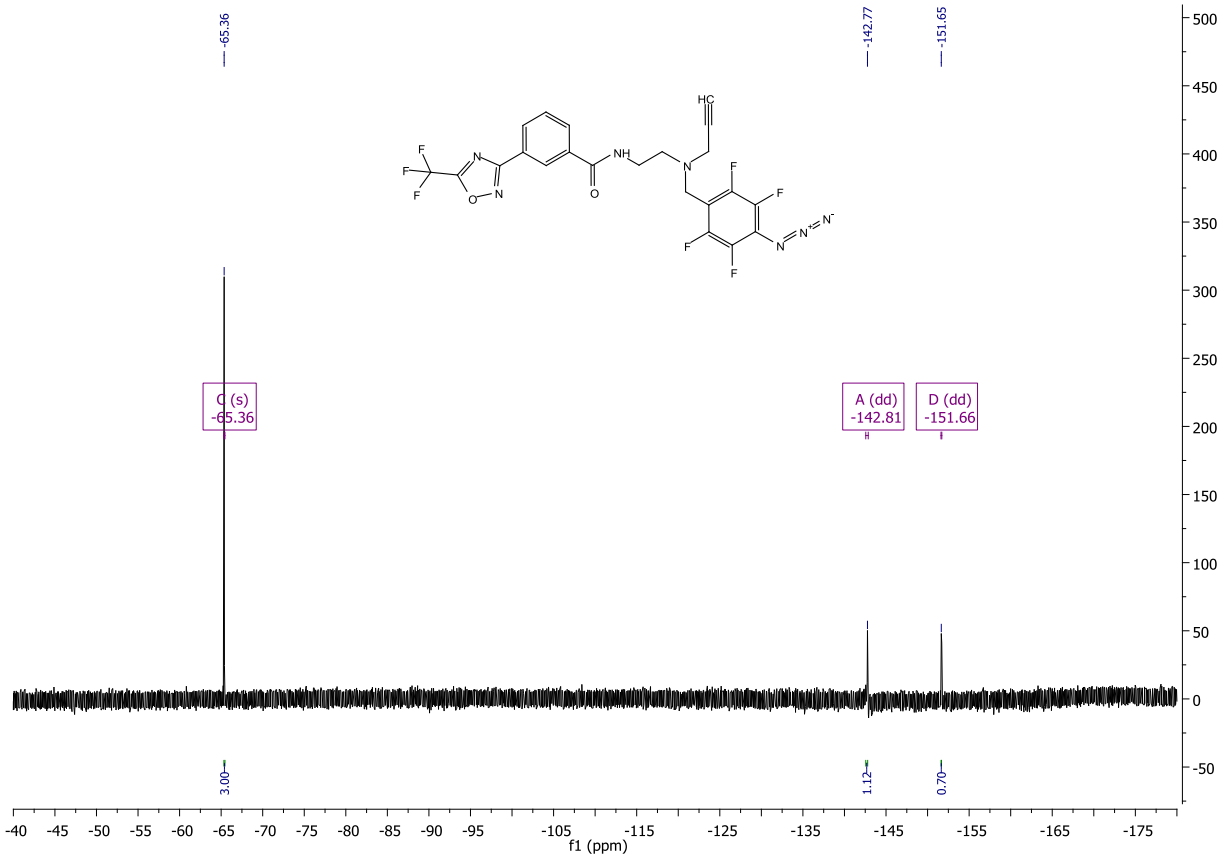

APPENDIX U: THE IMPACT OF HDACI TREATMENT ON THE SUBCELLULAR LOCALIZATION OF CLASS I HDACS.

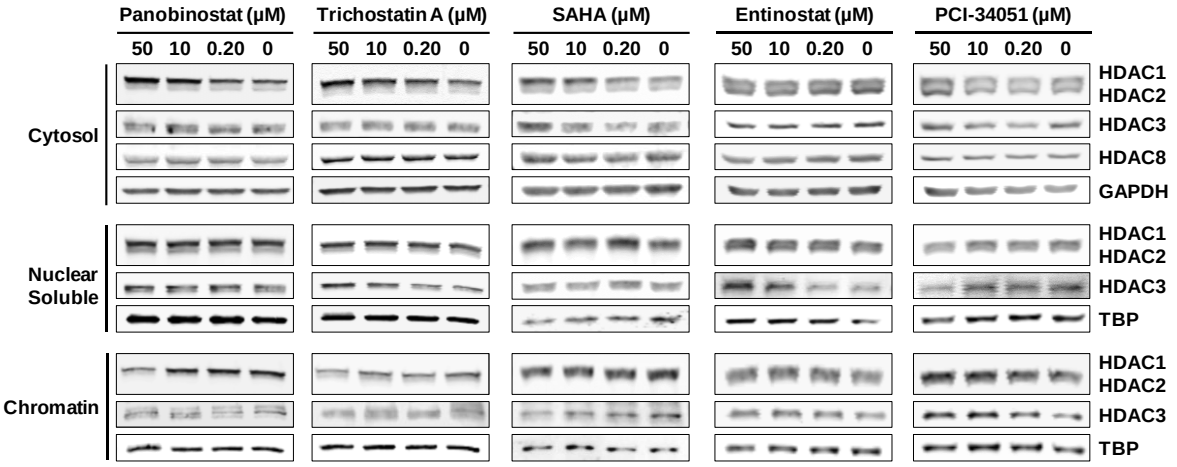

MCF-7 cells were treated with indicated concentrations of panobinostat, trichostatin A, SAHA, Entinostat, or PCI-34051 for 12 hours and then fractionated biochemically. The abundance of class I HDACs was characterized by Western blot analysis in the cytosolic (top panel), nuclear soluble (middle panel), and chromatin bound (bottom panel) fractions. Western blots shown are representative of at least two independent experiments.

APPENDIX V: HDACI TREATMENT DOES NOT SIGNIFICANTLY AFFECT MCF-7 CELL VIABILITY.

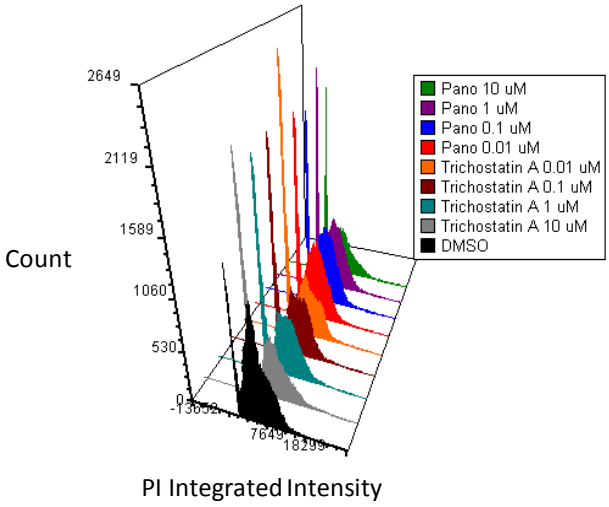

Treatment	Sub G_0/G_1 (apoptotic) cell population, %
DMSO	11.8 ± 0.7
Panobinostat 0.01 µM	16.5 ± 1.5
Panobinostat 0.1 µM	16.0 ± 2.2
Panobinostat 1 µM	18.8 ± 1.5
Panobinostat 10 µM	19.9 ± 6.9
Trichostatin A 0.01 µM	22.2 ± 3.3
Trichostatin A 0.1 µM	18.7 ± 3.2
Trichostatin A 1 µM	17.9 ± 1.1
Trichostatin A 10 µM	21.8 ± 0.9

HDACi treatment does not significantly affect MCF-7 cell viability. MCF-7 cells were serum starved for 12 hours and treated with indicated concentrations of panobinostat or trichostatin A. Cells were fixed, stained with propidium iodide (PI), and cell cycle analysis was conducted with Celigo image cytometer. Three-dimensional plot on left shows integrated PI intensity and table on right shows percentage of apoptotic cell population for each treatment. Percentage values are expressed as mean ± standard deviation of three replicates.

APPENDIX W: TRICHOSTATIN A TREATMENT INDUCES RE-EQUILIBRATION OF HDAC1 SUBCELLULAR LOCALIZATION IN MDA-MB-231 CELLS.

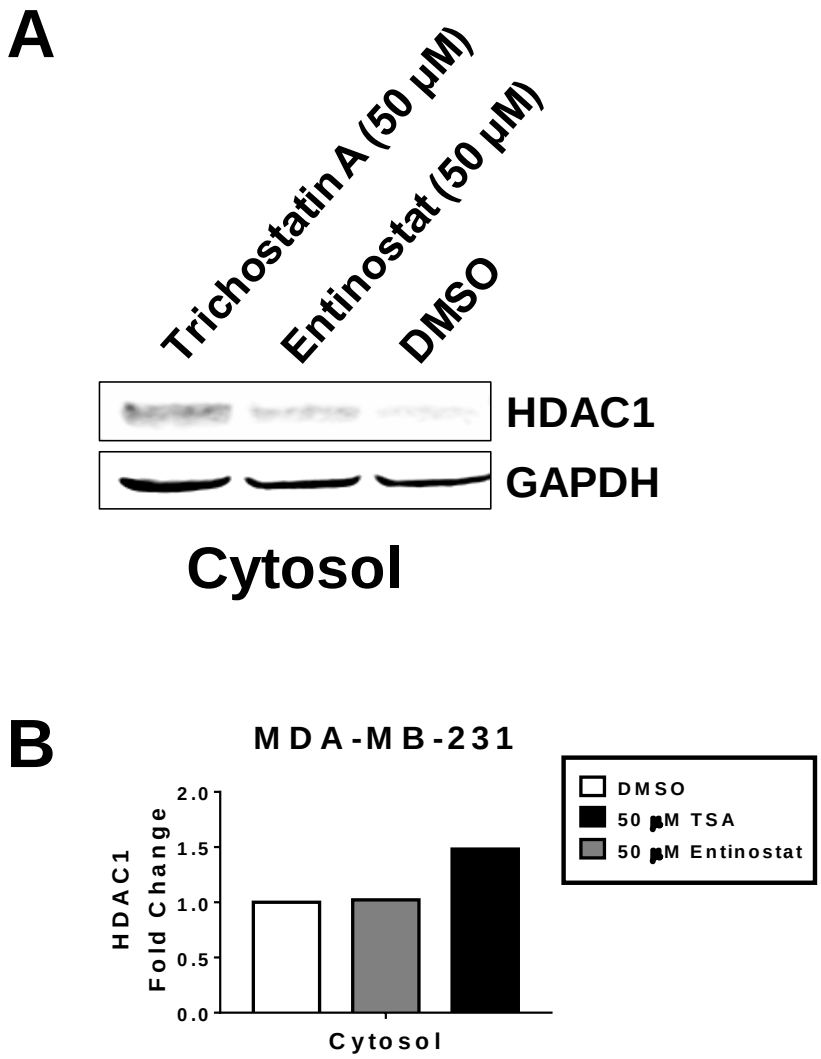

Trichostatin A treatment induces re-equilibration of HDAC1 subcellular localization in MDA-MB-231 cells. MDA-MB-231 cells were treated with 50 µM trichostatin A or entinostat for 12 hours and then fractionated biochemically. A) The abundance of HDAC1 was characterized by Western blot analysis in the cytosolic (top panel), and chromatin bound (bottom panel) fractions. B) Densitometry analysis of the abundance of HDAC1 normalized to GAPDH loading control.

APPENDIX X: HDACI-INDUCED RE-EQUILIBRATION OF HDAC1 ANALYSIS BY CONFOCAL MICROSCOPY.

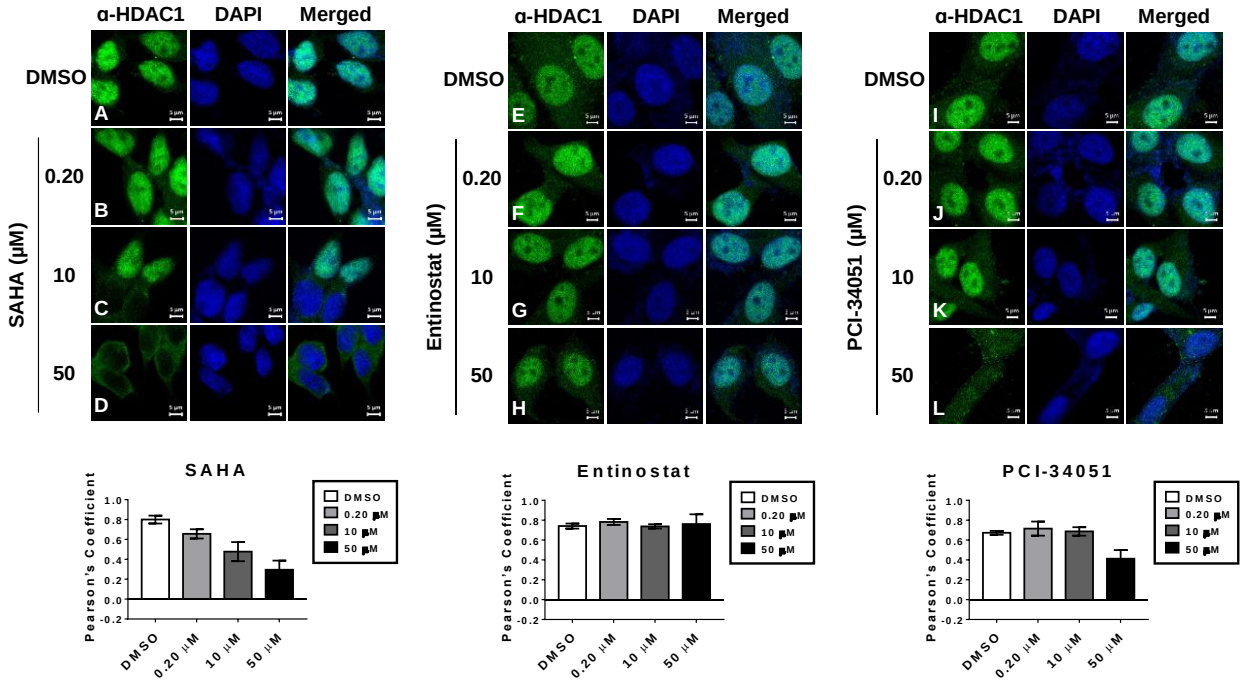

HDACi-induced re-equilibration of HDAC1 analysis by confocal microscopy. MCF-7 cells were treated indicated concentrations of SAHA (optical sections A-D, respectively), entinostat (optical sections E-H, respectively), or PCI-34051 (optical sections I-L, respectively) for 12 hours, fixed, permeabilized and optical sections were obtained by laser scanning confocal microscopy. Fluorescence signal for HDAC1 is shown in green (left panels), DAPI staining is shown in blue (middle panels), and merged optical sections are shown in the right panels. Colocalization analysis of HDAC1 fluorescence signal and the DAPI stain signal was performed with JACoP (ImageJ). Pearson's Coefficient is presented as the mean of at least two independent experiments ± standard deviation. Optical sections shown are representatives of at least two independent experiments.

APPENDIX Y: MATLAB SCRIPT FOR ANALYSI OF MS/MS DATA

```
Exp_Probeonly = readtable('1-
2_NoKeratin_PSMabove1_final.xlsx','ReadVariableNames',true);%imports excel
file (need to change to correct directory and filename) and saves array as
Exp_Probeonly
[~,Exp1]=unique(Exp_Probeonly(:,'Accession'));%wrtie unique 'geneNames' in
the data set to Exp1
Exp1 = sort(Exp1);%sort unique 'geneNames' in the data set to original order
Exp1_Final = Exp_Probeonly(Exp1,:); %write the rest of the row back into each
unique entry from original dataset
Exp_Competition = readtable('2-
2_NoKeratin_PSMabove1_final.xlsx','ReadVariableNames',true);
[~,Exp2]=unique(Exp_Competition(:,'Accession'));
Exp2 = sort(Exp2);
Exp2_Final = Exp_Competition(Exp2,:);
Exp_Blank = readtable('3-
2_NoKeratin_PSMabove1_final.xlsx','ReadVariableNames',true);
[~,Exp3]=unique(Exp_Blank(:,'Accession'));
Exp3 = sort(Exp3);
Exp3_Final = Exp_Blank(Exp3,:);
[~,Difference_Probe_Blank] =
setdiff(Exp1_Final(:,'Accession'),Exp3_Final(:,'Accession'));% sets
difference betweeen probe only and comp experiment
Difference_Probe_Blank = sort(Difference_Probe_Blank);
Difference_Probe_Blank_Final = Exp1_Final(Difference_Probe_Blank,:);

[~,Difference_Probe_Comp_Blank] =
setdiff(Difference_Probe_Blank_Final(:,'Accession'),Exp2_Final(:,'Accession')
);% sets difference betweeen probe comp final and blank experiment
Difference_Probe_Comp_Blank = sort(Difference_Probe_Comp_Blank);
Difference_Probe_Comp_Blank_Final =
Difference_Probe_Blank_Final(Difference_Probe_Comp_Blank,:);
filename = 'difference-exp8.xlsx'; % sets the name of the excel file to
export to
writetable(Difference_Probe_Comp_Blank_Final,filename,'Sheet',1); % exports
the experiment as an excel file to the specified filename
```

CITED LITERATURE

1. Carroll, S. B. (2001) Chance and necessity: the evolution of morphological complexity and diversity, *Nature 409*, 1102-1109.

2. Jaenisch, R., and Bird, A. (2003) Epigenetic regulation of gene expression: how the genome integrates intrinsic and environmental signals, *Nature genetics 33 Suppl*, 245-254.

3. Kornberg, R. D. (1974) Chromatin structure: a repeating unit of histones and DNA, *Science 184*, 868-871.

4. Oudet, P., Gross-Bellard, M., and Chambon, P. (1975) Electron microscopic and biochemical evidence that chromatin structure is a repeating unit, *Cell 4*, 281-300.

5. Ou, H. D., Phan, S., Deerinck, T. J., Thor, A., Ellisman, M. H., and O'Shea, C. C. (2017) ChromEMT: Visualizing 3D chromatin structure and compaction in interphase and mitotic cells, *Science 357*.

6. Li, B., Carey, M., and Workman, J. L. (2007) The role of chromatin during transcription, *Cell 128*, 707-719.

7. Van Holde, K. E. (1988) *Chromatin*, Springer.

8. Goldberg, A. D., Allis, C. D., and Bernstein, E. (2007) Epigenetics: a landscape takes shape, *Cell 128*, 635-638.

9. Workman, J. L., and Kingston, R. E. (1998) Alteration of nucleosome structure as a mechanism of transcriptional regulation, *Annual review of biochemistry 67*, 545-579.

10. Narlikar, G. J., Sundaramoorthy, R., and Owen-Hughes, T. (2013) Mechanisms and functions of ATP-dependent chromatin-remodeling enzymes, *Cell 154*, 490-503.

11. Allfrey, V. G., Faulkner, R., and Mirsky, A. E. (1964) ACETYLATION AND METHYLATION OF HISTONES AND THEIR POSSIBLE ROLE IN THE REGULATION OF RNA SYNTHESIS, *Proceedings of the National Academy of Sciences of the United States of America 51*, 786-794.

12. Holliday, R., and Pugh, J. E. (1975) DNA modification mechanisms and gene activity during development, *Science 187*, 226-232.

13. Stricker, S. H., Koferle, A., and Beck, S. (2017) From profiles to function in epigenomics, *Nat Rev Genet 18*, 51-66.

14. Strahl, B. D., and Allis, C. D. (2000) The language of covalent histone modifications, *Nature 403*, 41-45.

15. Consortium, E. P. (2012) An integrated encyclopedia of DNA elements in the human genome, *Nature 489*, 57-74.

16. Rivera, Chloe M., and Ren, B. Mapping Human Epigenomes, *Cell 155*, 39-55.

17. Noh, K. M., Wang, H., Kim, H. R., Wenderski, W., Fang, F., Li, C. H., Dewell, S., Hughes, S. H., Melnick, A. M., Patel, D. J., Li, H., and Allis, C. D. (2015) Engineering of a Histone-Recognition Domain in Dnmt3a Alters the Epigenetic Landscape and Phenotypic Features of Mouse ESCs, *Mol Cell 59*, 89-103.

18. Hilton, I. B., D'Ippolito, A. M., Vockley, C. M., Thakore, P. I., Crawford, G. E., Reddy, T. E., and Gersbach, C. A. (2015) Epigenome editing by a CRISPR-Cas9-based acetyltransferase activates genes from promoters and enhancers, *Nat Biotech 33*, 510-517.

19. Gama-Sosa, M. A., Slagel, V. A., Trewyn, R. W., Oxenhandler, R., Kuo, K. C., Gehrke, C. W., and Ehrlich, M. (1983) The 5-methylcytosine content of DNA from human tumors, *Nucleic acids research 11*, 6883-6894.

20. Feinberg, A. P., and Vogelstein, B. (1983) Hypomethylation distinguishes genes of some human cancers from their normal counterparts, *Nature 301*, 89-92.

21. Ginsburg, E., Salomon, D., Sreevalsan, T., and Freese, E. (1973) Growth inhibition and morphological changes caused by lipophilic acids in mammalian cells, *Proceedings of the National Academy of Sciences of the United States of America 70*, 2457-2461.

22. Candido, E. P., Reeves, R., and Davie, J. R. (1978) Sodium butyrate inhibits histone deacetylation in cultured cells, *Cell 14*, 105-113.

23. Vidali, G., Boffa, L. C., Bradbury, E. M., and Allfrey, V. G. (1978) Butyrate suppression of histone deacetylation leads to accumulation of multiacetylated forms of histones H3 and H4 and increased DNase I sensitivity of the associated

DNA sequences, *Proceedings of the National Academy of Sciences of the United States of America 75*, 2239-2243.

24. Polak, P., Karlic, R., Koren, A., Thurman, R., Sandstrom, R., Lawrence, M. S., Reynolds, A., Rynes, E., Vlahovicek, K., Stamatoyannopoulos, J. A., and Sunyaev, S. R. (2015) Cell-of-origin chromatin organization shapes the mutational landscape of cancer, *Nature 518*, 360-364.

25. Fraga, M. F., Ballestar, E., Villar-Garea, A., Boix-Chornet, M., Espada, J., Schotta, G., Bonaldi, T., Haydon, C., Ropero, S., Petrie, K., Iyer, N. G., Perez-Rosado, A., Calvo, E., Lopez, J. A., Cano, A., Calasanz, M. J., Colomer, D., Piris, M. A., Ahn, N., Imhof, A., Caldas, C., Jenuwein, T., and Esteller, M. (2005) Loss of acetylation at Lys16 and trimethylation at Lys20 of histone H4 is a common hallmark of human cancer, *Nature genetics 37*, 391-400.

26. Shen, H., and Laird, Peter W. Interplay between the Cancer Genome and Epigenome, *Cell 153*, 38-55.

27. Plass, C., Pfister, S. M., Lindroth, A. M., Bogatyrova, O., Claus, R., and Lichter, P. (2013) Mutations in regulators of the epigenome and their connections to global chromatin patterns in cancer, *Nat Rev Genet 14*, 765-780.

28. Hodgkinson, A., Chen, Y., and Eyre-Walker, A. (2012) The large-scale distribution of somatic mutations in cancer genomes, *Human mutation 33*, 136-143.

29. Schuster-Bockler, B., and Lehner, B. (2012) Chromatin organization is a major influence on regional mutation rates in human cancer cells, *Nature 488*, 504-507.

30. Taunton, J., Hassig, C. A., and Schreiber, S. L. (1996) A mammalian histone deacetylase related to the yeast transcriptional regulator Rpd3p, *Science 272*, 408-411.

31. de Ruijter, A. J., van Gennip, A. H., Caron, H. N., Kemp, S., and van Kuilenburg, A. B. (2003) Histone deacetylases (HDACs): characterization of the classical HDAC family, *The Biochemical journal 370*, 737-749.

32. Jenuwein, T., and Allis, C. D. (2001) Translating the histone code, *Science 293*, 1074-1080.

33. Chien, C. T., Buck, S., Sternglanz, R., and Shore, D. (1993) Targeting of SIR1 protein establishes transcriptional silencing at HM loci and telomeres in yeast, *Cell 75*, 531-541.

34. Karlić, R., Chung, H.-R., Lasserre, J., Vlahoviček, K., and Vingron, M. (2010) Histone modification levels are predictive for gene expression, *Proceedings of the National Academy of Sciences of the United States of America 107*, 2926-2931.

35. Whitaker, J. W., Chen, Z., and Wang, W. (2015) Predicting the human epigenome from DNA motifs, *Nat Meth 12*, 265-272.

36. Wang, Z., Zang, C., Rosenfeld, J. A., Schones, D. E., Barski, A., Cuddapah, S., Cui, K., Roh, T. Y., Peng, W., Zhang, M. Q., and Zhao, K. (2008) Combinatorial patterns of histone acetylations and methylations in the human genome, *Nature genetics 40*, 897-903.

37. Glaser, K. B., Staver, M. J., Waring, J. F., Stender, J., Ulrich, R. G., and Davidsen, S. K. (2003) Gene expression profiling of multiple histone deacetylase (HDAC) inhibitors: defining a common gene set produced by HDAC inhibition in T24 and MDA carcinoma cell lines, *Molecular cancer therapeutics 2*, 151-163.

38. Mitsiades, C. S., Mitsiades, N. S., McMullan, C. J., Poulaki, V., Shringarpure, R., Hideshima, T., Akiyama, M., Chauhan, D., Munshi, N., Gu, X., Bailey, C., Joseph, M., Libermann, T. A., Richon, V. M., Marks, P. A., and Anderson, K. C. (2004) Transcriptional signature of histone deacetylase inhibition in multiple myeloma: biological and clinical implications, *Proceedings of the National Academy of Sciences of the United States of America 101*, 540-545.

39. Katan-Khaykovich, Y., and Struhl, K. (2002) Dynamics of global histone acetylation and deacetylation in vivo: rapid restoration of normal histone acetylation status upon removal of activators and repressors, *Genes & development 16*, 743-752.

40. West, A. C., and Johnstone, R. W. (2014) New and emerging HDAC inhibitors for cancer treatment, *The Journal of clinical investigation 124*, 30-39.

41. Jamaladdin, S., Kelly, R. D., O'Regan, L., Dovey, O. M., Hodson, G. E., Millard, C. J., Portolano, N., Fry, A. M., Schwabe, J. W., and Cowley, S. M. (2014) Histone deacetylase (HDAC) 1 and 2 are essential for accurate cell division and the pluripotency of embryonic stem cells, *Proceedings of the National Academy of Sciences of the United States of America 111*, 9840-9845.

42. Reichert, N., Choukrallah, M. A., and Matthias, P. (2012) Multiple roles of class I HDACs in proliferation, differentiation, and development, *Cellular and molecular life sciences : CMLS 69*, 2173-2187.

43. Minucci, S., and Pelicci, P. G. (2006) Histone deacetylase inhibitors and the promise of epigenetic (and more) treatments for cancer, *Nature reviews. Cancer 6*, 38-51.

44. Martin, M., Kettmann, R., and Dequiedt, F. (2007) Class IIa histone deacetylases: regulating the regulators, *Oncogene 26*, 5450-5467.

45. Yang, X. J., and Gregoire, S. (2005) Class II histone deacetylases: from sequence to function, regulation, and clinical implication, *Molecular and cellular biology 25*, 2873-2884.

46. Gao, L., Cueto, M. A., Asselbergs, F., and Atadja, P. (2002) Cloning and functional characterization of HDAC11, a novel member of the human histone deacetylase family, *The Journal of biological chemistry 277*, 25748-25755.

47. Villagra, A., Cheng, F., Wang, H. W., Suarez, I., Glozak, M., Maurin, M., Nguyen, D., Wright, K. L., Atadja, P. W., Bhalla, K., Pinilla-Ibarz, J., Seto, E., and Sotomayor, E. M. (2009) The histone deacetylase HDAC11 regulates the expression of interleukin 10 and immune tolerance, *Nature immunology 10*, 92-100.

48. Dereeper, A., Audic, S., Claverie, J. M., and Blanc, G. (2010) BLAST-EXPLORER helps you building datasets for phylogenetic analysis, *BMC evolutionary biology 10*, 8.

49. Anisimova, M., and Gascuel, O. (2006) Approximate likelihood-ratio test for branches: A fast, accurate, and powerful alternative, *Systematic biology 55*, 539-552.

50. Guindon, S., and Gascuel, O. (2003) A simple, fast, and accurate algorithm to estimate large phylogenies by maximum likelihood, *Systematic biology 52*, 696-704.

51. Edgar, R. C. (2004) MUSCLE: multiple sequence alignment with high accuracy and high throughput, *Nucleic acids research 32*, 1792-1797.

52. Dereeper, A., Guignon, V., Blanc, G., Audic, S., Buffet, S., Chevenet, F., Dufayard, J. F., Guindon, S., Lefort, V., Lescot, M., Claverie, J. M., and Gascuel,

O. (2008) Phylogeny.fr: robust phylogenetic analysis for the non-specialist, *Nucleic acids research 36*, W465-469.

53. Johnson, C. A., White, D. A., Lavender, J. S., O'Neill, L. P., and Turner, B. M. (2002) Human class I histone deacetylase complexes show enhanced catalytic activity in the presence of ATP and co-immunoprecipitate with the ATP-dependent chaperone protein Hsp70, *The Journal of biological chemistry 277*, 9590-9597.

54. Lagger, G., O'Carroll, D., Rembold, M., Khier, H., Tischler, J., Weitzer, G., Schuettengruber, B., Hauser, C., Brunmeir, R., Jenuwein, T., and Seiser, C. (2002) Essential function of histone deacetylase 1 in proliferation control and CDK inhibitor repression, *The EMBO journal 21*, 2672-2681.

55. Zupkovitz, G., Tischler, J., Posch, M., Sadzak, I., Ramsauer, K., Egger, G., Grausenburger, R., Schweifer, N., Chiocca, S., Decker, T., and Seiser, C. (2006) Negative and positive regulation of gene expression by mouse histone deacetylase 1, *Molecular and cellular biology 26*, 7913-7928.

56. Bradner, J. E., Mak, R., Tanguturi, S. K., Mazitschek, R., Haggarty, S. J., Ross, K., Chang, C. Y., Bosco, J., West, N., Morse, E., Lin, K., Shen, J. P., Kwiatkowski, N. P., Gheldof, N., Dekker, J., DeAngelo, D. J., Carr, S. A., Schreiber, S. L., Golub, T. R., and Ebert, B. L. (2010) Chemical genetic strategy identifies histone deacetylase 1 (HDAC1) and HDAC2 as therapeutic targets in sickle cell disease, *Proceedings of the National Academy of Sciences 107*, 12617-12622.

57. Sun, Z., Feng, D., Fang, B., Mullican, S. E., You, S. H., Lim, H. W., Everett, L. J., Nabel, C. S., Li, Y., Selvakumaran, V., Won, K. J., and Lazar, M. A. (2013) Deacetylase-independent function of HDAC3 in transcription and metabolism requires nuclear receptor corepressor, *Molecular cell 52*, 769-782.

58. Montgomery, R. L., Potthoff, M. J., Haberland, M., Qi, X., Matsuzaki, S., Humphries, K. M., Richardson, J. A., Bassel-Duby, R., and Olson, E. N. (2008) Maintenance of cardiac energy metabolism by histone deacetylase 3 in mice, *The Journal of clinical investigation 118*, 3588-3597.

59. Lagger, S., Meunier, D., Mikula, M., Brunmeir, R., Schlederer, M., Artaker, M., Pusch, O., Egger, G., Hagelkruys, A., Mikulits, W., Weitzer, G., Muellner, E. W., Susani, M., Kenner, L., and Seiser, C. (2010) Crucial function of histone deacetylase 1 for differentiation of teratomas in mice and humans, *The EMBO journal 29*, 3992-4007.

60. Hubbert, C., Guardiola, A., Shao, R., Kawaguchi, Y., Ito, A., Nixon, A., Yoshida, M., Wang, X.-F., and Yao, T.-P. (2002) HDAC6 is a microtubule-associated deacetylase, *Nature 417*, 455-458.

61. Khoury, G. A., Baliban, R. C., and Floudas, C. A. (2011) Proteome-wide post-translational modification statistics: frequency analysis and curation of the swiss-prot database, *Scientific reports 1*.

62. Leder, A., and Leder, P. Butyric acid, a potent inducer of erythroid differentiation in cultured erythroleukemic cells, *Cell 5*, 319-322.

63. Richon, V. M., Webb, Y., Merger, R., Sheppard, T., Jursic, B., Ngo, L., Civoli, F., Breslow, R., Rifkind, R. A., and Marks, P. A. (1996) Second generation hybrid polar compounds are potent inducers of transformed cell differentiation, *Proceedings of the National Academy of Sciences of the United States of America 93*, 5705-5708.

64. Yoshida, M., Kijima, M., Akita, M., and Beppu, T. (1990) Potent and specific inhibition of mammalian histone deacetylase both in vivo and in vitro by trichostatin A, *The Journal of biological chemistry 265*, 17174-17179.

65. Kijima, M., Yoshida, M., Sugita, K., Horinouchi, S., and Beppu, T. (1993) Trapoxin, an antitumor cyclic tetrapeptide, is an irreversible inhibitor of mammalian histone deacetylase, *The Journal of biological chemistry 268*, 22429-22435.

66. Administration, F. a. D. (2017) Electronic Orange Book, https://www.fda.gov/downloads/Drugs/DevelopmentApprovalProcess/UCM071436.pdf.

67. Vannini, A., Volpari, C., Gallinari, P., Jones, P., Mattu, M., Carfi, A., De Francesco, R., Steinkuhler, C., and Di Marco, S. (2007) Substrate binding to histone deacetylases as shown by the crystal structure of the HDAC8-substrate complex, *EMBO reports 8*, 879-884.

68. Lauffer, B. E., Mintzer, R., Fong, R., Mukund, S., Tam, C., Zilberleyb, I., Flicke, B., Ritscher, A., Fedorowicz, G., Vallero, R., Ortwine, D. F., Gunzner, J., Modrusan, Z., Neumann, L., Koth, C. M., Lupardus, P. J., Kaminker, J. S., Heise, C. E., and Steiner, P. (2013) Histone deacetylase (HDAC) inhibitor kinetic rate constants correlate with cellular histone acetylation but not transcription and cell viability, *The Journal of biological chemistry 288*, 26926-26943.

69. Xu, W. S., Parmigiani, R. B., and Marks, P. A. (2007) Histone deacetylase inhibitors: molecular mechanisms of action, *Oncogene 26*, 5541-5552.

70. Van Lint, C., Emiliani, S., and Verdin, E. (1996) The expression of a small fraction of cellular genes is changed in response to histone hyperacetylation, *Gene expression 5*, 245-253.

71. Richon, V. M., Sandhoff, T. W., Rifkind, R. A., and Marks, P. A. (2000) Histone deacetylase inhibitor selectively induces p21WAF1 expression and gene-associated histone acetylation, *Proceedings of the National Academy of Sciences of the United States of America 97*, 10014-10019.

72. He, L. Z., Tolentino, T., Grayson, P., Zhong, S., Warrell, R. P., Jr., Rifkind, R. A., Marks, P. A., Richon, V. M., and Pandolfi, P. P. (2001) Histone deacetylase inhibitors induce remission in transgenic models of therapy-resistant acute promyelocytic leukemia, *The Journal of clinical investigation 108*, 1321-1330.

73. Della Ragione, F., Criniti, V., Della Pietra, V., Borriello, A., Oliva, A., Indaco, S., Yamamoto, T., and Zappia, V. (2001) Genes modulated by histone acetylation as new effectors of butyrate activity, *FEBS letters 499*, 199-204.

74. Rees, M. G., Seashore-Ludlow, B., Cheah, J. H., Adams, D. J., Price, E. V., Gill, S., Javaid, S., Coletti, M. E., Jones, V. L., Bodycombe, N. E., Soule, C. K., Alexander, B., Li, A., Montgomery, P., Kotz, J. D., Hon, C. S., Munoz, B., Liefeld, T., Dancik, V., Haber, D. A., Clish, C. B., Bittker, J. A., Palmer, M., Wagner, B. K., Clemons, P. A., Shamji, A. F., and Schreiber, S. L. (2016) Correlating chemical sensitivity and basal gene expression reveals mechanism of action, *Nature chemical biology 12*, 109-116.

75. Zwergel C, S. G., Valente S, et al. Histone Deacetylase Inhibitors: Updated Studies in Various Epigenetic-Related Diseases. J Clin Epigenet, *Journal of Clinical Epigenetics 2*.

76. Qiu, T., Zhou, L., Zhu, W., Wang, T., Wang, J., Shu, Y., and Liu, P. (2013) Effects of treatment with histone deacetylase inhibitors in solid tumors: a review based on 30 clinical trials, *Future oncology (London, England) 9*, 255-269.

77. Nebbioso, A., Carafa, V., Benedetti, R., and Altucci, L. (2012) Trials with 'epigenetic' drugs: an update, *Mol Oncol 6*, 657-682.

78. Grignani, F., De Matteis, S., Nervi, C., Tomassoni, L., Gelmetti, V., Cioce, M., Fanelli, M., Ruthardt, M., Ferrara, F. F., Zamir, I., Seiser, C., Grignani, F., Lazar,

M. A., Minucci, S., and Pelicci, P. G. (1998) Fusion proteins of the retinoic acid receptor-alpha recruit histone deacetylase in promyelocytic leukaemia, *Nature 391*, 815-818.

79. Nguyen, A. T., Taranova, O., He, J., and Zhang, Y. (2011) DOT1L, the H3K79 methyltransferase, is required for MLL-AF9-mediated leukemogenesis, *Blood 117*, 6912-6922.

80. Kakizuka, A., Miller, W. H., Jr., Umesono, K., Warrell, R. P., Jr., Frankel, S. R., Murty, V. V., Dmitrovsky, E., and Evans, R. M. (1991) Chromosomal translocation t(15;17) in human acute promyelocytic leukemia fuses RAR alpha with a novel putative transcription factor, PML, *Cell 66*, 663-674.

81. Insinga, A., Monestiroli, S., Ronzoni, S., Gelmetti, V., Marchesi, F., Viale, A., Altucci, L., Nervi, C., Minucci, S., and Pelicci, P. G. (2005) Inhibitors of histone deacetylases induce tumor-selective apoptosis through activation of the death receptor pathway, *Nature medicine 11*, 71-76.

82. Nebbioso, A., Clarke, N., Voltz, E., Germain, E., Ambrosino, C., Bontempo, P., Alvarez, R., Schiavone, E. M., Ferrara, F., Bresciani, F., Weisz, A., de Lera, A. R., Gronemeyer, H., and Altucci, L. (2005) Tumor-selective action of HDAC inhibitors involves TRAIL induction in acute myeloid leukemia cells, *Nature medicine 11*, 77-84.

83. Gelmetti, V., Zhang, J., Fanelli, M., Minucci, S., Pelicci, P. G., and Lazar, M. A. (1998) Aberrant recruitment of the nuclear receptor corepressor-histone deacetylase complex by the acute myeloid leukemia fusion partner ETO, *Molecular and cellular biology 18*, 7185-7191.

84. Dhordain, P., Quief, S., Lantoine, D., Kerckaert, J.-P., Albagli, O., Lin, R. J., and Evans, R. M. (1998) The LAZ3(BCL-6) oncoprotein recruits a SMRT/mSIN3A/histone deacetylase containing complex to mediate transcriptional repression, *Nucleic acids research 26*, 4645-4651.

85. Dimopoulos, K., Gimsing, P., and Gronbaek, K. (2014) The role of epigenetics in the biology of multiple myeloma, *Blood cancer journal 4*, e207.

86. Hu, D., and Shilatifard, A. (2016) Epigenetics of hematopoiesis and hematological malignancies, *Genes Dev 30*, 2021-2041.

87. Richon, V. M., Emiliani, S., Verdin, E., Webb, Y., Breslow, R., Rifkind, R. A., and Marks, P. A. (1998) A class of hybrid polar inducers of transformed cell

differentiation inhibits histone deacetylases, *Proceedings of the National Academy of Sciences of the United States of America 95*, 3003-3007.

88. Pili, R., Salumbides, B., Zhao, M., Altiok, S., Qian, D., Zwiebel, J., Carducci, M. A., and Rudek, M. A. (2012) Phase I study of the histone deacetylase inhibitor entinostat in combination with 13-cis retinoic acid in patients with solid tumours, *Br J Cancer 106*, 77-84.

89. Luu, T. H., Morgan, R. J., Leong, L., Lim, D., McNamara, M., Portnow, J., Frankel, P., Smith, D. D., Doroshow, J. H., Gandara, D. R., Aparicio, A., Somlo, G., and Wong, C. (2008) A Phase II Trial of Vorinostat (Suberoylanilide Hydroxamic Acid) in Metastatic Breast Cancer: A California Cancer Consortium Study, *Clinical Cancer Research 14*, 7138-7142.

90. Yardley, D. A., Ismail-Khan, R. R., Melichar, B., Lichinitser, M., Munster, P. N., Klein, P. M., Cruickshank, S., Miller, K. D., Lee, M. J., and Trepel, J. B. (2013) Randomized Phase II, Double-Blind, Placebo-Controlled Study of Exemestane With or Without Entinostat in Postmenopausal Women With Locally Recurrent or Metastatic Estrogen Receptor-Positive Breast Cancer Progressing on Treatment With a Nonsteroidal Aromatase Inhibitor, *Journal of Clinical Oncology 31*, 2128-2135.

91. Conte, P., Campone, M., Pronzato, P., Amadori, D., Frank, R., Schuetz, F., Rea, D., Wardley, A., Britten, C., and Elias, A. (2009) Phase I trial of panobinostat (LBH589) in combination with trastuzumab in pretreated HER2-positive metastatic breast cancer (mBC): Preliminary safety and tolerability results, *Journal of Clinical Oncology 27*, 1081-1081.

92. Subik, K., Lee, J. F., Baxter, L., Strzepek, T., Costello, D., Crowley, P., Xing, L., Hung, M. C., Bonfiglio, T., Hicks, D. G., and Tang, P. (2010) The Expression Patterns of ER, PR, HER2, CK5/6, EGFR, Ki-67 and AR by Immunohistochemical Analysis in Breast Cancer Cell Lines, *Breast cancer : basic and clinical research 4*, 35-41.

93. Chavez, K. J., Garimella, S. V., and Lipkowitz, S. (2010) Triple negative breast cancer cell lines: one tool in the search for better treatment of triple negative breast cancer, *Breast disease 32*, 35-48.

94. Ni, M., Chen, Y., Lim, E., Wimberly, H., Bailey, S. T., Imai, Y., Rimm, D. L., Liu, X. S., and Brown, M. (2011) Targeting androgen receptor in estrogen receptor-negative breast cancer, *Cancer cell 20*, 119-131.

95. Zhao, M., and Ramaswamy, B. (2014) Mechanisms and therapeutic advances in the management of endocrine-resistant breast cancer, *World journal of clinical oncology 5*, 248-262.

96. Torre, L. A., Bray, F., Siegel, R. L., Ferlay, J., Lortet-Tieulent, J., and Jemal, A. (2015) Global cancer statistics, 2012, *CA: a cancer journal for clinicians 65*, 87-108.

97. Hortobagyi, G. N. (1998) Treatment of breast cancer, *The New England journal of medicine 339*, 974-984.

98. Fernandez, Y., Cueva, J., Palomo, A. G., Ramos, M., de Juan, A., Calvo, L., Garcia-Mata, J., Garcia-Teijido, P., Pelaez, I., and Garcia-Estevez, L. (2010) Novel therapeutic approaches to the treatment of metastatic breast cancer, *Cancer treatment reviews 36*, 33-42.

99. Tate, C. R., Rhodes, L. V., Segar, H. C., Driver, J. L., Pounder, F. N., Burow, M. E., and Collins-Burow, B. M. (2012) Targeting triple-negative breast cancer cells with the histone deacetylase inhibitor panobinostat, *Breast cancer research : BCR 14*, R79.

100. Rhodes, L. V., Tate, C. R., Segar, H. C., Burks, H. E., Phamduy, T. B., Hoang, V., Elliott, S., Gilliam, D., Pounder, F. N., Anbalagan, M., Chrisey, D. B., Rowan, B. G., Burow, M. E., and Collins-Burow, B. M. (2014) Suppression of triple-negative breast cancer metastasis by pan-DAC inhibitor panobinostat via inhibition of ZEB family of EMT master regulators, *Breast cancer research and treatment 145*, 593-604.

101. Macaluso, M., Cinti, C., Russo, G., Russo, A., and Giordano, A. (2003) pRb2/p130-E2F4/5-HDAC1-SUV39H1-p300 and pRb2/p130-E2F4/5-HDAC1-SUV39H1-DNMT1 multimolecular complexes mediate the transcription of estrogen receptor-alpha in breast cancer, *Oncogene 22*, 3511-3517.

102. Meehan, W. J., Samant, R. S., Hopper, J. E., Carrozza, M. J., Shevde, L. A., Workman, J. L., Eckert, K. A., Verderame, M. F., and Welch, D. R. (2004) Breast cancer metastasis suppressor 1 (BRMS1) forms complexes with retinoblastoma-binding protein 1 (RBP1) and the mSin3 histone deacetylase complex and represses transcription, *The Journal of biological chemistry 279*, 1562-1569.

103. Sabnis, G. J., Goloubeva, O., Chumsri, S., Nguyen, N., Sukumar, S., and Brodie, A. M. H. (2011) Functional activation of the estrogen receptor-α and aromatase by

the HDAC inhibitor, entinostat, sensitizes of ER-negative tumors to letrozole, *Cancer research 71*, 1893-1903.

104. Sharma, D., Saxena, N. K., Davidson, N. E., and Vertino, P. M. (2006) Restoration of tamoxifen sensitivity in estrogen receptor-negative breast cancer cells: tamoxifen-bound reactivated ER recruits distinctive corepressor complexes, *Cancer Res 66*, 6370-6378.

105. Zhou, Q., Atadja, P., and Davidson, N. E. (2007) Histone deacetylase inhibitor LBH589 reactivates silenced estrogen receptor alpha (ER) gene expression without loss of DNA hypermethylation, *Cancer biology & therapy 6*, 64-69.

106. Yang, X., Ferguson, A. T., Nass, S. J., Phillips, D. L., Butash, K. A., Wang, S. M., Herman, J. G., and Davidson, N. E. (2000) Transcriptional activation of estrogen receptor alpha in human breast cancer cells by histone deacetylase inhibition, *Cancer research 60*, 6890-6894.

107. de Cremoux, P., Dalvai, M., N'Doye, O., Moutahir, F., Rolland, G., Chouchane-Mlik, O., Assayag, F., Lehmann-Che, J., Kraus-Berthie, L., Nicolas, A., Lockhart, B. P., Marangoni, E., de The, H., Depil, S., Bystricky, K., and Decaudin, D. (2015) HDAC inhibition does not induce estrogen receptor in human triple-negative breast cancer cell lines and patient-derived xenografts, *Breast cancer research and treatment 149*, 81-89.

108. Yang, X., Phillips, D. L., Ferguson, A. T., Nelson, W. G., Herman, J. G., and Davidson, N. E. (2001) Synergistic activation of functional estrogen receptor (ER)-alpha by DNA methyltransferase and histone deacetylase inhibition in human ER-alpha-negative breast cancer cells, *Cancer Res 61*, 7025-7029.

109. Fan, J., Yin, W. J., Lu, J. S., Wang, L., Wu, J., Wu, F. Y., Di, G. H., Shen, Z. Z., and Shao, Z. M. (2008) ER alpha negative breast cancer cells restore response to endocrine therapy by combination treatment with both HDAC inhibitor and DNMT inhibitor, *Journal of cancer research and clinical oncology 134*, 883-890.

110. Raha, P., Thomas, S., Thurn, K. T., Park, J., and Munster, P. N. (2015) Combined histone deacetylase inhibition and tamoxifen induces apoptosis in tamoxifen-resistant breast cancer models, by reversing Bcl-2 overexpression, *Breast Cancer Research 17*, 26.

111. (2015) NCT01194908 Re-expression of ER in Triple Negative Breast Cancers, National Institutes of Health, ClinicalTrials.gov.

112. Zeng, H., Qu, J., Jin, N., Xu, J., Lin, C., Chen, Y., Yang, X., He, X., Tang, S., Lan, X., Yang, X., Chen, Z., Huang, M., Ding, J., and Geng, M. Feedback Activation of Leukemia Inhibitory Factor Receptor Limits Response to Histone Deacetylase Inhibitors in Breast Cancer, *Cancer cell 30*, 459-473.

113. Eom, M., Oh, S. S., Lkhagvadorj, S., Han, A., and Park, K. H. (2012) HDAC1 Expression in Invasive Ductal Carcinoma of the Breast and Its Value as a Good Prognostic Factor, *J Pathol Transl Med 46*, 311-317.

114. Seo, J., Min, S. K., Park, H.-R., Kim, D. H., Kwon, M. J., Kim, L. S., and Ju, Y.-S. (2014) Expression of Histone Deacetylases HDAC1, HDAC2, HDAC3, and HDAC6 in Invasive Ductal Carcinomas of the Breast, *Journal of Breast Cancer 17*, 323-331.

115. Lapierre, M., Linares, A., Dalvai, M., Duraffourd, C., Bonnet, S., Boulahtouf, A., Rodriguez, C., Jalaguier, S., Assou, S., Orsetti, B., Balaguer, P., Maudelonde, T., Blache, P., Bystricky, K., Boulle, N., and Cavailles, V. (2016) Histone deacetylase 9 regulates breast cancer cell proliferation and the response to histone deacetylase inhibitors, *Oncotarget 7*, 19693-19708.

116. Zhang, Z., Yamashita, H., Toyama, T., Sugiura, H., Ando, Y., Mita, K., Hamaguchi, M., Hara, Y., Kobayashi, S., and Iwase, H. (2005) Quantitation of HDAC1 mRNA expression in invasive carcinoma of the breast*, *Breast cancer research and treatment 94*, 11-16.

117. Muller, B. M., Jana, L., Kasajima, A., Lehmann, A., Prinzler, J., Budczies, J., Winzer, K. J., Dietel, M., Weichert, W., and Denkert, C. (2013) Differential expression of histone deacetylases HDAC1, 2 and 3 in human breast cancer--overexpression of HDAC2 and HDAC3 is associated with clinicopathological indicators of disease progression, *BMC cancer 13*, 215.

118. Hsieh, C. L., Ma, H. P., Su, C. M., Chang, Y. J., Hung, W. Y., Ho, Y. S., Huang, W. J., and Lin, R. K. (2016) Alterations in histone deacetylase 8 lead to cell migration and poor prognosis in breast cancer, *Life sciences 151*, 7-14.

119. Krusche, C. A., Wulfing, P., Kersting, C., Vloet, A., Bocker, W., Kiesel, L., Beier, H. M., and Alfer, J. (2005) Histone deacetylase-1 and -3 protein expression in human breast cancer: a tissue microarray analysis, *Breast cancer research and treatment 90*, 15-23.

120. Zhang, Z., Yamashita, H., Toyama, T., Sugiura, H., Omoto, Y., Ando, Y., Mita, K., Hamaguchi, M., Hayashi, S., and Iwase, H. (2004) HDAC6 expression is

correlated with better survival in breast cancer, *Clinical cancer research : an official journal of the American Association for Cancer Research 10*, 6962-6968.

121. Duong, V., Bret, C., Altucci, L., Mai, A., Duraffourd, C., Loubersac, J., Harmand, P.-O., Bonnet, S., Valente, S., Maudelonde, T., Cavailles, V., and Boulle, N. (2008) Specific activity of class II histone deacetylases in human breast cancer cells, *Molecular Cancer Research 6*, 1908-1919.

122. Dovey, O. M., Foster, C. T., Conte, N., Edwards, S. A., Edwards, J. M., Singh, R., Vassiliou, G., Bradley, A., and Cowley, S. M. (2013) Histone deacetylase 1 and 2 are essential for normal T-cell development and genomic stability in mice, *Blood 121*, 1335-1344.

123. Santoro, F., Botrugno, O. A., Dal Zuffo, R., Pallavicini, I., Matthews, G. M., Cluse, L., Barozzi, I., Senese, S., Fornasari, L., Moretti, S., Altucci, L., Pelicci, P. G., Chiocca, S., Johnstone, R. W., and Minucci, S. (2013) A dual role for Hdac1: oncosuppressor in tumorigenesis, oncogene in tumor maintenance, *Blood 121*, 3459-3468.

124. Bhaskara, S., Knutson, S. K., Jiang, G., Chandrasekharan, M. B., Wilson, A. J., Zheng, S., Yenamandra, A., Locke, K., Yuan, J.-l., Bonine-Summers, A. R., Wells, C. E., Kaiser, J. F., Washington, M. K., Zhao, Z., Wagner, F. F., Sun, Z.-W., Xia, F., Holson, E. B., Khabele, D., and Hiebert, S. W. (2010) Hdac3 is essential for the maintenance of chromatin structure and genome stability, *Cancer cell 18*, 436-447.

125. West, A. C., and Johnstone, R. W. (2014) New and emerging HDAC inhibitors for cancer treatment, *The Journal of clinical investigation 124*, 30-39.

126. Lobera, M., Madauss, K. P., Pohlhaus, D. T., Wright, Q. G., Trocha, M., Schmidt, D. R., Baloglu, E., Trump, R. P., Head, M. S., Hofmann, G. A., Murray-Thompson, M., Schwartz, B., Chakravorty, S., Wu, Z., Mander, P. K., Kruidenier, L., Reid, R. A., Burkhart, W., Turunen, B. J., Rong, J. X., Wagner, C., Moyer, M. B., Wells, C., Hong, X., Moore, J. T., Williams, J. D., Soler, D., Ghosh, S., and Nolan, M. A. (2013) Selective class IIa histone deacetylase inhibition via a nonchelating zinc-binding group, *Nature chemical biology 9*, 319-325.

127. Marek, L., Hamacher, A., Hansen, F. K., Kuna, K., Gohlke, H., Kassack, M. U., and Kurz, T. (2013) Histone Deacetylase (HDAC) Inhibitors with a Novel Connecting Unit Linker Region Reveal a Selectivity Profile for HDAC4 and HDAC5 with Improved Activity against Chemoresistant Cancer Cells, *Journal of medicinal chemistry 56*, 427-436.

128. Wang, D.-F., Helquist, P., Wiech, N. L., and Wiest, O. (2005) Toward Selective Histone Deacetylase Inhibitor Design: Homology Modeling, Docking Studies, and Molecular Dynamics Simulations of Human Class I Histone Deacetylases, *Journal of medicinal chemistry 48*, 6936-6947.

129. Lapierre, M., Linares, A., Dalvai, M., Duraffourd, C., Bonnet, S., Boulahtouf, A., Rodriguez, C., Jalaguier, S., Assou, S., Orsetti, B., Balaguer, P., Maudelonde, T., Blache, P., Bystricky, K., Boulle, N., and Cavaillès, V. (2016) Histone deacetylase 9 regulates breast cancer cell proliferation and the response to histone deacetylase inhibitors, *Oncotarget 7*, 19693-19708.

130. Chao, M. W., Chu, P. C., Chuang, H. C., Shen, F. H., Chou, C. C., Hsu, E. C., Himmel, L. E., Huang, H. L., Tu, H. J., Kulp, S. K., Teng, C. M., and Chen, C. S. (2016) Non-epigenetic function of HDAC8 in regulating breast cancer stem cells by maintaining Notch1 protein stability, *Oncotarget 7*, 1796-1807.

131. Medler, T. R., Craig, J. M., Fiorillo, A. A., Feeney, Y. B., Harrell, J. C., and Clevenger, C. V. (2016) HDAC6 Deacetylates HMGN2 to Regulate Stat5a Activity and Breast Cancer Growth, *Molecular cancer research : MCR 14*, 994-1008.

132. Wen, Y. D., Cress, W. D., Roy, A. L., and Seto, E. (2003) Histone deacetylase 3 binds to and regulates the multifunctional transcription factor TFII-I, *The Journal of biological chemistry 278*, 1841-1847.

133. Doetzlhofer, A., Rotheneder, H., Lagger, G., Koranda, M., Kurtev, V., Brosch, G., Wintersberger, E., and Seiser, C. (1999) Histone Deacetylase 1 Can Repress Transcription by Binding to Sp1, *Molecular and cellular biology 19*, 5504-5511.

134. Xue, Y., Wong, J., Moreno, G. T., Young, M. K., Cote, J., and Wang, W. (1998) NURD, a novel complex with both ATP-dependent chromatin-remodeling and histone deacetylase activities, *Molecular cell 2*, 851-861.

135. Lai, A. Y., and Wade, P. A. (2011) Cancer biology and NuRD: a multifaceted chromatin remodelling complex, *Nature reviews. Cancer 11*, 588-596.

136. Fischle, W., Dequiedt, F., Fillion, M., Hendzel, M. J., Voelter, W., and Verdin, E. (2001) Human HDAC7 histone deacetylase activity is associated with HDAC3 in vivo, *The Journal of biological chemistry 276*, 35826-35835.

137. Fischle, W., Dequiedt, F., Hendzel, M. J., Guenther, M. G., Lazar, M. A., Voelter, W., and Verdin, E. Enzymatic Activity Associated with Class II HDACs Is Dependent on a Multiprotein Complex Containing HDAC3 and SMRT/N-CoR, *Molecular cell 9*, 45-57.

138. Guenther, M. G., Barak, O., and Lazar, M. A. (2001) The SMRT and N-CoR corepressors are activating cofactors for histone deacetylase 3, *Molecular and cellular biology 21*, 6091-6101.

139. Hayakawa, T., and Nakayama, J. (2011) Physiological roles of class I HDAC complex and histone demethylase, *Journal of biomedicine & biotechnology 2011*, 129383.

140. Zhang, X., Ozawa, Y., Lee, H., Wen, Y. D., Tan, T. H., Wadzinski, B. E., and Seto, E. (2005) Histone deacetylase 3 (HDAC3) activity is regulated by interaction with protein serine/threonine phosphatase 4, *Genes & development 19*, 827-839.

141. Zhang, Y., Ng, H. H., Erdjument-Bromage, H., Tempst, P., Bird, A., and Reinberg, D. (1999) Analysis of the NuRD subunits reveals a histone deacetylase core complex and a connection with DNA methylation, *Genes & development 13*, 1924-1935.

142. Andres, M. E., Burger, C., Peral-Rubio, M. J., Battaglioli, E., Anderson, M. E., Grimes, J., Dallman, J., Ballas, N., and Mandel, G. (1999) CoREST: a functional corepressor required for regulation of neural-specific gene expression, *Proc Natl Acad Sci U S A 96*, 9873-9878.

143. Guenther, M. G., Lane, W. S., Fischle, W., Verdin, E., Lazar, M. A., and Shiekhattar, R. (2000) A core SMRT corepressor complex containing HDAC3 and TBL1, a WD40-repeat protein linked to deafness, *Genes & development 14*, 1048-1057.

144. Yoon, H.-G., Chan, D. W., Huang, Z.-Q., Li, J., Fondell, J. D., Qin, J., and Wong, J. (2003) Purification and functional characterization of the human N-CoR complex: the roles of HDAC3, TBL1 and TBLR1, *The EMBO journal 22*, 1336-1346.

145. Zhang, J., Kalkum, M., Chait, B. T., and Roeder, R. G. (2002) The N-CoR-HDAC3 nuclear receptor corepressor complex inhibits the JNK pathway through the integral subunit GPS2, *Molecular cell 9*, 611-623.

146. Guenther, M. G., Barak, O., and Lazar, M. A. (2001) The SMRT and N-CoR Corepressors Are Activating Cofactors for Histone Deacetylase 3, *Molecular and cellular biology 21*, 6091-6101.

147. Sun, Z., Feng, D., Fang, B., Mullican, S. E., You, S.-H., Lim, H.-W., Everett, L. J., Nabel, C. S., Li, Y., Selvakumaran, V., Won, K.-J., and Lazar, M. A. (2013) Deacetylase-Independent Function of HDAC3 in Transcription and Metabolism Requires Nuclear Receptor Corepressor, *Molecular cell 52*, 10.1016/j.molcel.2013.1010.1022.

148. Guenther, M. G., Lane, W. S., Fischle, W., Verdin, E., Lazar, M. A., and Shiekhattar, R. (2000) A core SMRT corepressor complex containing HDAC3 and TBL1, a WD40-repeat protein linked to deafness, *Genes & development 14*, 1048-1057.

149. Zhang, J., Kalkum, M., Chait, B. T., and Roeder, R. G. (2002) The N-CoR-HDAC3 Nuclear Receptor Corepressor Complex Inhibits the JNK Pathway through the Integral Subunit GPS2, *Molecular cell 9*, 611-623.

150. Oberoi, J., Fairall, L., Watson, P. J., Yang, J.-C., Czimmerer, Z., Kampmann, T., Goult, B. T., Greenwood, J. A., Gooch, J. T., Kallenberger, B. C., Nagy, L., Neuhaus, D., and Schwabe, J. W. R. (2011) Structural basis for the assembly of the SMRT/NCoR core transcriptional repression machinery, *Nat Struct Mol Biol 18*, 177-184.

151. Pflum, M. K., Tong, J. K., Lane, W. S., and Schreiber, S. L. (2001) Histone deacetylase 1 phosphorylation promotes enzymatic activity and complex formation, *The Journal of biological chemistry 276*, 47733-47741.

152. Segre, C. V., and Chiocca, S. (2011) Regulating the regulators: the post-translational code of class I HDAC1 and HDAC2, *Journal of biomedicine & biotechnology 2011*, 690848.

153. Parra, M., and Verdin, E. (2010) Regulatory signal transduction pathways for class IIa histone deacetylases, *Current opinion in pharmacology 10*, 454-460.

154. Khan, D. H., He, S., Yu, J., Winter, S., Cao, W., Seiser, C., and Davie, J. R. (2013) Protein kinase CK2 regulates the dimerization of histone deacetylase 1 (HDAC1) and HDAC2 during mitosis, *The Journal of biological chemistry 288*, 16518-16528.

155. Di Giorgio, E., and Brancolini, C. (2016) Regulation of class IIa HDAC activities: it is not only matter of subcellular localization, *Epigenomics 8*, 251-269.

156. Gao, Z., He, Q., Peng, B., Chiao, P., and Ye, J. (2006) REGULATION OF NUCLEAR TRANSLOCATION OF HDAC3 BY IKBα IS REQUIRED FOR TNF-INHIBITION OF PPARγ FUNCTION, *The Journal of biological chemistry 281*, 4540-4547.

157. Yang, W. M., Tsai, S. C., Wen, Y. D., Fejer, G., and Seto, E. (2002) Functional domains of histone deacetylase-3, *The Journal of biological chemistry 277*, 9447-9454.

158. Alam, N., Zimmerman, L., Wolfson, Noah A., Joseph, Caleb G., Fierke, Carol A., and Schueler-Furman, O. Structure-Based Identification of HDAC8 Non-histone Substrates, *Structure 24*, 458-468.

159. Wolfson, N. A., Pitcairn, C. A., and Fierke, C. A. (2013) HDAC8 substrates: Histones and beyond, *Biopolymers 99*, 112-126.

160. Verdin, E., Dequiedt, F., and Kasler, H. G. (2003) Class II histone deacetylases: versatile regulators, *Trends in genetics : TIG 19*, 286-293.

161. Singh, A., Thornton, E. R., and Westheimer, F. H. (1962) The photolysis of diazoacetylchymotrypsin, *The Journal of biological chemistry 237*, 3006-3008.

162. Xu, C., Soragni, E., Chou, C. J., Herman, D., Plasterer, H. L., Rusche, J. R., and Gottesfeld, J. M. (2009) Chemical probes identify a role for histone deacetylase 3 in Friedreich's ataxia gene silencing, *Chem Biol 16*, 980-989.

163. Kotake, Y., Sagane, K., Owa, T., Mimori-Kiyosue, Y., Shimizu, H., Uesugi, M., Ishihama, Y., Iwata, M., and Mizui, Y. (2007) Splicing factor SF3b as a target of the antitumor natural product pladienolide, *Nature chemical biology 3*, 570-575.

164. Jessen, K. A., English, N. M., Yu Wang, J., Maliartchouk, S., Archer, S. P., Qiu, L., Brand, R., Kuemmerle, J., Zhang, H. Z., Gehlsen, K., Drewe, J., Tseng, B., Cai, S. X., and Kasibhatla, S. (2005) The discovery and mechanism of action of novel tumor-selective and apoptosis-inducing 3,5-diaryl-1,2,4-oxadiazole series using a chemical genetics approach, *Molecular cancer therapeutics 4*, 761-771.

165. Smith, E., and Collins, I. (2015) Photoaffinity labeling in target- and binding-site identification, *Future medicinal chemistry 7*, 159-183.

166. Gritsan, N., and Platz, M. (2010) Photochemistry of Azides: The Azide/Nitrene Interface, In *Organic Azides*, pp 311-372, John Wiley & Sons, Ltd.

167. Schnapp, K. A., Poe, R., Leyva, E., Soundararajan, N., and Platz, M. S. (1993) Exploratory photochemistry of fluorinated aryl azides. Implications for the design of photoaffinity labeling reagents, *Bioconjugate chemistry 4*, 172-177.

168. Terstappen, G. C., Schlupen, C., Raggiaschi, R., and Gaviraghi, G. (2007) Target deconvolution strategies in drug discovery, *Nature reviews. Drug discovery 6*, 891-903.

169. MacKinnon, A. L., and Taunton, J. (2009) Target Identification by Diazirine Photo-Cross-linking and Click Chemistry, *Current protocols in chemical biology 1*, 55-73.

170. Sadakane, Y., and Hatanaka, Y. (2006) Photochemical fishing approaches for identifying target proteins and elucidating the structure of a ligand-binding region using carbene-generating photoreactive probes, *Analytical sciences : the international journal of the Japan Society for Analytical Chemistry 22*, 209-218.

171. Wittelsberger, A., Thomas, B. E., Mierke, D. F., and Rosenblatt, M. (2006) Methionine acts as a "magnet" in photoaffinity crosslinking experiments, *FEBS letters 580*, 1872-1876.

172. Garin, J., Michel, L., Dupuis, A., Issartel, J. P., Lunardi, J., Hoppe, J., and Vignais, P. (1989) Photolabeling of the phosphate binding site of mitochondrial F1-ATPase by [32P]azidonitrophenyl phosphate. Identification of the photolabeled amino acid residues, *Biochemistry 28*, 1442-1448.

173. Janssen, M. J., van Voorst, F., Ploeger, G. E., Larsen, P. M., Larsen, M. R., de Kroon, A. I., and de Kruijff, B. (2002) Photolabeling identifies an interaction between phosphatidylcholine and glycerol-3-phosphate dehydrogenase (Gut2p) in yeast mitochondria, *Biochemistry 41*, 5702-5711.

174. Sadaghiani, A. M., Verhelst, S. H., and Bogyo, M. (2007) Tagging and detection strategies for activity-based proteomics, *Current opinion in chemical biology 11*, 20-28.

175. Speers, A. E., and Cravatt, B. F. (2009) Activity-Based Protein Profiling (ABPP) and Click Chemistry (CC)-ABPP by MudPIT Mass Spectrometry, *Current protocols in chemical biology 1*, 29-41.

176. Kolb, H. C., Finn, M. G., and Sharpless, K. B. (2001) Click Chemistry: Diverse Chemical Function from a Few Good Reactions, *Angewandte Chemie 40*, 2004-2021.

177. Speers, A. E., Adam, G. C., and Cravatt, B. F. (2003) Activity-based protein profiling in vivo using a copper(i)-catalyzed azide-alkyne [3 + 2] cycloaddition, *Journal of the American Chemical Society 125*, 4686-4687.

178. Parker, C. G., Galmozzi, A., Wang, Y., Correia, B. E., Sasaki, K., Joslyn, C. M., Kim, A. S., Cavallaro, C. L., Lawrence, R. M., Johnson, S. R., Narvaiza, I., Saez, E., and Cravatt, B. F. (2017) Ligand and Target Discovery by Fragment-Based Screening in Human Cells, *Cell 168*, 527-541 e529.

179. Martell, J., Seo, Y., Bak, D. W., Kingsley, S. F., Tissenbaum, H. A., and Weerapana, E. (2016) Global Cysteine-Reactivity Profiling during Impaired Insulin/IGF-1 Signaling in C. elegans Identifies Uncharacterized Mediators of Longevity, *Cell Chem Biol 23*, 955-966.

180. Salisbury, C. M., and Cravatt, B. F. (2007) Activity-based probes for proteomic profiling of histone deacetylase complexes, *Proceedings of the National Academy of Sciences of the United States of America 104*, 1171-1176.

181. Salisbury, C. M., and Cravatt, B. F. (2008) Optimization of activity-based probes for proteomic profiling of histone deacetylase complexes, *Journal of the American Chemical Society 130*, 2184-2194.

182. Albrow, V. E., Grimley, R. L., Clulow, J., Rose, C. R., Sun, J., Warmus, J. S., Tate, E. W., Jones, L. H., and Storer, R. I. (2016) Design and development of histone deacetylase (HDAC) chemical probes for cell-based profiling, *Molecular bioSystems 12*, 1781-1789.

183. Shan, B., Xu, C., Zhang, Y., Xu, T., Gottesfeld, J. M., and Yates, J. R., 3rd. (2014) Quantitative proteomic analysis identifies targets and pathways of a 2-aminobenzamide HDAC inhibitor in Friedreich's ataxia patient iPSC-derived neural stem cells, *Journal of proteome research 13*, 4558-4566.

184. Glozak, M. A., and Seto, E. (2007) Histone deacetylases and cancer, *Oncogene 26*, 5420-5432.

185. Munster, P. N., Marchion, D., Thomas, S., Egorin, M., Minton, S., Springett, G., Lee, J. H., Simon, G., Chiappori, A., Sullivan, D., and Daud, A. (2009) Phase I

trial of vorinostat and doxorubicin in solid tumours: histone deacetylase 2 expression as a predictive marker, *Brit J Cancer 101*, 1044-1050.

186. Luu, T. H., Morgan, R. J., Leong, L., Lim, D., McNamara, M., Portnow, J., Frankel, P., Smith, D. D., Doroshow, J. H., Wong, C., Aparicio, A., Gandara, D. R., and Somlo, G. (2008) A phase II trial of vorinostat (suberoylanilide hydroxamic acid) in metastatic breast cancer: a California Cancer Consortium study, *Clinical cancer research : an official journal of the American Association for Cancer Research 14*, 7138-7142.

187. Taylor, B. S., DeCarolis, P. L., Angeles, C. V., Brenet, F., Schultz, N., Antonescu, C. R., Scandura, J. M., Sander, C., Viale, A. J., Socci, N. D., and Singer, S. (2011) Frequent alterations and epigenetic silencing of differentiation pathway genes in structurally rearranged liposarcomas, *Cancer discovery 1*, 587-597.

188. Ropero, S., Fraga, M. F., Ballestar, E., Hamelin, R., Yamamoto, H., Boix-Chornet, M., Caballero, R., Alaminos, M., Setien, F., Paz, M. F., Herranz, M., Palacios, J., Arango, D., Orntoft, T. F., Aaltonen, L. A., Schwartz, S., Jr., and Esteller, M. (2006) A truncating mutation of HDAC2 in human cancers confers resistance to histone deacetylase inhibition, *Nature genetics 38*, 566-569.

189. Bhaskara, S., Knutson, S. K., Jiang, G., Chandrasekharan, M. B., Wilson, A. J., Zheng, S., Yenamandra, A., Locke, K., Yuan, J. L., Bonine-Summers, A. R., Wells, C. E., Kaiser, J. F., Washington, M. K., Zhao, Z., Wagner, F. F., Sun, Z. W., Xia, F., Holson, E. B., Khabele, D., and Hiebert, S. W. (2010) Hdac3 is essential for the maintenance of chromatin structure and genome stability, *Cancer cell 18*, 436-447.

190. Heideman, M. R., Wilting, R. H., Yanover, E., Velds, A., de Jong, J., Kerkhoven, R. M., Jacobs, H., Wessels, L. F., and Dannenberg, J. H. (2013) Dosage-dependent tumor suppression by histone deacetylases 1 and 2 through regulation of c-Myc collaborating genes and p53 function, *Blood 121*, 2038-2050.

191. Pulukuri, S. M., Gorantla, B., and Rao, J. S. (2007) Inhibition of histone deacetylase activity promotes invasion of human cancer cells through activation of urokinase plasminogen activator, *The Journal of biological chemistry 282*, 35594-35603.

192. Ontoria, J. M., Altamura, S., Di Marco, A., Ferrigno, F., Laufer, R., Muraglia, E., Palumbi, M. C., Rowley, M., Scarpelli, R., Schultz-Fademrecht, C., Serafini, S., Steinkuhler, C., and Jones, P. (2009) Identification of novel, selective, and stable inhibitors of class II histone deacetylases. Validation studies of the inhibition of

the enzymatic activity of HDAC4 by small molecules as a novel approach for cancer therapy, *J Med Chem 52*, 6782-6789.

193. Khan, N., Jeffers, M., Kumar, S., Hackett, C., Boldog, F., Khramtsov, N., Qian, X., Mills, E., Berghs, S. C., Carey, N., Finn, P. W., Collins, L. S., Tumber, A., Ritchie, J. W., Jensen, P. B., Lichenstein, H. S., and Sehested, M. (2008) Determination of the class and isoform selectivity of small-molecule histone deacetylase inhibitors, *The Biochemical journal 409*, 581-589.

194. Fournel, M., Bonfils, C., Hou, Y., Yan, P. T., Trachy-Bourget, M. C., Kalita, A., Liu, J., Lu, A. H., Zhou, N. Z., Robert, M. F., Gillespie, J., Wang, J. J., Ste-Croix, H., Rahil, J., Lefebvre, S., Moradei, O., Delorme, D., Macleod, A. R., Besterman, J. M., and Li, Z. (2008) MGCD0103, a novel isotype-selective histone deacetylase inhibitor, has broad spectrum antitumor activity in vitro and in vivo, *Molecular cancer therapeutics 7*, 759-768.

195. Balasubramanian, S., Ramos, J., Luo, W., Sirisawad, M., Verner, E., and Buggy, J. J. (2008) A novel histone deacetylase 8 (HDAC8)-specific inhibitor PCI-34051 induces apoptosis in T-cell lymphomas, *Leukemia 22*, 1026-1034.

196. Mottamal, M., Zheng, S., Huang, T. L., and Wang, G. (2015) Histone deacetylase inhibitors in clinical studies as templates for new anticancer agents, *Molecules 20*, 3898-3941.

197. Gray, G. K., McFarland, B. C., Rowse, A. L., Gibson, S. A., and Benveniste, E. N. (2014) Therapeutic CK2 inhibition attenuates diverse prosurvival signaling cascades and decreases cell viability in human breast cancer cells, *Oncotarget 5*, 6484-6496.

198. Gharbi, S. I., Zvelebil, M. J., Shuttleworth, S. J., Hancox, T., Saghir, N., Timms, J. F., and Waterfield, M. D. (2007) Exploring the specificity of the PI3K family inhibitor LY294002, *The Biochemical journal 404*, 15-21.

199. Bardai, F. H., and D'Mello, S. R. (2011) Selective toxicity by HDAC3 in neurons: regulation by Akt and GSK3beta, *The Journal of neuroscience : the official journal of the Society for Neuroscience 31*, 1746-1751.

200. Li, Y., Jia, L., Ren, D., Liu, C., Gong, Y., Wang, N., Zhang, X., and Zhao, Y. (2014) Axl mediates tumor invasion and chemosensitivity through PI3K/Akt signaling pathway and is transcriptionally regulated by slug in breast carcinoma, *IUBMB life 66*, 507-518.

201. Frasor, J., Chang, E. C., Komm, B., Lin, C. Y., Vega, V. B., Liu, E. T., Miller, L. D., Smeds, J., Bergh, J., and Katzenellenbogen, B. S. (2006) Gene expression preferentially regulated by tamoxifen in breast cancer cells and correlations with clinical outcome, *Cancer research 66*, 7334-7340.

202. Cossu-Rocca, P., Orru, S., Muroni, M. R., Sanges, F., Sotgiu, G., Ena, S., Pira, G., Murgia, L., Manca, A., Uras, M. G., Sarobba, M. G., Urru, S., and De Miglio, M. R. (2015) Analysis of PIK3CA Mutations and Activation Pathways in Triple Negative Breast Cancer, *PloS one 10*, e0141763.

203. Jonas, B. A., and Privalsky, M. L. (2004) SMRT and N-CoR corepressors are regulated by distinct kinase signaling pathways, *The Journal of biological chemistry 279*, 54676-54686.

204. Uehara, N., Kanematsu, S., Miki, H., Yoshizawa, K., and Tsubura, A. (2012) Requirement of p38 MAPK for a cell-death pathway triggered by vorinostat in MDA-MB-231 human breast cancer cells, *Cancer letters 315*, 112-121.

205. Insinga, A., Monestiroli, S., Ronzoni, S., Gelmetti, V., Marchesi, F., Viale, A., Altucci, L., Nervi, C., Minucci, S., and Pelicci, P. G. (2005) Inhibitors of histone deacetylases induce tumor-selective apoptosis through activation of the death receptor pathway (vol 11, pg 71, 2005), *Nat Med 11*, 233-233.

206. Singh, T. R., Shankar, S., and Srivastava, R. K. (2005) HDAC inhibitors enhance the apoptosis-inducing potential of TRAIL in breast carcinoma, *Oncogene 24*, 4609-4623.

207. Chakraborty, A. R., Robey, R. W., Luchenko, V. L., Zhan, Z. R., Piekarz, R. L., Gillet, J. P., Kossenkov, A. V., Wilkerson, J., Showe, L. C., Gottesman, M. M., Collie, N. L., and Bates, S. E. (2013) MAPK pathway activation leads to Bim loss and histone deacetylase inhibitor resistance: rationale to combine romidepsin with an MEK inhibitor, *Blood 121*, 4115-4125.

208. Ruefli, A. A., Ausserlechner, M. J., Bernhard, D., Sutton, V. R., Tainton, K. M., Kofler, R., Smyth, M. J., and Johnstone, R. W. (2001) The histone deacetylase inhibitor and chemotherapeutic agent suberoylanilide hydroxamic acid (SAHA) induces a cell-death pathway characterized by cleavage of Bid and production of reactive oxygen species, *P Natl Acad Sci USA 98*, 10833-10838.

209. Sandor, V., Senderowicz, A., Mertins, S., Sackett, D., Sausville, E., Blagosklonny, M. V., and Bates, S. E. (2000) P21-dependent g(1)arrest with downregulation of

cyclin D1 and upregulation of cyclin E by the histone deacetylase inhibitor FR901228, *Br J Cancer 83*, 817-825.

210. Garnett, M. J., Edelman, E. J., Heidorn, S. J., Greenman, C. D., Dastur, A., Lau, K. W., Greninger, P., Thompson, I. R., Luo, X., Soares, J., Liu, Q., Iorio, F., Surdez, D., Chen, L., Milano, R. J., Bignell, G. R., Tam, A. T., Davies, H., Stevenson, J. A., Barthorpe, S., Lutz, S. R., Kogera, F., Lawrence, K., McLaren-Douglas, A., Mitropoulos, X., Mironenko, T., Thi, H., Richardson, L., Zhou, W., Jewitt, F., Zhang, T., O'Brien, P., Boisvert, J. L., Price, S., Hur, W., Yang, W., Deng, X., Butler, A., Choi, H. G., Chang, J. W., Baselga, J., Stamenkovic, I., Engelman, J. A., Sharma, S. V., Delattre, O., Saez-Rodriguez, J., Gray, N. S., Settleman, J., Futreal, P. A., Haber, D. A., Stratton, M. R., Ramaswamy, S., McDermott, U., and Benes, C. H. (2012) Systematic identification of genomic markers of drug sensitivity in cancer cells, *Nature 483*, 570-575.

211. Liu, X. F., and Bagchi, M. K. (2004) Recruitment of distinct chromatin-modifying complexes by tamoxifen-complexed estrogen receptor at natural target gene promoters in vivo, *The Journal of biological chemistry 279*, 15050-15058.

212. Gao, Z., Chiao, P., Zhang, X., Zhang, X., Lazar, M. A., Seto, E., Young, H. A., and Ye, J. (2005) Coactivators and corepressors of NF-kappaB in IkappaB alpha gene promoter, *The Journal of biological chemistry 280*, 21091-21098.

213. Mahlknecht, U., Will, J., Varin, A., and Herbein, G. (2004) HDAC3, a class I histone deacetylase, interacts with the p38 pathway and suppresses MAPK11-Mediated ATF-2 activation and TNF gene expression., *Blood 104*, 599a-599a.

214. Weiss, C., Schneider, S., Wagner, E. F., Zhang, X., Seto, E., and Bohmann, D. (2003) JNK phosphorylation relieves HDAC3-dependent suppression of the transcriptional activity of c-Jun, *The EMBO journal 22*, 3686-3695.

215. Ellis, M. J., Ding, L., Shen, D., Luo, J., Suman, V. J., Wallis, J. W., Van Tine, B. A., Hoog, J., Goiffon, R. J., Goldstein, T. C., Ng, S., Lin, L., Crowder, R., Snider, J., Ballman, K., Weber, J., Chen, K., Koboldt, D. C., Kandoth, C., Schierding, W. S., McMichael, J. F., Miller, C. A., Lu, C., Harris, C. C., McLellan, M. D., Wendl, M. C., DeSchryver, K., Allred, D. C., Esserman, L., Unzeitig, G., Margenthaler, J., Babiera, G. V., Marcom, P. K., Guenther, J. M., Leitch, M., Hunt, K., Olson, J., Tao, Y., Maher, C. A., Fulton, L. L., Fulton, R. S., Harrison, M., Oberkfell, B., Du, F., Demeter, R., Vickery, T. L., Elhammali, A., Piwnica-Worms, H., McDonald, S., Watson, M., Dooling, D. J., Ota, D., Chang, L. W., Bose, R., Ley, T. J., Piwnica-Worms, D., Stuart, J. M., Wilson, R. K., and Mardis, E. R. (2012)

Whole-genome analysis informs breast cancer response to aromatase inhibition, *Nature 486*, 353-360.

216. Lai, C. J., Bao, R., Tao, X., Wang, J., Atoyan, R., Qu, H., Wang, D. G., Yin, L., Samson, M., Forrester, J., Zifcak, B., Xu, G. X., DellaRocca, S., Zhai, H. X., Cai, X., Munger, W. E., Keegan, M., Pepicelli, C. V., and Qian, C. (2010) CUDC-101, a multitargeted inhibitor of histone deacetylase, epidermal growth factor receptor, and human epidermal growth factor receptor 2, exerts potent anticancer activity, *Cancer research 70*, 3647-3656.

217. Bruzzese, F., Leone, A., Rocco, M., Carbone, C., Piro, G., Caraglia, M., Di Gennaro, E., and Budillon, A. (2011) HDAC inhibitor vorinostat enhances the antitumor effect of gefitinib in squamous cell carcinoma of head and neck by modulating ErbB receptor expression and reverting EMT, *Journal of cellular physiology 226*, 2378-2390.

218. He, B., Velaparthi, S., Pieffet, G., Pennington, C., Mahesh, A., Holzle, D. L., Brunsteiner, M., van Breemen, R., Blond, S. Y., and Petukhov, P. A. (2009) Binding ensemble profiling with photoaffinity labeling (BEProFL) approach: mapping the binding poses of HDAC8 inhibitors, *Journal of medicinal chemistry 52*, 7003-7013.

219. Neelarapu, R., Holzle, D. L., Velaparthi, S., Bai, H., Brunsteiner, M., Blond, S. Y., and Petukhov, P. A. (2011) Design, synthesis, docking, and biological evaluation of novel diazide-containing isoxazole- and pyrazole-based histone deacetylase probes, *Journal of medicinal chemistry 54*, 4350-4364.

220. Falkenberg, K. J., and Johnstone, R. W. (2014) Histone deacetylases and their inhibitors in cancer, neurological diseases and immune disorders, *Nature reviews. Drug discovery 13*, 673-691.

221. Mathias, R. A., Guise, A. J., and Cristea, I. M. (2015) Post-translational modifications regulate class IIa histone deacetylase (HDAC) function in health and disease, *Molecular & cellular proteomics : MCP 14*, 456-470.

222. You, A., Tong, J. K., Grozinger, C. M., and Schreiber, S. L. (2001) CoREST is an integral component of the CoREST- human histone deacetylase complex, *Proceedings of the National Academy of Sciences of the United States of America 98*, 1454-1458.

223. Remiszewski, S. W., Sambucetti, L. C., Bair, K. W., Bontempo, J., Cesarz, D., Chandramouli, N., Chen, R., Cheung, M., Cornell-Kennon, S., Dean, K.,

Diamantidis, G., France, D., Green, M. A., Howell, K. L., Kashi, R., Kwon, P., Lassota, P., Martin, M. S., Mou, Y., Perez, L. B., Sharma, S., Smith, T., Sorensen, E., Taplin, F., Trogani, N., Versace, R., Walker, H., Weltchek-Engler, S., Wood, A., Wu, A., and Atadja, P. (2003) N-hydroxy-3-phenyl-2-propenamides as novel inhibitors of human histone deacetylase with in vivo antitumor activity: discovery of (2E)-N-hydroxy-3-[4-[[(2-hydroxyethyl)[2-(1H-indol-3-yl)ethyl]amino]methyl]phenyl]-2-propenamide (NVP-LAQ824), *Journal of medicinal chemistry 46*, 4609-4624.

224. Lobera, M., Madauss, K. P., Pohlhaus, D. T., Wright, Q. G., Trocha, M., Schmidt, D. R., Baloglu, E., Trump, R. P., Head, M. S., Hofmann, G. A., Murray-Thompson, M., Schwartz, B., Chakravorty, S., Wu, Z., Mander, P. K., Kruidenier, L., Reid, R. A., Burkhart, W., Turunen, B. J., Rong, J. X., Wagner, C., Moyer, M. B., Wells, C., Hong, X., Moore, J. T., Williams, J. D., Soler, D., Ghosh, S., and Nolan, M. A. (2013) Selective class IIa histone deacetylase inhibition via a nonchelating zinc-binding group, *Nature chemical biology 9*, 319-325.

225. Balasubramanian, S., Ramos, J., Luo, W., Sirisawad, M., Verner, E., and Buggy, J. J. (2008) A novel histone deacetylase 8 (HDAC8)-specific inhibitor PCI-34051 induces apoptosis in T-cell lymphomas, *Leukemia 22*, 1026-1034.

226. Marks, P. A., and Breslow, R. (2007) Dimethyl sulfoxide to vorinostat: development of this histone deacetylase inhibitor as an anticancer drug, *Nature biotechnology 25*, 84-90.

227. Chou, C. J., Herman, D., and Gottesfeld, J. M. (2008) Pimelic diphenylamide 106 is a slow, tight-binding inhibitor of class I histone deacetylases, *The Journal of biological chemistry 283*, 35402-35409.

228. Buggy, J. J., Balasubramanian, S., Verner, E., Tai, V. W. F., and Lee, C. S. (2013) Indole derivatives as inhibitors of histone deacetylase, Google Patents.

229. Hanigan TW, A. S., Taha TY, Frasor JM, Petukhov PA. (2017) Divergent JNK Phosphorylation of HDAC3 in Triple Negative Breast Cancer Cells Determines HDAC Inhibitor Binding and Selectivity, *Cell Chemical Biology In-Press*.

230. Falkenberg, K. J., and Johnstone, R. W. (2014) Histone deacetylases and their inhibitors in cancer, neurological diseases and immune disorders, *Nat. Rev. Drug Discov. 13*, 673-691.

231. de Ruijter, A. J., van Gennip, A. H., Caron, H. N., Kemp, S., and van Kuilenburg, A. B. (2003) Histone deacetylases (HDACs): characterization of the classical HDAC family, *Biochem. J. 370*, 737-749.

232. Gao, L., Cueto, M. A., Asselbergs, F., and Atadja, P. (2002) Cloning and functional characterization of HDAC11, a novel member of the human histone deacetylase family, *The Journal of biological chemistry 277*, 25748-25755.

233. Butler, L. M., Zhou, X., Xu, W. S., Scher, H. I., Rifkind, R. A., Marks, P. A., and Richon, V. M. (2002) The histone deacetylase inhibitor SAHA arrests cancer cell growth, up-regulates thioredoxin-binding protein-2, and down-regulates thioredoxin, *Proc. Natl. Acad. Sci. U. S. A. 99*, 11700-11705.

234. Andrin, C., and Hendzel, M. J. (2004) F-actin-dependent insolubility of chromatin-modifying components, *The Journal of biological chemistry 279*, 25017-25023.

235. Galasinski, S. C., Resing, K. A., Goodrich, J. A., and Ahn, N. G. (2002) Phosphatase inhibition leads to histone deacetylases 1 and 2 phosphorylation and disruption of corepressor interactions, *The Journal of biological chemistry 277*, 19618-19626.

236. He, S., Khan, D. H., Winter, S., Seiser, C., and Davie, J. R. (2013) Dynamic distribution of HDAC1 and HDAC2 during mitosis: association with F-actin, *J. Cell Physiol. 228*, 1525-1535.

237. Ishii, S., Kurasawa, Y., Wong, J. M., and Yu-Lee, L. Y. (2008) Histone deacetylase 3 localizes to the mitotic spindle and is required for kinetochore-microtubule attachment, *Proc. Natl. Acad. Sci. U. S. A. 105*, 4179-4184.

238. Basile, V., Mantovani, R., and Imbriano, C. (2006) DNA damage promotes histone deacetylase 4 nuclear localization and repression of G(2)/M promoters, via p53 C-terminal lysines, *The Journal of biological chemistry 281*, 2347-2357.

239. McKinsey, T. A., Zhang, C. L., Lu, J. R., and Olson, E. N. (2000) Signal-dependent nuclear export of a histone deacetylase regulates muscle differentiation, *Nature 408*, 106-111.

240. Rosato, R. R., Almenara, J. A., and Grant, S. (2003) The histone deacetylase inhibitor MS-275 promotes differentiation or apoptosis in human leukemia cells through a process regulated by generation of reactive oxygen species and induction of p21(CIP1/WAF1), *Cancer Res. 63*, 3637-3645.

241. Beckers, T., Burkhardt, C., Wieland, H., Gimmnich, P., Ciossek, T., Maier, T., and Sanders, K. (2007) Distinct pharmacological properties of second generation HDAC inhibitors with the benzamide or hydroxamate head group, *Int. J. Cancer 121*, 1138-1148.

242. Singh, T. R., Shankar, S., and Srivastava, R. K. (2005) HDAC inhibitors enhance the apoptosis-inducing potential of TRAIL in breast carcinoma, *Oncogene 24*, 4609-4623.

243. Fortunati, N., Marano, F., Bandino, A., Frairia, R., Catalano, M. G., and Boccuzzi, G. (2014) The pan-histone deacetylase inhibitor LBH589 (panobinostat) alters the invasive breast cancer cell phenotype, *Int. J. Oncol. 44*, 700-708.

244. Tavakoli-Yaraki, M., Karami-Tehrani, F., Salimi, V., and Sirati-Sabet, M. (2013) Induction of apoptosis by Trichostatin A in human breast cancer cell lines: involvement of 15-Lox-1, *Tumour Biol. 34*, 241-249.

245. Savelieva, M., Woo, M. M., Schran, H., Mu, S., Nedelman, J., and Capdeville, R. (2015) Population pharmacokinetics of intravenous and oral panobinostat in patients with hematologic and solid tumors, *Eur. J. Clin. Pharmacol. 71*, 663-672.

246. Giles, F., Fischer, T., Cortes, J., Garcia-Manero, G., Beck, J., Ravandi, F., Masson, E., Rae, P., Laird, G., Sharma, S., Kantarjian, H., Dugan, M., Albitar, M., and Bhalla, K. (2006) A phase I study of intravenous LBH589, a novel cinnamic hydroxamic acid analogue histone deacetylase inhibitor, in patients with refractory hematologic malignancies, *Clin. Cancer Res. 12*, 4628-4635.

247. Sanderson, L., Taylor, G. W., Aboagye, E. O., Alao, J. P., Latigo, J. R., Coombes, R. C., and Vigushin, D. M. (2004) Plasma pharmacokinetics and metabolism of the histone deacetylase inhibitor trichostatin a after intraperitoneal administration to mice, *Drug. Metab. Dispos. 32*, 1132-1138.

248. Pili, R., Salumbides, B., Zhao, M., Altiok, S., Qian, D., Zwiebel, J., Carducci, M. A., and Rudek, M. A. (2012) Phase I study of the histone deacetylase inhibitor entinostat in combination with 13-cis retinoic acid in patients with solid tumours, *Br. J. Cancer 106*, 77-84.

249. O'Connor, O. A., Heaney, M. L., Schwartz, L., Richardson, S., Willim, R., MacGregor-Cortelli, B., Curly, T., Moskowitz, C., Portlock, C., Horwitz, S., Zelenetz, A. D., Frankel, S., Richon, V., Marks, P., and Kelly, W. K. (2006) Clinical experience with intravenous and oral formulations of the novel histone

deacetylase inhibitor suberoylanilide hydroxamic acid in patients with advanced hematologic malignancies, *J. Clin. Oncol. 24*, 166-173.

250. Sutherland, R. L., Hall, R. E., and Taylor, I. W. (1983) Cell proliferation kinetics of MCF-7 human mammary carcinoma cells in culture and effects of tamoxifen on exponentially growing and plateau-phase cells, *Cancer Res. 43*, 3998-4006.

251. Van den Wyngaert, I., de Vries, W., Kremer, A., Neefs, J. M., Verhasselt, P., Luyten, W. H. M. L., and Kass, S. U. (2000) Cloning and characterization of human histone deacetylase 8, *FEBS Lett. 478*, 77-83.

252. Buggy, J. J., Sideris, M. L., Mak, P., Lorimer, D. D., McIntosh, B., and Clark, J. M. (2000) Cloning and characterization of a novel human histone deacetylase, HDAC8, *Biochem. J. 350*, 199-205.

253. Ververis, K., and Karagiannis, T. C. (2012) An atlas of histone deacetylase expression in breast cancer: fluorescence methodology for comparative semi-quantitative analysis, *Am. J. Transl. Res. 4*, 24-43.

254. Atadja, P. (2009) Development of the pan-DAC inhibitor panobinostat (LBH589): successes and challenges, *Cancer Lett. 280*, 233-241.

255. Huber, K., Doyon, G., Plaks, J., Fyne, E., Mellors, J. W., and Sluis-Cremer, N. (2011) Inhibitors of histone deacetylases: correlation between isoform specificity and reactivation of HIV type 1 (HIV-1) from latently infected cells, *J. Biol. Chem. 286*, 22211-22218.

256. Kruhlak, M. J., Hendzel, M. J., Fischle, W., Bertos, N. R., Hameed, S., Yang, X. J., Verdin, E., and Bazett-Jones, D. P. (2001) Regulation of global acetylation in mitosis through loss of histone acetyltransferases and deacetylases from chromatin, *J. Biol. Chem. 276*, 38307-38319.

257. Hanigan TW, Aboukhatwa SM, Taha TY, Frasor J, Petukhov PA. (2017) Divergent JNK Phosphorylation of HDAC3 in Triple Negative Breast Cancer Cells Determines HDAC Inhibitor Binding and Selectivity, *Cell Chem. Biol.*, Forthcoming, CELL-CHEMICAL-BIOLOGY-D-17-00077R00071.

258. Tate, C. R., Rhodes, L. V., Segar, H. C., Driver, J. L., Pounder, F. N., Burow, M. E., and Collins-Burow, B. M. (2012) Targeting triple-negative breast cancer cells with the histone deacetylase inhibitor panobinostat, *Breast Cancer Res. 14*, R79.

259. Glaser, K. B., Staver, M. J., Waring, J. F., Stender, J., Ulrich, R. G., and Davidsen, S. K. (2003) Gene expression profiling of multiple histone deacetylase (HDAC) inhibitors: defining a common gene set produced by HDAC inhibition in T24 and MDA carcinoma cell lines, *Mol. Cancer Ther. 2*, 151-163.

260. Min, A., Im, S. A., Kim, D. K., Song, S. H., Kim, H. J., Lee, K. H., Kim, T. Y., Han, S. W., Oh, D. Y., Kim, T. Y., O'Connor, M. J., and Bang, Y. J. (2015) Histone deacetylase inhibitor, suberoylanilide hydroxamic acid (SAHA), enhances anti-tumor effects of the poly (ADP-ribose) polymerase (PARP) inhibitor olaparib in triple-negative breast cancer cells, *Breast Cancer Res. 17*, 33.

261. Vijayaraghavalu, S., Dermawan, J. K., Cheriyath, V., and Labhasetwar, V. (2013) Highly synergistic effect of sequential treatment with epigenetic and anticancer drugs to overcome drug resistance in breast cancer cells is mediated via activation of p21 gene expression leading to G2/M cycle arrest, *Mol. Pharm. 10*, 337-352.

262. Gray, S. G., and Ekstrom, T. J. (1998) Effects of cell density and trichostatin A on the expression of HDAC1 and p57Kip2 in Hep 3B cells, *Biochem. Biophys. Res. Commun. 245*, 423-427.

263. Taubert, S., Gorrini, C., Frank, S. R., Parisi, T., Fuchs, M., Chan, H. M., Livingston, D. M., and Amati, B. (2004) E2F-dependent histone acetylation and recruitment of the Tip60 acetyltransferase complex to chromatin in late G1, *Mol. Cell Biol. 24*, 4546-4556.

264. Lauffer, B. E., Mintzer, R., Fong, R., Mukund, S., Tam, C., Zilberleyb, I., Flicke, B., Ritscher, A., Fedorowicz, G., Vallero, R., Ortwine, D. F., Gunzner, J., Modrusan, Z., Neumann, L., Koth, C. M., Lupardus, P. J., Kaminker, J. S., Heise, C. E., and Steiner, P. (2013) Histone deacetylase (HDAC) inhibitor kinetic rate constants correlate with cellular histone acetylation but not transcription and cell viability, *J. Biol. Chem. 288*, 26926-26943.

265. Somoza, J. R., Skene, R. J., Katz, B. A., Mol, C., Ho, J. D., Jennings, A. J., Luong, C., Arvai, A., Buggy, J. J., Chi, E., Tang, J., Sang, B. C., Verner, E., Wynands, R., Leahy, E. M., Dougan, D. R., Snell, G., Navre, M., Knuth, M. W., Swanson, R. V., McRee, D. E., and Tari, L. W. (2004) Structural snapshots of human HDAC8 provide insights into the class I histone deacetylases, *Structure 12*, 1325-1334.

266. Wang, Z., Qin, G., and Zhao, T. C. (2014) HDAC4: mechanism of regulation and biological functions, *Epigenomics 6*, 139-150.

267. Smith, K. T., Martin-Brown, S. A., Florens, L., Washburn, M. P., and Workman, J. L. (2010) Deacetylase inhibitors dissociate the histone-targeting ING2 subunit from the Sin3 complex, *Chem. Biol. 17*, 65-74.

268. Maolanon, Alex R., Madsen, Andreas S., and Olsen, Christian A. Innovative Strategies for Selective Inhibition of Histone Deacetylases, *Cell Chemical Biology 23*, 759-768.

269. Matsuoka, H., Fujimura, T., Hayashi, M., Matsuda, K., Ishii, Y., Aramori, I., and Mutoh, S. (2007) Disruption of HDAC4/N-CoR complex by histone deacetylase inhibitors leads to inhibition of IL-2 gene expression, *Biochemical pharmacology 74*, 465-476.

270. Smith, K. T., Martin-Brown, S. A., Florens, L., Washburn, M. P., and Workman, J. L. (2010) Deacetylase inhibitors dissociate the histone-targeting ING2 subunit from the Sin3 complex, *Chemistry & biology 17*, 65-74.

271. Bantscheff, M., Hopf, C., Savitski, M. M., Dittmann, A., Grandi, P., Michon, A. M., Schlegl, J., Abraham, Y., Becher, I., Bergamini, G., Boesche, M., Delling, M., Dumpelfeld, B., Eberhard, D., Huthmacher, C., Mathieson, T., Poeckel, D., Reader, V., Strunk, K., Sweetman, G., Kruse, U., Neubauer, G., Ramsden, N. G., and Drewes, G. (2011) Chemoproteomics profiling of HDAC inhibitors reveals selective targeting of HDAC complexes, *Nature biotechnology 29*, 255-265.

272. Robers, M. B., Dart, M. L., Woodroofe, C. C., Zimprich, C. A., Kirkland, T. A., Machleidt, T., Kupcho, K. R., Levin, S., Hartnett, J. R., Zimmerman, K., Niles, A. L., Ohana, R. F., Daniels, D. L., Slater, M., Wood, M. G., Cong, M., Cheng, Y.-Q., and Wood, K. V. (2015) Target engagement and drug residence time can be observed in living cells with BRET, *6*, 10091.

273. Munster, P. N., Thurn, K. T., Thomas, S., Raha, P., Lacevic, M., Miller, A., Melisko, M., Ismail-Khan, R., Rugo, H., Moasser, M., and Minton, S. E. (2011) A phase II study of the histone deacetylase inhibitor vorinostat combined with tamoxifen for the treatment of patients with hormone therapy-resistant breast cancer, *British journal of cancer 104*, 1828-1835.

274. Gerber, D. E., Boothman, D. A., Fattah, F. J., Dong, Y., Zhu, H., Skelton, R. A., Priddy, L. L., Vo, P., Dowell, J. E., Sarode, V., Leff, R., Meek, C., Xie, Y., and Schiller, J. H. (2015) Phase 1 study of romidepsin plus erlotinib in advanced non-small cell lung cancer, *Lung cancer (Amsterdam, Netherlands) 90*, 534-541.

275. Han, J.-Y., Lee, S. H., Lee, G. K., Yun, T., Lee, Y. J., Hwang, K. H., Kim, J. Y., and Kim, H. T. (2015) Phase I/II study of gefitinib (Iressa(®)) and vorinostat (IVORI) in previously treated patients with advanced non-small cell lung cancer, *Cancer chemotherapy and pharmacology 75*, 475-483.

276. Shimizu, T., LoRusso, P. M., Papadopoulos, K. P., Patnaik, A., Beeram, M., Smith, L. S., Rasco, D. W., Mays, T. A., Chambers, G., Ma, A., Wang, J., Laliberte, R., Voi, M., and Tolcher, A. W. (2014) Phase I first-in-human study of CUDC-101, a multitargeted inhibitor of HDACs, EGFR, and HER2 in patients with advanced solid tumors, *Clinical cancer research : an official journal of the American Association for Cancer Research 20*, 5032-5040.

277. Napoli, M., Venkatanarayan, A., Raulji, P., Meyers, B. A., Norton, W., Mangala, L. S., Sood, A. K., Rodriguez-Aguayo, C., Lopez-Berestein, G., Vin, H., Duvic, M., Tetzlaff, M. B., Curry, J. L., Rook, A. H., Abbas, H. A., Coarfa, C., Gunaratne, P. H., Tsai, K. Y., and Flores, E. R. (2016) DeltaNp63/DGCR8-Dependent MicroRNAs Mediate Therapeutic Efficacy of HDAC Inhibitors in Cancer, *Cancer cell 29*, 874-888.

278. Ree, A. H., Saelen, M. G., Kalanxhi, E., Østensen, I. H. G., Schee, K., Røe, K., Abrahamsen, T. W., Dueland, S., and Flatmark, K. (2014) Biomarkers of Histone Deacetylase Inhibitor Activity in a Phase 1 Combined-Modality Study with Radiotherapy, *PloS one 9*, e89750.

279. de Bono, J. S., Kristeleit, R., Tolcher, A., Fong, P., Pacey, S., Karavasilis, V., Mita, M., Shaw, H., Workman, P., Kaye, S., Rowinsky, E. K., Aherne, W., Atadja, P., Scott, J. W., and Patnaik, A. (2008) Phase I pharmacokinetic and pharmacodynamic study of LAQ824, a hydroxamate histone deacetylase inhibitor with a heat shock protein-90 inhibitory profile, in patients with advanced solid tumors, *Clinical cancer research : an official journal of the American Association for Cancer Research 14*, 6663-6673.

280. Bates, S. E., Zhan, Z., Steadman, K., Obrzut, T., Luchenko, V., Frye, R., Robey, R. W., Turner, M., Gardner, E. R., Figg, W. D., Steinberg, S. M., Ling, A., Fojo, T., To, K. W., and Piekarz, R. L. (2010) Laboratory correlates for a phase II trial of romidepsin in cutaneous and peripheral T-cell lymphoma, *British journal of haematology 148*, 256-267.

281. Qu, K., Zaba, L. C., Satpathy, A. T., Giresi, P. G., Li, R., Jin, Y., Armstrong, R., Jin, C., Schmitt, N., Rahbar, Z., Ueno, H., Greenleaf, W. J., Kim, Y. H., and Chang, H. Y. Chromatin Accessibility Landscape of Cutaneous T Cell Lymphoma and Dynamic Response to HDAC Inhibitors, *Cancer cell 32*, 27-41.e24.

Vita

Thomas W. Hanigan

Education

2012-present	University of Illinois at Chicago Ph.D in Medicinal Chemistry Expected Graduation date: 2017 GPA 3.75
2007-2010	Iowa State University B.S. in Materials Engineering B.A. in Chemistry Graduation date: May 2012 GPA: 3.56

Research Experience

Graduate

2012-present	University of Illinois Department of Medicinal Chemistry Project 1: Development of method for detecting change in catalytic activity of histone deacetylase enzymes Project 2: Development of method to identify genomic loci targeted by small molecule inhibitors Project 3: general synthetic strategy for the development of diverse histone deacetylase inhibitor photoreactive probes and characterization of their cell based selectivity Project 4: Potent Hydroxamic Acid HDAC Inhibitors Re-equilibrate the Subcellular Localization and Post-Translational Modification State of Class I HDACs Advisement: Dr. Pavel Petukhov, Dr. Jonna Frasor
2017-present	Internship at Adello Biologics in Chicago Project: Identification of PEGylation site modification of GCSF. Advisement: Hari Ranpura Ph.D, Michelle Zheng Ph.D

Undergraduate

2011	Iowa State Materials Engineering Project: Ammonia Nurse Tank Fatigue Cracking: Noninvasive fatigue crack detection to decrease risk of catastrophic failure Advisement: Dr. Scott Chumbley and Dr. Alan Russell
2009-2010	NASA Space Center at Cal State LA Project: Researching manufacturing and process techniques for unmanned aerial vehicles Advisement: Dr. Chivey Wu and Dr. Helen Boussalis

---

Awards and Fellowships

2017 PIIPS Fellowship: American Society for Pharmacology and Experimental Therapeutics
2017 Charles Wesley Petranek Memorial Scholar
2016 UIC Research Day, Cancer center award for best poster
2015 UI Cancer Center Research Forum, Best Poster Award
2014 W.E. van Doren Scholar
American Association for the Advancement of Science Nominee
Alpha Lambda Delta and Phi Eta Sigma (ALD/PES) National Honors Societies
Dean's List for the college of engineering 2008-2012

Experimental Expertise

Biology
Cell culture (MCF-7, MDA-MB-231, MCF10A, BT474, T47-D, BT20, MDA-MB-453, MDA-MB468, ZR75-1, HeLa),
Real Time PCR (primer design, reverse transcription, DNA amplification) Protein expression and Purification
Enzyme Kinetics (fluorometric Based Assay for IC50 and Ki determination, Luminescence-Based Assay for IC_{50} and Ki determination)
Chromatin Immunoprecipitation
Antibody based affinity enrichments
SDS-polyacrylamide gel electrophoresis and Western blotting.
Bottom up proteomics
Top down proteomics
Cell based small molecule target identification
In vitro/In Situ click chemistry
Antibody covalent modification, click chemistry

Chemistry
Synthetic Organic Chemistry: photoreactive probes, heterocyclic HDAC inhibitors, Lignan Based analogues of Helioxanthins
Synthetic Alterations to Natural Products: Biotinylation of oligopeptide antibiotics derived from several strains of strepromycetes.

Spectroscopic Techniques:
NMR: 1D NMR experiments (H1, C13, F19, and DEPT), 2D NMR experiments (COSY, HMBS, HSQC)
Mass Spectrometry: LC-MS, MALDI-TOF, UPLC-MS/MS, bottom up proteomics, top down proteomics

Computer Assisted Drug Design:
MOE (Molecular Operating environment), OpenEye (molecular docking to protein/energy minimization, novel scaffold development, fragment based drug design)

Computer Programming
Proficient in FORTRAN, MATLAB, and PYTHON computer languages

Presentations

2017 UIC Research Day
"Divergent Phosphorylation of Histone Deacetylase in Breast Cancer Determines Inhibitor Binding and Selectivity", poster

2016 MIKI Medicinal Chemistry Symposium
"The Importance of Determining Target Engagement in a Native Environment", oral presentation

2016 UIC Research Day
"Cell Based Strategy to Improve HDAC Inhibitor Efficacy as Breast Cancer Therapeutics", poster

2015 Cancer Center Research Forum
"Cell Based Strategy to Improve HDAC Inhibitor Efficacy as Breast Cancer Therapeutics", poster

28th Annual ASPET Scientific Meeting, Chicago 2015
"Having a Complex: Implications on HDAC-Ligand Interactions", poster

7th Yao Yuan Biotech-Pharma Symposium, At the interface of Chemistry and Biology for Drug Discovery, Chicago 2015
"Having a Complex: Implications on HDAC-Ligand Interactions", poster

ACS chemistry conference, San Francisco 2014

"Optimization of Photolabeling and Cisualization of Histone Deacetylase 2 in cell lysates", poster

---

Publications

Thomas W. Hanigan, Jonna Frasor, Pavel Petukhov. "Divergent JNK Phosphorylation of HDAC3 in Breast Cancer Cells Determines HDAC Inhibitor Binding and Selectivity" In-Press. *Cell Chemical Biology* (2017)

Thomas W. Hanigan, Taha Y. Taha, Pavel Petukhov. "Potent Hydroxamic Acid HDAC Inhibitors Re-equilibrate the Subcellular Localization and Post-Translational Modification State of Class I HDACs" In-Press *PLOS One* (2017)

Thomas W Hanigan, Jeanne Danes, Taha Taha, Jonna Frasor, Pavel Petukhov. "Histone Deacetylase Inhibitor-Based Chromatin Precipitation for Identification of Targeted Genomic Loci" Under review at *Journal of Biological Methods* (2017)

Thomas W. Hanigan, Shaimaa Aboukhatwa, Jonna Frasor, Pavel Petukhov. "General Synthetic Strategy for the Development of Diverse HDAC inhibitor based Photoreactive Probes and Characterization of their Cell Based Selectivity" Under review *ACS Chemical Biology* (2017)

Alan M. Russell; Andrew T Becker, PhD; Leonard S Chumbley, PhD; Darrel A Enyart, B.S.; Brian L Bowersox, B.S.; Thomas W Hanigan, B.S.; Jason L Labbe, B.S.; James S Moran, B.S.; Emily L, Spicher, B.S. "A Survey of Flaws Near Welds Detected by Side-angle Ultrasound Examination of 532 Nurse Tanks." *Journal of Loss Prevention in the Process Industries* (2016): 263-272

Patents

Hanigan TW, Frasor J, Petukhov P. (2017). Superior anti-cancer combination of HDAC and JNK/p38 pathway kinase inhibitors as treatment for triple-negative breast cancer. Provisional Application for Patent. Application Number 62/457,244

Hanigan TW, Frasor J, Petukhov P. (2017). Convergent synthetic strategy to synthesis of photoreactive probes and their histone deacetylase target engagement evaluation in live cells. Provisional Application for Patent. Application Number 62/457,251

Hanigan TW, Frasor J, Petukhov P. (2017). HDAC3 Phosphorylation as a Diagnostic Marker for HDAC Inhibitor Effiicacy. Provisional Application for Patent. Application Number 62/457,254
